ENZYME IMMOBILISATION USING POROUS FRAMEWORKS

A thesis presented to

The School of Physical Sciences

at

The University of Adelaide

in fulfilment of the requirements for

The Degree of

Doctor of Philosophy in Chemical Science

by

Natasha K. Maddigan

THE UNIVERSITY of ADELAIDE

Adelaide, Australia

March 2020

Contents

Declaration

I certify that this work contains no material which has been accepted for the award of any other degree or diploma in my name, in any university or other tertiary institution and, to the best of my knowledge and belief, contains no material previously published or written by another person, except where due reference has been made in the text. In addition, I certify that no part of this work will, in the future, be used in a submission in my name, for any other degree or diploma in any university or other tertiary institution without the prior approval of the University of Adelaide and where applicable, any partner institution responsible for the joint-award of this degree.

I acknowledge that copyright of published works contained within this thesis resides with the copyright holder(s) of those works.

I also give permission for the digital version of my thesis to be made available on the web, via the University's digital research repository, the Library Search and also through web search engines, unless permission has been granted by the University to restrict access for a period of time.

I acknowledge the support I have received for my research through the provision of an Australian Government Research Training Program Scholarship.

Natasha Maddigan

Acknowledgements

There are many people that I would like to acknowledge for their support and guidance during the past 4 years of my PhD.

Firstly, I would like to thank my supervisors, A/Prof. Stephen Bell, and Prof. Christian Doonan for providing insight and advice that assisted in getting me this far. Thank you for the many opportunities you have given me to travel and present my work. It has pushed me outside of my comfort zone, but I feel I have become a better researcher and presenter because of it. Additionally, thank you for countless hours put into drafting this thesis, and other work I have been a part of. Special thanks also goes to my 'unofficial' supervisor Prof. Chris Sumby, who has been a valuable source of advice throughout my PhD.

I would like to extend my gratitude to past and present members of both the Bell and Sumby-Doonan-Keene-Bloch groups, as well as the Chemistry Department as a whole. In particular, Dr. Cam Coghlan, Dr. Jesse Teo, and Dr. Weibin Liang, who have all assisted with this research at various stages of its progression. Thanks for introducing me to new techniques, and for guiding my understanding of this research project. I would also like to thank Dr. Andrew "Co-pick of the week" Tarzia and A/Prof. David Huang for their valuable contributions to our paper, and for Prof. Paolo Falcaro for his insights and expert figure making skills. A big thanks must also go to Matt Bull for both his technical support and advice/general lab chats. To Kate, Harley and Oliver, thank you for being a part of all of the good times, and for your support through the less than good times. The endless dancing, singing, coffee and beers, have definitely been a highlight. Additionally, thanks to Rohan, Pat and Aimee for all of your support both in and outside of Uni. I appreciate you guys checking in.

Oliver, I wouldn't be where I am without your support. Thanks for always being there to help when I have needed it, especially during the hard times when Uncle Neil passed away. I am incredibly grateful to have had you by side during this journey.

Lastly, I would like to thank my friends and family outside of Uni for sharing in this journey with me. Thank you, Mum and Dad (Anita and Peter), Matthew, Terri, Aaron, Tianyi and the whole Linder-Patton family (David, Simone, Phoebe and Nathaniel), for your kind words, support and company, during the highs and lows of the past few years. Big shout-out also goes to Swathi and Bowie for your incredible support (and many meals), over the years. I owe you one, that's for sure.

Abbreviations

General Abbreviations

BET	Brunauer-Emmet-Teller
BID	Barrier discharge ionisation discharge
CLEA	Cross-linked enzyme aggregates
CLSM	Confocal Laser Scanning Microscopy
Dia	Diamondoid
EDX	Energy dispersive X-ray
FITC	Fluorescein isothiocyanate
FID	Flame ionisation detector
GC	Gas chromatography
HOF	Hydrogen-bonded organic framework
ICA	Imidazole-2-carboxaldehyde
MOF	Metal-organic framework
pI	Isoelectric point
***p*-NPB**	*para*-nitrophenyl butyrate
PXRD	Powder X-ray diffraction
Sod	Sodalite
SEM	Scanning electron microscopy
ZIF-8	Zeolitic imidazolate framework-8
ZIF-90	Zeolitic imidazolate framework-90
2-mIM	2-methyl imidazole
1,2-DBE	1,2- dibromoethane
1,3-DBP	1,3-dibromopropane

Protein/Enzyme Abbreviations

BSA	Bovine serum albumin
CALB	Lipase B from *Candida antarctica*
Cat	Catalase
Hb	Haemoglobin
HRP	Horseradish peroxidase
Mb	Myoglobin
LinB	Dehalogenase from *Sphingomonas paucimobilis*

Publications

The following publication is included as a chapter:

Maddigan, N. K.; Tarzia, A.; Huang, D. M.; Sumby, C. J.; Bell, S. G.; Falcaro, P.; Doonan, C. J., Protein surface functionalisation as a general strategy for facilitating biomimetic mineralisation of ZIF-8. *Chem. Sci.* **2018,** *9* (18), 4217-4223.

Additional contributions were made to the following publications:

Liang, W.; Ricco, R.; **Maddigan, N. K**.; Dickinson, R. P.; Xu, H.; Li, Q.; Sumby, C. J.; Bell, S. G.; Falcaro, P.; Doonan, C. J., Control of Structure Topology and Spatial Distribution of Biomacromolecules in Protein@ZIF-8 Biocomposites. *Chem. Mater.* **2018,** *30* (3), 1069-1077.

Liang, W.; Xu, H.; Carraro, F.; **Maddigan, N. K**.; Li, Q.; Bell, S. G.; Huang, D. M.; Tarzia, A.; Solomon, M. B.; Amenitsch, H.; Vaccari, L.; Sumby, C. J.; Falcaro, P.; Doonan, C. J., Enhanced Activity of Enzymes Encapsulated in Hydrophilic Metal–Organic Frameworks. *J. Am. Chem. Soc.* **2019,** *141* (6), 2348-2355.

Abstract

Enzymes are often sought after for applications in industry and synthetic chemistry due to their high reactivity and substrate selectivity, often surpassing their chemical counterparts. They are, however, limited by their structural instability and require restrictive environmental conditions that are often not compatible with industrial processing. As such, new technologies are required to protect enzymes from non-biological conditions. This thesis investigates enzyme immobilisation using porous frameworks including metal-organic frameworks (MOFs) and hydrogen-bonded organic frameworks (HOFs). The diverse nature of both the enzyme and MOF/HOF components offers great potential for creating a broad library of biocomposites with novel function. There are however inherent challenges in finding appropriate conditions for immobilisation in which the enzyme remains active, and where the overall biocomposite is stable.

Initial studies utilised Zeolitic Imidazolate Framework 8 (ZIF-8), a subclass of MOFs, for protein immobilisation. The addition of biomacromolecules, such as proteins, can promote the self-assembly of ZIF-8 by a process known as “biomimetic mineralisation”. Systematic screening studies established that this process is biomacromolecule dependent, with a subset of proteins requiring the addition of organic solvent or increased ligand concentrations to promote ZIF-8 nucleation. These reaction conditions were also instrumental in controlling the topology, morphology, and particle size of the biocomposites. Investigations into the influence of the protein revealed that biomimetic mineralisation is governed by the surface chemistry of the biomacromolecules, with a more negative surface charge promoting rapid nucleation, resulting from enhanced zinc ion concentration at the surface. Chemical functionalisation can be implemented, to alter the electrostatic potential of the protein surface and control the biomimetic mineralisation process.

The biocomposites from different immobilisation strategies for ZIF-8 were assessed for biocatalytic activity using two distinct enzymes, a lipase, and a dehalogenase. The activity was analysed relative to the free enzyme to interrogate the impact of immobilisation on the function and stability of the biocatalyst. Variation in support stability and biocomposite activity were observed. Each were dependent on the method of immobilisation with some strategies yielding inactive or unstable biocomposites. For lipase, the ZIF-8 framework provided enzymatic stability to organic solvent, whilst the framework itself was susceptible to degradation by phosphate buffer. In the case of the dehalogenase biocomposite, substrate dependent crystal

degradation was observed that was deemed responsible for variations in the observed enzyme activity. These findings highlight the potential limitations of ZIF-8 for enzyme immobilisation and as such, alternative porous supports were targeted.

Framework chemistry and porosity were further investigated utilising Zeolitic Imidazolate Framework-90 (ZIF-90) and a biologically compatible HOF (BioHOF-1) to immobilise the lipase and dehalogenase enzymes. Relative to ZIF-8, enhanced activity was observed for both enzymes upon immobilisation using these frameworks, with the lipase biocomposites demonstrating retention of enantioselectivity, comparable to the free enzyme. However, the metal based ZIF-90 material faced similar challenges to ZIF-8, being unstable towards phosphate buffer and the dehalogenation reaction conditions. The preliminary results for BioHOF-1 were promising, with both enzyme biocomposites maintaining high levels of activity, and enzyme stability. BioHOF-1 was capable of protecting the enzymes to denaturing conditions including thermal treatment (dehalogenase) and organic solvents (lipase). Additionally, both biocomposites could be recycled five times without a significant reduction in activity.

Chapter 1.

Introduction

Chapter 1: Introduction

1.1 Biocatalysis Overview

Biocatalysis is a diverse field of research that utilises biological systems to increase the rate of complex chemical reactions. Protein catalysts, known as enzymes, are responsible for mediating a wide variety of chemical transformations in nature, operating with high specificity and catalytic activity.[1-2] More specifically, biocatalysis refers to the study of these naturally occurring reactions, with the goal of extending their application into new settings beyond the cell.[3] Early examples of biocatalysis involved the use of whole-cell systems, such as fermentation in yeast cells, which utilise the molecular components of the cells for cascading, multi-enzyme reaction pathways.[4] As such, whole-cell catalysis is a cost-effective technique, which minimises the need for the extraction and purification of enzymes and cofactors, allowing for both the synthesis and metabolism of complicated molecules.[5-6] However, due to the intricate nature of whole-cell systems there are inherent challenges in maintaining cell viability and control over the reaction selectivity which complicates product extraction and waste separation steps.[6]

Alternatively, enzymes can be isolated from these systems and applied as crude or purified cell extracts, essentially uncoupling the cell growth phase from enzyme catalysis. Enzyme purification simplifies the investigation of biological transformations in several ways; by reducing the number of enzyme catalysts and unwanted side reactions, and allowing for the step-wise assessment of complicated processes.[6] Additionally, utilising pure enzymes enables the selective screening of potential substrate compounds which can provide insight into the structural and functional properties of each enzyme. Novel substrates can be screened, to understand an enzyme's natural function, potentially expand its application to compounds beyond their biological targets.[7] With this understanding, the complexity of the biocatalytic system can be systematically increased by introducing complementary enzymes that mediate controlled, multi-step reactions or those that act on toxic by-products.[8-10] For example, enzymes that break down hydrogen peroxide (H_2O_2) can be a useful addition to reactions that generate H_2O_2 as by-product, thus extending the life of the primary enzyme.[11-12]

1.2. Structure-Function Relationship

One of the advantages of using enzymes over standard chemical catalysts revolves around their highly selective nature where they can distinguish between substrates of similar functionality and structure.[1-2] Enzymes are able to catalyse a broad range of reactions under mild conditions. In comparison, chemical catalysts often require harsher reaction conditions to afford similar activity and selectivity, including elevated temperature and pressure, making enzymes a more environmentally friendly alternative to chemical catalysts.[12-13] As such, enzyme usage has become more commonplace in industry,[14-16] and include applications in the production of biofuels,[17-18] and pharmaceuticals,[19-20] as well as in food technology,[21-22] and the textile industry.[23]

The activity and selectivity of enzymes is closely tied to their complex structure, which dictates substrate accessibility and the chemistry of the reactions they can catalyse.[1, 24] Protein structure can be broken down into four basic levels of classification; primary through to quaternary, which describes the biomacromolecule from its amino acid sequence to its three-dimensional fold, including subunit interactions **(Figure 1.1).** Enzyme catalysis is dependent on the chemistry of the catalytic residues in the active site and is tightly controlled in terms of activity and specificity by the spatial arrangement of surrounding amino acid residues.[13]

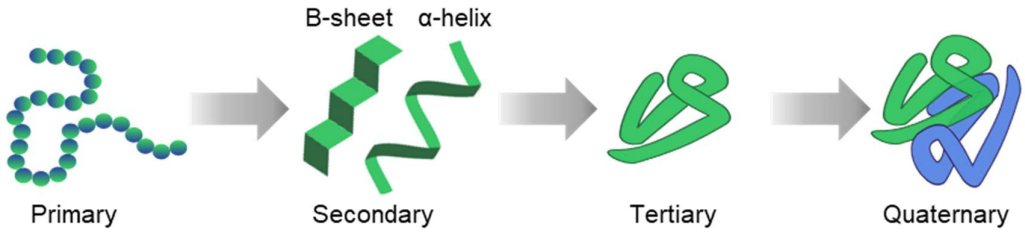

Figure 1.1: Schematic of the four protein structural levels in order of increasing complexity. The primary structure refers to the amino acid (polypeptide) sequence which can fold through hydrogen bonding interactions of the chain backbone to yield secondary structure motifs of α-helices and β-sheets. Amino acid side chain interactions (hydrophobic, hydrogen bonding, ionic and covalent [disulphide]) lead to the overall folded, tertiary structure of the protein. Multiple subunits can interact to form the functional, quaternary structure of the protein.

Enzymes are categorised by an enzyme commission number (EC) into four different levels of classification, dependant on the reactions they catalyse and the substrates they utilise.[25] The first level classifies enzymes by their general reaction type (**Table 1.1**), however there is significant diversity within each sub-class in terms of reaction mechanism and substrate targets. For example, both *Candida antarctica* lipase B (EC.3.1.1.3) and the LinB dehalogenase (E.3.8.1.5) described in **Chapters 4, 5, & 6**, are classified as hydrolases despite significant differences in substrate recognition and active site mechanisms.[25]

Table 1.1: Top level Enzyme Commission (EC) number for enzyme classification.[25]

Class	Reaction
1. Oxidoreductase	Hydrogen, oxygen or electron transfer
2. Transferase	Functional group transfer
3. Hydrolase	Hydrolytic bond cleavage
4. Lyase	Non-hydrolytic cleavage (addition or elimination)
5. Isomerase	Re-arrangement between isomers
6. Ligase	Bond formation between molecules (ATP dependant)
7. Translocase	Movement of ions across membranes

The diversity of reactions that encompasses the lower level EC classifications can be attributed to the complexity of the protein folding, and thus the accessibility, binding affinity and orientation of substrates within the active site. Pathways that connect the exterior surface of the protein to the active site can discriminate between potential substrates based on size, and their general interactions with amino acids.[26-27] Additionally, residues within the active site provide further control through positioning, and alignment of the target molecule towards the catalytic constituents. [28-29] The complexity of these interactions allow for enzymes to distinguish between structurally similar compounds, reacting in a chemo-, regio- and enantio-selective manner. Active site residues also play key roles in proton abstraction/donation, nucleophilic bond formation, intermediate stabilisation, radical formation and substrate/co-factor bond activation.[29] Sequence homology to known enzymes can be used to predict function and substrate range, however minor variations in active site residues can alter the recognition of target compounds.[3, 30] Binding and activity screening, in combination with structure based crystallographic studies, can provide insight into the binding interactions of substrates. With an understanding of the mechanism of binding, amino acid residues can be directly targeted for

protein engineering, where specific amino acids can be changed to create enzyme mutants with novel binding and function.[31-32] The industrial application of enzymes can benefit from these protein engineering strategies, enabling the development of a diverse range of biocatalysts. Through the rational design of enzymes, substrate ranges can be altered to target more industrially relevant compounds, and has the potential to enhance activity, selectivity, and stability.[26]

1.3. Stability

Despite the potential of enzymes for industrial biocatalysis, the feasibility of their application is often impeded by their inherently weak structural interactions (hydrogen bonding, hydrophobic interactions, van der Waals and salt bridges).[28, 33] To maintain the molecular integrity of the enzyme, stringent control of environmental conditions is required, often restricting biocatalysis to aqueous media, mild temperatures and narrow pH ranges. Enzyme structure is held together by a fine balance of entropic (protein folding and water loss) and enthalpic (hydrogen bond formation) contributions that can be easily perturbed by minimal energy input (10 $kJ.mol^{-1}$).[28,34] Disruptions to bonding forces by physical, chemical and biological denaturing agents (**Table 1.2**) can lead to protein unfolding that results in either enzyme denaturation or inactivation and thus loss of function.[33] Polypeptide unfolding (denaturation) can be reversed upon removal of the denaturing agent allowing for the protein to refold, however excessive loss of structure or the formation of polypeptide aggregates can cause an irreversible loss of function (inactivation).[35]

Table 1.2: Denaturing agents and the structural interactions they target (adapted from Iyer *et. al.,*2008).[33]

Chemical	**Target**
Acid/Base	Charged amino acids
Organic solvent	Hydrophobic interactions, solvation
Surfactant	Hydrophobic and/or charged amino acids
Physical	
Heat/Cold	Hydrogen bonds, hydrophobic bonding, protein solvation
Radiation	Disulphide and peptide bonds
Force	Protein solvation and void space
Biological	
Protease	Peptide bonds

1.3.1. Organic Solvent

The solvent utilised for biocatalysis can have a significant influence on the rate, and selectively of the reaction, impacting both substrate solubility and the structure of the enzyme. To achieve maximum catalytic activity, the substrate and product compounds need to be soluble in the conditions that the enzyme is most active. Since the majority of these reactions require aqueous media there is an inherent limitation to the substrate range. Organic solvents can be included to increase substrate solubility and reduce competing side reactions, however, in their native form enzymes are susceptible to solvent effects and often show significantly reduced catalytic activity as the concentration of organic solvent is increased.[33, 36-37] Water plays a fundamental role in preserving the intermolecular interactions that are essential to both protein folding and structural flexibility.[38] Organic solvents can disrupt these interactions by multiple mechanisms that include the stripping of key water molecules from within the protein structure, or direct contact/binding of solvent molecules.[37, 39] These processes induce polarity changes within the protein that can initiate unfolding and aggregation. It is often desirable to lower the water content of the reaction, to increase product formation and supress water dependant degradation (e.g. hydrolysis). For example, lipase enzymes can mediate competitive hydrolytic and esterification reactions, requiring finely tuned reaction conditions to maximise the desired product formation.[39] Consequently, the solvent composition can have a significant impact on the equilibrium of the enzymatic reaction through substrate solubility constraints and solvent induced structural variation of the enzyme.

1.3.2. Temperature

The rate of enzymatic catalysis is dependent on protein structural dynamics, and thus is influenced by the temperature and duration of the reaction. Increasing the temperature can enhance the enzyme's movement, accelerating the rate of catalysis up to an 'optimum temperature' that is specific to the enzyme. Enzymes can reversibly transition into unfavourable conformations that prelude irreversible structural changes, aggregation and permanent loss of activity.[35, 40-41] Maintaining temperatures near this apparent optimum can reduce the longevity of the catalyst by shifting the equilibrium of the enzyme into the inactive conformation, thus increasing the probability of permanent deactivation.[35, 40-41] As such, even at ambient temperatures, enzymes are generally not stable to extended storage or catalytic conditions, and would require frequent replacement.[42]

1.4. Stabilisation Strategies

The development of new technologies that promote enzyme stability in non-biological conditions is required to maximise the productivity and longevity of enzymes for industrial catalysis.[43] There are micro-organisms, known collectively as extremophiles, that are naturally more stable to the temperatures, solvents, substrate/product concentrations and pressures of industrial catalysis.[44-46] Activity of the enzymes within these organisms is maintained in extreme conditions by the unique spatial arrangement of the protein and tight structural interactions that are more resistant to modification and conformational change.[47-48] Incorporating similar structural restraints to enzymes from non-extremophiles (mesophiles) has the potential to enhance their stability towards the desired reaction conditions.

In their native form enzymes act as homogeneous catalysts and require separation from the reaction mixture using processes that are often challenging, expensive and denaturing to the protein structure.[49-51] One means to do so, is to attach the protein to an inert support, in a technique known as enzyme immobilisation, where enzymes can be anchored to a surface, thereby restraining enzyme movement and protecting key residues from alteration. Immobilisation transforms enzymes into a heterogeneous form, thus providing an alternate method of separation to maximise their reusability.[43, 52] As such, immobilisation strategies can afford enzyme composites that are more tolerant of harsh environments, whilst increasing their overall longevity. Methods of immobilisation that are utilised in both a research and industrial setting include enzyme cross-linking, covalent attachment/adsorption, and encapsulation/entrapment within biological or synthetic materials (**Figure 1.2**).[43, 53-54]

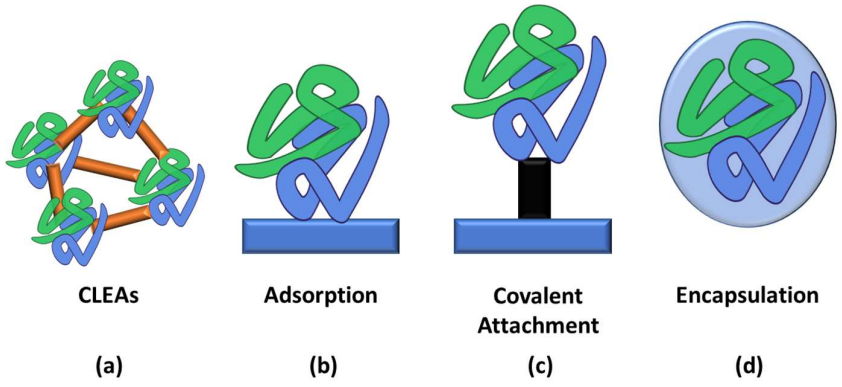

Figure 1.2. Schematic of the four general processes of enzyme immobilisation. (a) Enzyme cross-linking (cross-linked enzyme aggregates, CLEA), (b-c) physical adsorption and covalent attachment onto a solid support, and (d) encapsulation/entrapment into biological or synthetic material.

1.5. Immobilisation

1.5.1. General Considerations

The primary goal of immobilisation is to stabilise enzymes in their active conformations, however, the properties of the support can lead to enzyme biocomposites of differing activity and stability.[55] Careful consideration of the support material, the immobilisation method, and the final application, is therefore necessary when developing immobilised enzymes for use in challenging conditions. The chemical and physical properties of the support will play a pivotal role in the orientation, conformation and microenvironment (local solvent and substrate concentration) of the enzyme, which can influence substrate accessibility and binding.[55] Immobilisation conditions including solvent choice, temperature, pH, and reagents need to be compatible to ensure the enzyme maintains its active structure during the immobilisation process and catalysis. As mentioned previously, enzymes require some structural movement for activity so there must be a compromise made between enzyme flexibility and stabilisation. Too much freedom may insufficiently protect the enzyme, whereas high levels of order may prevent the movement required for activity. Hence, an enzyme's activity will likely differ at the solid-liquid interface, in comparison to homogenous catalysis in aqueous media, and careful consideration of the enzyme-support interactions is necessary.

1.5.2. Cross-linked Enzyme Aggregates (CLEAs)

One stabilisation method that does not require an external support material is that of cross-linked enzymes aggregates (CLEAs). This process involves the addition of precipitating agents (salts, solvent, non-ionic polymers) to an enzyme solution, that leads to the formation of insoluble, but active conformation enzyme clusters.[56-57] The interactions holding the enzyme molecules together are reversible, i.e. the enzyme can easily be resolubilised, and thus an addition of bi-functional cross-linking reagents, such as glutaraldehyde, is required to maintain integrity of the enzyme aggregates.[58-59] This process yields a catalyst with a high enzyme loading, circumventing the need for expensive support materials. However, difficulties arise during formation, where polydisperse materials can form due to poor control over the aggregation and cross-linking processes.[60-61] This can impact the material in several ways; the overall stability of the enzyme material, the ease in which the CLEAs can be separated and recycled, as well as the mass transfer of substrates to the internal surfaces of the aggregate.[62] Additionally, CLEAs have been reported to not retain enzyme activity over long periods of storage which limits their reusability and reduces their applicability.

1.5.3. Adsorption

A simple approach for immobilisation is enzyme adsorption onto a support material. Enzyme adherence typically occurs through reversible interactions that minimise perturbation to the enzyme structure including, van der Waals, ionic, and hydrogen bonding.[63] Electrostatic enzyme-support interactions are inherently weak, meaning that in aqueous solutions there is a high chance for enzyme leaching. This method is therefore best suited for catalysis in organic solvents where low enzyme solubility disfavours its separation from the support.[54] As the enzyme is not a fundamental component of the support structure, if enzyme inactivation were to occur, the support can be easily cleared and regenerated via adsorption of fresh catalyst. In many cases, this process can be applied directly to the native enzyme without any modification steps, however the mode of adsorption will be enzyme dependent and determined by the exterior surface chemistry of the protein.[43, 54] For example, lipase enzymes tend to have large areas of exposed lipophilic regions, and thus can be paired with a hydrophobic material such as octyl-agarose or polypropylene. [64-65] These support materials can sometimes lead to 'hyper-activation' of lipases, where the immobilisation process induces conformational changes that favour substrate accessibility and enzymatic activity.[66-67] In general, lipases possess an active site 'lid' that restricts access of substrate compounds in aqueous solutions, and requires a hydrophobic interface, such as an immobilisation support, to transform the enzyme into an active or 'open' conformation.[65, 68] Whilst this in an interesting phenomena for lipases, conformational changes that result in a loss of secondary structure are prominent for many enzymes immobilised on hydrophobic supports.[69-70] It has been postulated that these structural changes expose internal hydrophobic residues of the protein, which may lead to tighter binding to the support and/or structure dependent deactivation.[71]

An alternative would be to use hydrophilic surfaces (e.g. celite, cellulose), however these interactions are often reported to be weaker than hydrophobic supports, due to the different conformational changes induced.[69, 72] A benefit of hydrophilic support materials is that their increased affinity for water can favour the fundamental solvent enzyme interactions that assist in maintaining structural integrity in bulk non-aqueous solutions.[54-55] Chemical modification of the support or the enzyme can be used to increase the affinity of the binding, or to stabilise and align the enzyme in the active form.[63] This can include the incorporation of branched polymers to increase the number of binding interactions,[73-74] and sugar moieties to mimic solvent interactions.[55, 75] Enzyme-support interactions can also be made stronger and more permanent via covalent bond formation which is an alternative to physical adsorption.

1.5.4. Covalent Attachment

Covalent attachment generally relies on the availability of reactive residues (lysine; NH_3, aspartate and glutamate; COOH, cysteine; SH) or other functional groups (sugars) that can be covalently bound to the support via a linking reagent. Covalent attachment strengthens the enzyme support interactions compared to adsorption, reducing the risk of enzyme leaching that is prominent in aqueous solutions.[55] Additionally, the presence of multiple reactive sites on an enzymes surface can allow for multi-point attachment to the support, to increase its rigidity and the strength of interaction. The binding is often non-specific and the abundance of reactive residues (lysine, aspartate, glutamate) and can lead to multiple orientations, binding affinities and structural flexibility of the enzyme.[55, 76] For enzymes where uniform alignment is required for active site access, site-directed attachment can sometimes be achieved by targeting uncommon surface amino acids such as cysteine. Enzyme engineering techniques to include and remove surface exposed cysteines can afford greater control over the orientation of the enzyme which can significantly improve enzymatic activity.[77-78] For example, incorporation of cysteine residues into the sequence of a dehalogenase enzyme (LinB), controlled the orientation of the enzyme on a functionalised glass support.[79] Greater activity was reported for controlled covalent attachment technique (42%), relative to non-specific adsorption (0%), highlighting the impact of orientation and spacing of the enzyme on the support.[79]

1.5.5. Entrapment and Encapsulation

Attachment to the external surface of a solid support, would exhibit the greatest stabilisation at regions closest to the site of attachment. Unfortunately, immobilisation in this manner still means that regions of the protein remain exposed to the environment and would be susceptible to physical, chemical, and biological denaturing agents. Entrapment methods are designed to completely surround the enzyme, providing additional stabilising interactions and creating a microenvironment that is compatible with the enzyme in terms of solvation, hydrophobicity/hydrophilicity, and pH. Early encapsulation methods typically involved the use of polymer matrices, capsules (polymersomes) and inverse micelles, however these materials are often affected by slow substrate diffusion caused by low structural order of the material or poor membrane permeability.[80-82] Materials that are intrinsically porous, can overcome substrate diffusion restraints by providing access pathways to the encapsulated enzyme. Enzymes can be immobilised into porous materials via two general processes: infiltration and *in situ* encapsulation/entrapment. Infiltration involves the adsorption of enzymes into the pores

of pre-synthesised materials, for example mesoporous silicas, and requires careful matching of the pore size to the enzyme to maximise loading and minimise leaching.[83-84] Alternatively, the porous material can be synthesised around the enzyme, (e.g. hydrogels and sol-gels) which can prevent enzyme leaching through entrapment,[80, 85] however the synthetic conditions (solvents, reagents, and timeframe) create additional challenges in preventing enzyme denaturation.[86]

1.6. Metal-organic Frameworks

Metal-organic frameworks are a class of network solids composed of metal nodes and organic linkers that self-assemble into an extended crystalline network (**Figure 1.3**).[87-88] These materials can be tailored through the modular synthesis and selection of the inorganic and organic building blocks which give rise to a diverse range of chemical and physical properties. MOFs are widely known for their crystallinity, high internal surface areas, and tuneable porosity and chemical functionality. Collectively, these properties have led to the exploration of MOFs for application to areas including gas storage/separation,[89-91] catalysis,[92] and more recently biomacromolecule immobilisation.[51, 93]

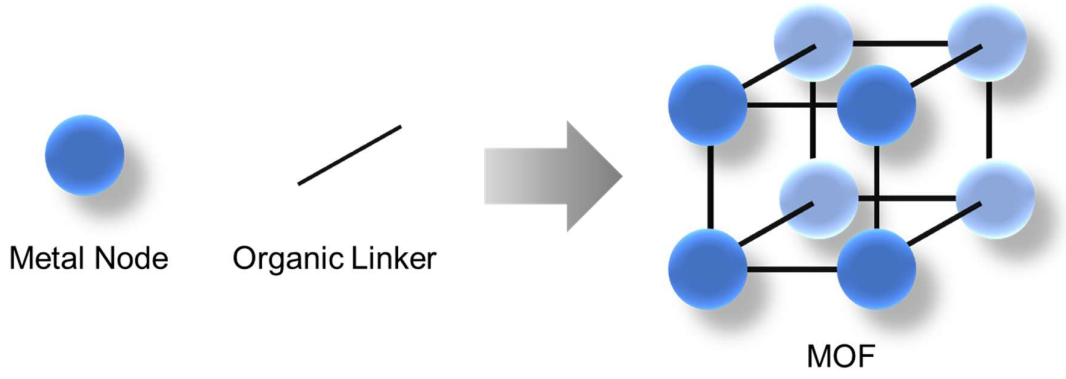

Figure 1.3: Metal-organic frameworks (MOFs) form from the self-assembly of metal nodes (blue sphere) and organic linkers (black rod) to form an extended, crystalline network.

The modular nature of the MOF synthesis means that the framework chemistry itself can be tuned to facilitate the immobilisation of enzymes via three general strategies a). Bio-conjugation (adsorption/covalent attachment), b) Infiltration, and c) Encapsulation (**Figure 1.4)**. Bio-conjugation via adsorption or covalent attachment methods give rise to similar challenges to other porous supports i.e. leaching, conformational changes, and environmental exposure. Nevertheless, the vast range of chemically and functionally different frameworks has led to the development of an extensive library of biocomposites (**Table 1.3**).

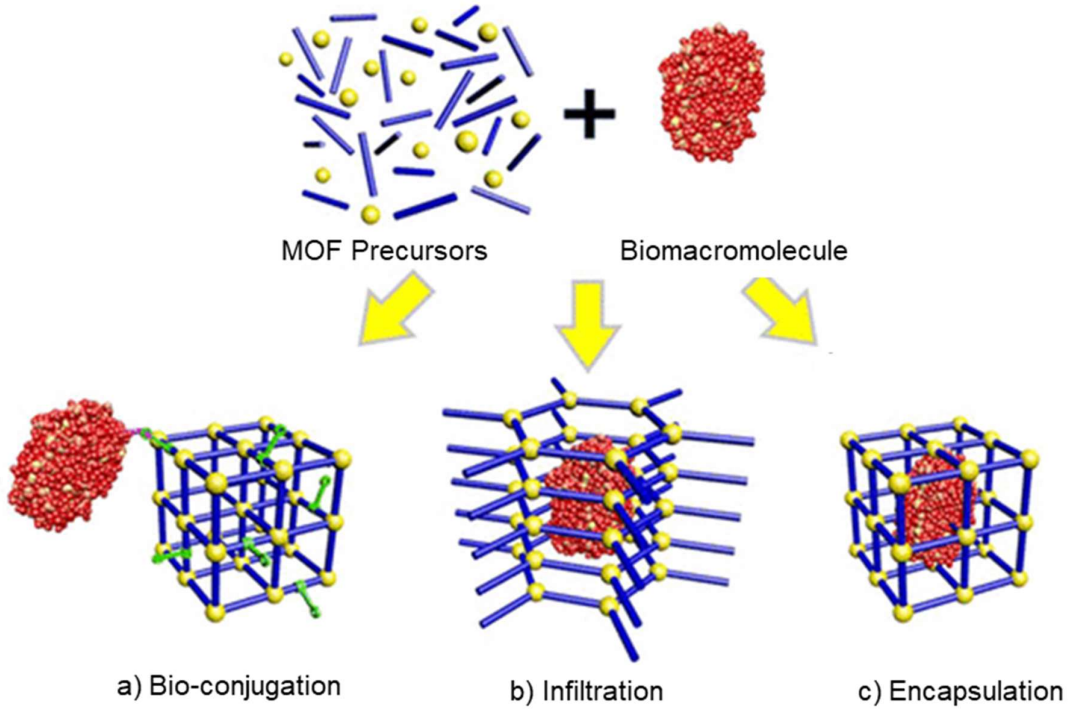

Figure 1.4: Schematic representation of enzyme immobilisation with MOFs; bio-conjugation, infiltration and encapsulation. Figure adapted from Doonan *et. al*.[93]

Table 1.3: Examples of enzyme adsorption and covalent attachment to MOFs.

Enzyme	MOF	Method	Application	Ref.
GDH	ZIF-7, ZIF-67, ZIF-68, ZIF-70,	Adsorption	Sensing	[94]
GOx	MIL-100-Fe	Adsorption	Sensing	[95]
Trypsin	CYCU-4, UiO66(Zr), ZIF-8	Adsorption	Immobilisation	[96-98]
Lipase	UiO68(Zr), NH_2-UiO66(Zr), MIL53 (Al), HKUST-1	Adsorption	Catalysis	[99-100]
MP-11	$[Cu(BPDC)(DABCO)]_n$	Adsorption	Catalysis	[101]
Trypsin	NH_2-MIL88B (Cr)	Covalent	Proteomics	[102]
β-glucosidase	NH_2-MIL53	Covalent	Catalysis	[103]
GDH	ZIF	Covalent	Sensing	[94]
Lipase	NH_2-UiO66, IrMOF	Covalent	Catalysis	[104]

Abbreviations: GDH: glucose dehydrogenase, GOx: Glucose Oxidase, MP-11:Microperoxidase, ZIF: zeolitic imidazolate framework, MIL: Materials of Institut Lavoisier, UiO: University of Oslo, HKUST: Hong Kong University of Science and Technology, (BPDC)(DABCO):4'4 biphenyldicarboxylate, 1,4-diazabicyclo[2.2. 2]octane.

Infiltrating enzymes within the pores of MOFs provides the attributes of simple adsorption techniques with the advantages of an increased number of stabilising interactions, and greater coverage and control of the enzyme microenvironment (**Table 1.4**) MOFs, however, typically comprise of a microporous structure that is not large enough to post synthetically accommodate enzymes and as such, this methodology is limited to MOF materials that possess mesopores exceeding the size of the enzyme. The structural diversity of enzyme size and shape means that the infiltration method poses the challenges described in **Section 1.5.3**, to favour enzyme loading and reduce leaching.

Table 1.4: Examples of enzyme infiltration into MOFs.

Enzyme	MOF	Method	Application	Ref.
Cyt c	Tb-mesoMOF	Infiltration	Catalysis	[105]
HRP, GOx	PCN-888	Infiltration	Catalysis	[106]
HRP, Cyt c, MP-11	PCN-332,PCN-333	Infiltration	Catalysis	[107]
Lipase	HKUST-1	Infiltration	Catalysis	[99]
MP-11	Tb-mesoMOF, PCN-333	Infiltration	Catalysis, Sensing	[108-110]
Mb	IRMOF-74	Infiltration	Storage	[111]
Insulin	MOF-818	Infiltration	Storage	[112]

Abbreviations: Cyt c: cytochrome c, HRP: horseradish peroxidase, GOx: glucose oxidase, MP-11: microperoxidase, PCN: porous coordination network, Mb: myoglobin,

Alternatively, enzymes can be encapsulated within a microporous MOF material. Unlike the previously described methods (adsorption, covalent attachment, infiltration), encapsulation involves the MOF formation around the enzyme, via a 'one pot' approach, and thus requires biocompatible synthetic conditions.[51, 93, 113] Employing this strategy, enzymes larger than the average pore size of the MOF material can be encased within a microporous framework that prevents leaching of the enzyme, whilst retaining free substrate diffusion. The method of enzyme encapsulation within MOFs was first proposed in 2014, by Lyu *et. al.* where an enzyme (cytochrome c) was coated with a protective layer of PVP, and encapsulated within a MOF; Zeolitic Imidazolate Framework-8; ZIF-8.[114] In this work, the encapsulation process involved the co-precipitation of the framework in a methanolic solution, generating large cavities that are not present in the standard MOF preparation, within which the enzyme was contained. Presumably, the PVP coating offered the enzyme a degree of protection from the effects of the alcohol. The cytochrome c-ZIF-8 biocomposite demonstrated enhanced activity relative to the free enzyme, due to a combined effect of exposure to methanol and the metal source (Zn^{2+}) inducing conformational changes that exposed the catalytically active haem group.[114] Methanol, and many organic solvents can have deleterious effect on enzyme structure,[33, 36-37] and their addition is not desirable for enzyme co-precipitation/immobilisation. A preferred method of immobilisation would involve the use of water based synthetic protocols. These were first developed, also using the Zn^{2+} based Zeolitic Imidazolate Framework (ZIFs) materials.

1.6. Zeolitic Imidazolate Frameworks (ZIFs)

The two most commonly studied ZIF frameworks for protein encapsulation are ZIF-8 and ZIF-90, which form via the self-assembly of Zn^{2+} ions and imidazolate based linkers; 2-methyl-imidazole (2-mIM) and imidazole-2-carboxaldehyde respectively **(Figure 1.5)**.[115-116] Both of these frameworks can be synthesised under biocompatible conditions (in water and at room temperature) forming highly porous crystalline materials with large internal surface areas (Brunauer-Emmet-Teller, BET, surface area *ca.* 1200 $m^2.g^{-1}$).[117-119] These ZIF frameworks display negligible cytotoxicity and are stable to elevated temperatures (~400 °C) and a wide range of organic solvents, making them an appropriate candidate for enzyme stabilisation.[115, 120-121] Additionally, they possess small crystallographic pore apertures (~3.4 Å) that would prevent enzyme leaching, but still enables diffusion of small substrate compounds. Furthermore, the ZIF-8 framework exhibits a degree of flexibility through linker rotation, that enables the diffusion of substrates larger than the pore aperture of the framework (~5 Å).[122-123]

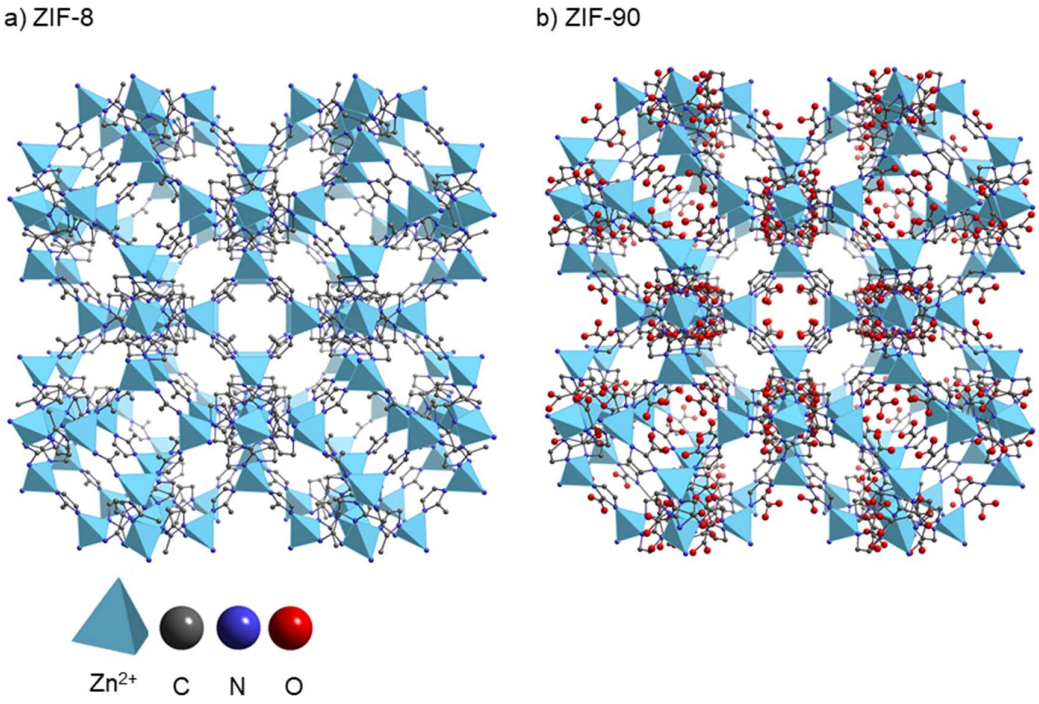

Figure 1.5: Representations of the crystal structures of (a) ZIF-8 and (b) ZIF-90 viewed along the b axis, showing the continuous network of these frameworks, with Zn^{2+}, C, N and O atoms represented by light blue polyhedral and grey, blue and red spheres respectively.

The aqueous co-precipitation of a protein within ZIF-90 was first described by Shieh *et.al.* in 2015.[124] This method involved the coating of catalase with polyvinyl pyrrolidone (PVP), followed by the addition of ZIF-90 precursors (Zn^{2+} and ICA) to form a catalase-PVP-ZIF-90 composite. This biocomposite retained full activity after exposure to protease (a peptide cleaving enzyme), whilst complete denaturation and loss of activity was observed for the free enzyme. Due to the small pore size of the framework, the encapsulation process restricted protease access to catalase, whilst allowing for diffusion of the substrate compound (hydrogen peroxide). An alternate method was established in the same year by Liang *et. al.,* where ZIF-8 encapsulation of proteins and DNA was developed using aqueous conditions without additives or precipitating agents (**Figure 1.6**).[125] This method was distinguished from co-precipitation, by the observation via NMR, that biomolecules (proteins etc.) can concentrate Zn^{2+} at their surface and thus initiate the nucleation of ZIF-8.[125] This phenomenon was termed "biomimetic mineralisation" due to its similarity to natural self-assembly of exoskeletons around biological tissues (biomineralisation).[126] In addition to the protection from proteolytic enzymes, the ZIF-8 biocomposites were tested for their stability to organic solvent, and elevated temperature. The ZIF-8 framework demonstrated the protection of horseradish peroxidase (HRP) where conditions that inactivate the free enzyme, such as boiling water and boiling dimethylformamide (DMF, 150 °C), had minimal impact on the encapsulated enzyme.

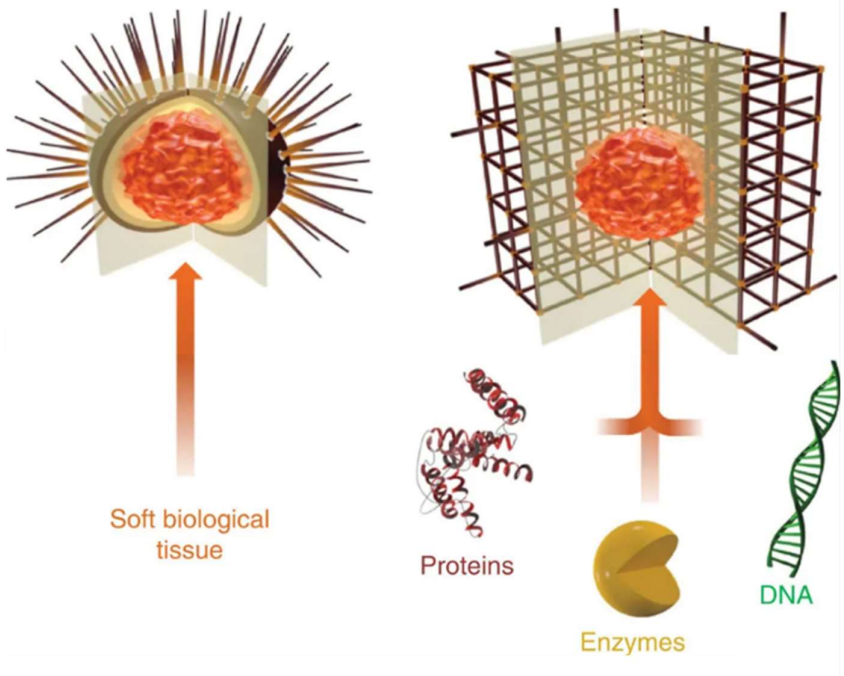

Figure 1.6: Schematic of the biomimetic mineralisation strategy. Adapted from Liang *et. al*.[125]

These studies by Shieh and Liang, highlighted the potential of ZIF materials for enzyme protection and instigated extensive research in this field. Over the past five years, efforts have been made to advance the field of bioencapsulation by creating novel biocomposites, testing the limits of the protective capacity, and understanding and developing the immobilisation process. As such, there is an extensive library of enzyme-ZIF literature, focussing on different aspects and application of these materials (**Table 1.5**).

Whilst there have been a large number of studies on enzyme-ZIF-8 biocomposites, there is also considerable diversity of the synthetic protocols utilised for biocomposite synthesis (ligand concentrations, additives, formation time). For example, different ZIF-8 synthetic procedures have yielded conflicting data for catalase, with both activity and enzyme deactivation being reported for the same enzyme and reaction.[127-132] A systematic characterisation of biocomposite synthesis (and sample handling) is therefore necessary to understand the mechanisms of ZIF-8 formation and its impact of enzymatic activity and stability. This thesis focusses on the screening and the development of protocols to synthesise consistent ZIF-8 biocomposites (henceforth referred to as protein@ZIF-8). This work aims to investigate the influence of the protein and MOF precursors on biocomposite formation to determine what impact the formation mechanism has on enzymatic activity. Additionally, it has been shown that the hydrophobicity of the ZIF-8 framework can impact the activity of some enzymes (catalase and urease).[129] Comparatively, the ZIF-90 framework, is significantly more hydrophilic than ZIF-8, as determined via water vapor adsorption studies, and influences enzyme activity differently.[133-134] Catalase was one enzyme that was reported to be impacted by hydrophobic interactions with ZIF-8 causing a loss in secondary structure of the enzyme (α-helix and β-sheets). The more hydrophilic ZIF-90 provided more favourable structural interactions, which resulted in activity retention. As such, in the work presented hereafter, both ZIF-8 and ZIF-90 biocomposites were tested in analogous activity studies.

Table 1.5: Examples enzyme encapsulation in ZIF-8 highlighting the novel findings.

Enzyme	Year	Comment	Ref
Cyt C, HRP, Lipase	**2014**	Enhanced activity upon immobilisation	[114]
HRP,(PQQ)GDH, Urease	**2015**	Stable to boiling water, DMF and proteolytic agents	[125]
GOx, HRP	**2015**	Two enzyme cascade reaction	[135]
GOx	**2015**	Polydopamine tethering of ZIF-8 crystals for better handling and recycling	[136]
GOx	**2016**	Combined with a molecular catalyst (hemin)	[137]
Lipase	**2016**	Mechanical grinding synthesis	[138]
Urease	**2016**	Biomimetic mineralisation/ co-precipitation comparison	[139]
Catalase	**2017**	Polyacrylamide coating prior to encapsulation	[128]
β-gal and *S. cerevisiae.*	**2017**	*S. cerevisiae* coated with β-gal and ZIF-8 for cell survival	[140]
β-gal, GOx, HRP	**2018**	Two and three enzyme cascade reaction	[141]
HRP, Lysozyme	**2018**	Enzymes@ZIF-8 on gold nanorods	[142]
Ace	**2018**	Recombinantly expressed enzyme tested	[143]
Lipase	**2018**	Thermostable, ultrasound stable	[142]
HRP, Urease, GOx	**2019**	Amino acid assisted ZIF-8 nucleation	[145]
Laccase	**2019**	Enhanced selectivity upon immobilisation	[146]
AChE	**2019**	Co-encapsulation with magnetic nanoparticles	[147]

Abbreviations: Cyt C: Cytochrome C, HRP: Horseradish Peroxidase, (PQQ)GDH: Pyrroloquinoline glucose dehydrogenase, GOx: Glucose oxidase, β-gal: β-galactosidase, S. cerevisiae: Saccharomyces cerevisiae, ACE: Acetyl esterase, AChE: acetylcholinesterase

1.7. Hydrogen-bonded Organic Frameworks (HOFs)

ZIFs are not ideal universal support materials for enzyme immobilisation as the synthetic conditions, enzyme-support interactions, and pore size can all contribute to reduced catalytic output caused by enzyme denaturation and inhibited substrate diffusion. Additionally, ZIFs are not stable to pH <6,[121] certain buffers,[131, 148-149] and metal chelating agents,[150] thus limiting their potential application. As such, our group has been continually investigating the development of novel porous materials, utilising protein friendly ligands for framework formation.

Recently, a hydrogen-bonded organic framework (HOF) made from tetra-amidinium and tetra-carboxylate building units was developed,[151-152] and later used for enzyme encapsulation.[153] Hereafter, this framework is termed BioHOF-1, named for its biocompatible synthesis and capacity to encapsulate and stabilise biomolecules. BioHOF-1 self assembles in water, taking advantage of non-covalent secondary interactions to yield a continuous crystalline solid (**Figure 1.7**). This framework has a larger pore aperture (~6.4 Å)[151-152] than the ZIF materials that have been previously investigated, and thus may be advantageous for applications that require diffusion of larger substrates. Within the pores of BioHOF-1, there are water molecules that assist in maintaining the structural integrity of the framework. Indeed, upon activation (desolvation under reduced pressure) this material is known to be non-porous to N_2 (77 K) due to the removal of these water molecules that caused a loss of long-range order (crystallinity). However, in solution phase experiments, fluorescein (7 Å) was shown to homogenously diffuse into the framework, confirming solution accessible porosity. Due to the retention of water within the pores, BioHOF-1 may favour enzyme stabilisation and activity. As described in **Section 1.5.3**, water may assist in maintaining enzyme structural integrity. Additionally, enzymes that require water as a cofactor for reactivity may benefit from immobilisation within BioHOF-1.

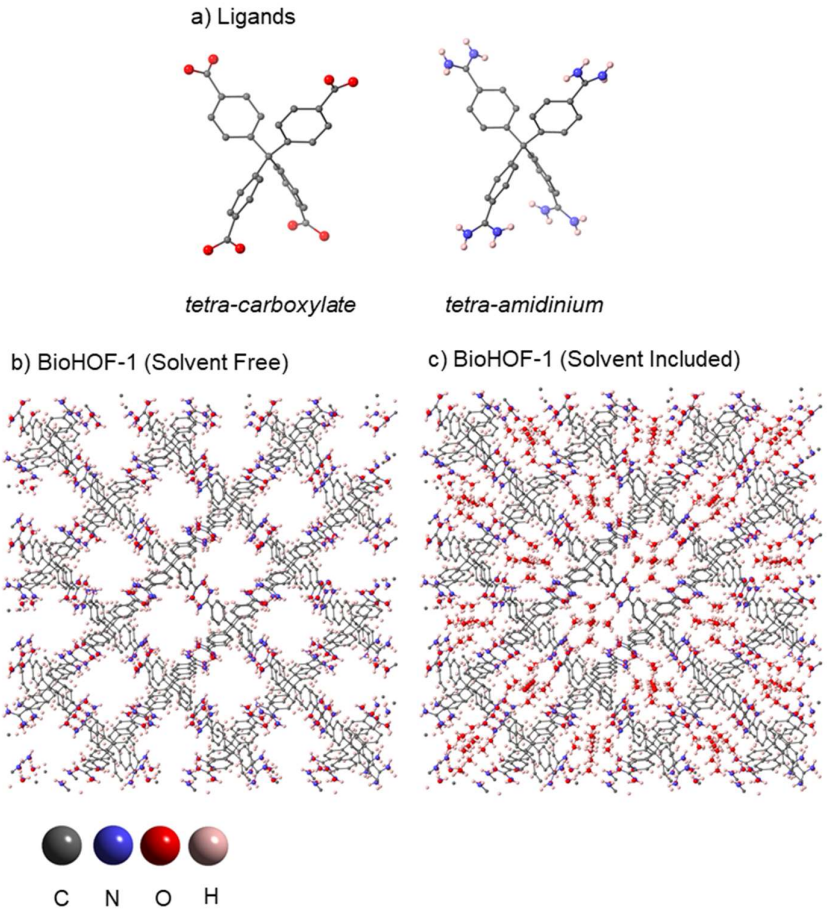

Figure 1.7: (a) Crystallographic representation of the tetra-carboxylate and tetra-amidinium ligands. (b-c) Representations of the crystal structures of BioHOF-1 showing the continuous network of this framework, with C, N and O atoms represented by grey, blue, red and pink spheres, respectively.(a) Solvent (water) molecules have been excluded to show porosity. (b) Structurally important water molecules included.

In the initial enzyme immobilisation study, catalase and alcohol oxidase enzymes were immobilised using BioHOF-1, which yielded biocomposites of high crystallinity, enzyme loading and framework stability.[153] A promising finding of this study was that BioHOF-1 was capable forming active biocomposites with enzymes, which, when immobilised within ZIF-8, were inactive. Additionally, in initial testing, BioHOF-1 has been proven to stabilise enzymes to denaturing conditions such as extreme pH (5-10), proteolytic agents (trypsin), thermal treatment (60 °C in water), and an unfolding agent (urea). As such, this thesis also describes an investigation into the formation, and resulting activity of novel enzyme@BioHOF-1 composites, broadening the scope of this burgeoning field of research.

1.8. Thesis Coverage

This thesis consists of five research chapters. **Chapter 3** has been published in a peer-reviewed international journal, whilst **Chapters 4**, is written in manuscript style and are intended to be submitted for peer-review. **Chapters 2, 5, and 6** are written as stand-alone thesis chapters. Each chapter contains their own introduction and experimental section. The statement of authorship can be found at the beginning of the appropriate chapters.

Chapter 1 introduces the field of biocatalysis, providing context for the immobilisation strategies utilised. Here, the challenges associated with enzyme catalysis are described, and the technologies currently employed to enhance enzyme stability are presented. Additionally, this chapter introduces the porous support materials that are the focus of this thesis, ZIF-8, ZIF-90 and BioHOF-1.

Chapter 2 describes the initial screening protocols that were tested to find a general immobilisation strategy for ZIF-8. Here it was established that synthetic conditions could be controlled to encapsulate a broad range of proteins which contributed to a peer reviewed publication.[154] This study developed the protocols that were used in later chapters.

Chapter 3 is a peer reviewed study and provides additional details into the screening of successful/unsuccessful proteins, investigating the impact of protein electrostatics on the immobilisation protocol.[155] Supporting computational studies, analysing the surface charge and isoelectric point of the protein, were used to predict this phenomenon and are detailed within this chapter alongside experimental studies. Methods to manipulate the biomineralisation process by surface functionalisation of the protein were presented.

Chapter 4 builds on the work of the previous chapters, with an extension to activity testing. A lipase enzyme was immobilised via the different protocols described in **Chapter 2**, and was used to test the impact of synthetic conditions on biocomposite activity and stability.

Chapters 5 and 6 introduced new frameworks (ZIF-90 and BioHOF-1) to test impact of new frameworks on the activity/stability of the lipase and a dehalogenase enzyme. In **Chapter 6,** the dehalogenase enzyme was recombinantly expressed and purified prior to immobilisation and testing of its activity and thermal stability.

Chapter 7 provides a summary of the research goals that were achieved in the previous chapters and discusses the potential directions in which the research can progress.

1.9. References

1. Benkovic, S. J.; Hammes-Schiffer, S., A perspective on enzyme catalysis. *Science* **2003,** *301* (5637), 1196-1202.

2. van Dongen, S. F. M.; Elemans, J. A. A. W.; Rowan, A. E.; Nolte, R. J. M., Processive catalysis. *Angew. Chem. Int. Ed.* **2014,** *53* (43), 11420-11428.

3. Bornscheuer, U. T.; Huisman, G. W.; Kazlauskas, R. J.; Lutz, S.; Moore, J. C.; Robins, K., Engineering the third wave of biocatalysis. *Nature* **2012,** *485* (7397), 185-194.

4. Hughes, G.; Lewis, J. C., Introduction: Biocatalysis in industry. *Chem.Rev* **2018,** *118* (1), 1-3.

5. Tufvesson, P.; Lima-Ramos, J.; Nordblad, M.; Woodley, J. M., Guidelines and cost analysis for catalyst production in biocatalytic processes. *Org. Process Rev. Dev* **2011,** *15* (1), 266-274.

6. Wachtmeister, J.; Rother, D., Recent advances in whole cell biocatalysis techniques bridging from investigative to industrial scale. *Curr. Opin. Biotech.* **2016,** *42*, 169-177.

7. Kuznetsova, E.; Proudfoot, M.; Sanders, S. A.; Reinking, J.; Savchenko, A.; Arrowsmith, C. H.; Edwards, A. M.; Yakunin, A. F., Enzyme genomics: Application of general enzymatic screens to discover new enzymes. *FEMS. Microbiol. Rev* **2005,** *29* (2), 263-279.

8. Hold, C.; Billerbeck, S.; Panke, S., Forward design of a complex enzyme cascade reaction. *Nat. Commun.* **2016,** *7* (1), 12971.

9. Dudley, Q. M.; Karim, A. S.; Jewett, M. C., Cell-free metabolic engineering: Biomanufacturing beyond the cell. *Biotech.* **2015,** *10* (1), 69-82.

10. Schoffelen, S.; van Hest, J. C. M., Multi-enzyme systems: bringing enzymes together in vitro. *Soft Matter.* **2012,** *8* (6), 1736-1746.

11. Rocha-Martin, J.; Acosta, A.; Guisan, J. M.; López-Gallego, F., Immobilizing systems biocatalysis for the selective oxidation of glycerol coupled to in situ cofactor recycling and hydrogen peroxide elimination. *ChemCatChem.* **2015,** *7* (13), 1939-1947.

12. Fessner, W.-D., How to meet the need for speed in protein evolution. *Nat. Catal.* **2019,** *2* (9), 738-739.

13. Sheldon, R. A.; Woodley, J. M., Role of biocatalysis in sustainable chemistry. *Chem.Rev.* **2018,** *118* (2), 801-838.

14. Kirk, O.; Borchert, T. V.; Fuglsang, C. C., Industrial enzyme applications. *Curr. Opin. Biotech.* **2002,** *13* (4), 345-351.

15. Beilen, J. B. v.; Li, Z., Enzyme technology: an overview. *Curr. Opin. Biotech.* **2002,** *13* (4), 338-344.

16. Schmid, A.; Dordick, J. S.; Hauer, B.; Kiener, A.; Wubbolts, M.; Witholt, B., Industrial biocatalysis today and tomorrow. *Nature* **2001,** *409* (6817), 258-268.

17. Yeoman, C. J.; Han, Y.; Dodd, D.; Schroeder, C. M.; Mackie, R. I.; Cann, I. K. O., Thermostable enzymes as biocatalysts in the biofuel industry. *Adv. Appl. Microbiol.* **2010,** *70*, 1-55.

18. Horn, S. J.; Vaaje-Kolstad, G.; Westereng, B.; Eijsink, V., Novel enzymes for the degradation of cellulose. *Biotechnol. Biofuels* **2012,** *5* (1), 45.

19. Savile, C. K.; Janey, J. M.; Mundorff, E. C.; Moore, J. C.; Tam, S.; Jarvis, W. R.; Colbeck, J. C.; Krebber, A.; Fleitz, F. J.; Brands, J.; Devine, P. N.; Huisman, G. W.; Hughes, G. J., Biocatalytic asymmetric synthesis of chiral amines from ketones applied to sitagliptin manufacture. *Science* **2010,** *329* (5989), 305.

20. Pollard, D. J.; Woodley, J. M., Biocatalysis for pharmaceutical intermediates: the future is now. *Trends Biotechnol.* **2007,** *25* (2), 66-73.

21. Couto, S. R.; Sanromán, M. A., Application of solid-state fermentation to food industry-A review. *J. Food. Eng.* **2006,** *76* (3), 291-302.

22. Gibbs, B. F.; Kermasha, S.; Alli, I.; Mulligan, C. N., Encapsulation in the food industry: a review. *Int. J. Food. Sci. Nutr.* **1999,** *50* (3), 213-224.

23. Soares, J. C.; Moreira, P. R.; Queiroga, A. C.; Morgado, J.; Malcata, F. X.; Pintado, M. E., Application of immobilized enzyme technologies for the textile industry: a review. *Biocatal. Biotransform.* **2011,** *29* (6), 223-237.

24. Fersht, A., *Structure and Mechanism in Protein Science: A Guide to Enzyme Catalysis and Protein Folding* W. H. Freeman and Company: London, **1999**.

25. IUPAC-IUBMB Joint commission on biochemical nomenclature (jcbn) and nomenclature committee of IUBMB (NC-IUBMB). *Eur. J. Biochem.* **1999,** *264* (2), 607-609.

26. Kokkonen, P.; Bednar, D.; Pinto, G.; Prokop, Z.; Damborsky, J., Engineering enzyme access tunnels. *Biotechnol. Adv.* **2019,** *37* (6), 107386.

27. Kingsley, L. J.; Lill, M. A., Substrate tunnels in enzymes: structure-function relationships and computational methodology. *Proteins* **2015,** *83* (4), 599-611.

28. Scharnagl, C.; Reif, M.; Friedrich, J., Stability of proteins: Temperature, pressure and the role of the solvent. *Biochim. Biophys. Acta, Proteins Proteomics* **2005,** *1749* (2), 187-213.

29. Bartlett, G. J.; Porter, C. T.; Borkakoti, N.; Thornton, J. M., Analysis of catalytic residues in enzyme active sites. *J. Mol. Biol.* **2002,** *324* (1), 105-121.

30. Höhne, M.; Schätzle, S.; Jochens, H.; Robins, K.; Bornscheuer, U. T., Rational assignment of key motifs for function guides in silico enzyme identification. *Nat. Chem. Biol.* **2010,** *6* (11), 807-813.

31. Kazlauskas, R. J.; Bornscheuer, U. T., Finding better protein engineering strategies. *Nat. Chem. Biol.* **2009,** *5* (8), 526-529.

32. Turner, N. J., Directed evolution drives the next generation of biocatalysts. *Nat. Chem. Biol.* **2009,** *5* (8), 567-573.

33. Iyer, P. V.; Ananthanarayan, L., Enzyme stability and stabilization—Aqueous and non-aqueous environment. *Process. Biochem.* **2008,** *43* (10), 1019-1032.

34. Chapman, R.; Stenzel, M. H., All wrapped up: Stabilization of enzymes within single enzyme nanoparticles. *J. Am. Chem. Soc.* **2019,** *141* (7), 2754-2769.

35. Peterson, M. E.; Daniel, R. M.; Danson, M. J.; Eisenthal, R., The dependence of enzyme activity on temperature: determination and validation of parameters. *Biochem. J.* **2007,** *402* (2), 331-337.

36. Klibanov, A. M., Improving enzymes by using them in organic solvents. *Nature* **2001,** *409* (6817), 241-246.

37. Serdakowski, A. L.; Dordick, J. S., Enzyme activation for organic solvents made easy. *Trends Biotechnol.* **2008,** *26* (1), 48-54.

38. Bizzarri, A. R.; Cannistraro, S., Molecular dynamics of water at the protein−solvent interface. *J. Phys. Chem. B* **2002,** *106* (26), 6617-6633.

39. Graber, M.; Irague, R.; Rosenfeld, E.; Lamare, S.; Franson, L.; Hult, K., Solvent as a competitive inhibitor for *Candida antarctica* lipase B. *Biochim. Biophys. Acta. Proteins Proteomics* **2007,** *1774* (8), 1052-1057.

40. Daniel, R. M.; Danson, M. J., Temperature and the catalytic activity of enzymes: A fresh understanding. *FEBS Letters* **2013,** *587* (17), 2738-2743.

41. Daniel, R. M.; Danson, M. J.; Eisenthal, R., The temperature optima of enzymes: a new perspective on an old phenomenon. *Trends Biochem. Sci.* **2001,** *26* (4), 223-225.

42. DiCosimo, R.; McAuliffe, J.; Poulose, A. J.; Bohlmann, G., Industrial use of immobilized enzymes. *Chem. Soc. Rev* **2013,** *42* (15), 6437-6474.

43. Mohamad, N. R.; Marzuki, N. H. C.; Buang, N. A.; Huyop, F.; Wahab, R. A., An overview of technologies for immobilization of enzymes and surface analysis techniques for immobilized enzymes. *Biotechnol. Biotechnol. Equip.* **2015,** *29* (2), 205-220.

44. Elleuche, S.; Schröder, C.; Sahm, K.; Antranikian, G., Extremozymes—biocatalysts with unique properties from extremophilic microorganisms. *Curr. Opin. Biotechnol.* **2014,** *29*, 116-123.

45. Adams, M. W. W.; Perler, F. B.; Kelly, R. M., Extremozymes: expanding the limits of biocatalysis. *Bio/Technology* **1995,** *13* (7), 662-668.

46. Bommarius, A. S.; Paye, M. F., Stabilizing biocatalysts. *Chem. Soc. Rev.* **2013,** *42* (15), 6534-6565.

47. Demirjian, D. C.; Morís-Varas, F.; Cassidy, C. S., Enzymes from extremophiles. *Curr. Opin. Biotech.* **2001,** *5* (2), 144-151.

48. D'Amico, S.; Marx, J.-C.; Gerday, C.; Feller, G., Activity-stability relationships in extremophilic enzymes. *J. Biol. Chem.* **2003,** *278* (10), 7891-7896.

49. Hartmann, M., Ordered mesoporous materials for bioadsorption and biocatalysis. *Chem. Mater.* **2005,** *17* (18), 4577-4593.

50. Hartmann, M.; Jung, D., Biocatalysis with enzymes immobilized on mesoporous hosts: the status quo and future trends. *J. Mater. Chem.* **2010,** *20* (5), 844-857.

51. Drout, R. J.; Robison, L.; Farha, O. K., Catalytic applications of enzymes encapsulated in metal–organic frameworks. *Coord. Chem. Rev.* **2019,** *381*, 151-160.

52. Garcia-Galan, C.; Berenguer-Murcia, Á.; Fernandez-Lafuente, R.; Rodrigues, R. C., Potential of different enzyme immobilization strategies to improve enzyme performance. *Adv. Synth. Catal.* **2011,** *353* (16), 2885-2904.

53. Homaei, A. A.; Sariri, R.; Vianello, F.; Stevanato, R., Enzyme immobilization: an update. *J. Chem. Biol.* **2013,** *6* (4), 185-205.

54. Hanefeld, U.; Gardossi, L.; Magner, E., Understanding enzyme immobilisation. *Chem. Soc. Rev.* **2009,** *38* (2), 453-468.

55. Hoarau, M.; Badieyan, S.; Marsh, E. N. G., Immobilized enzymes: understanding enzyme – surface interactions at the molecular level. *Org. Biomol. Chem.* **2017,** *15* (45), 9539-9551.

56. Sheldon, R. A., Cross-linked enzyme aggregates (CLEA®s): stable and recyclable biocatalysts. *Biochem. Soc. Trans.* **2007,** *35* (6), 1583-1587.

57. Sheldon, R. A., Characteristic features and biotechnological applications of cross-linked enzyme aggregates (CLEAs). *Apple. Microbiol. Biotechnol.* **2011,** *92* (3), 467-477.

58. Cao, L.; van Langen, L. M.; van Rantwijk, F.; Sheldon, R. A., Cross-linked aggregates of penicillin acylase: robust catalysts for the synthesis of β-lactam antibiotics. *J. Mol. Catal. B. Enzym.* **2001,** *11* (4), 665-670.

59. Cao, L.; van Rantwijk, F.; Sheldon, R. A., Cross-linked enzyme aggregates: a simple and effective method for the immobilization of penicillin acylase. *Org. Lett.* **2000,** *2* (10), 1361-1364.

60. Roessl, U.; Nahálka, J.; Nidetzky, B., Carrier-free immobilized enzymes for biocatalysis. *Biotechnol. Lett.* **2010,** *32* (3), 341-350.

61. Velasco-Lozano, S.; López-Gallego, F.; Mateos-Díaz Juan, C.; Favela-Torres, E., Cross-linked enzyme aggregates (CLEA) in enzyme improvement – a review. In *Biocatalysis*, 2016; Vol. 1, p 166.

62. Cui, J. D.; Jia, S. R., Optimization protocols and improved strategies of cross-linked enzyme aggregates technology: current development and future challenges. *Crit. Rev. Biotechnol.* **2015,** *35* (1), 15-28.

63. Jesionowski, T.; Zdarta, J.; Krajewska, B., Enzyme immobilization by adsorption: a review. *Adsorption* **2014,** *20* (5), 801-821.

64. Mateo, C.; Palomo, J. M.; Fernandez-Lorente, G.; Guisan, J. M.; Fernandez-Lafuente, R., Improvement of enzyme activity, stability and selectivity via immobilization techniques. *Enzyme Microb. Technol.* **2007,** *40* (6), 1451-1463.

65. Persson, M.; Mladenoska, I.; Wehtje, E.; Adlercreutz, P., Preparation of lipases for use in organic solvents. *Enzyme Microb. Technol.* **2002,** *31* (6), 833-841.

66. Palomo, J. M.; Muñoz, G.; Fernández-Lorente, G.; Mateo, C.; Fernández-Lafuente, R.; Guisán, J. M., Interfacial adsorption of lipases on very hydrophobic support (octadecyl–Sepabeads): immobilization, hyperactivation and stabilization of the open form of lipases. *J. Mol. Catal. B. Enzym.* **2002,** *19-20*, 279-286.

67. Chen, Z.; Liu, L.; Yang, R., Improved performance of immobilized lipase by interfacial activation on Fe3O4@PVBC nanoparticles. *RSC Adv.* **2017,** *7* (56), 35169-35174.

68. Cabrera, Z.; Fernandez-Lorente, G.; Fernandez-Lafuente, R.; Palomo, J. M.; Guisan, J. M., Novozym 435 displays very different selectivity compared to lipase from *Candida antarctica* B adsorbed on other hydrophobic supports. *J. Mol. Catal. B. Enzym.* **2009,** *57* (1), 171-176.

69. Rabe, M.; Verdes, D.; Seeger, S., Understanding protein adsorption phenomena at solid surfaces. *Adv. Colloid. Interface Sci.* **2011,** *162* (1), 87-106.

70. Zoungrana, T.; Findenegg, G. H.; Norde, W., Structure, Stability, and Activity of Adsorbed Enzymes. *J. Colloid Interface Sci.* **1997,** *190* (2), 437-448.

71. Anand, G.; Sharma, S.; Dutta, A. K.; Kumar, S. K.; Belfort, G., Conformational transitions of adsorbed proteins on surfaces of varying polarity. *Langmuir* **2010,** *26* (13), 10803-10811.

72. Grimaldi, J.; Radhakrishna, M.; Kumar, S. K.; Belfort, G., Stability of proteins on hydrophilic surfaces. *Langmuir* **2015,** *31* (3), 1005-1010.

73. Wang, S.; Su, P.; Ding, F.; Yang, Y., Immobilization of cellulase on polyamidoamine dendrimer-grafted silica. *J. Mol. Catal. B. Enzym.* **2013,** *89*, 35-40.

74. Xiao, P.; Lv, X.; Deng, Y., Immobilization of chymotrypsin on silica beads based on high affinity and specificity aptamer and its applications. *Anal. Lett.* **2012,** *45* (10), 1264-1273.

75. Li, Y.; Zhang, X.; Myers, J.; Abbott, N. L.; Chen, Z., Room temperature freezing and orientational control of surface-immobilized peptides in air. *Chem. Commun.* **2015,** *51* (55), 11015-11018.

76. Duckworth, B. P.; Xu, J.; Taton, T. A.; Guo, A.; Distefano, M. D., Site-specific, covalent attachment of proteins to a solid surface. *Bioconj. Chem.* **2006,** *17* (4), 967-974.

77. Liu, Y.; Ogorzalek, T. L.; Yang, P.; Schroeder, M. M.; Marsh, E. N. G.; Chen, Z., Molecular orientation of enzymes attached to surfaces through defined chemical linkages at the solid–liquid interface. *J. Am. Chem. Soc.* **2013,** *135* (34), 12660-12669.

78. Spicer, C. D.; Pashuck, E. T.; Stevens, M. M., Achieving controlled biomolecule–biomaterial conjugation. *Chem. Rev.* **2018,** *118* (16), 7702-7743.

79. Badieyan, S.; Wang, Q.; Zou, X.; Li, Y.; Herron, M.; Abbott, N. L.; Chen, Z.; Marsh, E. N. G., Engineered surface-immobilized enzyme that retains high levels of catalytic activity in air. *J. Am. Chem. Soc.* **2017,** *139* (8), 2872-2875.

80. Lee, K. Y.; Yuk, S. H., Polymeric protein delivery systems. *Prog. Polym. Sci.* **2007,** *32* (7), 669-697.

81. Parthasarathy, R. V.; Martin, C. R., Synthesis of polymeric microcapsule arrays and their use for enzyme immobilization. *Nature* **1994,** *369* (6478), 298-301.

82. Pollak, A.; Blumenfeld, H.; Wax, M.; Baughn, R. L.; Whitesides, G. M., Enzyme immobilization by condensation copolymerization into crosslinked polyacrylamide gels. *J. Am. Chem. Soc.* **1980,** *102* (20), 6324-6336.

83. Ispas, C.; Sokolov, I.; Andreescu, S., Enzyme-functionalized mesoporous silica for bioanalytical applications. *Anal. Bioanal. Chem.* **2009,** *393* (2), 543-554.

84. Hudson, S.; Cooney, J.; Magner, E., Proteins in mesoporous silicates. *Angew. Chem. Int. Ed.* **2008,** *47* (45), 8582-8594.

85. Gill, I.; Ballesteros, A., Encapsulation of biologicals within silicate, siloxane, and hybrid sol−gel polymers: an efficient and generic approach. *J. Am. Chem. Soc.* **1998,** *120* (34), 8587-8598.

86. Pierre, A. C., The sol-gel encapsulation of enzymes. *Biocatal. Biotransform.* **2004,** *22* (3), 145-170.

87. Furukawa, H.; Cordova, K. E.; O'Keeffe, M.; Yaghi, O. M., The chemistry and applications of metal-organic frameworks. *Science* **2013,** *341* (6149), 1230444.

88. Kitagawa, S., Porous crystalline materials: closing remarks. *Faraday Discuss.* **2017,** *201* (0), 395-404.

89. Ma, S.; Zhou, H.-C., Gas storage in porous metal–organic frameworks for clean energy applications. *Chem. Commun.* **2010,** *46* (1), 44-53.

90. Murray, L. J.; Dincă, M.; Long, J. R., Hydrogen storage in metal-organic frameworks. *Chem. Soc. Rev* **2009,** *38* (5), 1294-1314.

91. Rosi, N. L.; Eckert, J.; Eddaoudi, M.; Vodak, D. T.; Kim, J.; O'Keeffe, M.; Yaghi, O. M., Hydrogen storage in microporous metal-organic frameworks. *Science* **2003,** *300* (5622), 1127-1129.

92. Doonan, C. J.; Sumby, C. J., Metal–organic framework catalysis. *CrystEngComm.* **2017,** *19* (29), 4044-4048.

93. Doonan, C.; Riccò, R.; Liang, K.; Bradshaw, D.; Falcaro, P., Metal–organic frameworks at the biointerface: synthetic strategies and applications. *Acc. Chem. Res.* **2017,** *50* (6), 1423-1432.

94. Ma, W.; Jiang, Q.; Yu, P.; Yang, L.; Mao, L., Zeolitic imidazolate framework-based electrochemical biosensor for in vivo electrochemical measurements. *Anal. Chem.* **2013,** *85* (15), 7550-7557.

95. Patra, S.; Hidalgo Crespo, T.; Permyakova, A.; Sicard, C.; Serre, C.; Chaussé, A.; Steunou, N.; Legrand, L., Design of metal organic framework–enzyme based bioelectrodes as a novel and highly sensitive biosensing platform. *J. Mater. Chem. B.* **2015,** *3* (46), 8983-8992.

96. Liu, W.-L.; Wu, C.-Y.; Chen, C.-Y.; Singco, B.; Lin, C.-H.; Huang, H.-Y., Fast Multipoint Immobilized MOF Bioreactor. *Chem. Eur. J.* **2014,** *20* (29), 8923-8928.

97. Liu, W.-L.; Lo, S.-H.; Singco, B.; Yang, C.-C.; Huang, H.-Y.; Lin, C.-H., Novel trypsin–FITC@MOF bioreactor efficiently catalyzes protein digestion. *J. Mater. Chem. B.* **2013,** *1* (7), 928-932.

98. Wen, L.; Gao, A.; Cao, Y.; Svec, F.; Tan, T.; Lv, Y., Layer-by-layer assembly of metal–organic frameworks in macroporous polymer monolith and their use for enzyme immobilization. *Macromol. Rapid Commun.* **2016,** *37* (6), 551-557.

99. Cao, Y.; Wu, Z.; Wang, T.; Xiao, Y.; Huo, Q.; Liu, Y., Immobilization of Bacillus subtilis lipase on a Cu-BTC based hierarchically porous metal–organic framework material: a biocatalyst for esterification. *Dalton Trans.* **2016,** *45* (16), 6998-7003.

100. Liu, W.-L.; Yang, N.-S.; Chen, Y.-T.; Lirio, S.; Wu, C.-Y.; Lin, C.-H.; Huang, H.-Y., Lipase-supported metal–organic framework bioreactor catalyzes warfarin synthesis. *Chem. Eur. J.* **2015,** *21* (1), 115-119.

101. Pisklak, T. J.; Macías, M.; Coutinho, D. H.; Huang, R. S.; Balkus, K. J., Hybrid materials for immobilization of MP-11 catalyst. *Top. Catal.* **2006,** *38* (4), 269-278.

102. Shih, Y.-H.; Lo, S.-H.; Yang, N.-S.; Singco, B.; Cheng, Y.-J.; Wu, C.-Y.; Chang, I. H.; Huang, H.-Y.; Lin, C.-H., Trypsin-immobilized metal–organic framework as a biocatalyst in proteomics analysis. *ChemPlusChem.* **2012,** *77* (11), 982-986.

103. Doherty, C. M.; Grenci, G.; Riccò, R.; Mardel, J. I.; Reboul, J.; Furukawa, S.; Kitagawa, S.; Hill, A. J.; Falcaro, P., Combining uv lithography and an imprinting technique for patterning metal-organic frameworks. *Adv. Mater.* **2013,** *25* (34), 4701-4705.

104. Jung, S.; Kim, Y.; Kim, S.-J.; Kwon, T.-H.; Huh, S.; Park, S., Bio-functionalization of metal–organic frameworks by covalent protein conjugation. *Chem. Commun.* **2011,** *47* (10), 2904-2906.

105. Chen, Y.; Lykourinou, V.; Vetromile, C.; Hoang, T.; Ming, L.-J.; Larsen, R. W.; Ma, S., How can proteins enter the interior of a MOF? Investigation of cytochrome c translocation into a MOF consisting of mesoporous cages with microporous windows. *J. Am. Chem. Soc.* **2012,** *134* (32), 13188-13191.

106. Lian, X.; Chen, Y.-P.; Liu, T.-F.; Zhou, H.-C., Coupling two enzymes into a tandem nanoreactor utilizing a hierarchically structured MOF. *Chem. Sci.* **2016,** *7* (12), 6969-6973.

107. Feng, D.; Liu, T.-F.; Su, J.; Bosch, M.; Wei, Z.; Wan, W.; Yuan, D.; Chen, Y.-P.; Wang, X.; Wang, K.; Lian, X.; Gu, Z.-Y.; Park, J.; Zou, X.; Zhou, H.-C., Stable metal-organic frameworks containing single-molecule traps for enzyme encapsulation. *Nat. Commun.* **2015,** *6* (1), 5979.

108. Lykourinou, V.; Chen, Y.; Wang, X.-S.; Meng, L.; Hoang, T.; Ming, L.-J.; Musselman, R. L.; Ma, S., Immobilization of mp-11 into a mesoporous metal–organic framework, mp-11@mesomof: a new platform for enzymatic catalysis. *J. Am. Chem. Soc.* **2011,** *133* (27), 10382-10385.

109. Chen, Y.; Han, S.; Li, X.; Zhang, Z.; Ma, S., Why does enzyme not leach from metal–organic frameworks (MOFs)? unveiling the interactions between an enzyme molecule and a MOF. *Inorg. Chem.* **2014,** *53* (19), 10006-10008.

110. Gong, C.; Shen, Y.; Chen, J.; Song, Y.; Chen, S.; Song, Y.; Wang, L., Microperoxidase-11@PCN-333 (Al)/three-dimensional macroporous carbon electrode for sensing hydrogen peroxide. *Sensors Actuators B.* **2017,** *239*, 890-897.

111. Deng, H.; Grunder, S.; Cordova, K. E.; Valente, C.; Furukawa, H.; Hmadeh, M.; Gándara, F.; Whalley, A. C.; Liu, Z.; Asahina, S.; Kazumori, H.; O'Keeffe, M.; Terasaki, O.; Stoddart, J. F.; Yaghi, O. M., Large-pore apertures in a series of metal-organic frameworks. *Science* **2012,** *336* (6084), 1018.

112. Liu, Q.; Song, Y.; Ma, Y.; Zhou, Y.; Cong, H.; Wang, C.; Wu, J.; Hu, G.; O'Keeffe, M.; Deng, H., Mesoporous cages in chemically robust MOFs created by a large number of vertices with reduced connectivity. *J. Am. Chem. Soc.* **2019,** *141* (1), 488-496.

113. Lian, X.; Fang, Y.; Joseph, E.; Wang, Q.; Li, J.; Banerjee, S.; Lollar, C.; Wang, X.; Zhou, H.-C., Enzyme–MOF (metal–organic framework) composites. *Chem. Soc. Rev.* **2017,** *46* (11), 3386-3401.

114. Lyu, F.; Zhang, Y.; Zare, R. N.; Ge, J.; Liu, Z., One-pot synthesis of protein-embedded metal–organic frameworks with enhanced biological activities. *Nano. Lett.* **2014,** *14* (10), 5761-5765.

115. Park, K. S.; Ni, Z.; Côté, A. P.; Choi, J. Y.; Huang, R.; Uribe-Romo, F. J.; Chae, H. K.; O'Keeffe, M.; Yaghi, O. M., Exceptional chemical and thermal stability of zeolitic imidazolate frameworks. *Proc. Nat. Acad. Sci.* **2006,** *103* (27), 10186.

116. Morris, W.; Doonan, C. J.; Furukawa, H.; Banerjee, R.; Yaghi, O. M., Crystals as molecules: postsynthesis covalent functionalization of zeolitic imidazolate frameworks. *J. Am. Chem. Soc.* **2008,** *130* (38), 12626-12627.

117. Kida, K.; Okita, M.; Fujita, K.; Tanaka, S.; Miyake, Y., Formation of high crystalline ZIF-8 in an aqueous solution. *CrystEngComm.* **2013,** *15* (9), 1794-1801.

118. Jian, M.; Liu, B.; Liu, R.; Qu, J.; Wang, H.; Zhang, X., Water-based synthesis of zeolitic imidazolate framework-8 with high morphology level at room temperature. *RSC Adv.* **2015,** *5* (60), 48433-48441.

119. Shieh, F.-K.; Wang, S.-C.; Leo, S.-Y.; Wu, K. C. W., Water-based synthesis of zeolitic imidazolate framework-90 (zif-90) with a controllable particle size. *Chem. Eur. J.* **2013,** *19* (34), 11139-11142.

120. Hayashi, H.; Côté, A. P.; Furukawa, H.; O'Keeffe, M.; Yaghi, O. M., Zeolite A imidazolate frameworks. *Nat. Mater.* **2007,** *6* (7), 501-506.

121. Sun, C.-Y.; Qin, C.; Wang, X.-L.; Yang, G.-S.; Shao, K.-Z.; Lan, Y.-Q.; Su, Z.-M.; Huang, P.; Wang, C.-G.; Wang, E.-B., Zeolitic imidazolate framework-8 as efficient pH-sensitive drug delivery vehicle. *Dalton Trans.* **2012,** *41* (23), 6906-6909.

122. Zhang, K.; Lively, R. P.; Zhang, C.; Chance, R. R.; Koros, W. J.; Sholl, D. S.; Nair, S., Exploring the framework hydrophobicity and flexibility of ZIF-8: from biofuel recovery to hydrocarbon separations. *J. Phys. Chem. Lett.* **2013,** *4* (21), 3618-3622.

123. Fairen-Jimenez, D.; Moggach, S. A.; Wharmby, M. T.; Wright, P. A.; Parsons, S.; Düren, T., Opening the gate: framework flexibility in ZIF-8 explored by experiments and simulations. *J. Am. Chem. Soc.* **2011,** *133* (23), 8900-8902.

124. Shieh, F.-K.; Wang, S.-C.; Yen, C.-I.; Wu, C.-C.; Dutta, S.; Chou, L.-Y.; Morabito, J. V.; Hu, P.; Hsu, M.-H.; Wu, K. C. W.; Tsung, C.-K., Imparting functionality to biocatalysts via embedding enzymes into nanoporous materials by a de novo approach: size-selective sheltering of catalase in metal–organic framework microcrystals. *J. Am. Chem. Soc.* **2015,** *137* (13), 4276-4279.

125. Liang, K.; Ricco, R.; Doherty, C. M.; Styles, M. J.; Bell, S.; Kirby, N.; Mudie, S.; Haylock, D.; Hill, A. J.; Doonan, C. J.; Falcaro, P., Biomimetic mineralization of metal-organic frameworks as protective coatings for biomacromolecules. *Nat. Commun.* **2015,** *6* (1), 7240.

126. Estroff, L. A., Introduction: biomineralization. *Chem.Rev.* **2008,** *108* (11), 4329-4331.

127. Du, Y.; Gao, J.; Liu, H.; Zhou, L.; Ma, L.; He, Y.; Huang, Z.; Jiang, Y., Enzyme@silica nanoflower@metal-organic framework hybrids: A novel type of integrated nanobiocatalysts with improved stability. *Nano. Res.* **2018,** *11* (8), 4380-4389.

128. Du, Y.; Gao, J.; Zhou, L.; Ma, L.; He, Y.; Huang, Z.; Jiang, Y., Enzyme nanocapsules armored by metal-organic frameworks: A novel approach for preparing nanobiocatalyst. *Chem. Eng. J.* **2017,** *327*, 1192-1197.

129. Liang, W.; Xu, H.; Carraro, F.; Maddigan, N. K.; Li, Q.; Bell, S. G.; Huang, D. M.; Tarzia, A.; Solomon, M. B.; Amenitsch, H.; Vaccari, L.; Sumby, C. J.; Falcaro, P.; Doonan, C. J., Enhanced activity of enzymes encapsulated in hydrophilic metal–organic frameworks. *J. Am. Chem. Soc.* **2019,** *141* (6), 2348-2355.

130. Feng, Y.; Zhong, L.; Bilal, M.; Tan, Z.; Hou, Y.; Jia, S.; Cui, J., Enzymes@ZIF-8 Nanocomposites with protection nanocoating: stability and acid-resistant evaluation. *Polymers (Basel)* **2018,** *11* (1), 27.

131. Cui, J.; Feng, Y.; Jia, S., Silica encapsulated catalase@metal-organic framework composite: A highly stable and recyclable biocatalyst. *Chem. Eng. J.* **2018,** *351*, 506-514.

132. Zhu, G.; Zhang, M.; Bu, Y.; Lu, L.; Lou, X.; Zhu, L., Enzyme-embedded metal–organic framework colloidosomes via an emulsion-based approach. *Chem. Asian J.* **2018,** *13* (19), 2891-2896.

133. Ortiz, A. U.; Freitas, A. P.; Boutin, A.; Fuchs, A. H.; Coudert, F.-X., What makes zeolitic imidazolate frameworks hydrophobic or hydrophilic? The impact of geometry and functionalization on water adsorption. *Phys. Chem. Chem. Phys.* **2014,** *16* (21), 9940-9949.

134. Zhang, J.-P.; Zhu, A.-X.; Lin, R.-B.; Qi, X.-L.; Chen, X.-M., Pore Surface Tailored SOD-Type Metal-Organic Zeolites. *Adv. Mater.* **2011,** *23* (10), 1268-1271.

135. Wu, X.; Ge, J.; Yang, C.; Hou, M.; Liu, Z., Facile synthesis of multiple enzyme-containing metal–organic frameworks in a biomolecule-friendly environment. *Chem. Commun.* **2015,** *51* (69), 13408-13411.

136. Wu, X.; Yang, C.; Ge, J.; Liu, Z., Polydopamine tethered enzyme/metal–organic framework composites with high stability and reusability. *Nanoscale* **2015,** *7* (45), 18883-18886.

137. Cheng, H.; Zhang, L.; He, J.; Guo, W.; Zhou, Z.; Zhang, X.; Nie, S.; Wei, H., Integrated nanozymes with nanoscale proximity for in vivo neurochemical monitoring in living brains. *Anal. Chem.* **2016,** *88* (10), 5489-5497.

138. He, H.; Han, H.; Shi, H.; Tian, Y.; Sun, F.; Song, Y.; Li, Q.; Zhu, G., Construction of thermophilic lipase-embedded metal–organic frameworks via biomimetic mineralization: a biocatalyst for ester hydrolysis and kinetic resolution. *ACS Appl. Mater.* **2016,** *8* (37), 24517-24524.

139. Liang, K.; Coghlan, C. J.; Bell, S. G.; Doonan, C.; Falcaro, P., Enzyme encapsulation in zeolitic imidazolate frameworks: a comparison between controlled co-precipitation and biomimetic mineralisation. *Chem. Commun.* **2016,** *52* (3), 473-476.

140. Liang, K.; Richardson, J. J.; Doonan, C. J.; Mulet, X.; Ju, Y.; Cui, J.; Caruso, F.; Falcaro, P., An enzyme-coated metal–organic framework shell for synthetically adaptive cell survival. *Angew. Chem. Int. Ed.* **2017,** *56* (29), 8510-8515.

141. Chen, W.-H.; Vázquez-González, M.; Zoabi, A.; Abu-Reziq, R.; Willner, I., Biocatalytic cascades driven by enzymes encapsulated in metal–organic framework nanoparticles. *Nat. Catal.* **2018,** *1* (9), 689-695.

142. Tadepalli, S.; Yim, J.; Cao, S.; Wang, Z.; Naik, R. R.; Singamaneni, S., Metal–organic framework encapsulation for the preservation and photothermal enhancement of enzyme activity. *Small* **2018,** *14* (7), 1702382.

143. Wang, Y.; Ryu, B. H.; Yoo, W.; Lee, C. W.; Kim, K. K.; Lee, J. H.; Kim, T. D., Identification, characterization, immobilization, and mutational analysis of a novel acetylesterase with industrial potential (LaAcE) from Lactobacillus acidophilus. *Biochim. Biophys. Acta.* **2018,** *1862* (1), 197-210.

144. Nadar, S. S.; Rathod, V. K., Encapsulation of lipase within metal-organic framework (MOF) with enhanced activity intensified under ultrasound. *Enzyme Microb. Technol.* **2018,** *108*, 11-20.

145. Chen, G.; Huang, S.; Kou, X.; Wei, S.; Huang, S.; Jiang, S.; Shen, J.; Zhu, F.; Ouyang, G., A convenient and versatile amino-acid-boosted biomimetic strategy for the nondestructive encapsulation of biomacromolecules within metal–organic frameworks. *Angew. Chem. Int. Ed.* **2019,** *58* (5), 1463-1467.

146. Knedel, T.-O.; Ricklefs, E.; Schlüsener, C.; Urlacher, V. B.; Janiak, C., Laccase encapsulation in zif-8 metal-organic framework shows stability enhancement and substrate selectivity. *ChemistryOpen* **2019,** *8* (11), 1337-1344.

147. Bagheri, N.; Khataee, A.; Hassanzadeh, J.; Habibi, B., Sensitive biosensing of organophosphate pesticides using enzyme mimics of magnetic ZIF-8. *Spectrochim. Acta. Pt. A* **2019,** *209*, 118-125.

148. Cui, J.; Feng, Y.; Lin, T.; Tan, Z.; Zhong, C.; Jia, S., Mesoporous metal–organic framework with well-defined cruciate flower-like morphology for enzyme immobilization. *ACS Appl. Mater.* **2017,** *9* (12), 10587-10594.

149. Velásquez-Hernández, M. d. J.; Ricco, R.; Carraro, F.; Limpoco, F. T.; Linares-Moreau, M.; Leitner, E.; Wiltsche, H.; Rattenberger, J.; Schröttner, H.; Frühwirt, P.; Stadler, E. M.; Gescheidt, G.; Amenitsch, H.; Doonan, C. J.; Falcaro, P., Degradation of ZIF-8 in phosphate buffered saline media. *CrystEngComm.* **2019,** *21* (31), 4538-4544.

150. Luzuriaga, M. A.; Benjamin, C. E.; Gaertner, M. W.; Lee, H.; Herbert, F. C.; Mallick, S.; Gassensmith, J. J., ZIF-8 degrades in cell media, serum, and some—but not all—common laboratory buffers. *Supramol. Chem.* **2019,** *31* (8), 485-490.

151. Boer, S. A.; Morshedi, M.; Tarzia, A.; Doonan, C. J.; White, N. G., Molecular tectonics: a node-and-linker building block approach to a family of hydrogen-bonded frameworks. *Chem. Eur. J.* **2019,** *25* (42), 10006-10012.

152. Morshedi, M.; Thomas, M.; Tarzia, A.; Doonan, C. J.; White, N. G., Supramolecular anion recognition in water: synthesis of hydrogen-bonded supramolecular frameworks. *Chem. Sci.* **2017,** *8* (4), 3019-3025.

153. Liang, W.; Carraro, F.; Solomon, M. B.; Bell, S. G.; Amenitsch, H.; Sumby, C. J.; White, N. G.; Falcaro, P.; Doonan, C. J., Enzyme encapsulation in a porous hydrogen-bonded organic framework. *J. Am. Chem. Soc.* **2019,** *141* (36), 14298-14305.

154. Liang, W.; Ricco, R.; Maddigan, N. K.; Dickinson, R. P.; Xu, H.; Li, Q.; Sumby, C. J.; Bell, S. G.; Falcaro, P.; Doonan, C. J., Control of structure topology and spatial distribution of biomacromolecules in protein@ZIF-8 biocomposites. *Chem. Mater.* **2018,** *30* (3), 1069-1077.

155. N. K.; Tarzia, A.; Huang, D. M.; Sumby, C. J.; Bell, S. G.; Falcaro, P.; Doonan, C. J., Protein surface functionalisation as a general strategy for facilitating biomimetic mineralisation of ZIF-8. *Chem. Sci.* **2018,** *9* (18), 4217-4223.

Chapter 2.

Screening Protein@ZIF-8 Biocomposite Synthesis

This work contributed to the following publication:

Liang, W.; Ricco, R.; **Maddigan, N. K**.; Dickinson, R. P.; Xu, H.; Li, Q.; Sumby, C. J.; Bell, S. G.; Falcaro, P.; Doonan, C. J., Control of Structure Topology and Spatial Distribution of Biomacromolecules in Protein@ZIF-8 Biocomposites. *Chem. Mater.* **2018,** *30* (3), 1069-1077.

Chapter 2. Screening Protein@ZIF-8 Biocomposite Synthesis

2.1. Introduction

One of the first, and most broadly utilised frameworks for protein encapsulation in metal-organic frameworks (MOFs), is the zinc based zeolitic imidazolate framework-8 (ZIF-8). This framework can be synthesised under a broad range of synthetic conditions, which can be modulated in terms of solvent selection, temperature, and formation time.[1-4] There has been extensive investigation into the synthetic conditions employed and their effect on the kinetics of ZIF-8 formation, with protocols established to yield ZIF-8 composites of varied crystal size, morphology and topology.[1-4] Typically, ZIF-8 forms crystals with rhombic dodecahedral morphology and sodalite (*sod*) topology, with large pore sizes and but small crystallographic pore apertures, 11.4 and 3.4 Å, respectively. Additionally, there are a number of distinct topologies (polymorphs) that can arise from aqueous ZIF-8 synthesis, which may impact the effectiveness of the framework for enzyme immobilisation, stabilisation and substrate diffusion.[5-7] One such polymorph is the thermodynamically stable diamondoid (dia) framework which, compared to the highly porous sodalite arrangement, is more densely packed and non-porous to N_2.[5] If this topology were to arise during enzyme@ZIF-8 immobilisation, the resulting biocomposite properties would likely differ from sod ZIF-8 in terms of enzyme spatial distribution and capacity for substrate diffusion.[8] Additionally, variation in crystal size and morphology can confer varied physical properties, including framework flexibility and stability.[9-11] Hence, when developing enzyme@ZIF-8 biocomposites, a systematic approach to the synthesis is paramount, to ensure consistent material formation and characterisation.

In the study by Liang *et. al.* in 2015, it was reported that bovine serum albumin (BSA) could rapidly induce nucleation of ZIF-8 to yield uniformly sized, rhombic dodecahedral crystals of the sodalite topology.[12] Liang *et. al* developed a protocol for ZIF-8 synthesis, whereby the driving force for biocomposite formation was the protein/biomacromolecule. The method involved the dissolution of a protein such as BSA into an aqueous 2-methyl imidazole (2-mIM) solution (160 mM), followed by the addition of an aqueous zinc acetate dihydrate ($Zn(OAc)_2.H_2O$) solution (40 mM). The mixing of precursors, led to precipitation of the biocomposite within seconds, however in the absence of a biomacromolecule, minimal precipitate (i.e. ZIF-8) formed over an extended timeframe (24 hours). This process was termed ‘biomimetic mineralisation’, where the pre-concentration of zinc at the surface of the biomacromolecule initiated the ZIF nucleation process.[12] This protocol was extended to

different proteins and biomacromolecules, however morphological variations were observed during characterisation by scanning electron microscopy (SEM) imaging.

The results of this study became the foundation for the work described in this thesis, as the morphology of the protein@ZIF-8 biocomposites appeared to be protein dependent. As such, we investigated the process of biomimetic mineralisation in a systematic manner, in order to establish new protocols for uniform ZIF formation, and to understand the impact of the synthetic conditions on biocomposite formation and thus enzyme activity. The studied conditions included variation to the precursor concentrations and solvent selection (for synthesis and solvent exchange), as well as the protein surface chemistry (described in **Chapter 3**). This chapter describes the initial screening of conditions, that contributed to two peer reviewed publications and established the protocols used in the latter chapters of this thesis.

2.2. Results and Discussion

2.2.1. Visual Inspection of Precipitate Formation

Low ratio 2-mIM:Zn^{2+}(160: 40 mM)

Initial screening was undertaken using the Zn^{2+} (40 mM) and 2-mIM (160 mM) concentrations reported by Liang *et. al* using a variety of different proteins to initiate nucleation.[13] As such, we were interested in investigating the impact that different proteins had on forming ZIF-8 in aqueous solutions. During the screening process, it was observed that the precipitation, formation rate and final yield of the biocomposite was protein dependent. For example, certain enzymes, including lipase from *Candida antarctica* (CALB) and catalase, initiated the instant formation of a precipitate upon mixing the precursors **(Figure 2.1)**. ZIF-8 nucleation was rapid (within seconds) yielding ~10-15 mg of biocomposite per sample with CALB, whereas, after the initial nucleation process for catalase (seconds), formation occurred at a slower rate, yielding ~5-10 mg of the ZIF-8 biocomposite. A selection of proteins, that included haemoglobin, resembled the protein free control, yielding only low levels of precipitate after 16 hours which could not be quantified in terms of yield **(Figure 2.1)**. A broader range of proteins were screened and subsequently classed 'successful' or 'unsuccessful', resultant from their ability/inability to enhance the rate of ZIF-8 formation relative to the no protein sample (**Table 2.1, Figure S2.1**). It is apparent from the screening data, that the biomimetic mineralisation process is heavily influenced by the choice of biomacromolecule which, in addition to the morphological differences previously reported,

affects the rate of formation and the quantity of biocomposite that is formed. Hence, immobilisation at the low 2-mIM:Zn^{2+} ratio is not applicable to all proteins.

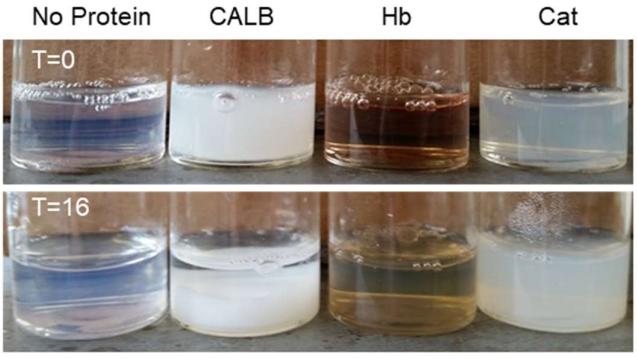

Figure 2.1: Images of the biomimetic mineralisation process using *Candida antarctica* Lipase B (CALB), Haemoglobin (Hb) and Catalase (Cat) after the initial mixing of Zn^{2+} and 2-mIM (t=0) and after 16 hours of formation (t=16). Additional screening using a more comprehensive selection of proteins is reported in **Figure S2.1**.

Table 2.1: The proteins tested for biomimetic mineralisation, categorised by their ability to seed the biomimetic mineralisation of ZIF-8 according to **Figure 2.1** and **Figure S2.1**.

Successful	**Unsuccessful**
Bovine Serum Albumin (BSA)	Haemoglobin
Horseradish peroxidase (HRP)	Myoglobin
Catalase	Trypsin
Lipase (CALB)	Lysozyme
Urease	
Pepsin	

High ratio 2-mIM:Zn^{2+} (1200: 40 mM)

In aqueous solutions, ZIF-8 can be formed utilising high ligand-to-metal ratios, where the basicity[1] of the solution promotes ligand deprotonation, nucleation and thus crystal formation. As such, higher ligand to metal ratios (8:1, 16:1, 20;1 and 30:1) were examined for protein free, haemoglobin, and pepsin ZIF-8 preparations in order to establish a more general method of protein encapsulation. Increasing the concentration of 2-mIM does favour precipitation in the presence of haemoglobin with the 30:1 molar ratio resulting in the largest yield (~20-30 mg) of biocomposite (**Figure 2.2**). Similar results were obtained in the absence

of protein, highlighting that an increased ligand concentration (30:1) is required for significant ZIF formation. Pepsin, however, induced rapid nucleation at all ratios (**Figure 2.2**).

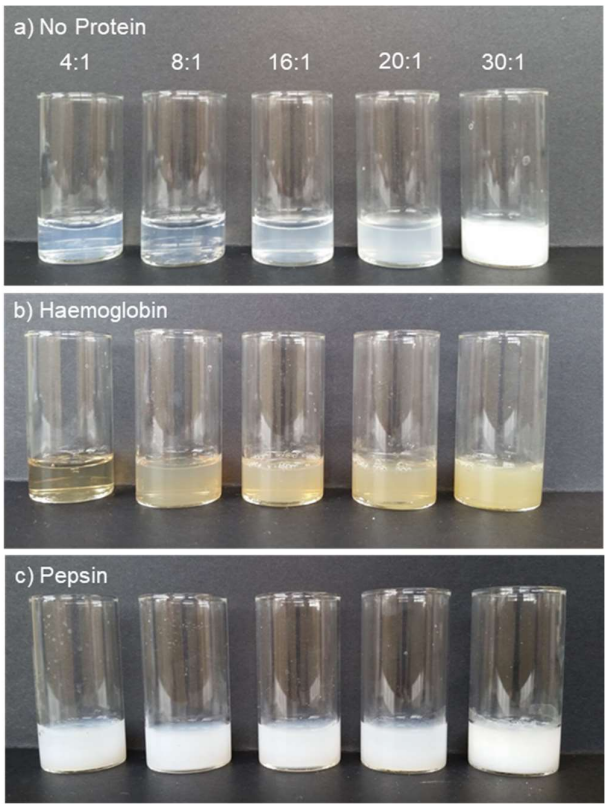

Figure 2.2: Images of the ZIF-8 formation 16 hours using different ratios of 2-mIM:Zn^{2+} for (a) no protein control, (b) haemoglobin and (c) pepsin. The Zn^{2+} concentration was kept constant at 20 mM (final concentration) and equal volumes of Zn^{2+} and 2-mIM were used in each preparation.

2.2.2. Morphology Investigation

Low ratio 2-mIM:Zn^{2+} (160: 40 mM)

To understand the variation in biocomposite formation at low 2-mIM to Zn^{2+} ratios, the influence of the protein was examined by characterising the precipitates that formed after 16 hours. Two proteins, pepsin (successful) and haemoglobin (unsuccessful) were selected for screening purposes. These were not extensively characterised in the initial study,[13] and thus would extend our understanding of this process to different proteins. Due to the low yields of the "unsuccessful" proteins, initial characterisation of the precipitate was limited to SEM analysis, where differences in the particle size and morphology could be observed (**Figure 2.3**). Using concentrations of 2-mIM (160 mM) and Zn^{2+} (40 mM), the haemoglobin preparation shared similar morphological features to the protein free control, generating large aggregates of material. In comparison, the addition of the pepsin afforded crystals of the characteristic rhombic dodecahedral morphology associated with ZIF-8 (**Figure 2.3c**). Pepsin, much like BSA, induced the formation of uniform ZIF-8 crystals, whereas haemoglobin did not significantly influence the precipitate formation, acting more as a spectator protein.

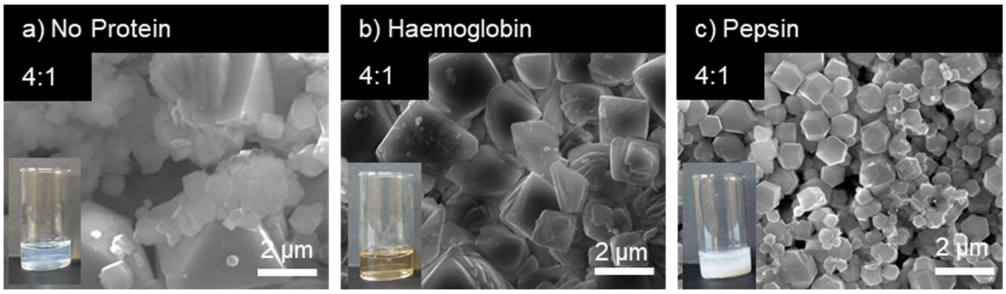

Figure 2.3: SEM images of the ZIF-8 preparations after16 hours formation using a) no protein control, b) haemoglobin, and c) pepsin. The Zn^{2+} and 2-mIM concentrations were held constant at 40 mM and 160 mM (stock concentration, prior to mixing). Inset are images of the precipitate after 16-hours.

High ratio 2-mIM:Zn^{2+} (1200: 40 mM)

At higher 2-mIM to Zn^{2+} ratios (1200:40 mM; 30:1), the particle sizes associated with each preparation were different. The no protein and pepsin samples affording homogeneously sized crystals after 16-hours of formation (1 μm) (**Figure 2.4a, c**). Under the same conditions, the haemoglobin sample produced significantly larger crystals (~2 μm) (**Figure 2.4b**), which would indicate that the protein is either influencing the initial nucleation, the crystal growth phase, or potentially both steps. It is of note that small molecule inhibitors, such as weak bases and amino acids have been utilised to modulate the crystal growth of ZIF-8.[9, 14-15] This phenomenon may translate to larger polypeptides and proteins, and thus may explain the effect that haemoglobin has on ZIF-8 formation.

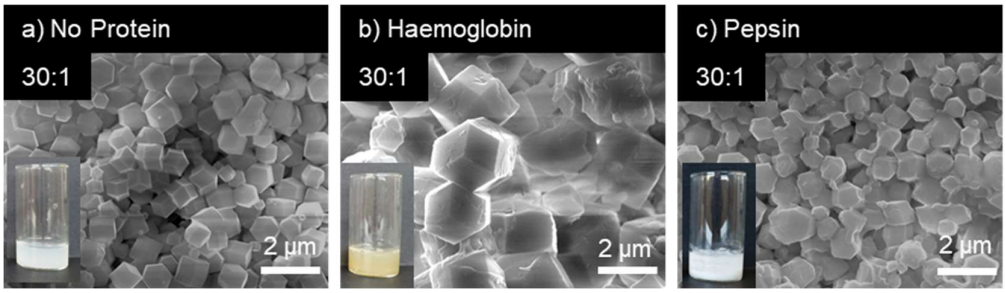

Figure 2.4: SEM images of the ZIF-8 preparations after 16 hours formation using a) no protein, b) haemoglobin, and c) pepsin. The Zn^{2+} and 2-mIM concentrations were held constant at 40 mM and 1200 mM (stock concentration, prior to mixing). Inset are images of the precipitate after 16 hours.

To understand the differences in crystal formation, the 30:1 haemoglobin and control (protein free) samples were analysed via SEM during the early stages of formation (between 0- and 120- minutes, **Figure S2.2-S2.3**). The presence of uniform, rhombic dodecahedral crystals first appeared after 30 minutes for the protein free control, whilst formation in the presence of haemoglobin was slower, yielding equivalent crystals to the no protein control sample after 120 minutes. Analysis of the supernatant of the 30:1 haemoglobin@ZIF-8 sample indicated that the protein was being immobilised by the higher ratio preparations (**Figure S2.4**). This observation highlights the possibility that 'unsuccessful' proteins, such as haemoglobin, may slow down the rate at which ZIF-8 forms, by acting like an inhibitor. [15] Thus, at low and high 2-mIM:Zn^{2+} ratios, the protein is likely to impact the final properties of the biocomposite that is formed, and as such this should be taken into consideration when comparing enzyme@ZIF-8 materials. Hence, all further studies in this thesis utilised 16-hour formation

times, to enable direct comparison of the impact of the different proteins/synthetic conditions and ensure consistent analysis of each biocomposite

2.2.3. Topological Investigation

In addition to the variation in crystal size and morphology, the connectivity and metal-ligand geometry can vary to yield different structural topologies. It has been shown that increasing the 2-mIM:Zn^{2+} ratio favours the formation of phase pure sodalite crystals that could immobilise the subset of proteins listed in **Table 2.1**. Increasing the ligand: metal ratio was established to encapsulate haemoglobin, with the sodalite topology appearing at the 16:1 ratio and above (**Figure 2.5**). Using haemoglobin and the 4:1, and 8:1 2-mIM:Zn^{2+} precursor ratios generated an unknown phase (later identified as ZIF-C[16]) and diamondoid topologies respectively.[8] When examined further, additional topologies, including katsenite, and unknown phases 12, 13, and 14 were identified.[8] Additionally, the precipitate that forms using the 'successful' proteins at a 4:1 ratio, is not the desired sodalite topology, and instead yields other topologies, including an amorphous phase (**Figure 2.6**). Upon solvent exchange with ethanol, these phases can transition to the sodalite topology, as was observed for biocomposites formed with HRP and CALB (**Figure 2.6**). The mechanism of the transition with ethanol is not well understood, however, the different phases are now known to impact the release profile of the protein.[16] For example, amorphous materials are known to release their protein cargo (BSA) more rapidly than the densely packed diamondoid topology.[16] As such, the characterisation of these different topologies may be important for understanding the activity and stability of each biocomposite.

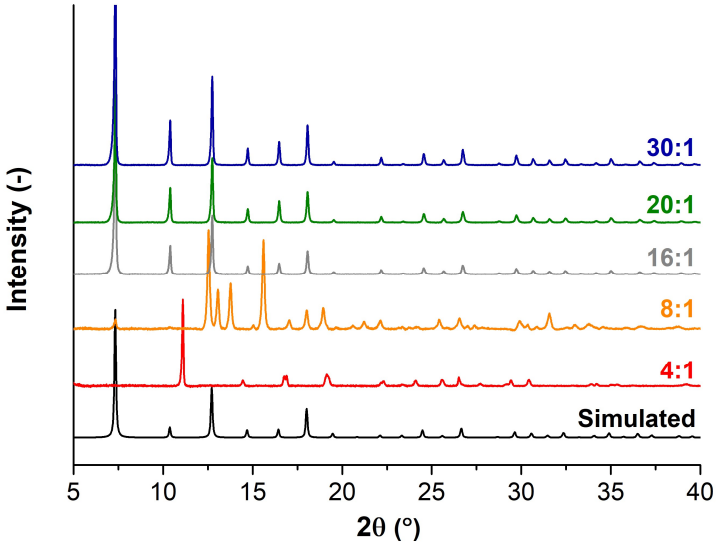

Figure 2.5: PXRD pattern of haemoglobin ZIF-8 preparations after water washes only using increasing 2-mIM:Zn^{2+} ratios. The 4:1 ratio yielded ZIF-C^{16}, whereas the 8:1 ratio yielded the densely packed diamondoid (*dia*) topology. 16:1, 20:1 and 30:1 all formed the sodalite topology.

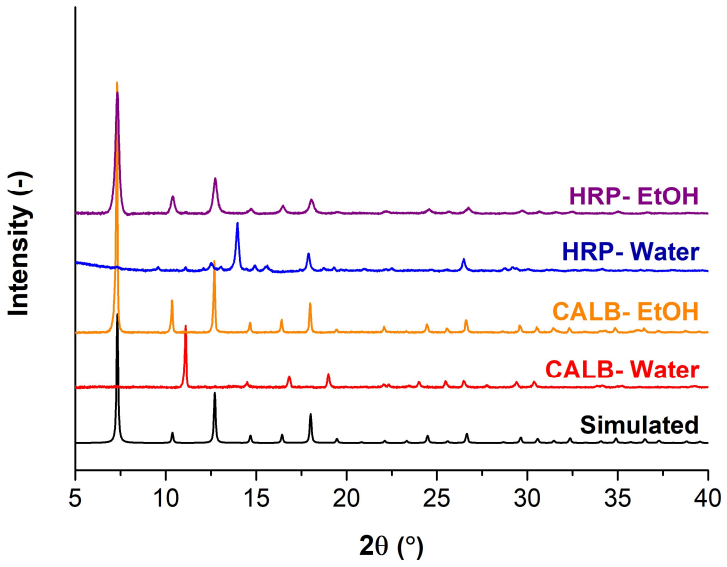

Figure 2.6: PXRD pattern of the 4:1 ratio of proteins CALB and HRP after water washes only (water), and sequential water and ethanol washes (EtOH). The initial precipitates of CALB and HRP were assigned as ZIF-C^{15} and Unknown 14 (U14) and could both transition to the sodalite topology after an ethanol wash.

The phase transition of the BSA biocomposites (160: 40 mM; 4:1, 16 hours) was investigated further by solvent exchanging the amorphous precipitates with primary alcohols of increasing length (methanol to octanol). Each of the alcohols had the capacity to mediate the phase transition from amorphous to sodalite, indicating that the conversion process was not limited to the short chain alcohols (**Figure 2.7**). SEM imaging of the ethanol, butanol and octanol washed BSA@ZIF-8 biocomposites highlighted alcohol dependent crystal degradation, with the longer chain alcohols (butanol and octanol) causing etching of the crystal surfaces (**Figure 2.8**). This observation is consistent with previous literature, where hydrophobic reagents with polar functional groups, were shown to degrade ZIF-8 crystals.[17] Whilst the transition between phases can be mediated by all lengths of the primary alcohols tested, the crystals are not stable to the solvent exchange process.

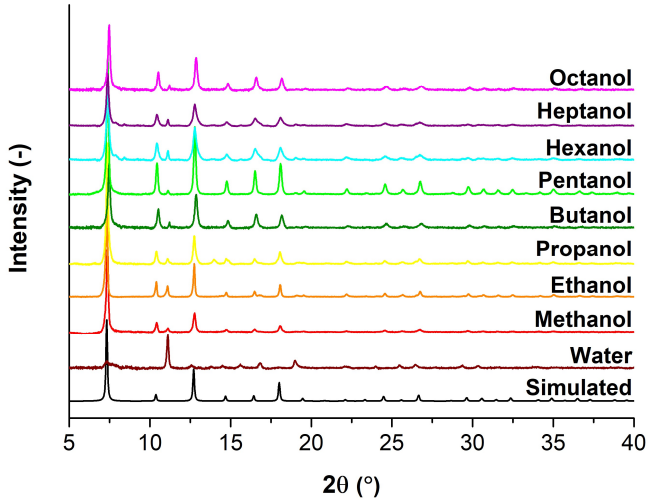

Figure 2.7: PXRD pattern of BSA@ZIF-8 samples after water washes or subsequent alcohol washes. The water wash sample consisted of mainly an amorphous phase mixed with ZIF-C. After each alcohol wash, the dominant phase was sodalite.

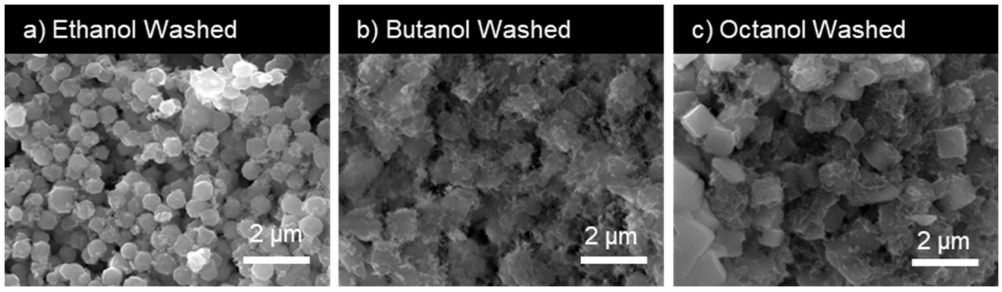

Figure 2.8: SEM images BSA@ZIF-8 with post solvent exchange with different alcohols, a) ethanol, b) butanol and c) octanol.

2.2.3. *Solvent Effects*

The impact of alcohol solvents on ZIF-8 formation and its role in topology transitions was investigated further. Protic solvents, such as ethanol and methanol are typically used for room temperature syntheses of ZIF-8 at low ligand: metal ratios facilitating rapid nucleation and greater control over particle size and crystallinity. As such the low ratio (160: 40 mM) protocol was tested with haemoglobin using an alcohol solvent. Changing the solvent system, of the low ratio Hb preparation, to a water: methanol composition (3:1, and 1:1) did appear to enhance ZIF-8 nucleation, forming a sodalite network without the need for additional (i.e. ethanol) washing steps. This rapid nucleation leads to the formation of smaller crystals. Small ZIF-8 crystals have been reported be more susceptible to degradation than larger crystals which may impact the longevity of the protein@ZIF-8 biocomposite (**Figure 2.9**).[17] It is favourable to utilise the water-based system for the initial synthesis of the ZIF-8 biocomposite to minimise the exposure time to solvents such as ethanol and methanol that may denature the enzyme during encapsulation.

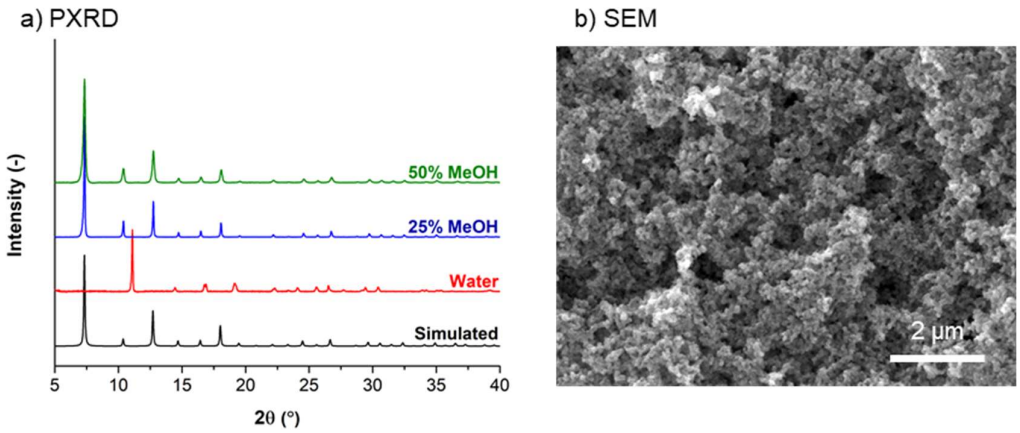

Figure 2.9: a) PXRD pattern of the haemoglobin, 4:1 sample, using solvent compositions of; 100% water, and 3:1 and 1:1 water: methanol ratios. The water-based haemoglobin synthesis yielded the ZIF-C.[15] b) SEM image of the haemoglobin@ZIF-8 biocomposite formed in 50:50 water: methanol.

2.3. Conclusions

In summary, the synthetic protocols for protein@ZIF-8 biocomposites were examined, investigating the effects of the protein, the precursor concentrations, washing protocol and solvent selection. In this study, significant variability of the encapsulation process was observed, and this work provided valuable insight into the encapsulation process, that was fundamental to the remainder of the work in this thesis.

The effectiveness of the biomimetic mineralisation process was not applicable to all proteins tested, and a subset of proteins were identified to be incapable of seeding ZIF-8 nucleation at low 2-mIM:Zn^{2+} ratios. This led to the investigation and development of synthetic conditions that enabled the immobilisation of a broader range of proteins. By increasing the concentration of the ligand (2-mIM), ZIF-8 nucleation was favoured, allowing the immobilisation of proteins during the ZIF-8 growth phase. Additionally, the ligand concentration was important in controlling the topology of the as-synthesised ZIF-8, with dilute 2-mIM solutions yielding a variety of amorphous or densely packed crystalline phases. Conversely, high 2-mIM concentrations favoured the formation of phase pure ZIF-8 biocomposites, however, the protein was shown to influence the final particle size, ranging from 500 nm to 2 μm depending on the protein. This work contributed to a peer reviewed publication, that extensively examined the impact of precursor concentrations, and synthetic conditions on the formation of protein@ZIF-8 biocomposites. Additionally, these findings stimulated further investigation on the effect of the protein chemistry that is presented in **Chapter 3**.

The aforementioned screening results also established the protocols used in **Chapters 4-6**, to ensure a systematic approach to characterisation and activity testing of different enzyme@ZIF-8 biocomposites. It was established in these initial screening studies, that the choice of protein and synthetic conditions was controlling the formation of ZIF-8. This resulted in biocomposites of different topology, morphology and particle size. As such, the activity screening studies focussed on a lipase (**Chapter 4, 5)** and a dehalogenase enzyme **(Chapter 6)** that were both capable of biomimetic mineralisation of ZIF-8 at low 2-mIM concentrations. In these studies, enzyme@ZIF-8 biocomposites were also formed at high ratios, to understand the impact of synthetic conditions on enzymatic activity. In both cases, careful reporting of the synthesis conditions and characterisation of the biocomposites was fundamental to the systematic analysis of these variables.

2.4. Experimental

2.4.1. Materials

All proteins (excluding lysozyme) were purchased from Merck as lyophilised powders and used without purification. Lysozyme was purchased from Astral Scientific. Product codes can be found in **Chapter 3, Table S3.1**. All chemicals were purchased from commercial sources and used as received. Ultra-pure Milli-Q (MQ) with resistivity of >18 MΩ cm^{-1} (Merck Millipore purification system) was used for all syntheses, wash protocols and buffer preparations.

2.4.2. ZIF Syntheses

All ZIF-biocomposites were synthesised in water using 2 mg of protein and varied ratios of zinc acetate dihydrate ($Zn(OAc)_2$) and 2-methylimidazole (2-mIM). $Zn(OAc)_2$ (40 mM 2 mL) was added to a solution of 2-mIM (160 mM/320 mM/640 mM/800 mM/1.2 M, 2mL) containing protein. The samples were left to form for 16 hours before being washed with water (2x) only, or water (2x) and an alcohol solvent (2x). For protocols using methanol as a solvent, the methanol concentration was equivalent in both the Zn^{2+} and 2-mIM solutions.

2.4.3 Characterisation

Powder X-ray Diffraction. Powder X-ray diffraction (PXRD) data were collected on a Bruker D8 Advanced X-ray powder diffractometer (parallel X-ray, capillary-loaded) using a Cu Kα λ=1.5418 Å radiation source, using 0.5 mm glass capillaries and data collected for between 2θ of 2° to 52.94° with Phi rotation at 20 rotations per min at 1-second exposure per step at 5001 steps. Simulated powder X-ray diffraction patterns were generated from the single crystal X-ray data using Mercury 3.9.[18]

Scanning Election Microscopy (SEM). SEM images were collected on either the Philips XL30 Field Emission Scanning Electron Microscope (FESEM). Samples were dry loaded onto carbon tabs on aluminium stages and sputter coated with carbon.

2.5. References

1. Katsenis, A. D.; Puškarić, A.; Štrukil, V.; Mottillo, C.; Julien, P. A.; Užarević, K.; Pham, M.-H.; Do, T.-O.; Kimber, S. A. J.; Lazić, P.; Magdysyuk, O.; Dinnebier, R. E.; Halasz, I.; Friščić, T., In situ X-ray diffraction monitoring of a mechanochemical reaction reveals a unique topology metal-organic framework. *Nat. Commun.* **2015,** *6* (1), 6662.

2. Akimbekov, Z.; Katsenis, A. D.; Nagabhushana, G. P.; Ayoub, G.; Arhangelskis, M.; Morris, A. J.; Friščić, T.; Navrotsky, A., Experimental and theoretical evaluation of the stability of true mof polymorphs explains their mechanochemical interconversions. *J. Am. Chem. Soc.* **2017,** *139* (23), 7952-7957.

3. Baburin, I. A.; Leoni, S., The energy landscapes of zeolitic imidazolate frameworks (ZIFs): towards quantifying the presence of substituents on the imidazole ring. *J. Mater. Chem.* **2012,** *22* (20), 10152-10154.

4. Baburin, I. A.; Leoni, S., Modelling polymorphs of metal–organic frameworks: a systematic study of diamondoid zinc imidazolates. *CrystEngComm.* **2010,** *12* (10), 2809-2816.

5. Shi, Q.; Chen, Z.; Song, Z.; Li, J.; Dong, J., Synthesis of ZIF-8 and ZIF-67 by steam-assisted conversion and an investigation of their tribological behaviors. *Angew. Chem. Int. Ed.* **2011,** *50* (3), 672-675.

6. Cui, J.; Feng, Y.; Lin, T.; Tan, Z.; Zhong, C.; Jia, S., Mesoporous metal–organic framework with well-defined cruciate flower-like morphology for enzyme immobilization. *ACS Appl. Mater.* **2017,** *9* (12), 10587-10594.

7. Jian, M.; Liu, B.; Liu, R.; Qu, J.; Wang, H.; Zhang, X., Water-based synthesis of zeolitic imidazolate framework-8 with high morphology level at room temperature. *RSC. Adv.* **2015,** *5* (60), 48433-48441.

8. Liang, W.; Ricco, R.; Maddigan, N. K.; Dickinson, R. P.; Xu, H.; Li, Q.; Sumby, C. J.; Bell, S. G.; Falcaro, P.; Doonan, C. J., Control of structure topology and spatial distribution of biomacromolecules in protein@zif-8 biocomposites. *Chem. Mater.* **2018,** *30* (3), 1069-1077.

9. Maddigan, N. K.; Tarzia, A.; Huang, D. M.; Sumby, C. J.; Bell, S. G.; Falcaro, P.; Doonan, C. J., Protein surface functionalisation as a general strategy for facilitating biomimetic mineralisation of ZIF-8. *Chem. Sci.* **2018,** *9* (18), 4217-4223.

10. Zhang, C.; Gee, J. A.; Sholl, D. S.; Lively, R. P., Crystal-size-dependent structural transitions in nanoporous crystals: adsorption-induced transitions in ZIF-8. *J. Phys. Chem. C.* **2014,** *118* (35), 20727-20733.

11. Tanaka, S.; Fujita, K.; Miyake, Y.; Miyamoto, M.; Hasegawa, Y.; Makino, T.; Van der Perre, S.; Cousin Saint Remi, J.; Van Assche, T.; Baron, G. V.; Denayer, J. F. M., Adsorption

and diffusion phenomena in crystal size engineered ZIF-8 MOF. *J. Phys. Chem. C.* **2015,** *119* (51), 28430-28439.

12. Sakata, Y.; Furukawa, S.; Kondo, M.; Hirai, K.; Horike, N.; Takashima, Y.; Uehara, H.; Louvain, N.; Meilikhov, M.; Tsuruoka, T.; Isoda, S.; Kosaka, W.; Sakata, O.; Kitagawa, S., Shape-memory nanopores induced in coordination frameworks by crystal downsizing. *Science* **2013,** *339* (6116), 193.

13. Liang, K.; Ricco, R.; Doherty, C. M.; Styles, M. J.; Bell, S.; Kirby, N.; Mudie, S.; Haylock, D.; Hill, A. J.; Doonan, C. J.; Falcaro, P., Biomimetic mineralization of metal-organic frameworks as protective coatings for biomacromolecules. *Nat. Commun.* **2015,** *6* (1), 7240.

14. Pan, Y.; Heryadi, D.; Zhou, F.; Zhao, L.; Lestari, G.; Su, H.; Lai, Z., Tuning the crystal morphology and size of zeolitic imidazolate framework-8 in aqueous solution by surfactants. *CrystEngComm.* **2011,** *13* (23), 6937-6940.

15. Liang, K.; Ricco, R.; Doherty, C. M.; Styles, M. J.; Falcaro, P., Amino acids as biomimetic crystallization agents for the synthesis of ZIF-8 particles. *CrystEngComm* **2016,** *18* (23), 4264-4267.

16. Carraro, F.; Velasquez, M.; Astria, E.; Liang, W.; Twight, L.; Parise, C.; Ge, M.; Huang, Z.; Ricco, R.; Zou, X.; villanova, L.; Kappe, C. O.; Doonan, C.; Falcaro, P., Phase dependent encapsulation and release profile of ZIF-based biocomposites. *Chem. Sci.* **2020**, *11*, 3397-3404.

17. Linder-Patton, O. M.; de Prinse, T. J.; Furukawa, S.; Bell, S. G.; Sumida, K.; Doonan, C. J.; Sumby, C. J., Influence of nanoscale structuralisation on the catalytic performance of ZIF-8: a cautionary surface catalysis study. *CrystEngComm.* **2018,** *20* (34), 4926-4934.

18. Macrae, C. F.; Edgington, P. R.; McCabe, P.; Pidcock, E.; Shields, G. P.; Taylor, R.; Towler, M.; van de Streek, J., Mercury: visualization and analysis of crystal structures. *J. Appl. Crystallogr.* **2006,** *39* (3), 453-457.

2.6. Supporting Information

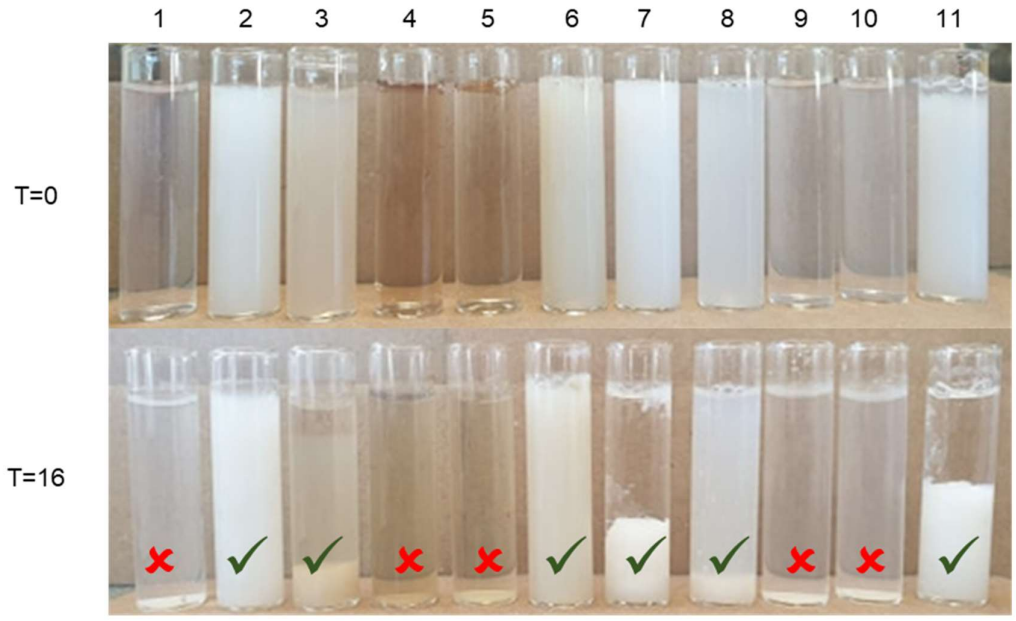

Figure S2.1: Images of the biomimetic mineralisation process after the initial mixing of Zn^{2+} and 2-mIM (t=0) and after 16 hours of formation (t=16).**(1)** No Protein (NP), **(2)** Bovine Serum Albumin (BSA), **(3)** Horseradish Peroxidase (HRP), **(4)** Haemoglobin (Hb), **(5)** Myoglobin (Mb), **(6)** Catalase (Cat), **(7)** Lipase (CALB), **(8)** Urease (Ure), **(9)** Trypsin (Tryp), **(10)** Lysozyme (Lys), **(11)** Pepsin (Pep).

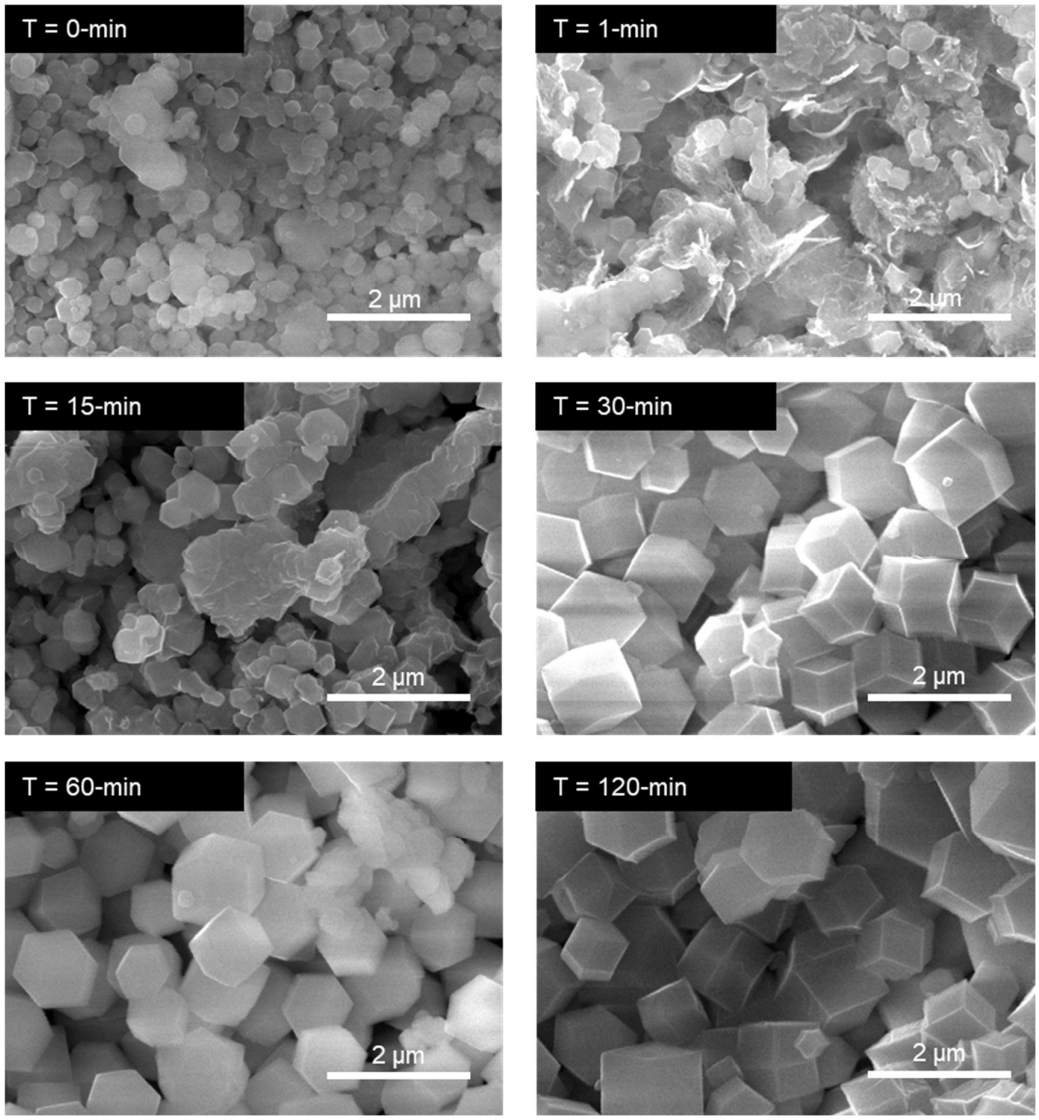

Figure S2.2: No protein control. SEM images of the no protein ZIF-8 control formed using the 30:1 2-mIM: Zn^{2+} ratio. Samples were taken at each of the corresponding time points which were washed with water and ethanol prior to imaging. The Zn^{2+} concentration was held constant at 20 mM (final concentration).

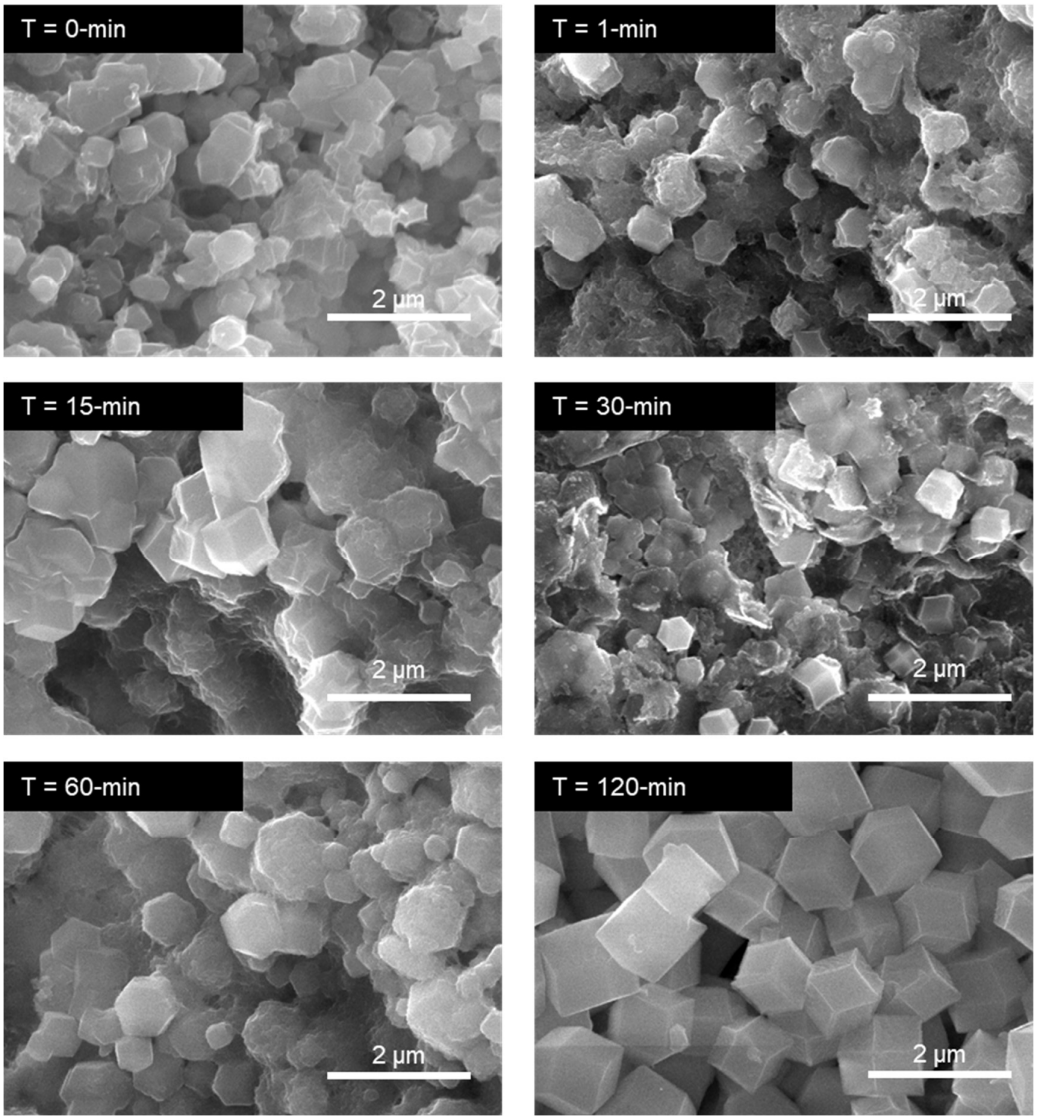

Figure S2.3: Haemoglobin. SEM images of the haemoglobin ZIF-8 sample formed using the 30:1 2-mIM: Zn^{2+} ratio. Samples were taken at each of the corresponding time points which were washed with water and ethanol prior to imaging. The Zn^{2+} concentration was held constant at 20 mM (final concentration).

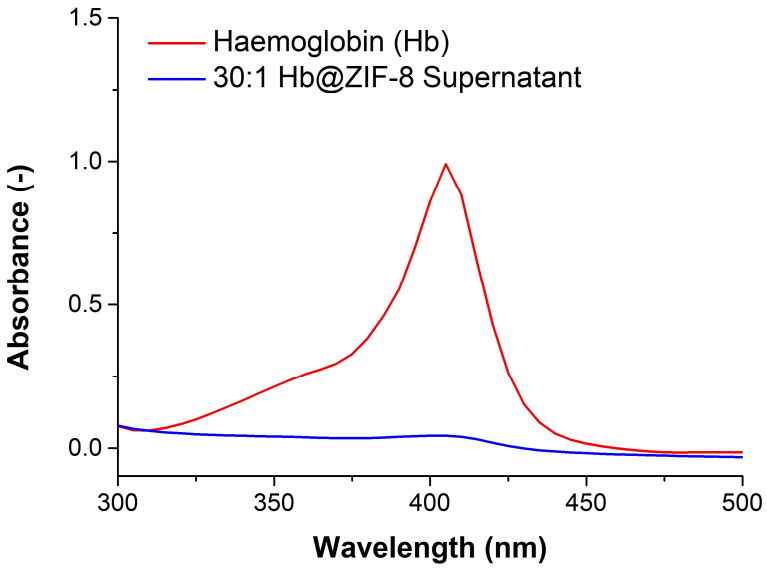

Figure S2.4: Absorbance spectrum of haemoglobin (red) and the supernatant of the 30:1 haemoglobin@ZIF-8 biocomposite. The decrease in Soret absorbance of haemoglobin (~400 nm), indicates that the protein is incorporated into the ZIF-8 material.

Chapter 3.

Protein Surface Functionalisation as a General Strategy for Facilitating Biomimetic Mineralisation of ZIF-8

This work appears in the following publication and has been re-formatted in thesis style.

Maddigan, N. K.; Tarzia, A.; Huang, D. M.; Sumby, C. J.; Bell, S. G.; Falcaro, P.; Doonan, C. J., Protein surface functionalisation as a general strategy for facilitating biomimetic mineralisation of ZIF-8. *Chem. Sci.* **2018,** *9* (18), 4217-4223.

Statement of Authorship

Title of Paper	Protein surface functionalisation as a general strategy for facilitating biomimetic mineralisation of ZIF-8
Publication Status	☑ Published ☐ Accepted for Publication ☐ Submitted for Publication ☐ Unpublished and Unsubmitted work written in manuscript style
Publication Details	N. K. Maddigan, A. Tarzia, D. M. Huang, C. J. Sumby, S. G. Bell, P. Falcaro and C. J. Doonan, *Chemical Science*, 2018, **9**, 4217-4223.

Principal Author

Name of Principal Author (Candidate)	Natasha K. Maddigan		
Contribution to the Paper	Experimental, manuscript writing, and editing		
Overall percentage (%)	85%		
Certification:	This paper reports on original research I conducted during the period of my Higher Degree by Research candidature and is not subject to any obligations or contractual agreements with a third party that would constrain its inclusion in this thesis. I am the primary author of this paper.		
Signature		Date	10/03/20

Co-Author Contributions

By signing the Statement of Authorship, each author certifies that:

i. the candidate's stated contribution to the publication is accurate (as detailed above);
ii. permission is granted for the candidate in include the publication in the thesis; and
iii. the sum of all co-author contributions is equal to 100% less the candidate's stated contribution.

Name of Co-Author	Andrew Tarzia		
Contribution to the Paper	Computation experiments. Manuscript writing and drafting.		
Signature		Date	10/03/20

Name of Co-Author	David M. Huang		
Contribution to the Paper	Aided in manuscript writing, and drafting.		
Signature		Date	17/03/20

Pleas

Name of Co-Author	Christopher J. Sumby		
Contribution to the Paper	Supervised experimental work. Aided in manuscript writing, and drafting.		
Signature		Date	17/03/2020

Name of Co-Author	Stephen. G. Bell		
Contribution to the Paper	Supervised experimental work. Aided in manuscript writing, and drafting.		
Signature		Date	17/03/2020.

Name of Co-Author	Paolo Falcaro		
Contribution to the Paper	Aided in manuscript writing, and drafting.		
Signature		Date	09/03/2020

Name of Co-Author	Christian J. Doonan		
Contribution to the Paper	Supervised experimental work. Aided in manuscript writing, and drafting.		
Signature		Date	17/03/2020

Chapter 3. Protein Surface Functionalisation as a General Strategy for Facilitating Biomimetic Mineralisation of ZIF-8

3.1. Abstract

The durability of enzymes in harsh conditions can be enhanced by encapsulation within metal–organic frameworks (MOFs) *via* process called biomimetic mineralisation. Herein we show that the surface charge and chemistry of a protein determines its ability to seed MOF growth. We demonstrate that chemical modification of amino acids on the protein surface is an effective method for systematically controlling biomimetic mineralisation by zeolitic imidazolate framework-8 (ZIF-8). Reaction of surface lysine residues with succinic (or acetic) anhydride facilitates biomimetic mineralisation by increasing the surface negative charge, whereas reaction of surface carboxylate moieties with ethylenediamine affords a more positively charged protein and hinders the process. Moreover, computational studies confirm that the surface electrostatic potential of a protein is a good indicator of its ability to induce biomimetic mineralisation. This study highlights the important role played by protein surface chemistry in encapsulation and outlines a general method for facilitating the biomimetic mineralisation of proteins.

3.2. Introduction

Metal–organic frameworks (MOFs) are a class of porous materials that are constructed from metal nodes connected *via* organic links.[1] The chemical mutability of these building units offers broad scope for tailoring the properties of MOFs for specific applications such as gas separations, drug delivery and catalysis.[2-10] A recent development in MOF chemistry is their use as matrices for encapsulating biomacromolecules, *e.g.* proteins and enzymes, *via* a one-pot synthetic approach termed 'biomimetic mineralisation'.[11-16] This strategy has also been extended to the synthesis of MOF-based biocomposites composed of viruses,[17] and cells,[18-19] and more recently to the co-encapsulation of gene-editing system CRISPR/CAS9.[20] A salient feature of the MOF coating is that it can protect an encapsulated enzyme from inhospitable external environments (*e.g.* elevated temperatures or proteolytic media) while facilitating size-selective transport of substrates to the active site *via* its pore network.[21-23] These properties are relevant to commercial bio-catalysis, for which strategies to improve enzyme durability are sought after.[24]

The most studied MOF for biomimetic mineralisation has been zeolitic imidazolate framework-8 (ZIF-8),[25] a material of sodalite topology comprising tetrahedral Zn^{2+} ions connected *via* 2-methylimidazole (mIM) bridging units. ZIF-8 is porous (BET surface area *ca.* 1200 m^2g^{-1}), stable in a wide range of organic solvents and can be synthesised in neat water.[26-27] Standard conditions for the biomimetic mineralisation of ZIF-8 employ a stoichiometric ratio metal ions and organic linker (160 mM of mIM and 40 mM of metal salt) in an aqueous solution of 2 mg of protein at room temperature.[21] While the presence of a biomacromolecule may enhance the kinetics, there are cases in which biomimetic mineralisation requires a higher excess of organic linker (mIM), or longer times, to engender ZIF formation.[28] In order to maximise the efficacy and versatility of this promising strategy for the protection of biomacromolecules, a general approach is desirable.

A detailed understanding of the chemistry at the interface of the MOF and the biomacromolecule is necessary to develop this burgeoning area. A first step towards this aim is to ascertain how the surface chemistry of the protein influences the biomimetic mineralisation process. Preliminary data showed that MOF crystallisation was facilitated by the capacity of the biomacromolecule to attract and concentrate metal cations and ligands; however, empirical data was only provided for a composite made with a single protein, bovine serum albumin (BSA).[21] Subsequently, we have observed that the kinetics of the biomimetic mineralisation process are protein dependent. Under identical reaction conditions the

precipitation of the biocomposite varies from seconds to hours and in some cases no composite is formed. For example, whilst BSA induces the formation of ZIF-8 within seconds, in our hands, a thorough study employing haemoglobin showed that aqueous solutions only yield a low quantity of non-ZIF-8 precipitate after several hours and that the precipitate does not contain protein. This observation suggests that the surface chemistry of the protein may have a significant effect on MOF crystallisation. Moreover, FTIR studies performed on proteins encapsulated within ZIF-8 point towards the existence of interactions between Zn^{2+} cations and carbonyl moieties at the protein surface.[16] To enhance our understanding of the biomimetic mineralisation process we carried out a combined computational and experimental study to investigate the role that protein surface chemistry plays in the formation of the MOF-based biocomposites. Specifically, we chemically modified the surface amino acid residues of a variety of proteins using succinic (or acetic) anhydride or ethylene diamine (**Scheme S3.1**). Analysis of these data indicates that converting the basic residues on the protein surface into acidic or non-ionisable moieties is a convenient strategy for facilitating the biomimetic mineralisation of proteins under standard conditions.

3.3. Results and Discussion

To determine the main features of the protein chemistry that induce ZIF-8 encapsulation, we screened a series of structurally distinct proteins under identical biomimetic mineralisation conditions (0.5 mg mL^{-1} of protein dissolved in a solution composed of a 1 : 4 : 278 molar ratio of Zn^{2+} : mIM : H_2O). These standard conditions were chosen because: (1) they have previously been shown to give rise to rapid (within seconds) biomimetic mineralisation;[21] (2) all proteins investigated are homogeneously dispersed; and (3) a visually observable ZIF-8 precipitate is not formed in the absence of a biomacromolecule for several hours. **Table 3.1** lists the proteins assessed for their capacity to induce the formation of a MOF-based biocomposite. Analysis of the data indicates that a biomimetically mineralised ZIF-8 precipitate is formed with proteins that have a low isoelectric point (pI) (see **Figure S3.1** and **S3.2**). These proteins contain a greater proportion of acidic residues (aspartate, pK_a 3.7, and glutamate, pK_a 4.3) which will be deprotonated, and thus negatively charged under the basic reaction process.[29] The proteins that did not induce ZIF-8 formation are those with higher pI values (above *ca.*7) which conversely possess a larger percentage of basic amino acids (lysine, pK_a 10.5, and arginine, pK_a 12.5).[29] We posit that basic amino acids will contribute to a positively charged protein surface, under the standard reaction conditions, and thus disfavour the accumulation of Zn^{2+} ions that engenders biomimetic mineralisation.

Amino acid modifications are commonly applied to increase the binding affinity of biomacromolecules for an immobilisation support by controlling the electrostatic interactions.[24] Thus, we proposed this technique could be applied as a general strategy for facilitating biomimetic mineralisation under mild, standard conditions. To explore this hypothesis, we chemically modified the basic surface amino acid residues of haemoglobin (Hb) and myoglobin (Mb) that would contribute to a positive surface charge. Surface lysine residues of Hb and Mb were reacted with succinic or acetic anhydride to convert these exposed basic residues into acidic or non-ionisable groups respectively (**Figure 3.1** and **Scheme S3.1**). The succinylated forms of Hb and Mb induced immediate precipitate formation upon precursor mixing. The precipitate was confirmed to have sodalite topology and rhombic dodecahedral crystal morphology characteristic of ZIF-8 by PXRD and SEM, respectively (**Figure S3.3–S3.5**). The acetylated variants, which do not provide carboxyl functional groups also facilitated precipitation of a crystalline product (**Figure S3.1**), but PXRD data indicated that the samples were not phase pure (**Figure S3.4**). These results confirm that the biomimetic mineralisation process is highly dependent on a protein's surface chemistry, with the ionisable carboxyl groups being more effective at facilitating biomimetic mineralisation of the desired ZIF-8 phase. **Figure S3.6** shows the UV-visible spectra of the supernatants obtained after centrifugation of the Hb and Mb biocomposites. The presence of the Soret band at 405 nm, indicates that the unmodified proteins remain in solution. To evaluate that the modified forms of these proteins were incorporated into the ZIF crystals, we performed UV-vis spectroscopy on dissolved samples of the biocomposite. We first washed the composites with SDS to ensure that surface bound protein was removed.[28] **Figure S3.7** shows the UV-vis spectra of the dissolved HbAc/Succ@ZIF-8 and MbAc/Succ@ZIF-8 biocomposites. The presence of the Soret band at 405 nm is evidence that the Hb and Mb proteins are encapsulated within the ZIF-8 crystals.

Table 3.1: Reported pI (pH at which the protein is uncharged), experimental zeta potential in a mIM solution at pH 11, and binary ZIF-8 growth result for each protein tested in this work. The yes/no descriptor for ZIF growth indicates the formation of a biocomposite with sodalite topology (determined by PXRD). Uncertainties are twice the standard error in the mean.

Protein	**pI**	**Ref**	**Zeta Potential [mV]**	**ZIF-8**	**Modification**	**Zeta Potential [mV]**	**ZIF-8**
Pepsin	2.9	[30]	-30.9 ± 1.4	Yes	Amination	-7.9 ± 0.6	No
BSA	5.3	[31]	-36.4 ± 1.4	Yes	Amination	-5.8 ± 0.2	No
Lipase	4-8[a]	[32]	-31.7 ± 0.3	Yes			
Catalase	5.4[b]	[33]	-30.4 ± 0.6	Yes			
HRP	3.0-9.0[c]	[34]	-36.4 ± 1.0	Yes			
Haemoglobin	8.1(α), 7.0(β)	[30]	-21.0 ± 2.4	No	Succinylation	-37.0 ± 2.7	Yes
					Acetylation	-35.9 ± 2.6	Yes[d]
Myoglobin	7.6	[30]	-14.7 ± 2.0	No	Succinylation	-36.6 ± 0.2	Yes
					Acetylation	-36.1 ± 3.6	Yes[d]
Trypsin	10.7	[30]	-9.0 ±1.05	No			
Lysozyme	11, 11.3	[30]	+6.6 ± 0.2	No			

[a] broad experimental isoelectric region, [b] computational value, [c] seven isozymes, [d] not phase pure.

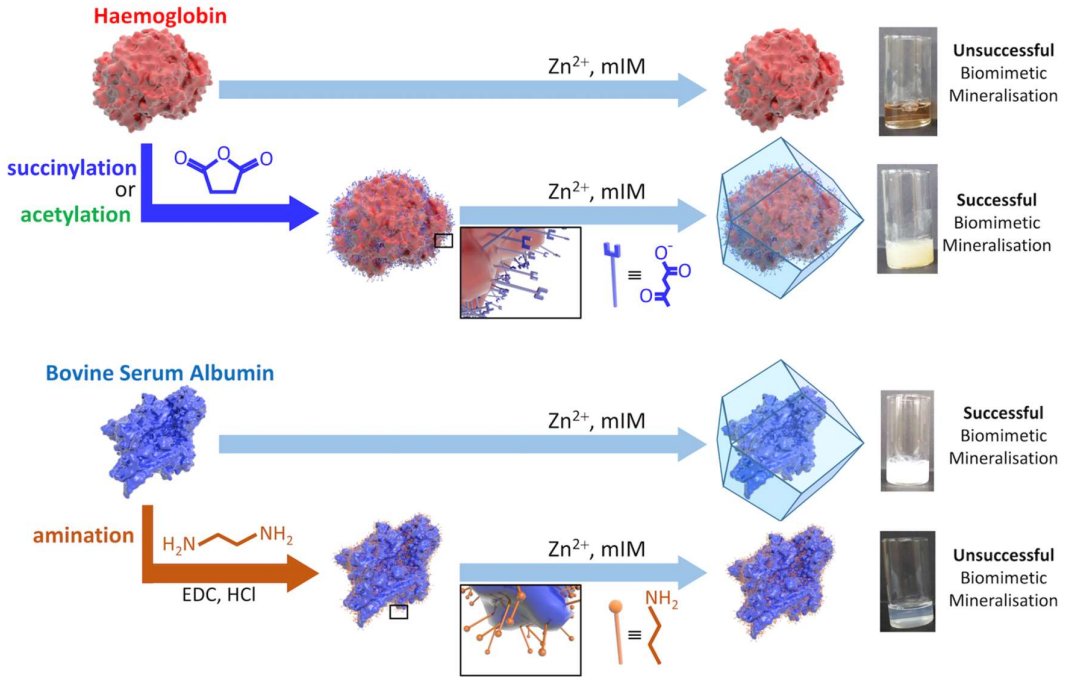

Figure 3.1: Schematic representations of the outcomes of biomimetic mineralisation for two proteins, namely haemoglobin (Hb) and bovine serum albumin (BSA). Hb does not undergo biomimetic mineralisation under standard conditions but can be chemically modified by acetylation or succinylation (shown) to increase the surface negative charge and facilitate ZIF-8 formation and encapsulation. BSA can be biomimetically mineralised but amination introduces surface amine groups that are protonated under the conditions used for ZIF-8 formation and thereby prevent mineralisation.

Both the pI values and surface modification experiments suggest that the biomimetic mineralisation of ZIF-8 depends on electrostatics of the protein surface. Thus, we measured the zeta potential of each protein in a 160 mM mIM precursor solution to estimate their charge under the reaction conditions. The zeta potential data presented in **Table 3.1** indicates that precipitation of ZIF-8 crystals is induced when the values are below *ca.*−30 mV. This trend explains why surface modification can switch the biomimetic mineralisation process 'on' or 'off'. For example, the zeta potentials of both Hb and Mb decrease from −21 and −15 mV respectively to values significantly below −30 mV upon succinylation or acetylation. To further demonstrate the importance of surface charge, BSA and pepsin were reacted with ethylene diamine to yield a more positively charged protein. Amination of the acidic residues was confirmed by a positive shift in the zeta potential measurements above this −30 mV threshold.

Both modified proteins yielded minimal precipitate, insufficient for PXRD, demonstrating an inhibition of the biomimetic mineralisation process (**Figure S3.2**).

The experimental data thus far confirm that the surface electrostatic potential of the biomacromolecule, which is related to, and for typical surfaces approximately equal to, the zeta potential,[35] can be used to predict whether ZIF-8 crystallisation will be induced. These findings are consistent with previous reports that hypothesised that biomacromolecules concentrate positively charged zinc ions at their surface.[21] Since the ion concentration varies approximately exponentially with the surface potential for purely electrostatic ion–surface interactions according to the Boltzmann equation (see Computational methods section), the surface zinc ion concentration is expected to double with each 9 mV decrease in the surface potential. This would result in an enhancement of the rate of encounters of zinc ions and mIM bridging units near the protein surface and thus to more rapid ZIF-8 formation.[36]

Both the surface electrostatic potential (zeta potential) and pI of a protein, both of which we have shown to be good discriminators of a protein's ability to seed ZIF-8 formation, can be determined from theory.[37-39] Therefore, whether a protein is likely to undergo biomimetic mineralisation can be predicted prior to experimental study.

From the peptide sequence and acid-base equilibria we calculated the pI for all the proteins studied and reproduce the trend in the experimental results shown in **Table 3.1** (**Figure 3.2, S3.9**). Furthermore, we have used the same method for computing a protein's pI to predict the effect of surface modification on propensity for ZIF-8 formation (**Figure 3.2, S3.9**).

Figure 3.2 shows the calculated pI for BSA, pepsin, Hb and Mb with and without the surface modifications used in the experiments. We assumed that any target residue (lysine for acetylation and succinylation, and glutamic acid and aspartic acid for the amination) will undergo the modification reaction. As the reaction efficiency may not be 100% and our method does not consider whether amino acids are exposed to solvent, the calculated change in the pI is expected to be an overestimate; however, we get reasonable agreement to experimental values (for example aminated BSA has a pI > 9.5).[40] As shown in **Figure 3.2** the calculated pI values (**Figure 3.2a**) show the same trend as the experimental zeta potential (**Figure 3.2b**) and clearly predicts the effect of surface modification on ZIF-8 formation for the proteins considered.

Finally, we have computed the electrostatic potential around each of the proteins studied experimentally by solving the Poisson–Boltzmann equation, from which we can approximate the protein zeta potential (see Computational methods section and **Figure S3.11–S3.13**).[37, 41] The calculated surface potential also provides comprehensive 3D information about the electrostatic interactions of the protein with the surrounding electrolyte solution. **Figure 3.3** highlights the differences in the calculated surface potential and zinc ion enhancement at pH 11 between a protein that seeds ZIF-8 and one that does not (see also **Figure S3.13**). While not quantitatively reproducing the experimental data, the calculated average surface potential follows the same trend as the experimental zeta potential at pH 7 and pH 11 for the proteins studied (**Figure S3.11**). Importantly, we show that the predictions made by a simple sequence-based model (pI calculations) and a more physical 3D structure-based model (surface potential calculations) are equivalent, and that both of these calculations agree with our experimental observations. Combined, this supports the idea that computational screening can obviate the need for more time-consuming experimental studies.

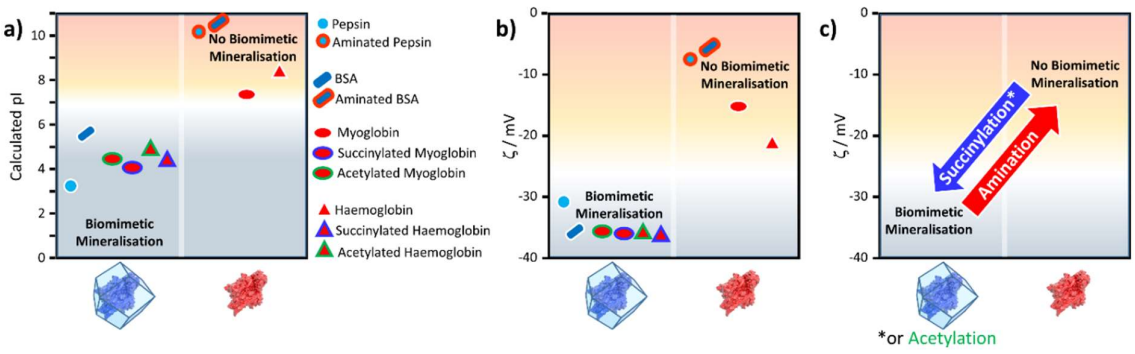

Figure 3.2: Plots of (a) the calculated pI for BSA, pepsin, Hb and Mb, with and without the surface modifications used in the experiments; (b) the experimental zeta (ζ) potentials for the same biomacromolecules and their modified variants; and (c) the general changes in zeta potential for the three types of chemical modifications used.

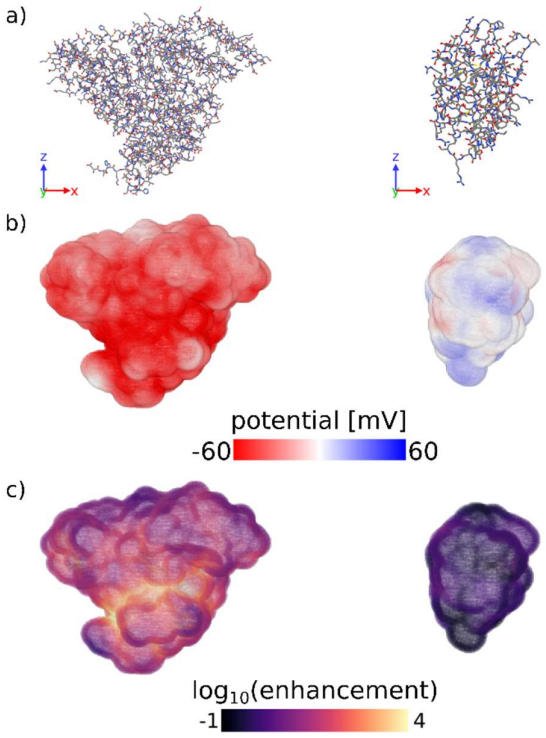

Figure 3.3: (a) Stick representations of protein crystal structures of (left) BSA and (right) lysozyme. Hydrogens are omitted for clarity. (b) Surface potential and (c) $\log_{10}$ of the zinc ion enhancement at the surface of both proteins. Zinc ion enhancement is defined as the ratio of the calculated zinc ion concentration due to the electrostatic potential and the bulk zinc ion concentration (0.04 M) at each point near the surface of the protein. **Figure S3.13** shows the calculated electrostatic surface of all proteins tested in this work. Figures were made using OVITO.[42]

3.4. Conclusions

In conclusion, we have shown that the electrostatic properties of a protein's surface, as described by its pI and zeta potential, are a good predictor of whether a protein will induce ZIF-8 growth from aqueous solution. Our findings explain why the biomimetic mineralisation of ZIF-8 is not observed under standard conditions for a variety of proteins and confirm the role of Zn^{2+} concentration in seeding crystallisation. These results are consistent with studies that describe the effect of metal ion concentration gradients on the nucleation and growth of ZIF crystals.[43] In addition, we have shown that simple chemical modification of surface ionisable residues is a convenient strategy for controlling the electrostatic potential of a protein and thus the formation of ZIF-8 biocomposites. We posit that chemical surface modification is a general strategy that can be applied to facilitate biomimetic mineralisation in a broad range of systems, including proteins, viruses and cells. Thus, this work significantly broadens the research scope and potential applications of this technique.

3.5. Experimental

3.5.1. Materials

All proteins were purchased from Sigma-Aldrich unless otherwise stated (**Table S3.1**). Each of the proteins tested were lyophilised powders and were used without further purification. 2-Methylimidazole (mIM) and *N*-(3-dimethylaminopropyl)-*N′*-ethylcarbodiimide hydrochloride (EDC·HCl) were purchased from Sigma-Aldrich, zinc acetate dihydrate from VWR Chemicals, succinic anhydride from BDH, acetic anhydride from Chem Supply, and ethylene diamine (EDA) from Merck. The water used was ultra-pure Milli-Q (MQ) with resistivity of 18 MΩ cm^{-1} (Merck Millipore purification system). All other buffers and solvents were purchased from commercial sources and used without further purification.

3.5.2. ZIF synthesis

$Zn(OAc)_2$ (40 mM, 2 mL) was mixed with a solution of mIM (160 mM, 2 mL) containing the protein (2 mg). The reaction mixture was left for 16 hours undisturbed, and collected by centrifugation at 4000 rpm. The pellet was washed with water twice, followed by ethanol and air dried at ambient temperature and pressure.

3.5.3. Succinylation and acetylation reactions

The method for the succinylation and acetylation of proteins was adapted from literature procedures.[44-46] The protein (20 mg, haemoglobin or myoglobin) was dissolved in 4 mL of phosphate buffered saline (PBS, 100 mM, pH 8). A 50-fold molar excess of succinic anhydride or acetic anhydride was added in small increments over 1 hour. The pH was adjusted back to 8 using 2 M NaOH after each addition and the solution was stirred for 1 hour after the final addition. The protein solution was washed by ultra-filtration once with PBS (100 mM, pH 7.4) and twice with MQ water to remove excess salts (Vivacell 100, Sartorius Stedim, 10 kDa at 4000 rpm/1699 g). The protein solution was concentrated to 4 mg mL^{-1} in MQ water.

3.5.4. Amination reactions

The method for the chemical amination of proteins was adapted from a literature procedure.[47] A 2 mL solution of EDA (0.268 mL, 4.01 mmol) dissolved in MQ water was prepared and the pH was adjusted to 4.5 using 6 M HCl. The protein (20 mg, BSA or pepsin) was dissolved in the EDA solution followed by EDC·HCl (7.2 mg, 0.038 mmol). The solution was stirred on ice for 120 minutes before being washed and concentrated as described above.

3.5.5. Characterisation

Powder X-ray diffraction (PXRD). PXRD data were collected on a Bruker D8-Advanced X-ray powder diffractometer (parallel X-ray, capillary-loaded) using a Cu Kα (λ= 1.5418 Å) radiation source. Samples were mounted in 0.5 mm glass capillaries and data collected for between 2θ of 2° to 52.94° with Phi rotation at 20 rotations per min at 1-second exposure per step at 5001 steps. The data were then converted into xye format and background-subtracted using WinPlotr 2000 software.[48] Simulated powder X-ray diffraction patterns were generated from the single crystal X-ray data using Mercury 3.9.[49]

Scanning electron microscopy (SEM). SEM images were collected using a Philips XL30 field emission scanning electron microscope (FESEM). Samples were dry loaded onto an adhesive carbon tab and sputter coated with 5 nm platinum thin film.

UV/Visible (UV/Vis). Spectra were recorded at 30 °C on an Agilent Cary 60 UV/Vis spectrophotometer. Samples were diluted to 4 mL prior to each measurement.

Zeta potential measurements. Measurements were recorded on a Malvern Zetasizer nano using a disposable folded cell capillary (DTS1070). Protein samples were dissolved in a HmIM solution (160 mM, pH 11) or MQ water (≈pH 7) with measurements recorded with the following parameters: Dispersant RI: 1.33, viscosity (C_p): 0.887, Dispersant dielectric constant 78.5, f(K_a): 1.5 (Smoluchowski approximation).

3.5.6. Computation methods

Calculation of the pI from protein sequence. For each protein, the sequence of natural amino acids was extracted from the FASTA file associated with each PDB entry (**Table S3.1**). Using the Biopython module[50] and the Henderson–Hasselbach equation, the average charge,

$$q_{\pm} = \frac{10^{\pm \mathrm{p}K_\mathrm{a} \mp \mathrm{pH}}}{10^{\pm \mathrm{p}K_\mathrm{a} \mp \mathrm{pH}} + 1}, \qquad (1)$$

of each ionisable residue as a function of pH was calculated. The total protein charge was calculated as the sum of the average charges of all ionisable residues and the pH varied until the total protein charge was $0 \pm 0.0001e$ to determine the sequence pI. The pK_a of all residue types were kept constant and defined within Biopython.

Surface modification of proteins. The pI of surface-modified proteins was calculated using Biopython and assuming 100% efficiency of modification reactions on all target residues. For the amination reaction, any aspartate or glutamate residues were treated as lysine residues with respect to their charge and pK_a. For the acetylation and succinylation reactions, any lysine residues were either ignored in the calculation of the protein charge (acetylation) or treated as glutamate residues with respect to their charge and pK_a (succinylation). See **Scheme S3.1** for the reaction schemes.

Calculation of average surface potentials. Crystal structures were obtained from the Protein Data Bank[51] for each protein (PDB accession codes given in **Table S3.1**). PROPKA 3.0,[52-53] was used to assign charge states to each ionisable residue in the PDB file and the PDB2PQR software[54-55] was used to prepare the protein structures for analysis. See ESI for details.

Using the SURFPOT module,[37] within the DELPHI software,[41] the linearised Poisson–Boltzmann equation,[56]

$$\nabla\,[\varepsilon(r)\nabla\psi(r)] - \varepsilon_0\varepsilon_r\kappa(r)^2\psi(r) = -\rho(r), \qquad (2)$$

was solved to calculate the electrostatic potential, $\psi(r)$, at position r. In the expression, $\rho(r)$ is the (fixed) charge density of the solute (protein), $\varepsilon(r)$ is the spatially varying dielectric permittivity, which is different in the protein and in the solution, and $\kappa(r)$ is the Debye screening parameter given by

$$\kappa = \left(\frac{\varepsilon_0 \varepsilon_r k_B T}{e^2 \sum_i c_{0i} z_i^{\,2}} \right)^{-1/2}, \qquad (3)$$

outside of the protein and is zero inside of the protein. In expression (3), e is the elementary charge, k_B is the Boltzmann constant, T is temperature, ε_0 is the vacuum permittivity, ε_r is the relative permittivity of water (80), and c_{0i} and z_i are the bulk concentration and valency of ions of type i, respectively. For all our calculations the Debye length (κ^{-1}) was 8.86 Å. The efficiency of the linearised Poisson–Boltzmann equation makes it more amenable to high-throughput computational screening than solving the full nonlinear equation and comparison of the calculated average surface potentials with experimental zeta potentials at pH 7 and pH 11 (see **Figure. S3.11**) suggest that the linearised equation is sufficiently accurate for our purposes.

The zeta potential for each protein was estimated to be the average electrostatic potential on a surface at 4 Å from the van der Waals surface of the protein. The zeta potential of a particle undergoing electrophoresis is defined by the electrostatic potential at the shear plane, which is not readily determined for heterogeneous and rough surfaces such as proteins. The chosen surface at which the zeta potential was calculated is expected to be a reasonable approximation for the shear plane and is similar to that used previously in the literature to estimate the zeta potential of proteins.[37] An interior protein dielectric coefficient of 4 was used

and it was confirmed that the average surface potential was not sensitive to this parameter (results not shown), which agrees well with literature.[37] We used a grid spacing of 0.5 Å, a probe radius (to define the protein surface) of 1.4 Å, which is equivalent to the radius of a water molecule, dipolar boundary conditions on the edge of the box, and a box size such that the longest dimension of the solute was 60% of the box size.

Ion concentrations and enhancements. The concentration of ions of type *i* at position *r* was calculated from the electrostatic potential ($\psi(r)$) using the Boltzmann equation,

$$c_i(r) = c_{0i} \exp\left[\frac{-z_i e \psi(r)}{k_B T}\right]. \qquad (4)$$

To match the experimental conditions, the bulk concentrations of the cations (zinc) and anions (acetate) in solution were taken to be c_{0+}= 0.04 M and c_{0-}= 0.08 M, respectively, and were assumed to be independent of pH. The cation and anion valencies were z_+ = +2 and z_- = −1, respectively. The zinc ion enhancement ($X(r)$) was calculated from the ion concentration as

$$X(r) = \frac{c_+(r)}{c_{0+}}.$$

3.6. Conflicts of interest

The Authors confirm that there are no conflicts to declare.

3.7. Acknowledgements

This work was supported by the Australian Research Council under the Discovery Projects Scheme (DP170103531). N. K. Maddigan and A. Tarzia acknowledge an Australian Government Research Training Program Scholarships. A. Tarzia thanks the CSIRO Materials Science and Engineering for a Ph.D. top-up scholarship. P. Falcaro acknowledges TU Graz for the Lead Project (LP-03). The authors acknowledge the facilities, and the scientific and technical assistance of the Australian Microscopy & Microanalysis Research Facility at the Adelaide Microscopy Unit, The University of Adelaide.

3.8. References

1. Furukawa, H.; Cordova, K. E.; O'Keeffe, M.; Yaghi, O. M., The chemistry and applications of metal-organic frameworks. *Science* **2013**, *341* (6149), 1230444.

2. Dechnik, J.; Gascon, J.; Doonan, C. J.; Janiak, C.; Sumby, C. J., Mixed-matrix membranes. *Angew. Chem. Int. Ed.* **2017,** *56* (32), 9292-9310.

3. Gascon, J.; Corma, A.; Kapteijn, F.; Llabrés i Xamena, F. X., Metal organic framework catalysis: quo vadis? *ACS Catal.* **2014,** *4* (2), 361-378.

4. Rogge, S. M. J.; Bavykina, A.; Hajek, J.; Garcia, H.; Olivos-Suarez, A. I.; Sepúlveda-Escribano, A.; Vimont, A.; Clet, G.; Bazin, P.; Kapteijn, F.; Daturi, M.; Ramos-Fernandez, E. V.; Llabrés i Xamena, F. X.; Van Speybroeck, V.; Gascon, J., Metal–organic and covalent organic frameworks as single-site catalysts. *Chem. Soc. Rev.* **2017,** *46* (11), 3134-3184.

5. Li, J.-R.; Kuppler, R. J.; Zhou, H.-C., Selective gas adsorption and separation in metal–organic frameworks. *Chem. Soc. Rev*. **2009,** *38* (5), 1477-1504.

6. Chen, W.; Wu, C., Synthesis, functionalization, and applications of metal–organic frameworks in biomedicine. *Dalton Trans.* **2018,** *47* (7), 2114-2133.

7. Wuttke, S.; Lismont, M.; Escudero, A.; Rungtaweevoranit, B.; Parak, W. J., Positioning metal-organic framework nanoparticles within the context of drug delivery – a comparison with mesoporous silica nanoparticles and dendrimers. *Biomaterials* **2017,** *123*, 172-183.

8. Lismont, M.; Dreesen, L.; Wuttke, S., Metal-organic framework nanoparticles in photodynamic therapy: current status and perspectives. *Adv. Funct. Mater.* **2017,** *27* (14), 1606314.

9. Giménez-Marqués, M.; Hidalgo, T.; Serre, C.; Horcajada, P., Nanostructured metal–organic frameworks and their bio-related applications. *Coord. Chem. Rev.* **2016,** *307*, 342-360.

10. Furukawa, S.; Reboul, J.; Diring, S.; Sumida, K.; Kitagawa, S., Structuring of metal–organic frameworks at the mesoscopic/macroscopic scale. *Chem. Soc. Rev.* **2014,** *43* (16), 5700-5734.

11. Riccò, R.; Liang, W.; Li, S.; Gassensmith, J. J.; Caruso, F.; Doonan, C.; Falcaro, P., Metal–organic frameworks for cell and virus biology: a perspective. *ACS Nano.* **2018,** *12* (1), 13-23.

12. Doonan, C.; Riccò, R.; Liang, K.; Bradshaw, D.; Falcaro, P., Metal–organic frameworks at the biointerface: synthetic strategies and applications. *Acc. Chem. Res.* **2017,** *50* (6), 1423-1432.

13. Ricco, R.; Pfeiffer, C.; Sumida, K.; Sumby, C. J.; Falcaro, P.; Furukawa, S.; Champness, N. R.; Doonan, C. J., Emerging applications of metal–organic frameworks. *CrystEngComm.* **2016,** *18* (35), 6532-6542.

14. Jiang, W.; Wang, X.; Chen, J.; Liu, Y.; Han, H.; Ding, Y.; Li, Q.; Tang, J., Deuterohemin-peptide enzyme mimic-embedded metal-organic frameworks through biomimetic mineralization with efficient ATRP catalytic activity. *ACS Appl. Mater. Interfaces.* **2017,** *9* (32), 26948-26957.

15. He, H.; Han, H.; Shi, H.; Tian, Y.; Sun, F.; Song, Y.; Li, Q.; Zhu, G., Construction of thermophilic lipase-embedded metal–organic frameworks via biomimetic mineralization: a biocatalyst for ester hydrolysis and kinetic resolution. *ACS Appl. Mater. Interfaces.* **2016,** *8* (37), 24517-24524.

16. Wang, C.; Sun, H.; Luan, J.; Jiang, Q.; Tadepalli, S.; Morrissey, J. J.; Kharasch, E. D.; Singamaneni, S., Metal–organic framework encapsulation for biospecimen preservation. *Chem. Mater.* **2018,** *30* (4), 1291-1300.

17. Li, S.; Dharmarwardana, M.; Welch, R. P.; Ren, Y.; Thompson, C. M.; Smaldone, R. A.; Gassensmith, J. J., Template-directed synthesis of porous and protective core–shell bionanoparticles. *Angew. Chem. Int. Ed*. **2016,** *55* (36), 10691-10696.

18. Liang, K.; Richardson, J. J.; Cui, J.; Caruso, F.; Doonan, C. J.; Falcaro, P., Metal–organic framework coatings as cytoprotective exoskeletons for living cells. *Adv. Mater.* **2016,** *28* (36), 7910-7914.

19. Liang, K.; Richardson, J. J.; Doonan, C. J.; Mulet, X.; Ju, Y.; Cui, J.; Caruso, F.; Falcaro, P., An enzyme-coated metal–organic framework shell for synthetically adaptive cell survival. *Angew. Chem. Int. Ed.* **2017,** *56* (29), 8510-8515.

20. Alsaiari, S. K.; Patil, S.; Alyami, M.; Alamoudi, K. O.; Aleisa, F. A.; Merzaban, J. S.; Li, M.; Khashab, N. M., Endosomal escape and delivery of CRISPR/cas9 genome editing machinery enabled by nanoscale zeolitic imidazolate framework. *J. Am. Chem. Soc.* **2018,** *140* (1), 143-146.

21. Liang, K.; Ricco, R.; Doherty, C. M.; Styles, M. J.; Bell, S.; Kirby, N.; Mudie, S.; Haylock, D.; Hill, A. J.; Doonan, C. J.; Falcaro, P., Biomimetic mineralization of metal-organic frameworks as protective coatings for biomacromolecules. *Nat. Commun.* **2015,** *6* (1), 7240.

22. Shieh, F.-K.; Wang, S.-C.; Yen, C.-I.; Wu, C.-C.; Dutta, S.; Chou, L.-Y.; Morabito, J. V.; Hu, P.; Hsu, M.-H.; Wu, K. C. W.; Tsung, C.-K., Imparting functionality to biocatalysts via embedding enzymes into nanoporous materials by a de novo approach: size-selective

sheltering of catalase in metal–organic framework microcrystals. *J. Am. Chem. Soc.* **2015,** *137* (13), 4276-4279.

23. Lyu, F.; Zhang, Y.; Zare, R. N.; Ge, J.; Liu, Z., One-pot synthesis of protein-embedded metal–organic frameworks with enhanced biological activities. *Nano Lett.* **2014,** *14* (10), 5761-5765.

24. Schmid, A.; Dordick, J. S.; Hauer, B.; Kiener, A.; Wubbolts, M.; Witholt, B., Industrial biocatalysis today and tomorrow. *Nature* **2001,** *409* (6817), 258-268.

25. Phan, A.; Doonan, C. J.; Uribe-Romo, F. J.; Knobler, C. B.; O'Keeffe, M.; Yaghi, O. M., Synthesis, structure, and carbon dioxide capture properties of zeolitic imidazolate frameworks. *Acc. Chem. Res.* **2010,** *43* (1), 58-67.

26. Kida, K.; Okita, M.; Fujita, K.; Tanaka, S.; Miyake, Y., Formation of high crystalline ZIF-8 in an aqueous solution. *CrystEngComm.* **2013,** *15* (9), 1794-1801.

27. Jian, M.; Liu, B.; Liu, R.; Qu, J.; Wang, H.; Zhang, X., Water-based synthesis of zeolitic imidazolate framework-8 with high morphology level at room temperature. *RSC Adv.* **2015,** *5* (60), 48433-48441.

28. Liang, W.; Ricco, R.; Maddigan, N. K.; Dickinson, R. P.; Xu, H.; Li, Q.; Sumby, C. J.; Bell, S. G.; Falcaro, P.; Doonan, C. J., Control of structure topology and spatial distribution of biomacromolecules in protein@ZIF-8 biocomposites. *Chem. Mater.* **2018,** *30* (3), 1069-1077.

29. Lide, D. R., CRC Handbook of Chemistry and Physics. 72 ed.; CRC Press: Boca Raton Florida, **1991**.

30. Patrickios, C. S.; Yamasaki, E. N., Polypeptide amino acid composition and isoelectric point ii. comparison between experiment and theory. *Anal. Biochem.* **1995,** *231* (1), 82-91.

31. Foster, J. F.; Kaplan, L. J., Isoelectric focussing behavior of bovine plasma albumin, mercaptalbumin, and β-lactoglobulins a and B. *Biochemistry* **1971,** *10* (4), 630-636.

32. Trodler, P.; Nieveler, J.; Rusnak, M.; Schmid, R. D.; Pleiss, J., Rational design of a new one-step purification strategy for *Candida antarctica* lipase b by ion-exchange chromatography. J. *Chromatogr.. A.* **2008,** *1179* (2), 161-7.

33. Samejima, T.; Kamata, M.; Shibata, K., Dissociation of bovine liver catalase at low pH. *The J. Biochem.* **1962,** *51* (3), 181-187.

34. Shannon, L. M.; Kay, E.; Lew, J. Y., Peroxidase isozymes from horseradish roots: I. isolation and physical properties. *J. Biochem*. **1966,** *241* (9), 2166-2172.

35. Hunter, R. J., Zeta potential in colloid science: principles and applications. 1 ed.; academic press: New York, **1981**.

36. Li, Z.; Zhou, G.; Dai, H.; Yang, M.; Fu, Y.; Ying, Y.; Li, Y., Biomineralization-mimetic preparation of hybrid membranes with ultra-high loading of pristine metal–organic frameworks grown on silk nanofibers for hazard collection in water. *J. Mater. Chem. A.* **2018,** *6* (8), 3402-3413.

37. Chakravorty, A.; Jia, Z.; Li, L.; Alexov, E., A new delphi feature for modeling electrostatic potential around proteins: role of bound ions and implications for zeta-potential. *Langmuir* **2017,** *33* (9), 2283-2295.

38. Bjellqvist, B.; Hughes, G. J.; Pasquali, C.; Paquet, N.; Ravier, F.; Sanchez, J.-C.; Frutiger, S.; Hochstrasser, D., The focusing positions of polypeptides in immobilized ph gradients can be predicted from their amino acid sequences. *Electrophoresis.* **1993,** *14* (1), 1023-1031.

39. Bjellqvist, B.; Basse, B.; Olsen, E.; Celis, J. E., Reference points for comparisons of two-dimensional maps of proteins from different human cell types defined in a ph scale where isoelectric points correlate with polypeptide compositions. *Electrophoresis.* **1994,** *15* (1), 529-539.

40. Muckerheide, A.; Apple, R. J.; Pesce, A. J.; Michael, J. G., Cationization of protein antigens. i. alteration of immunogenic properties. *J. Immunol.* **1987,** *138* (3), 833.

41. Li, L.; Li, C.; Sarkar, S.; Zhang, J.; Witham, S.; Zhang, Z.; Wang, L.; Smith, N.; Petukh, M.; Alexov, E., Delphi: a comprehensive suite for Delphi software and associated resources. *BMC Biophys.* **2012,** *5* (1), 9.

42. Stukowski, A., Visualization and Analysis of Atomistic Simulation Data With OVITO–the Open Visualization Tool. *Modell. Simul. Mater. Sci. Eng.* **2010,** *18* (1), 015012.

43. Saliba, D.; Ammar, M.; Rammal, M.; Al-Ghoul, M.; Hmadeh, M., Crystal growth of zif-8, zif-67, and their mixed-metal derivatives. *J. Am. Chem. Soc.* **2018,** *140* (5), 1812-1823.

44. Jamison, J. A.; Bryant, E. L.; Kadali, S. B.; Wong, M. S.; Colvin, V. L.; Matthews, K. S.; Calabretta, M. K., Altering protein surface charge with chemical modification modulates protein–gold nanoparticle aggregation. *J. Nanopart. Res.* **2011,** *13* (2), 625-636.

45. Glocker, M. O.; Borchers, C.; Fiedler, W.; Suckau, D.; Przybylski, M., Molecular characterization of surface topology in protein tertiary structures by amino-acylation and mass spectrometric peptide mapping. *Bioconjugate Chem.* **1994,** *5* (6), 583-590.

46. van der Veen, M.; Norde, W.; Stuart, M. C., Electrostatic interactions in protein adsorption probed by comparing lysozyme and succinylated lysozyme. *Colloids. Surf. B.* **2004,** *35* (1), 33-40.

47. Border, W. A.; Ward, H. J.; Kamil, E. S.; Cohen, A. H., Induction of membranous nephropathy in rabbits by administration of an exogenous cationic antigen: demonstration of a pathogenic role for electrical charge. *J. Clin. Invest.* **1982,** *69* (2), 451-461.

48. Rosinel, T.; Rodriguez-Carvajal, J., Proceedings of the seventh european powder diffraction conference (EPDIC 7) **2000**.

49. Macrae, C. F.; Edgington, P. R.; McCabe, P.; Pidcock, E.; Shields, G. P.; Taylor, R.; Towler, M.; van de Streek, J., Mercury: Visualization and analysis of crystal structures. *J. Appl. Crystallogr.* **2006,** *39* (3), 453-457.

50. Cock, P. J. A.; Antao, T.; Chang, J. T.; Chapman, B. A.; Cox, C. J.; Dalke, A.; Friedberg, I.; Hamelryck, T.; Kauff, F.; Wilczynski, B.; de Hoon, M. J. L., Biopython: freely available python tools for computational molecular biology and bioinformatics. *Bioinformatics* **2009,** *25* (11), 1422-1423.

51. Berman, H. M.; Westbrook, J.; Feng, Z.; Gilliland, G.; Bhat, T. N.; Weissig, H.; Shindyalov, I. N.; Bourne, P. E., The Protein Data Bank. *Nucleic Acids Res.* **2000,** *28* (1), 235-242.

52. Søndergaard, C. R.; Olsson, M. H. M.; Rostkowski, M.; Jensen, J. H., Improved treatment of ligands and coupling effects in empirical calculation and rationalization of pka values. *J. Chem. Theory Comput.* **2011,** *7* (7), 2284-2295.

53. Olsson, M. H. M.; Søndergaard, C. R.; Rostkowski, M.; Jensen, J. H., PROPKA3: consistent treatment of internal and surface residues in empirical pka predictions. *J. Chem. Theory Comput.* **2011,** *7* (2), 525-537.

54. Dolinsky, T. J.; Nielsen, J. E.; McCammon, J. A.; Baker, N. A., PDB2PQR: An automated pipeline for the setup of poisson–boltzmann electrostatics calculations. *Nucleic Acids Res.* **2004,** *32*, W665-W667.

55. Dolinsky, T. J.; Czodrowski, P.; Li, H.; Nielsen, J. E.; Jensen, J. H.; Klebe, G.; Baker, N. A., PDB2PQR: Expanding and upgrading automated preparation of biomolecular structures for molecular simulations. *Nucleic Acids Res.* **2007,** *35*, W522-W525.

56. Nicholls, A.; Honig, B., A rapid finite difference algorithm, utilizing successive over-relaxation to solve the poisson–boltzmann equation. *J. Comput. Chem.* **1991,** *12* (4), 435-445.

3.9. Supporting Information

3.9.1. Materials

Table S3.1. Details of the proteins, their sources, product codes and the Protein Data Bank (PDB) codes for the proteins investigated in this research.

Protein	Source	Product Code	PDB File Used
Pepsin	Porcine gastric mucosa	P6887	4pep[1]
Bovine serum albumin (BSA)	Bovine	A9418	4f5s[2]
Candida antarctica Lipase B (CALB)	*Aspergillus oryzae*	62288	1tca[3]
Catalase	Bovine Liver	C9322	3re8[4]
Peroxidase from horseradish (HRP)	Horseradish	77332	1w4w[5]
Myoglobin	Equine skeletal muscle	M0630	2frf[6]
Haemoglobin	Human	H7379	2dn2[7]
Trypsin	Porcine pancreas	T4799	1s81[8]
Lysozyme	Egg white	Astral Scientific (LDB0308)	2vb1[9]

[a] *Protein structures are from the same organism from which the protein sample is sourced.*

3.9.2. Protein surface modification reactions

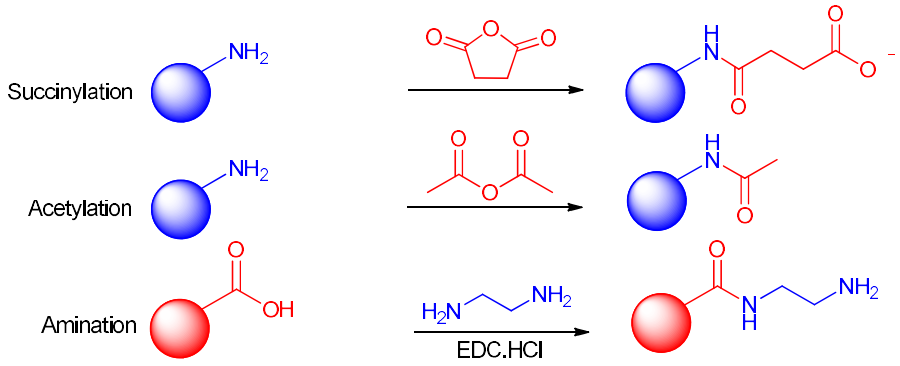

Scheme S3.1: Surface modification reactions. Succinylation and acetylation reactions lower the pI of a protein by modification of exposed amine groups. Amination reactions cap carboxyl groups with a free amine, thus increasing the pI.

3.9.3. Time course biomimetic mineralisation studies

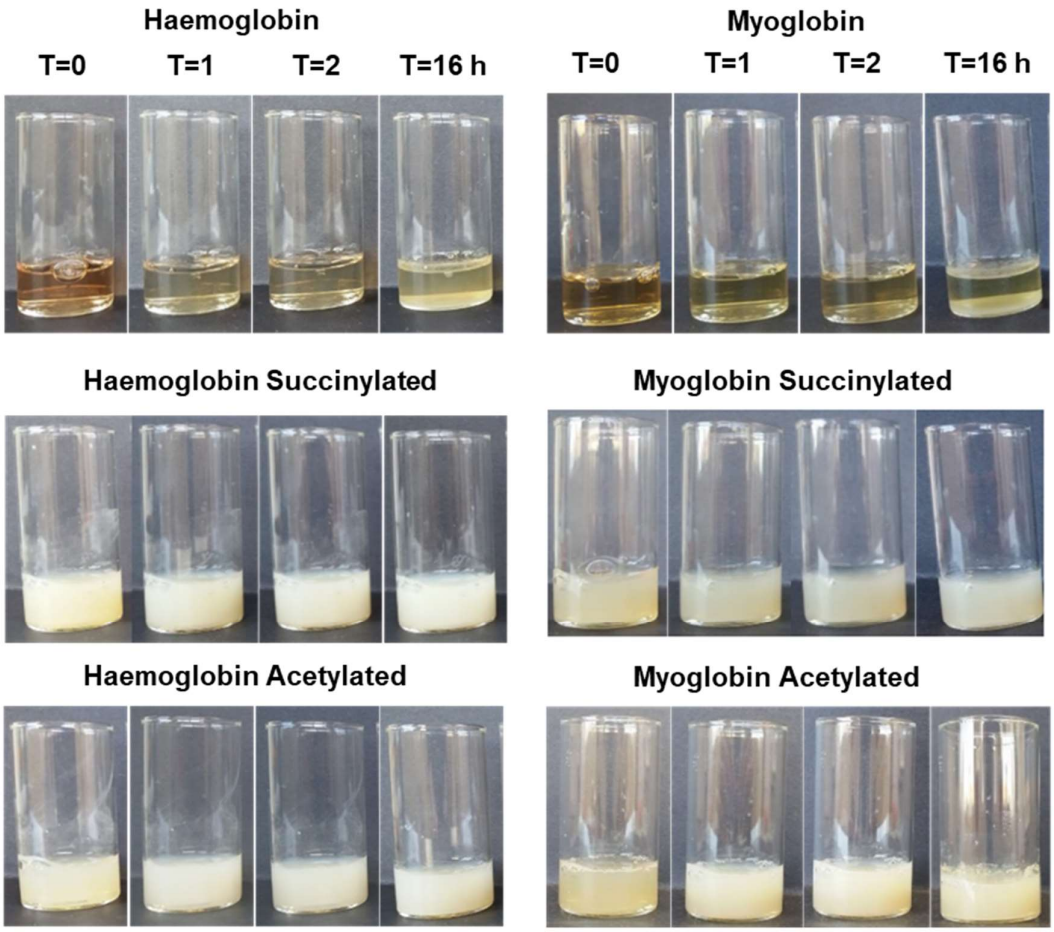

Figure S3.1: Sequential photographs of haemoglobin (Hb), succinylated haemoglobin (HbSucc), acetylated haemoglobin (HbAc), myoglobin (Mb), succinylated myoglobin (MbSucc), and acetylated myoglobin (MbAc) samples (2 mg protein) immediately after mixing of the mIM (160 mM) and zinc solutions (40 mM) (t=0) until immediately prior to centrifugation and washing (t=16 hours). The unmodified haemoglobin and myoglobin samples remain clear upon addition of the zinc solution, both yielding minimal product after 16 hours. The succinylated and acetylated forms of both proteins cause immediate precipitation of ZIF.

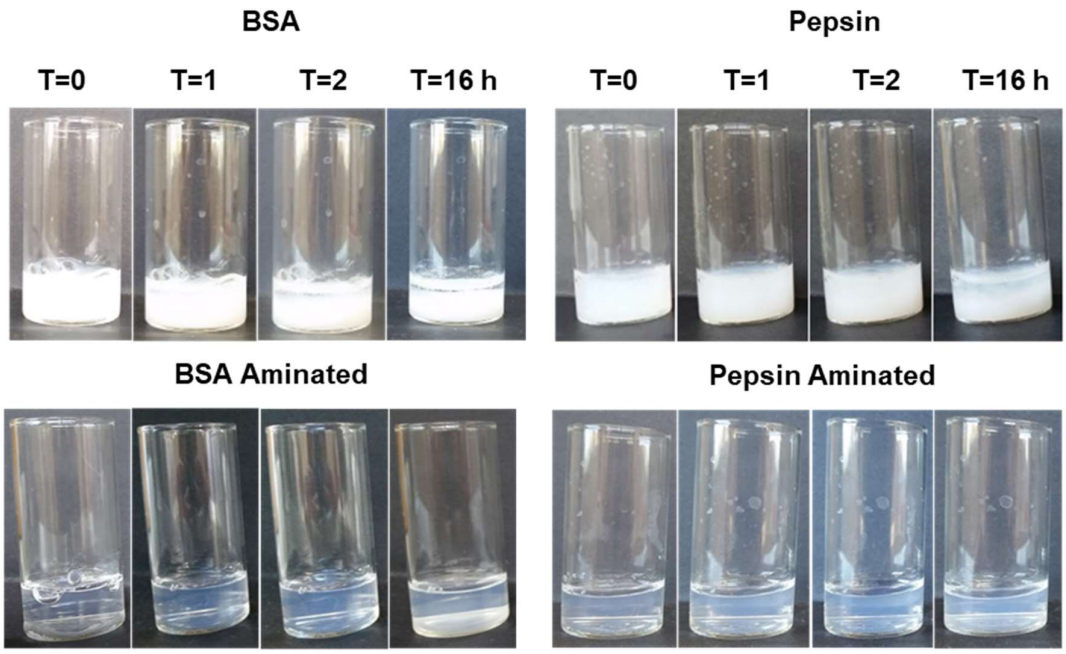

Figure S3.2: Sequential photographs of unmodified and aminated bovine serum albumin (BSA) and pepsin (2 mg protein) immediately after mixing of the mIM (160 mM) and zinc solutions (40 mM) (t=0) until immediately prior to centrifugation and washing (t=16 hours). The unmodified BSA and pepsin samples gave immediate biomineralization upon addition of the zinc solution. The aminated BSA and pepsin samples show a dramatic reduction in precipitation yielding only minimal product after 16 hours.

3.9.4. Powder X-ray diffraction (PXRD) data

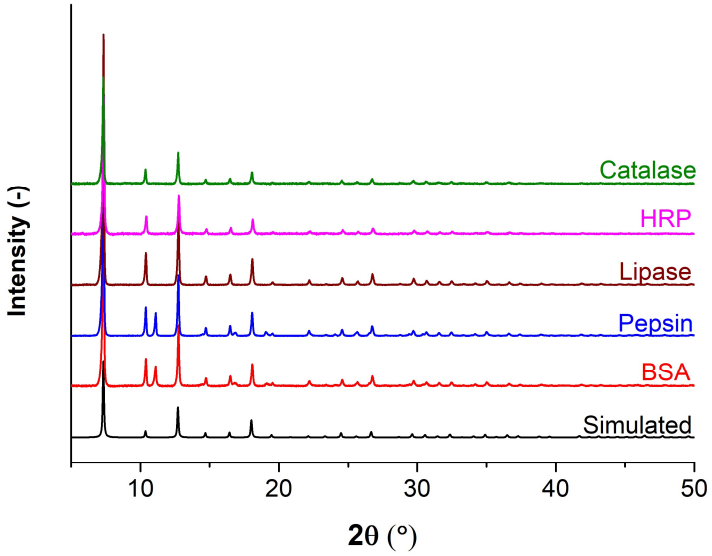

Figure S3.3: Powder X-ray diffraction patterns of biomimetically mineralised ZIF samples of unmodified proteins made under standard conditions (4:1 mIM:Zn^{2+}). Data collected on dried samples after washes with water and ethanol. Unmodified haemoglobin, myoglobin, lysozyme, and trypsin did not yield sufficient product for PXRD analysis. The simulated pattern relates to ZIF-8.

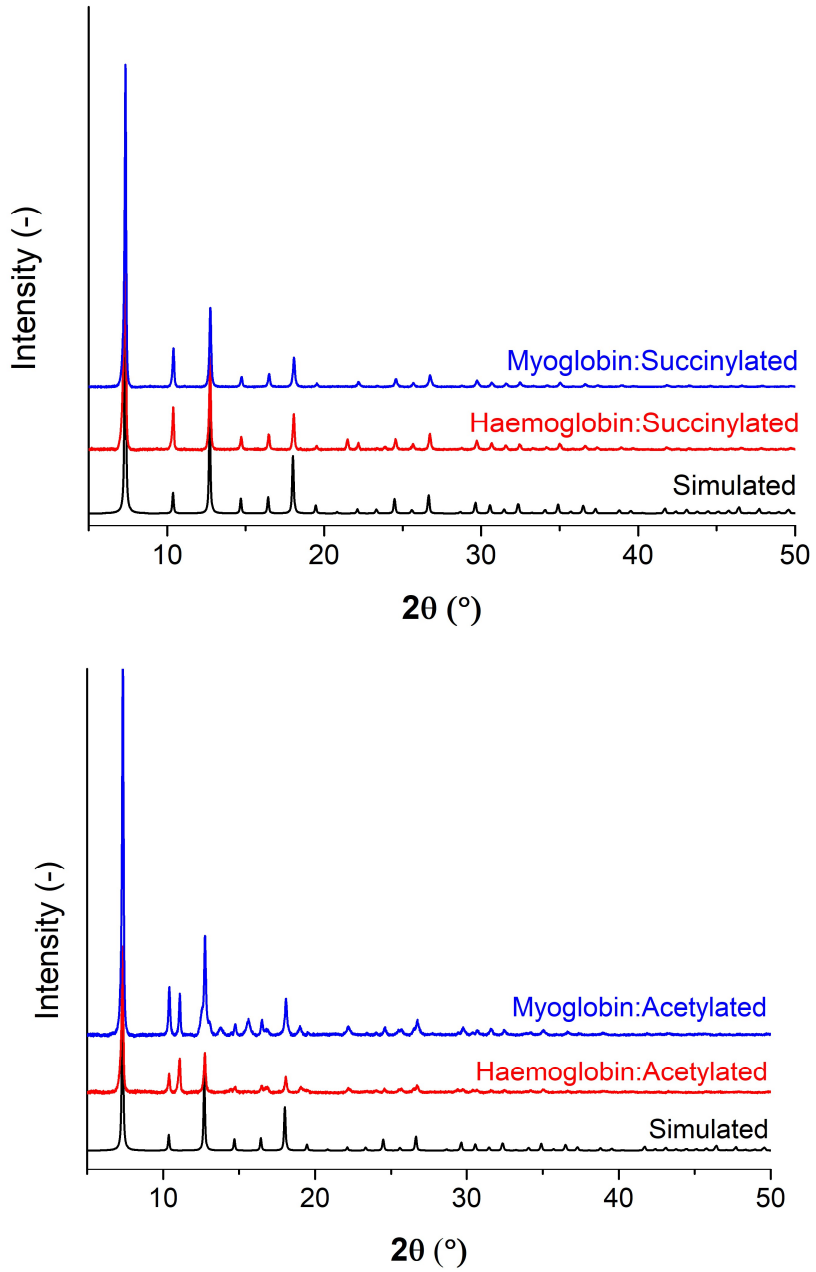

Figure S3.4: Powder X-ray diffraction patterns of biomimetically mineralised ZIF samples of HbSucc and MbSucc (top) and HbAc and MbAc (bottom) made under standard conditions (4:1 mIM:Zn^{2+}). Data collected on dried samples after washes with water and ethanol. Aminated BSA and pepsin, did not yield sufficient product for PXRD analysis. The simulated pattern relates to ZIF-8.

3.9.5. Scanning electron microscopy

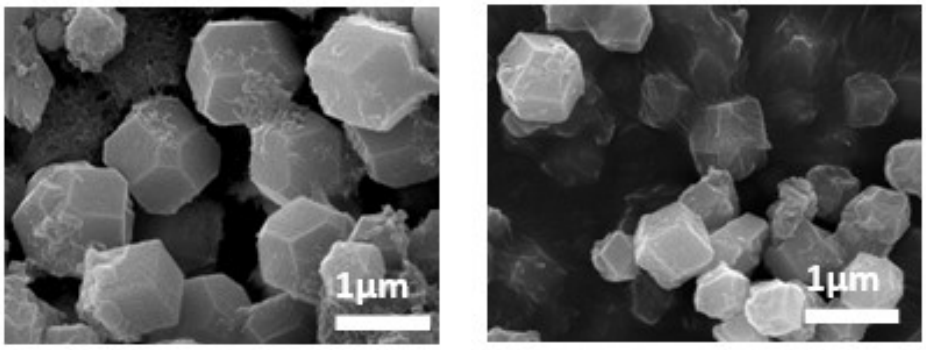

Figure S3.5: HbSucc@ZIF-8 (left) and MbSucc@ZIF-8 (right) after 16 hours from the beginning of the biomimetic mineralization reaction; the rhombic dodecahedral morphology can be observed.

3.9.6. UV-visible spectra

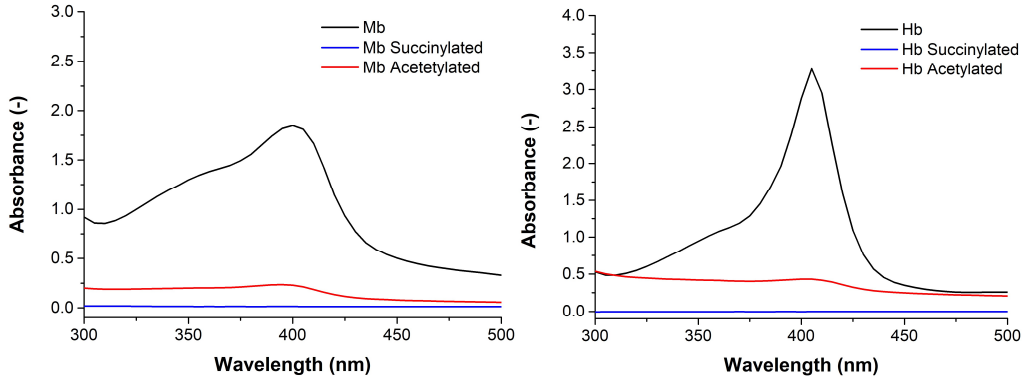

Figure S3.6: UV-visible spectra of the supernatant removed after centrifugation of the biocomposite samples where the protein was myoglobin (Mb), succinylated myoglobin (MbSucc), and acetylated myoglobin (MbAc) (left) and haemoglobin (Hb), succinylated haemoglobin (HbSucc), and acetylated haemoglobin (HbAc) (right). Unmodified haemoglobin and myoglobin formed minimal product and therefore show a large Soret absorbance in the removed solution, indicating that the protein has not been immobilised. In both the succinylated and acetylated variants, the absorbance has decreased thus indicating that the protein has been removed from solution and incorporated into ZIF-8 as it formed.

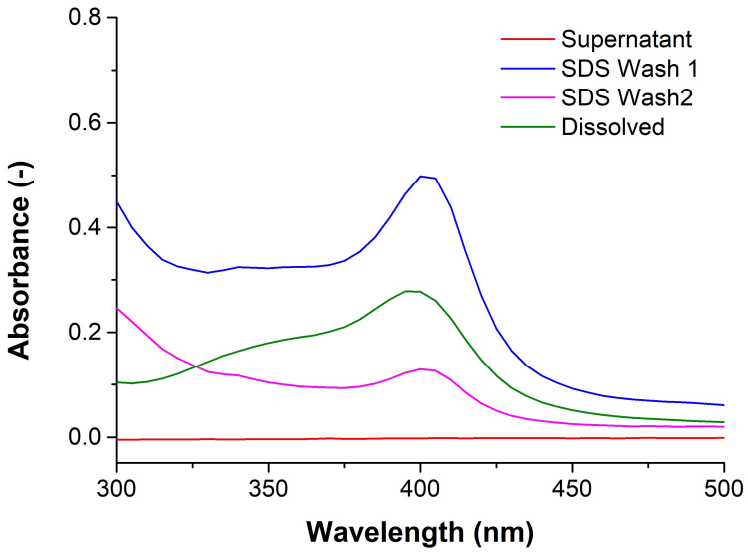

Figure S3.7: UV-visible spectra of the washings of succinylated haemoglobin ZIF-8 samples. The supernatant (red) was obtained after centrifugation of the product and shows no evidence of protein remaining in solution. SDS washes 1 (blue) and 2 (pink) show the appearance of the haemoglobin absorbance peak, indicating that some protein was surface bound had been washed off. After the SDS washes to remove surface bound protein showed nofurther protein, the ZIF-8 sample was dissolved in citric acid buffer (pH 6) containing EDTA (20 mM) and the absorbance was measured to show presence of encapsulated protein.

3.9.7. Additional computational methods

Calculation of the average hydropathic index. The hydropathic index is a measure of an amino acid sequences hydropathicity. Negative values imply an overall hydrophilic protein, whereas positive values imply an overall hydrophobic protein. The hydropathic index for a protein sequence was calculated using the Kyte and Doolittle scale of residue hydropathicity,[10] which quantifies the hydropathicity of each residue, and the Biopython module.[11-12] A single value is reported, which is the sum of the hydropathic indices of all residues divided by the length of the sequence.

Preparation of PDB files and calculation of protein charge state. Crystal structures were obtained from the Protein Data Bank[13] for each protein (PDB accession codes given in **Table S3.1)**. Where available a protein structure associated with the same organism as the experimental source was obtained. Each PDB file comes with one or more peptide chain, where each chain represents a separate sequence of amino acids in the crystal structure. For BSA, only the first polypeptide chain in the PDB file was used because this protein is expected to exist as a monomer in solution. In all other cases all chains in the PDB file were used. Heteroatoms (non-natural amino acid residues or ligands), bound ions or water molecules in the protein structures were removed.

PROPKA 3.0,[14-15] was used to estimate the pKa of each ionisable residue in each protein structure using a highly efficient, empirical method. PROPKA uses effective potentials to calculate the total environmental perturbation to the free energy of protonation due to moving the ionisable residue from water into the 3D environment of the protein. The resultant free energy was used to determine the shift in the known pKa of each residue due to the protein environment. We have confirmed that similar results are obtained for the calculated pKa's using the more sophisticated DELPHIPKA[16] to assign atom charges and protonation states (results not shown). DELPHIPKA uses a variable dielectric coefficient within the protein and the free energy difference between the protonated and deprotonated state of each ionisable residue within the 3D structure (using a Poisson–Boltzmann based approach to calculate the free energy difference) to obtain the pKa for each residue. The calculated pKa of each ionisable residue, given by PROPKA, was then used to calculate the 3D model pI of each protein using the Henderson–Hasselbach equation.

Before analysing each crystal structure, the PDB2PQR software[17-18] was used to add missing heavy atoms, to make sure there were no overlapping atoms in the structure, to

protonate the structure based on the pKa's calculated by PROPKA and the given pH (where a residue is protonated if its pKa is greater than the given pH) and to assign charges and radii from the AMBER[19] force field to each atom. We note that the AMBER force field included with PDB2PQR does not contain charge parameters for residues in certain protonation states derived by PROPKA (for example, a neutral N terminus state is not supported by the force field provided by PDB2PQR) and therefore some residues will always exist in their pH 7 state. 8. Additional computational results 8.1.

3.9.8. Additional computational results

Protein Metrics. In **Figure S3.8** we show the calculated average hydropathic index of the sequence of each protein. The results indicate that the proteins that seed ZIF-8 growth have hydropathicities that overlap completely with proteins that do not seed ZIF-8 growth. This finding further supports the dominant nature of electrostatic interactions in determining ZIF-8 formation, which allows for the use of such simplified screening methods.

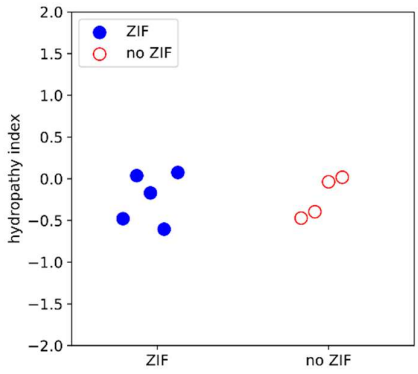

Figure S3.8: Categorical scatterplot of the average hydropathicity of the peptide sequences for all proteins. Closed circles are proteins that form ZIF-8 and open circles are proteins that do not form ZIF-8.

Comparison of pI from sequence models, 3D models and experiments. **Figure S3.9** shows categorical scatter plots of the calculated pIs from the 3D structure (obtained from PROPKA 3.0) and peptide sequence (obtained from Biopython) of each protein, which shows that both calculation methods predict ZIF-8 growth reasonably accurately. Parity plots of the pIs obtained from both calculation methods as well as a comparison between the pIs calculated from the 3D protein structure and the reported pIs (**Table 3.1**) are also shown. Importantly, reasonable agreement between the two calculation methods was obtained, indicating that the much simpler sequencebased model can be used without adversely affecting prediction

accuracy. We note that some experimental pIs are reported as a range of values, and so error bars are included in **Figure S3.9d**, for which the uncertainty encompasses the reported range and the pI is the mean of the reported range.

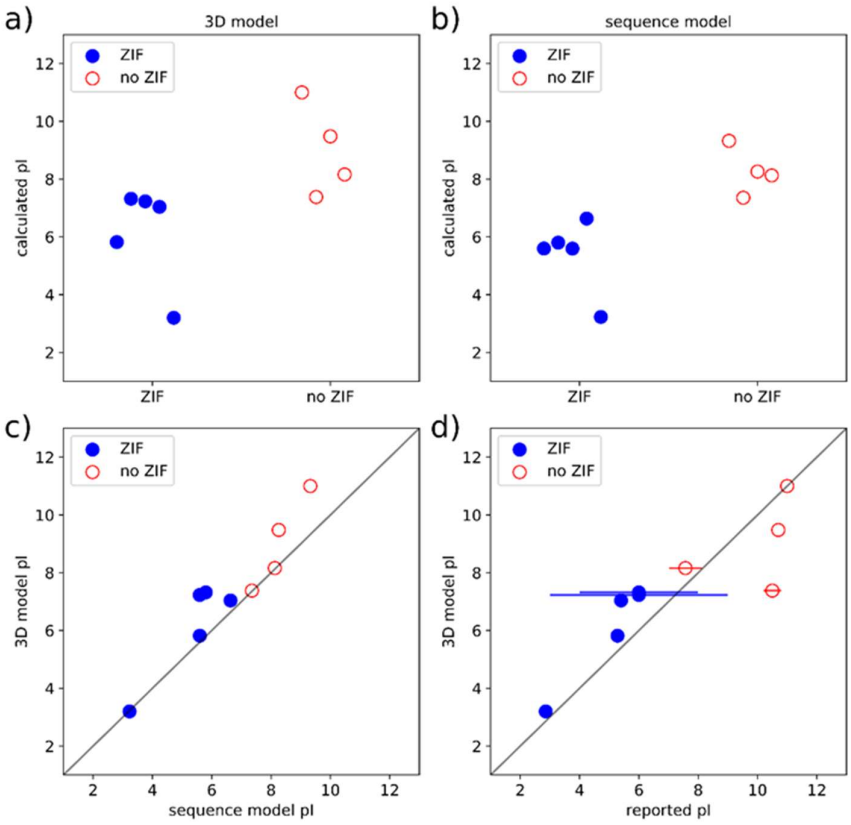

Figure S3.9: Categorical scatter plots of the calculated pI (a) from the 3D model and (b) sequence model of all proteins. Parity plots comparing the calculated pI from the 3D model and (c) the sequence model and (d) the reported pI values (the y = x line is shown). Error bars represent ranges of pI values reported from experiments. Closed circles are proteins that form ZIF-8 and open circles are proteins that do not form ZIF-8.

Experimental zinc ion enhancement. Figure S3.10 shows a categorical scatter plot of the enhancement of zinc ions calculated from the experimental zeta potentials in **Table 3.1** using Equation 4. Experimental zeta potentials give reasonable approximations of the surface electrostatic potential of each protein in solution and, therefore, a proteins ability to enhance zinc ion concentrations near the surface and, hence, seed ZIF-8 growth. Based on **Figure S3.10**, a surface zinc ion enhancement of > 10, which is a zinc ion concentration of 0.4 M, leads to ZIF-8 formation under experimental conditions.

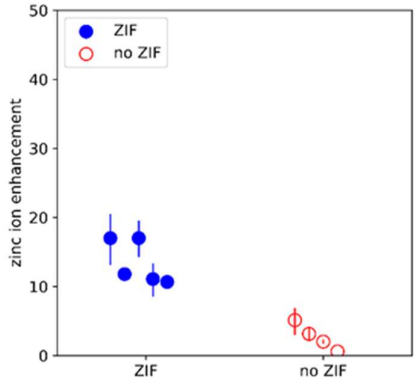

Figure S3.10: Categorical scatterplots of the zinc ion enhancements calculated from the experimental zeta potentials at pH 11 for all proteins. Closed circles are proteins that form ZIF-8 and open circles are proteins that do not form ZIF-8.

Zinc ion enhancement from 3D model. The calculated average surface potentials from the 3D model of each protein show reasonable agreement with the experimental zeta potentials (**Figure S3.11**). The main discrepancies are the overestimation of the average surface potential compared with experimental zeta potentials for very highly charged proteins, such as BSA, catalase and pepsin. This result is not unexpected, given the use of the linearised Poisson–Boltzmann equation, which breaks down in regimes of high zeta potential ($(|\zeta| > \left|\frac{k_B T}{z_+ e}\right| \approx$ 12 mV). The underestimation of the average surface potential compared with experimental zeta potentials for lipase and HRP is likely a result of experimental impurities. Both proteins are expected to be glycosylated,[20-21] which is known to affect zeta potential measurements,[22] whereas the calculations used non-glycosylated structures. Additionally, HRP could be a mixture of different iso-enzymes with vastly different electrostatic properties.[23] We note that both proteins have reported pIs that span a broad range of values (**Table 3.1**), indicating a broad range of electrostatic properties for different samples. Our calculation methodology used static 3D structures of each protein obtained from X-ray crystallography, which are unlikely to be representative of the protein structure in solution at a pH of 11. At high pHs, the presence of high-charge regions would lead to repulsion and a degree of unfolding, which such a simple model could not take into account. We also note that it has been shown previously that the interior of a protein has a highly variable dielectric coefficient and assuming a constant dielectric coefficient, as we have, can give rise to errors near the surface of proteins.[24] Furthermore, by taking the average surface potential to be equal to the experimental zeta potential for a heterogenous protein surface we assumed that the electric double layer

surrounding the protein is thin compared with the size of the protein and that the linearised Poisson–Boltzmann equation applies, which may not always be the case for the systems studied (discussed above).[25] The semi-quantitative agreement with experiment in most cases is very encouraging, considering the approximations in the calculations.

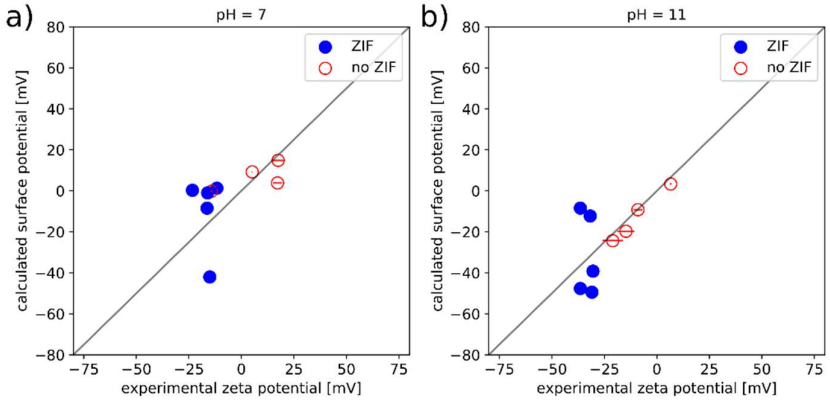

Figure S3.11: Parity plots comparing the calculated surface potential from our 3D model and experimental zeta potentials at (a) pH 7 and (b) pH 11 for all proteins (the y = x line is shown). Closed circles are proteins that form ZIF-8 and open circles are proteins that do not form ZIF-8. **Figure S3.12** shows a categorical scatter plot of the calculated average surface potentials at pH 9 and pH 11 for all proteins. These results support the experimental findings and show a reasonable ability to predict a protein's propensity to seed ZIF-8 formation. Results at pH 9 and pH 11 are shown as the initial solution (before zinc ions are added) is at approximately pH 11, but upon zinc ion addition, the pH quickly decreases to around 9, likely because of ZIF nucleation.[26] Finally, **Figure S3.13** shows the variation in the surface potential around all proteins at pH 11 calculated from our 3D model.

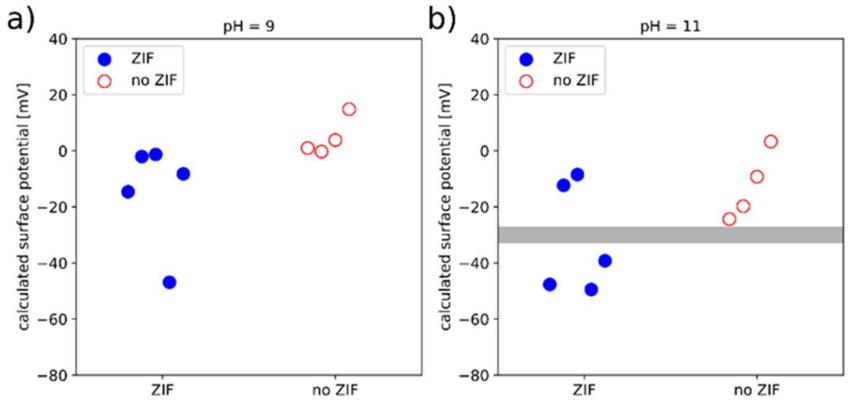

Figure S3.12: Categorical scatterplots of the calculated surface potential from the 3D model (a) at pH 9 and (b) pH 11 for all proteins. Closed circles are proteins that form ZIF-8 and open circles are proteins that do not form ZIF-8. The shaded region highlights the approximate boundary of the zeta potential in the experiments for proteins that do and do not seed ZIF-8 growth.

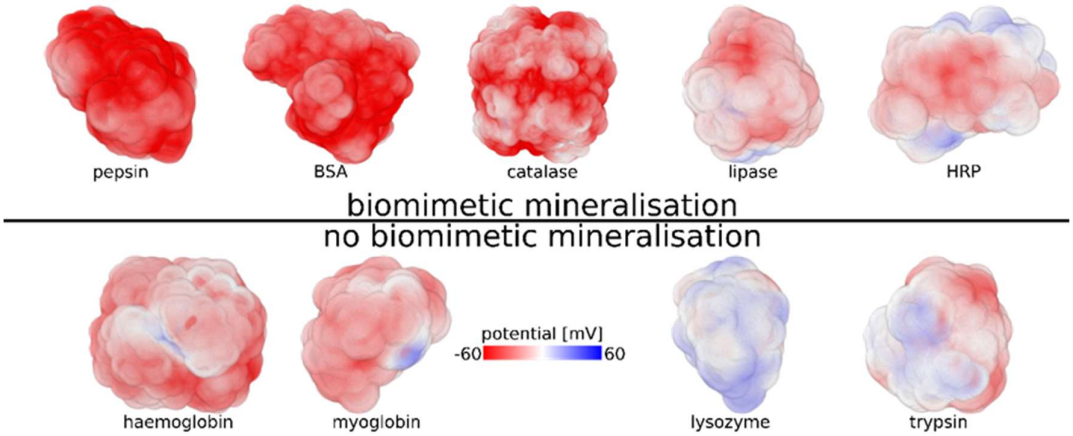

Figure S3.13: Surface potential surrounding all proteins calculated from our 3D model at pH 11. Lipase and HRP are outliers based on our analysis.

Supporting Information 3.9. References

1. Sielecki, A. R.; Fedorov, A. A.; Boodhoo, A.; Andreeva, N. S.; James, M. N. G., Molecular and crystal structures of monoclinic porcine pepsin refined at 1.8Å resolution. *J. Mol. Biol.* **1990,** *214* (1), 143-170.

2. Bujacz, A., Structures of bovine, equine and leporine serum albumin. *Acta Crystallogr. Sect. D. Biol. Crystallogr.* **2012,** *68* (10), 1278-1289.

3. Uppenberg, J.; Hansen, M. T.; Patkar, S.; Jones, T. A., The sequence, crystal structure determination and refinement of two crystal forms of lipase B from *Candida antarctica*. *Structure* **1994,** *2* (4), 293-308.

4. Purwar, N.; McGarry, J. M.; Kostera, J.; Pacheco, A. A.; Schmidt, M., Interaction of nitric oxide with catalase: structural and kinetic analysis. *Biochemistry* **2011,** *50* (21), 4491-4503.

5. Carlsson, G. H.; Nicholls, P.; Svistunenko, D.; Berglund, G. I.; Hajdu, J., Complexes of horseradish peroxidase with formate, acetate, and carbon monoxide. *Biochemistry* **2005,** *44* (2), 635-642.

6. Copeland, D. M.; Soares, A. S.; West, A. H.; Richter-Addo, G. B., Crystal structures of the nitrite and nitric oxide complexes of horse heart myoglobin. *J. Inorg. Biochem.* **2006,** *100* (8), 1413-1425.

7. Park, S.-Y.; Yokoyama, T.; Shibayama, N.; Shiro, Y.; Tame, J. R. H., 1.25 Å Resolution crystal structures of human haemoglobin in the oxy, deoxy and carbonmonoxy forms. *J. Mol. Biol.* **2006,** *360* (3), 690-701.

8. Transue, T. R.; Krahn, J. M.; Gabel, S. A.; DeRose, E. F.; London, R. E., X-ray and NMR characterization of covalent complexes of trypsin, borate, and alcohols. *Biochemistry* **2004,** *43* (10), 2829-2839.

9. Wang, J.; Dauter, M.; Alkire, R.; Joachimiak, A.; Dauter, Z., Triclinic lysozyme at 0.65 A resolution. *Acta Crystallogr. Sect. D. Biol. Crystallogr.* **2007,** *63* (12), 1254-1268.

10. Kyte, J.; Doolittle, R. F., A simple method for displaying the hydropathic character of a protein. *J. Mol. Biol.* **1982,** *157* (1), 105-132.

11. Hamelryck, T.; Manderick, B., PDB file parser and structure class implemented in Python. *Bioinformatics* **2003,** *19* (17), 2308-2310.

12. Cock, P. J. A.; Antao, T.; Chang, J. T.; Chapman, B. A.; Cox, C. J.; Dalke, A.; Friedberg, I.; Hamelryck, T.; Kauff, F.; Wilczynski, B.; de Hoon, M. J. L., Biopython: freely

available Python tools for computational molecular biology and bioinformatics. *Bioinformatics* **2009,** *25* (11), 1422-1423.

13. Berman, H. M.; Westbrook, J.; Feng, Z.; Gilliland, G.; Bhat, T. N.; Weissig, H.; Shindyalov, I. N.; Bourne, P. E., The Protein Data Bank. *Nucleic Acids Res.* **2000,** *28* (1), 235-242.

14. Søndergaard, C. R.; Olsson, M. H. M.; Rostkowski, M.; Jensen, J. H., Improved treatment of ligands and coupling effects in empirical calculation and rationalization of pKa values. *J. Chem. Theory. Comput.* **2011,** *7* (7), 2284-2295.

15. Olsson, M. H. M.; Søndergaard, C. R.; Rostkowski, M.; Jensen, J. H., PROPKA3: Consistent treatment of internal and surface residues in empirical pKa predictions. *J. Chem. Theory. Comput.* **2011,** *7* (2), 525-537.

16. Wang, L.; Li, L.; Alexov, E., pKa predictions for proteins, RNAs, and DNAs with the Gaussian dielectric function using DelPhi pKa. *Proteins* **2015,** *83* (12), 2186-2197.

17. Dolinsky, T. J.; Nielsen, J. E.; McCammon, J. A.; Baker, N. A., PDB2PQR: an automated pipeline for the setup of Poisson–Boltzmann electrostatics calculations. *Nucleic Acids Res.* **2004,** *32*, W665-W667.

18. Dolinsky, T. J.; Czodrowski, P.; Li, H.; Nielsen, J. E.; Jensen, J. H.; Klebe, G.; Baker, N. A., PDB2PQR: expanding and upgrading automated preparation of biomolecular structures for molecular simulations. *Nucleic Acids Res.* **2007,** *35*, W522-W525.

19. Wang, J.; Cieplak, P.; Kollman, P. A., How well does a restrained electrostatic potential (RESP) model perform in calculating conformational energies of organic and biological molecules? *J. Comput. Chem.* **2000,** *21* (12), 1049-1074.

20. Spadiut, O.; Rossetti, L.; Dietzsch, C.; Herwig, C., Purification of a recombinant plant peroxidase produced in Pichia pastoris by a simple 2-step strategy. *Protein Expr. Purif.* **2012,** *86* (2), 89-97.

21. Høegh, I.; Patkar, S.; Halkier, T.; Hansen, M. T., Two lipases from *Candida antarctica*: cloning and expression in aspergillus oryzae. *Can. J. Bot.* **1995,** *73* (S1), 869-875.

22. Kreuß, M.; Strixner, T.; Kulozik, U., The effect of glycosylation on the interfacial properties of bovine caseinomacropeptide. *Food Hydrocol.* **2009,** (7), 1818-1826.

23. Hoyle, M. C., High resolution of peroxidase-indoleacetic acid oxidase isoenzymes from horseradish by isoelectric focusing. *Plant. Physiol.* **1977,** *60* (5), 787-793.

24. Li, L.; Li, C.; Zhang, Z.; Alexov, E., On the dielectric "constant" of proteins: smooth dielectric function for macromolecular modeling and its implementation in DelPhi. *J. Chem. Theory Comput.* **2013,** *9* (4), 2126-2136.

25. Fogolari, F.; Zuccato, P.; Esposito, G.; Viglino, P., Biomolecular electrostatics with the linearized Poisson-Boltzmann equation. *Biophys. J.* **1999,** *76* (1 Pt 1), 1-16.

26. Jian, M.; Liu, B.; Liu, R.; Qu, J.; Wang, H.; Zhang, X., Water-based synthesis of zeolitic imidazolate framework-8 with high morphology level at room temperature. *RSC. Adv.* **2015,** *5* (60), 48433-48441.

Chapter 4.

Influence of Fabrication Conditions and Formation Kinetics on the Activity of *Candida antarctica* Lipase B ZIF-8 Biocomposites

This work is to be submitted for publication.

Statement of Authorship

Title of Paper	Influence of Fabrication Conditions and Formation Kinetics on the Activity of *Candida antarctica* Lipase B ZIF-8 Biocomposites.
Publication Status	☐ Published ☐ Accepted for Publication ☐ Submitted for Publication ☑ Unpublished and Unsubmitted work written in manuscript style
Publication Details	Unsubmitted, written in manuscript style

Principal Author

Name of Principal Author (Candidate)	Natasha K. Maddigan		
Contribution to the Paper	Experimental, manuscript writing, and editing		
Overall percentage (%)	90%		
Certification:	This paper reports on original research I conducted during the period of my Higher Degree by Research candidature and is not subject to any obligations or contractual agreements with a third party that would constrain its inclusion in this thesis. I am the primary author of this paper.		
Signature		Date	10/03/20

Co-Author Contributions

By signing the Statement of Authorship, each author certifies that:

i. the candidate's stated contribution to the publication is accurate (as detailed above);
ii. permission is granted for the candidate in include the publication in the thesis; and
iii. the sum of all co-author contributions is equal to 100% less the candidate's stated contribution.

Name of Co-Author	Oliver Linder-Patton		
Contribution to the Paper	Sample characterisation (SEM). Aided in manuscript drafting		
Signature		Date	17/03/20

Name of Co-Author	Paolo Falcaro		
Contribution to the Paper	Aided in manuscript writing, and drafting.		
Signature		Date	09/03/2020

Pleas

Name of Co-Author	Christopher J. Sumby
Contribution to the Paper	Supervised experimental work. Aided in manuscript writing, and drafting.
Signature	Date 17/03/2020

Name of Co-Author	Stephen. G. Bell
Contribution to the Paper	Supervised experimental work. Aided in manuscript writing, and drafting.
Signature	Date 17/03/2020

Name of Co-Author	Christian J. Doonan
Contribution to the Paper	Supervised experimental work. Aided in manuscript writing, and drafting.
Signature	Date 17/03/2020

Chapter 4. Influence of Fabrication Conditions and Formation Kinetics on the Activity of *Candida antarctica* Lipase B ZIF-8 Biocomposites

4.1. Abstract

The biomimetic mineralisation of ZIF-8 has been widely reported as a strategy for enzyme immobilisation, enabling the heterogenisation and protection of biomacromolecules. Here, we report the preparation of different *Candida antarctica* lipase B biocomposites (CALB@ZIF-8) of different particle size by altering the concentrations of Zn^{2+} and 2-methylimidazole (2-mIM). The influence of synthetic conditions on the catalytic activity of CALB was measured by hydrolysis and transesterification assays. We demonstrated that for both reactions, activity was retained for the biocomposites formed at low 2-mIM:Zn^{2+} but almost entirely lost when the ligand concentration was increased. Additionally, phosphate buffer could regenerate the activity of larger particles by degrading the crystal surfaces and releasing encapsulated CALB into solution. The transesterification reactions were undertaken in 100% hexane, giving rise to enhanced CALB activity relative to the free enzyme. These observations highlight the fundamental importance of synthetic protocols and solvent selection for developing enzyme MOF biocomposites with improved activity in challenging conditions.

4.2. Introduction

Enzymes are protein catalysts that function under mild biological conditions, providing an alternate, low energy pathway for complex chemical reactions.[1] In general, enzyme reactions are rapid and highly selective under ambient conditions and as such they are sought after for application to industrial processes.[2-3] However, their catalytic output is often restricted by the necessity of aqueous conditions which limits the substrate range and concentration that is tolerated by the enzyme.[4-5] Thus, challenges include improving the tolerance of enzymes to high substrate concentration and challenging conditions, such as organic solvents and elevated temperatures.[6]

Immobilisation of enzymes directly onto, or within a solid support, is one strategy that has been explored to protect enzymes from harsh conditions whilst additionally facilitating reusability.[7-8] Metal-organic frameworks (MOFs) are a class of extended solids that have recently shown promise for enzyme immobilisation.[8-13] Enzyme-MOF composites can be synthesised via infiltrating biomacromolecules into the framework pores,[14] surface adsorption,[15] covalent attachment,[16] and 'one-pot' encapsulation of enzymes within MOF crystals.[17] Zeolitic imidazolate-8 (ZIF-8), a porous framework composed of tetrahedral Zn^{2+} ions linked via 2-methylimidazole (2-mIM), is commonly utilised for its porosity and thermal stability.[18-19] Recently it has been shown that enzymes can induce the growth of ZIF-8 crystals from its precursors (Zn^{2+} and 2-mIM) in aqueous conditions.[20] This process termed 'biomimetic mineralisation' yields enzyme@MOF biocomposites where the biomacromolecule is encapsulated within the ZIF-8 crystals. The formation of enzyme@ZIF-8 biocomposites of uniform size (ca. 1 μm), topology (sodalite; *sod*), and morphology (rhombic dodecahedral; RD) can be achieved using either high precursor concentrations or a high 2-mIM: Zn^{2+} ratio.[21] Conversely, dilute or low ratio precursors give rise to a variety of network topologies and morphologies including an amorphous phase that requires ethanol washing to generate, crystalline, phase pure sodalite frameworks.[22] Presumably, modulating the biocomposite synthesis conditions and precursor concentration/ ratio, gives rise to the different nucleation and growth rates, that determine the wide variety of observed ZIF phases. Understanding the synthetic conditions required to predicably yield a ZIF-based biocomposite of a specific topology/morphology is essential as each ZIF phase possesses distinct physical properties that have a direct input on catalysis. For

example, ZIF-8 (sodalite; *sod*) is porous whereas its denser counterpart ZIF-8 (diamondoid; *dia*) is non-porous.[23]

It can be anticipated that the crystal properties will influence the catalytic output of the biocomposite as the particle size will affect composite stability, enzyme spatial distribution, and mass transfer (diffusion) of substrates and products. In addition, reports have shown that phosphate containing solutions cause rapid degradation of ZIF particles due to the high affinity of Zn^{2+} for the phosphate anions.[24-26] The rate of this degradation is known to be size dependent and may account for conflicting reports of biocomposite activity reported in the literature. For example, we have previously shown that catalase immobilisation within ZIF-8 generates an inactive biocomposite due to the frameworks hydrophobicity.[27] However, there are literature reports that catalase@ZIF-8 biocomposites are active when stored and tested in phosphate buffered saline (PBS).[28-30] Accordingly, we were motivated to understand the underlying chemistry of how biocomposite activity is related to crystal size and handling conditions.

In this present work, we synthesised ZIF-based biocomposites of *Candida antarctica lipase B* (CALB) using different metal : ligand ratios (yielding particle sizes of 500 nm to 1 μm) and assessed how activity was influenced by handling conditions (phosphate buffer) and crystal size. Though lipases have been immobilised onto various MOF supports, to date the effect of synthetic conditions, particle size, topology, and solvents have not been systematically investigated.[17, 31-33] We found that phosphate buffer mediated degradation facilitated hydrolytic activity after prolonged exposure regardless of the crystal preparation conditions (**Figure 4.1**). However, an additional and noteworthy result is that the activity of CALB@ZIF-8 biocomposites was dependent on crystal size, which is determined by the precursor concentrations used to synthesise ZIF-8. These findings highlight that both preparation and handling conditions can affect the biocatalytic activity of ZIF-based biocomposites

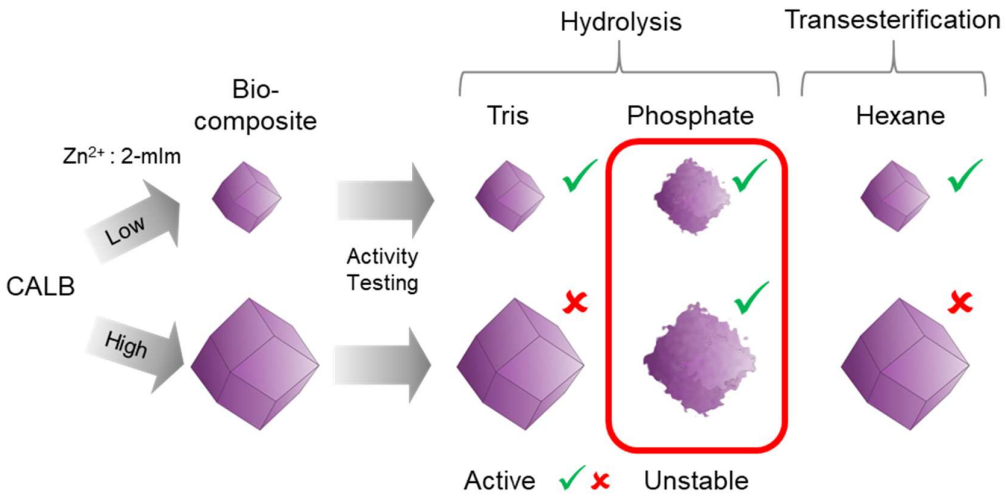

Figure 4.1: Schematic representation of the relationship between particle size, solvent stability and enzymatic activity of CALB@ZIF -8 biocomposites. Small (500 nm) particles can be synthesised using a low 2-mIM: Zn^{2+} ratio, which generate active (✓) CALB@ZIF-8 biocomposites whilst larger (1 µm) crystals are formed using a higher 2-mIM: Zn^{2+} ratio and are inactive (✗). Standard activity was measured via two reactions: hydrolysis in aqueous tris buffered media and transesterification in hexane. An additional hydrolysis reaction in phosphate buffer caused size dependant crystal degradation that led to the restoration of activity of the larger biocomposites (**Figure 4.6**, **S4.12**).

4.3. Results and Discussion

4.3.1. CALB@ZIF-8 Synthesis

Lipase B from *Candida antarctica* (CALB) was chosen as the enzyme for this study for its low isoelectric point that can mediate ZIF-8 biomimetic mineralisation at low 2-mIM concentrations, and for its proven stability to a broad pH range.[34-35] CALB@ZIF-8 biocomposites were synthesised using a range of Zn^{2+} and 2-mIM ratios with the ligand concentration ranging from 80-640 mM in the final solution. Specifically, a zinc acetate dihydrate solution (2 mL) was mixed with a solution of 2-mIM (2 mL) containing CALB (2 mg powder) such that the final Zn^{2+}: 2-mIM concentrations were 20:80, 20:160, 20:400, and 40:640 mM. This procedure gave rise to biocomposites with particle size distributions of 0.57 ± 0.02 μm, 0.71 ± 0.02 μm, 1.06 ± 0.03 μm, and 1.13 ± 0.03 μm, respectively (**Figure 4.2**). At low ratios, the rate of precipitate formation is accelerated in the presence of CALB, however this effect was reduced as the 2-mIM concentration increased (**Figure S4.1**). This suggests that the formation of the crystalline biocomposites is influenced by the enzyme at low ratios but is dominated by the 2-mIM concentration at high ratios. As such, we chose precursor ratios that would generate ZIF-8 biocomposites via competing nucleation mechanisms. For example, at low Zn^{2+}: 2-mIM ratios (20:80, 20:160 mM), crystal formation is induced by the presence of the biomacromolecule, whereas higher ratio preparations (20:400, 40:640 mM) can form from the precursors alone (**Figure S4.1**). This is consistent with previous observations where excess ligand (Zn^{2+}: 2-mIM ratios, 40:1200 and 40:1600 mM) precipitate crystals, albeit of reduced particle size, with a loss of edge definition. In this case the basic solution, that results from excess 2-mIM, controls crystal formation.[21]

Low 2-MIM: Zn^{2+} ratios can produce a number of different phases which when washed with ethanol yield a phase change to pure, sodalite (*sod*) topology. However, high ratios form sodalite samples without requiring an ethanol wash.[21-22] Consistent with previously reported data, the water washed samples of 20:80 and 20:160 generated ZIF-C,[22, 36] and diamondoid (*dia*) topologies, respectively, whilst the higher ratio samples (20:400, 40:640) favoured the sodalite topology (**Figure 4.3a**). For consistency, each sample was also washed with ethanol to ensure that only sodalite ZIF-8 was present (confirmed by PXRD) (**Figure 4.3b**). This yielded two sets of samples for activity studies (water vs ethanol washed).

We also ensured that the free enzyme maintained full activity after exposure to the most concentrated 2-mIM (~pH 11) solution to confirm that initial enzyme exposure to the precursors did not modify its activity (**Figure S4.2**). Given that deactivation was not observed, enzyme activity upon immobilisation could be analysed relative to each CALB@ZIF-8 biocomposite synthetic protocol.

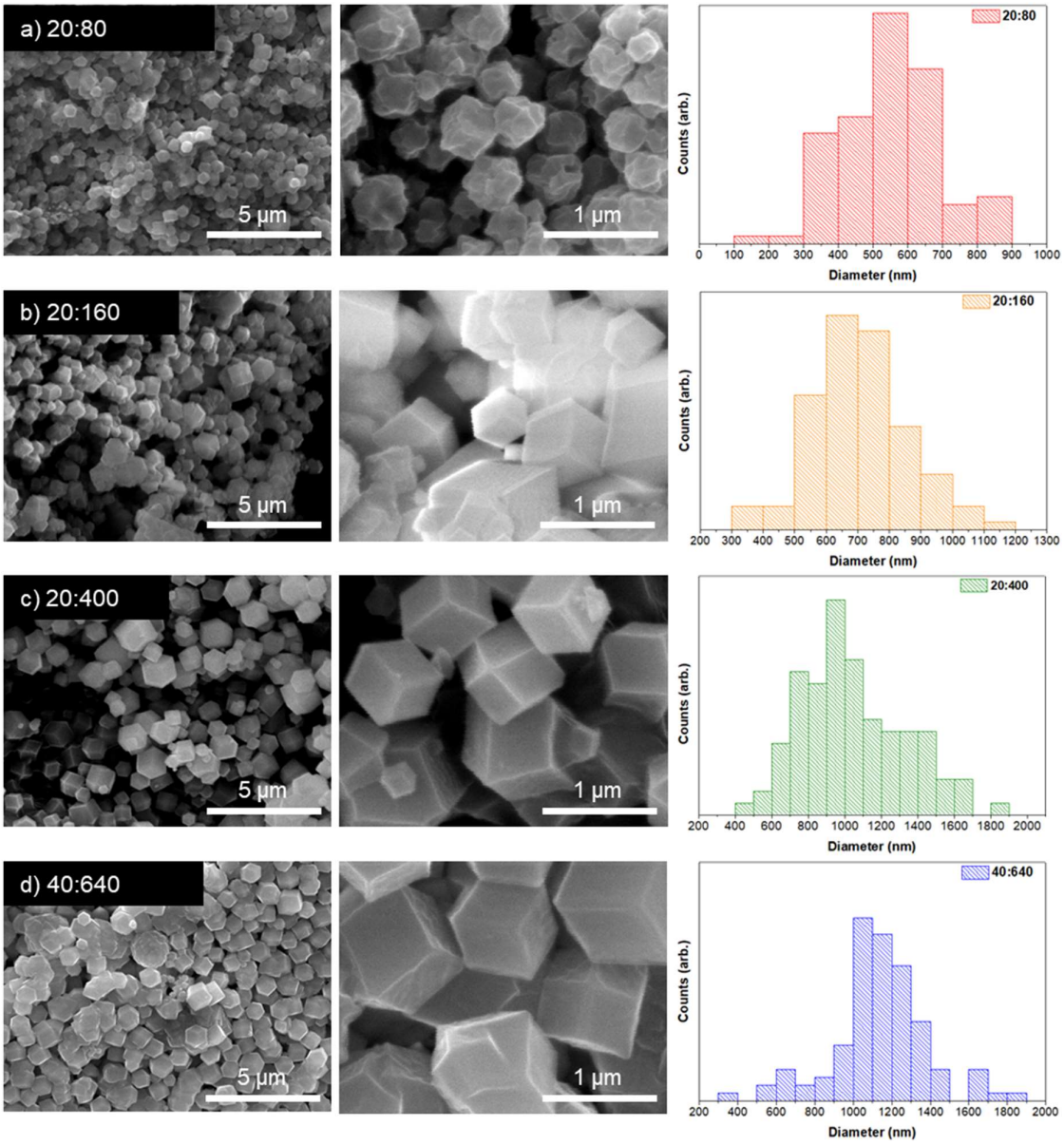

Figure 4.2: SEM images of each CALB@ ZIF-8 preparation (Zn^{2+}:2-mIM concentrations, mM) with corresponding particle size distributions. Mean particle sizes were calculated to be a) 571 ± 18 nm, b) 709 ± 15 nm, c) 1.06 ± 0.03 µm, d) 1.13 ± 0.03 µm.

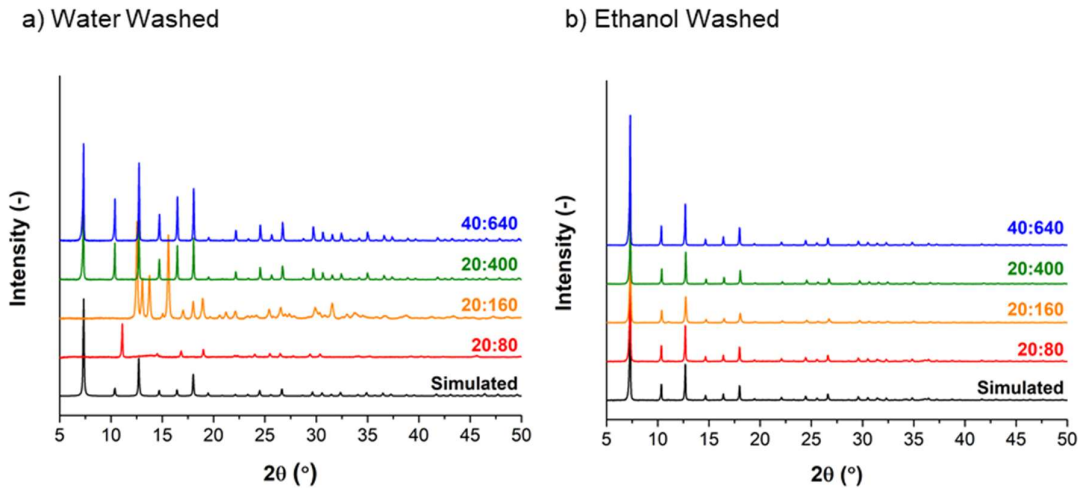

Figure 4.3: Powder X-ray Diffraction (PXRD) patterns of each CALB@ZIF-8 biocomposite after two water washes (a) and two additional ethanol washes (b). Samples were air dried at room temperature overnight, and gently ground prior to analysis.

4.3.3. Spatial Distribution Analysis with ZIF-8 Biocomposites

We investigated the spatial localisation of CALB within the ZIF-8 crystals by performing Confocal Laser Scanning Microscopy (CLSM) on biocomposites synthesised from fluorescein isothiocyanate tagged CALB (FITC-CALB) (**Figure 4.4, S4.3**). Close inspection of the CLSM images indicated co-localisation of the enzyme with the crystals; however, the precise spatial distribution could not be determined due to small particle size and crystal aggregation (**Figure 4.4**). Analysis of the supernatants via UV-Vis spectroscopy and SDS-PAGE detected no protein, indicating complete protein immobilisation for all biocomposites (**Figure S4.4**).

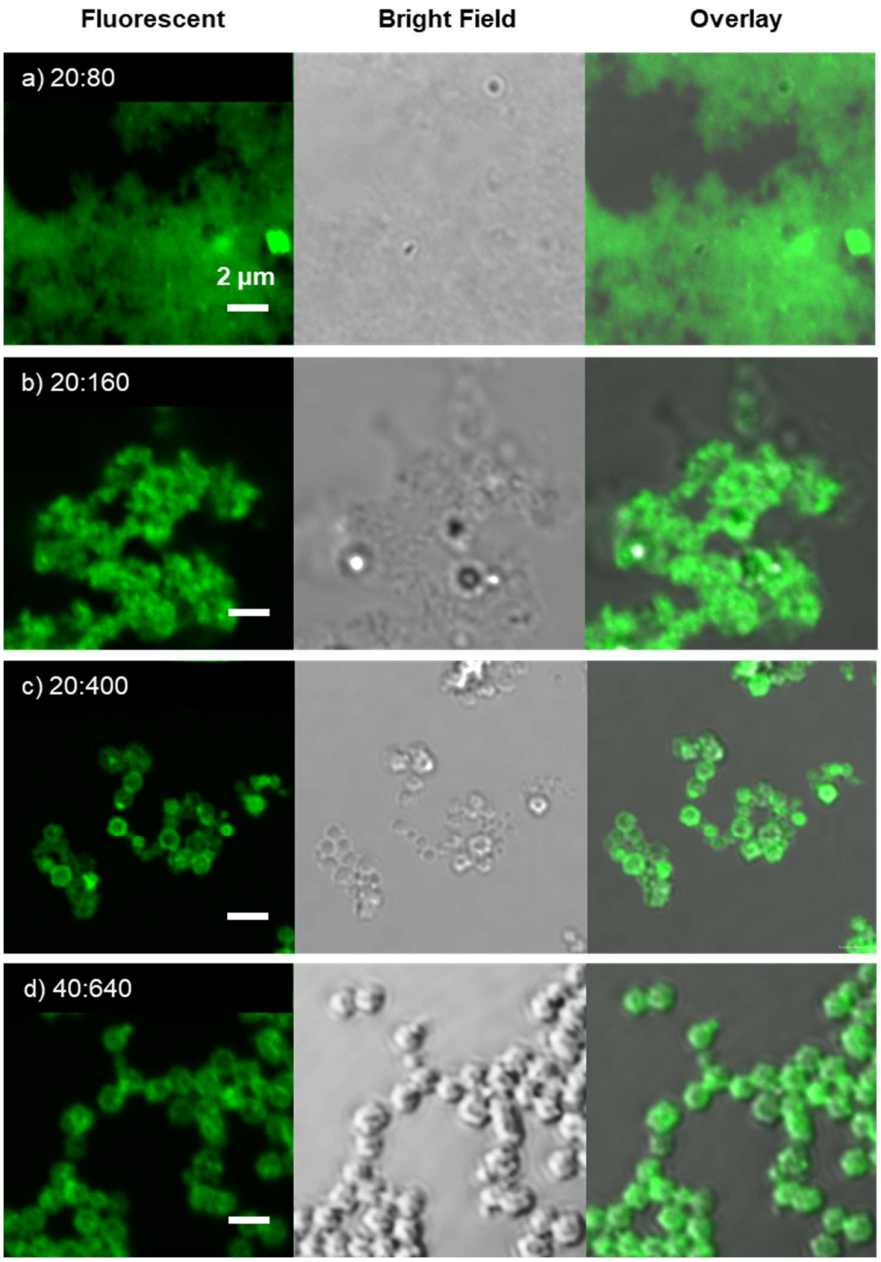

Figure 4.4: Confocal Laser Scanning Microscopy (CLSM) images of ethanol washed FITC-CALB@ZIF-8 biocomposites, showing the fluorescence, bright field and overlay images. All samples were dispersed in ethanol and dried on a glass slide prior to analysis. Attempts were then made to treat the different biomineralised ZIF-8 samples to remove surface bound enzyme however, due to the small sample sizes, 100% removal of surface enzyme could not be confirmed (**Figure S4.22-S4.24**).

4.3.4. CALB@ZIF-8 Activity Testing (Hydrolysis)

The hydrolysis activity of each CALB@ZIF-8 biocomposite was determined for water and ethanol washed samples, by measuring the rate of *p*-nitrophenyl butyrate (*p*-NPB) hydrolysis in tris buffer, 50 mM, pH 7.4 containing 0.1% Triton X-100 (**Figure 4.5, Table 4.1, Figure S4.5**). The water washed 20:80 CALB@ZIF-8 sample, i.e. the biocomposite with the smallest particle size and ZIF-C topology, showed an enhanced rate of *p*-NPB hydrolysis compared to the BSA@ZIF-8 controls (BSA = Bovine serum Albumin, **Figure S4.6**). Slightly lower activity was observed for the 20:160 biocomposite, however materials prepared using 2-mIM: Zn^{2+} ratios of 20:400 and 40:640 showed significantly reduced *p*-nitrophenol production. The post ethanol washed 20:80 (i.e. ZIF-C to *sod*) sample showed a 50% reduction in activity whilst the 20:160 (*dia* to *sod*) sample maintained full activity (**Figure S4.5**). In comparison, the 20:400 and 40:640 ethanol washed samples (*sod*) were inactive.

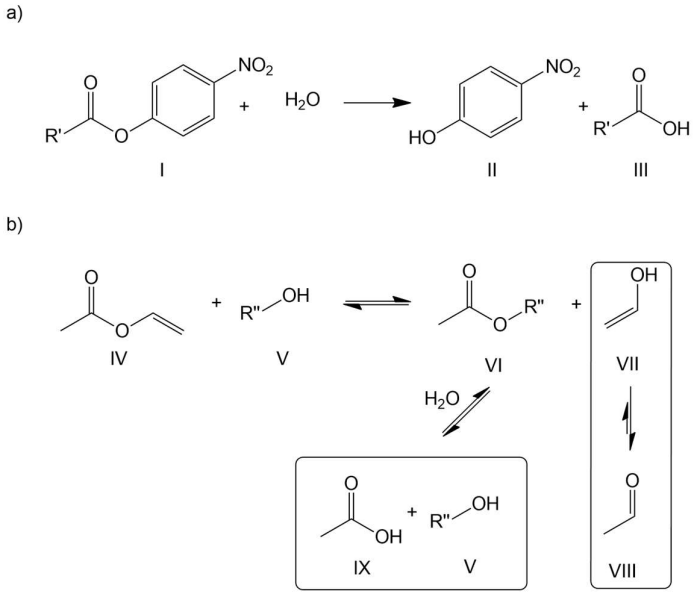

Figure 4.5: General reaction scheme showing the reactions catalysed by CALB. a) The hydrolysis of *p*-nitrophenyl esters **I** (R'=4, *p*-nitrophenyl butyrate; *p*-NPB) to generate *p*-nitrophenol **II** and a carboxylic acid **III** (butyric acid). b) The transesterification of vinyl acetate **IV** with an alcohol V (R"=6, hexanol) to generate an ester **VI** (hexyl acetate) and vinyl alcohol **VII**. Vinyl alcohol rapidly tautomerises to acetaldehyde **VIII**, inhibiting the reverse reaction. In the presence of water, the ester product **VI** can be hydrolysed to form acetic acid **IX** and the initial alcohol **V**.

Given that CALB was stable to the highest 2-mIM concentration, (**Figure S4.2**) we hypothesized that the variation in activity may arise from structural differences between the biocomposites. Accordingly, we analysed the porosity of the CALB@ZIF-8 samples by performing 77 K N_2 adsorption isotherms (**Figure S4.7**). Brunauer-Emmett-Teller (BET) analysis yielded surface areas of 1026 ± 4, 248 ± 2, 1570 ± 11 1956 ± 20 m^2/g, for the 20:80, 20:160, 20:400, and 40:640 samples respectively (**Figure S4.7a**). The 20:80 and 20:160 samples were not stable to activation conditions used for the 20:400 and 40:640 samples and required the use of milder activation conditions that allowed for BET surface area and pore size analysis of the 20:80 sample. Furthermore, pore size distribution analysis, (**Figure S4.7b**), calculated via DFT N_2 model (DFT = density functional theory), revealed the presence of larger pores (10.9, 17.3 Å) in the samples formed at lower Zn^{2+}:2-mIM ratios (20:80) compared to the 20:400 and 40:640 samples (10.9,13.6 Å). These data indicate that the biocomposites of smaller crystal size, which retain activity, possess a more hierarchical pore structure which also reflects the qualitative difference in biocomposite formation kinetics. In summary, the different pore structure of the CALB@ZIF-8 biocomposites may influence the activity of the biocomposites as larger pore size would favour the diffusion of substrate molecules.[37] Furthermore, the more heterogeneous pore structure could facilitate trapping partially embedded enzymes that are not hindered by mass transfer to the same extent as fully embedded enzymes.[38]

Table 4.1: a) Rate of hydrolysis measured as of *p*-nitrophenol production of each ZIF-8 biocomposite in tris and phosphate buffer after 0 minutes of incubation. b) Percentage conversion of hexanol into hexyl acetate after 24 hours in hexane.

Biocomposite		**Hydrolysis (μM.min^{-1})[a]**				**Transesterification (% conversion)[b]**
(Zn2+: 2-mIM)	Size (μm)	Tris		Phosphate		Hexane
		Water Washed	Ethanol Washed	Water Washed	Ethanol Washed	Ethanol Washed
20:80	0.57 ± 0.02	3.7 ± 0.1	2.5 ± 0.1	4.7 ± 0.1	2.5 ± 0.1	97
20:160	0.71 ± 0.02	3.6 ± 0.1	3.6 ± 0.4	3.8 ± 0.3	4.6 ± 0.1	97
20:400	1.06 ± 0.03	0.5 ± 0.0	0.3 ± 0.1	0.5 ± 0.0	0.6 ± 0.0	5
40:640	1.13 ± 0.03	0.2 ± 0.1	0.0 ± 0.2	0.7± 0.0	0.6 ± 0.1	2

To assess the contribution of surface bound enzyme to the biocomposite activity CALB was adsorbed onto the surface of protein free samples of ZIF-8, 1 μm synthesised using a

Zn^{2+}:2-mIM ratio of 40:640 (Supporting information **Section 4.9.6, Figure S4.9-S4.10**). For these materials the rate of hydrolysis of *p*-NPB did not increase significantly relative to the biomimetically mineralised sample (**Figure S4.10a**). To assess the potential effects of surface enzyme crowding on activity, we decreased the mass of support used to increase coverage on the ZIF surface. Thus, potentially increasing favourable enzyme-enzyme interactions that could reduce the inhibitory effect of the ZIF-enzyme surface interactions on enzyme activity. However, the increased enzyme surface coverage did not alter the rate, reinforcing the idea that large ZIF-8 particles are unsuitable for CALB immobilisation (**Table S4.1, Figure S4.10**). Analysis of the supernatant of the surface only samples, indicated that near 100% adsorption of CALB (and FITC-CALB) was possible, but this reduced when the mass of support was decreased. It has been reported for non-MOF immobilisation that the support particle size can effect activity due to variations in the degree of enzyme-enzyme interaction, enzyme-support interaction, and enzyme position and orientation on the support.[39-41] We therefore postulate, that there is a feature of the larger, more stable and highly crystalline ZIF-8 that is disfavours CALB activity. Encapsulating the enzyme within or adsorbing the enzyme to the surface of the crystals (40:640 sample) gave rise to inactive biocomposites, indicating that the enzyme-ZIF surface interactions are deactivating the enzyme.

Next, we sought to understand the effect of different buffers on biocomposite activity. Each biocomposite, both water and ethanol washed samples, were assayed in 50 mM phosphate buffer, pH 7.4 containing 0.1% Triton X-100. All ZIF-8 bio composites were marginally more active than in the tris assay, however the trend in the small versus large samples remained unchanged (**Table 4.1, Figure 4.6, Figure S4.11**). Incubating the sample in phosphate buffer for 15- or 30- minutes prior to substrate addition resulted in an increase in enzymatic activity that was not observed for the tris samples (**Figure 4.6, S4.12**). The larger crystal samples increased in activity to a rate that is comparable to the smaller, ethanol washed samples, 3.0 ± 0.0 and 4.6 ± 0.0 $\mu M.min^{-1}$ respectively. After incubation in buffer, each composite was pelletised via centrifugation and filtered through a 0.2 μm filter to remove particles larger than the membrane and the flow through was assayed for the same reaction. The filtrate of all the active samples retained activity in the filtrate suggesting that either enzyme had leached off of the surface of the crystals, and/or CALB@ZIF-8 particles smaller than the membrane were contributing to the activity (**Figure 4.2, 4.6, S4.12**).

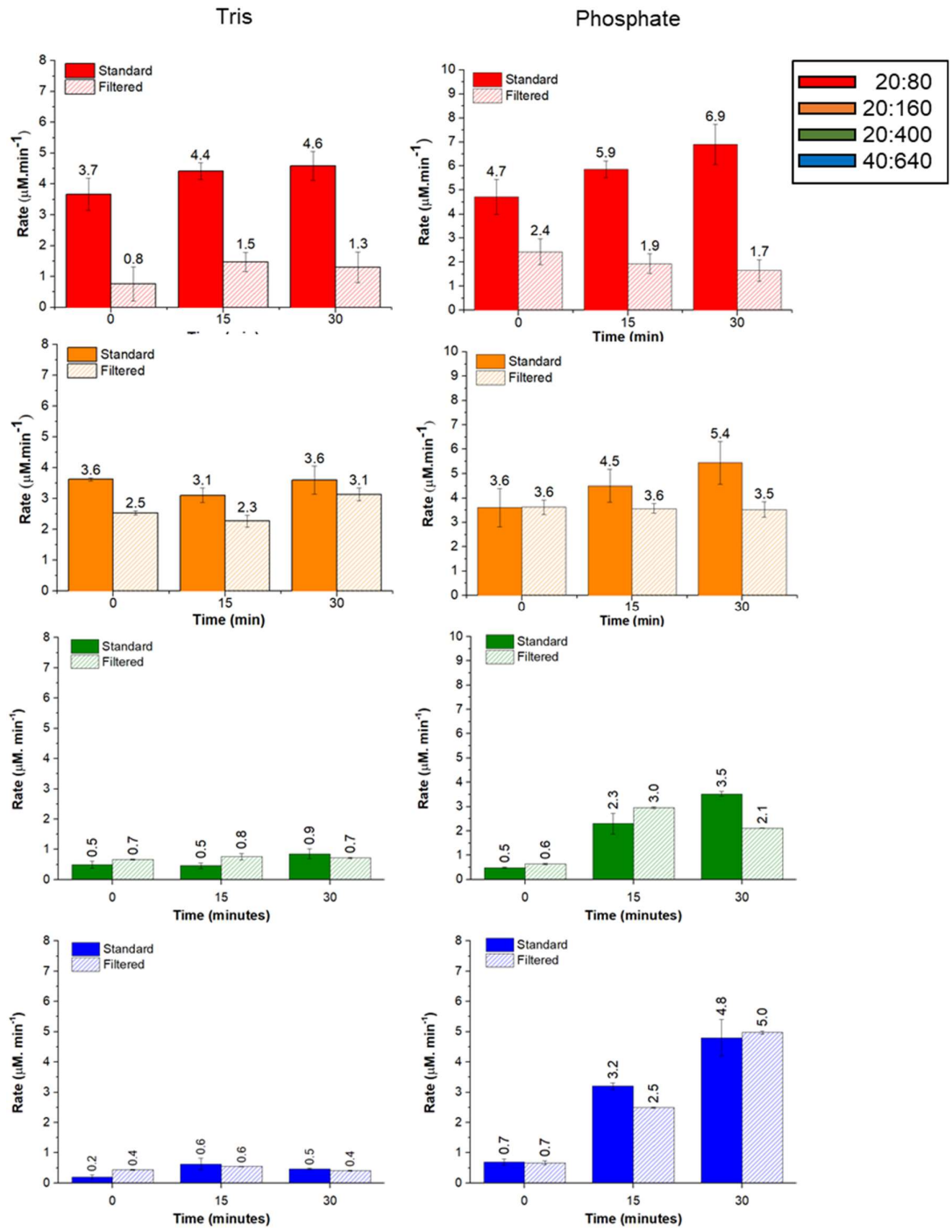

Figure 4.6: Average rates of *p*-NPB production using the water washed samples after exposure to tris or phosphate buffer for 0, 15, or 30 minutes (solid colours). Equivalent samples were filtered prior to commencement of the assay to account for small particle size and leached enzyme (dashed). The effectiveness of centrifugation was affected by particle size and buffer related aggregation, which may account for variation of filtered versus non-filtered assays between samples. The equivalent ethanol samples are shown in **Figure S4.12**.

4.3.5. CALB@ZIF-8 Stability Testing

The stability of each biocomposites to the buffered solutions was further examined by exposing the crystals to tris and phosphate buffers (50 mM, pH 7.4) (**Figure S4.13-S4.16**). When exposed to tris buffer, the larger crystals of 20:400 and 40:640 remained well dispersed in solution and could not be easily pelletised by centrifugation, requiring the addition of ethanol to enable collection of the crystals. The smaller samples could easily be obtained from the buffer solution by centrifugation, however for consistency, ethanol was used for collection of all crystals. Scanning Electron Microscopy (SEM) images showed no noticeable etching to the crystal surface, however an increase in surface charging, aggregation and a reduction in the definition of the crystal edge was observed, attributed to an observable tris coating on the crystal surfaces (**Figure S4.13**). Tris has a reduced solubility in ethanol compared to water, and thus favours aggregation and pelletisation upon addition of ethanol. In contrast, phosphate buffer led to size dependent degradation of the crystals after 30 minutes of exposure as shown by SEM (**Figure S4.14**) and PXRD (**Figure S4.15**). The smaller crystals (20:80 and 20:160) transitioned to an amorphous material, whereas the larger crystals retained long range order however demonstrated surface conversion to zinc phosphate by SEM. Energy Dispersive X-ray (EDX) analysis showed high levels of phosphorous in the remaining material due to zinc phosphate formation. (**Figure S4.16**).[24]

Next, 100 μm protein free crystals were synthesised,[42] and exposed to the same buffers to obtain more insight into the changes occurring at the crystal surfaces. Similar to the CALB@ZIF-8 samples, tris appeared to coat the surface the surface of the 100 μm sized crystals, whereas phosphate buffer caused etching of the crystal surface and led to the formation of zinc phosphate (**Figure 4.7, S4.17**). The PXRD pattern of the bulk material demonstrated retention of long-range order, but no crystalline zinc phosphate was observed (**Figure S4.18**). These combined results may help explain the variations in activity that are reported for some enzyme@ZIF-8 composites in the literature where differences in synthetic procedures, particle size, and treatment/storage in buffer can impact the observed activities. These results also suggest that tris is a suitable buffer to increase the solubility and dispersion of hydrophobic ZIF-8 crystals, however the change in surface chemistry may lead to issues regarding collection, handling and re-usability.

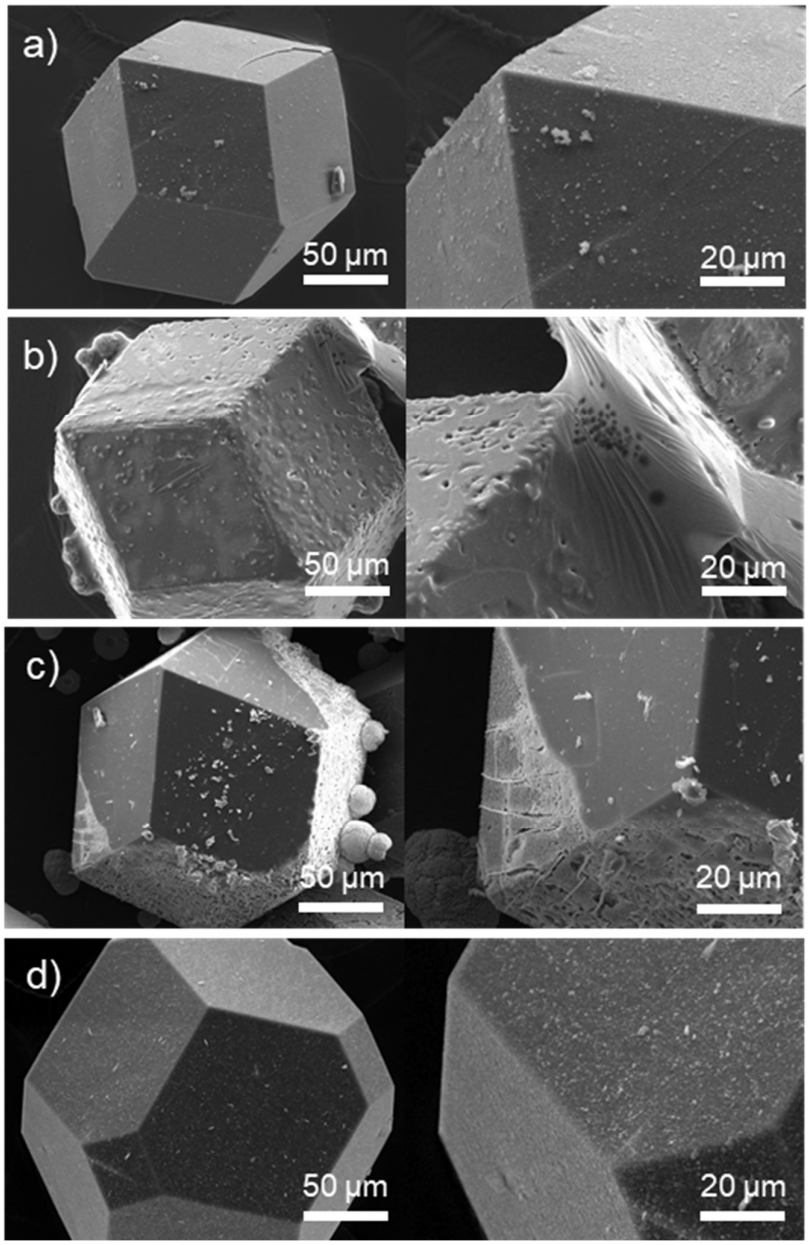

Figure 4.7: SEM images of >100 µm protein free crystals, (a) as-synthesised and after exposure to (b) tris buffer (50 mM, pH 7.4), (c) phosphate buffer (50 mM, pH 7.4) and (d) 100% hexane.

4.3.5. CALB@ZIF-8 Activity Testing (Transesterification)

Given that ZIF-8 crystals were stable to hexane (**Figure 4.7**), we were interested in assessing the activity of CALB@ZIF-8 for transesterification reactions in organic solvent. This would be advantageous in this research, as it could broaden the scope of solvents and reactions for ZIF-8 biocatalysis and provide an effective means to stabilise CALB in non-biological conditions. For example, lyophilised CALB cannot be solubilised in 100% organic solvent, and requires immobilisation to maintain activity in non-aqueous conditions.[41] The catalytic performance of CALB@ZIF-8 biocomposites for the transesterification of hexanol with vinyl acetate (forming hexyl acetate and vinyl alcohol) were examined using hexane as the organic solvent (**Figure 4.5b**). This reaction has been reported previously for pure ZIF-8, however the conditions for catalysis required elevated temperature and high reactant concentrations (alcohol solvent), which led to etching of the crystal surface and release of catalytically active Zn^{2+}.[42] Immobilised CALB can catalyse the transesterification at room temperature, utilising lower substrate concentrations and different solvent systems, which can negate crystal etching and increase the longevity of the catalyst.[43-44]

Initial screening conditions utilised a 50:50 water/hexane solvent system to develop baseline level of activity of the free enzyme for comparison to the immobilised variants. The catalytic activity of the free enzyme was tested using a 5:1 molar ratio of vinyl acetate: n-hexanol with aliquots taken from the hexane layer for analysis (**Figure S4.19**). As expected, the free enzyme showed rapid transesterification in the early stages of the reaction (for both 5:1 and 10:1 substrate ratios), measuring a conversion of approximately 53% at the 1-hour timepoint. In later aliquots, the concentration of hexyl acetate decreased, due to CALB mediated hydrolysis (**Figure S4.19**).

The catalytic activity of the water washed 20:80 and 40:640 CALB@ZIF-8 samples were tested in 50% hexane under the same conditions described for the free enzyme. First, we measured the activity of BSA@ZIF-8 control samples which showed minimal activity (<1%), indicating that at mild reaction conditions the reaction is not catalysed by framework or by leached Zn^{2+}. For the CALB@ZIF-8 biocomposites, the 20:80 sample(small crystals) showed the fastest hexyl acetate production of the ZIF biocomposites (**Figure 4.8**), yielding 65% conversion after 8 hours. However, the activity of the 40:640 sample (large crystals) was negligible and only slightly above that of the BSA@ZIF-8 controls (**Figure 4.8**). Washing the 20:80 sample with ethanol to transition to the sodalite topology led to a reduction in both the initial rate, and the overall maximum conversion of 43% (**Figure 4.9a**).

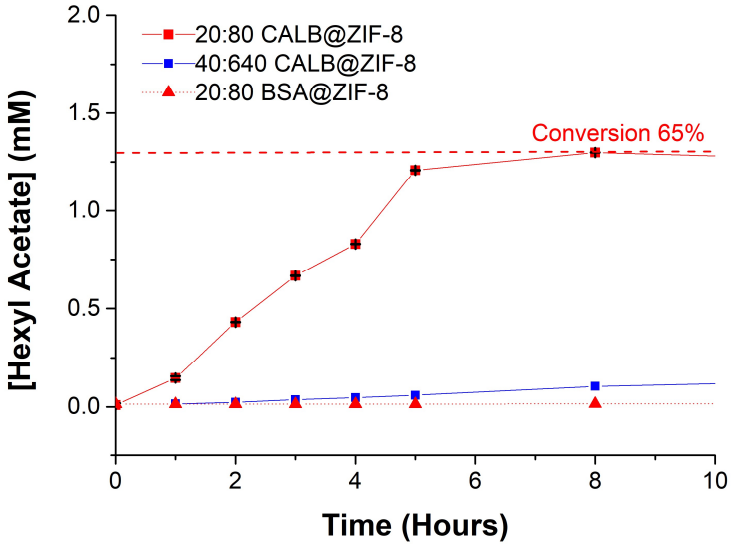

Figure 4.8: Transesterification of vinyl acetate and hexanol in 50:50 water: hexane using the 20:80 CALB@ZIF-8 sample. Maximum measured conversion (65 %) occurred after 8 hours, which reduced to 60% after 24 hours, likely due to competitive transesterification and hydrolysis that occurred during these timepoints. Product conversion is calculated from the concentration of hexyl acetate detected, relative to the limiting reagent (hexanol). No production was observed for the 40:640 when compared to a 20:80 BSA@ZIF-8 sample under identical conditions. Concentrations refer to the hexane layer of the biphasic system (See **Figure S4.21** for GC-FID retention times).

To minimise the observed hydrolysis in the biphasic system, 100% hexane was used as the solvent. Under these conditions no transesterification activity was observed for the free enzyme. Additionally, the initial rate of the 20:80 (ethanol washed) sample remained unchanged (relative to the biphasic system), however, generated hexyl acetate to a yield of 97% after 24 hours (**Figure 4.9a**). The ethanol washed 20:160 sample reached maximum conversions of 50% and 100% for biphasic and hexane solvents respectively, (**Figure 4.9b**) whilst the 20:400 and 40:640 remained inactive in both cases (**Figure 4.9c-d**). The 20:80 was reused five times, with no loss of activity (**Figure 4.10**), indicating that high retention of active enzyme on the support was possible after multiple reaction cycles and washes in hexane.

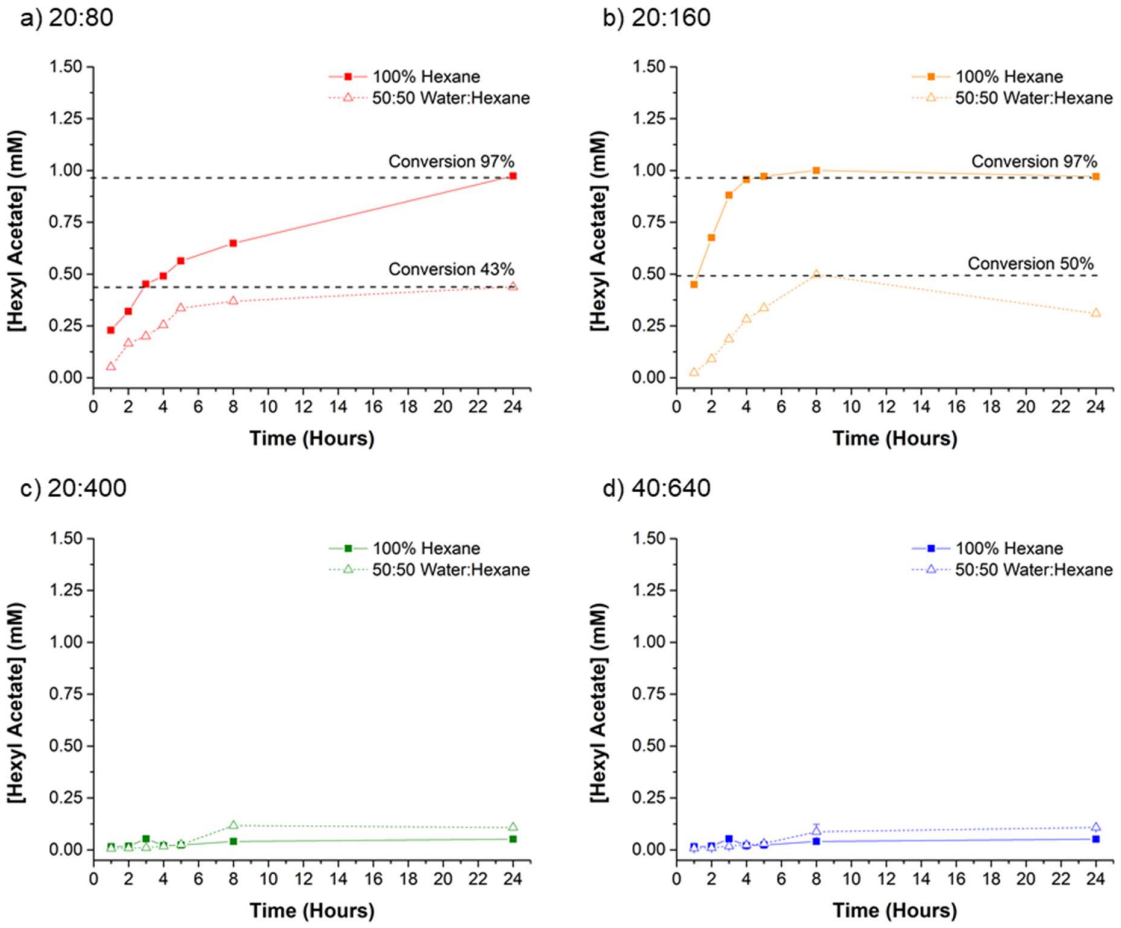

Figure 4.9: Transesterification plots of each biocomposites in 50:50 hexane: water (Δ) and 100% hexane (■). All samples were treated with an ethanol wash for sodalite topology comparison, which led to a reduction in rate for the 20:80 CALB@ZIF-8 sample, relative to the water washed sample in the biphasic systems (**Figure 4.8**). All concentrations are expressed using the total volume of the biphasic or 100% hexane system.

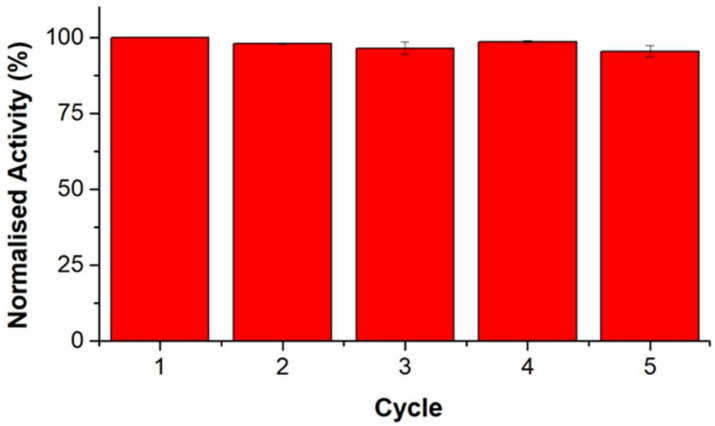

Figure 4.10: Activity of the 20:80 CALB@ZIF-8 sample in 100% (normalised to the first cycle). After each cycle, the hexane was removed, and the sample was washed three times with fresh hexane to remove reactant/ product from the previous reaction. Activity was maintained after each 24-hour cycle and with the first cycle equalling 97% conversion.

4.4. Conclusion

Herein, we showed that the rate of CALB@ZIF-8 catalysis was strongly influenced by the crystal size of the biocomposite. Gas adsorption experiments suggest this may be due to hierarchical porosity in the smaller sized samples resulting from different formation kinetics. Specifically, the rate of CALB@ZIF-8 catalysis for model hydrolysis and transesterification reactions was highly dependent on the synthetic conditions of the biocomposite. At low 2-mIM:Zn^{2+} ratios (20:80 mM, and 20:160 mM), sub-micron particles were generated which demonstrated higher activity for both reactions compared to larger crystals that were formed at increasing ratios (20:400, 40:640 mM). Further, we observed that phosphate buffer could be used to regenerate activity for the larger samples, by degrading the exterior surfaces of the crystals, thus changing the microenvironment surrounding the enzyme and allowing for greater exposure to the reactants and potential enzyme release. In addition to the framework hydrophobicity, [27] the kinetics of formation can influence the structure and activity of ZIF-based biocomposites. We are currently investigating the generality of this concept by examining the properties of a number enzyme@ZIF-8 biocomposites.

4.5. Experimental

4.5.1. Materials

Lipase B from *Candida antarctica* (CALB) recombinant from *Aspergillus oryzae* (Product Code 62288) was purchased from Merck as a lyophilised powder and used without purification. All chemicals were purchased from commercial sources and used as received. Ultra-pure Milli-Q (MQ) with resistivity of >18 MΩ cm^{-1} (Merck Millipore purification system) was used for all syntheses, wash protocols and buffer preparations.

4.5.2. Fluorescein Tagged CALB

CALB was tagged using fluorescein isothiocyanate (FITC) as per previously reported protocols. CALB (15 mg) was dissolved in carbonate-bicarbonate buffer (0.1 M, pH 9.2, 2 mL). FITC in acetone (20 µL, 10 mg. mL^{-1}, 0.2 mg) was added and the protein solution was gently stirred at room temperature for 2 hours in darkness. The tagged enzyme was recovered using Illustra NAP-25 column (GE Healthcare Life Sciences, NSW, Australia) and concentrated and exchanged into ultra-pure water using a 10 KDa membrane and centrifugation (3400 rpm 3 x 15 minutes 4°C). The FITC-CALB was stored in darkness at 4°C prior to use.

4.5.3. ZIF-8 Syntheses

All ZIF-8 biocomposites were synthesised in water using 2 mg of CALB (lyophilised powder or FITC-CALB solution) using varied ratios of zinc acetate dihydrate ($Zn(OAc)_2$) and 2-methylimidazole (2-mIM). $Zn(OAc)_2$ (40 mM/80 mM, 2 mL) was added to a solution of 2-mIM (160 mM/320 mM/800 mM/1.2M, 2mL) containing CALB. The samples were left to form for 16 hours before being washed with water (2x) only, or water (2x) and ethanol (2x).

Surface Adsorption of CALB (CALB-on-ZIF-8). CALB (2 mg lyophilised powder) in water (0.5 mL) was combined with ZIF-8 in water (1 mL) that had been synthesised without protein using the 40 mM:640 mM Zn^{2+}:2-mIM (final concentration) protocol. The CALB on ZIF-8 sample was gently shaken for 4 hours and washed with water (2x) to remove loosely bound enzyme.

4.5.4. Activity Testing

Hydrolysis. The hydrolysis of *p*-nitrophenyl butyrate (*p*-NPB) assay was adapted from the protocol available online from Sigma.[45] Each ZIF biocomposite sample made to a final volume of 1 mL in water. The ZIF sample (50 µL) was added to a tris buffer solution (50 mM, 4.9 mL) pH 7.4 containing Triton X-100 (0.1%) and *p*-NPB (50 µl, 25 mM). Triton X-100 is used to solubilise and activate the enzyme and is known to be ineffective at removing surface

bound enzyme.[21] An equivalent stock concentration of CALB or BSA (2 mg mL^{-1}) was used for free enzyme and control reactions respectively. At each time point 100 µL of the reaction mixture was collected and centrifuged before measuring the absorbance between 380-600 nm. The absorbance of A_{405}-A_{500} was used for activity determination to account for scattering due to remaining particulate matter. The rate of activity was measured using the molar extinction coefficient of *p*-nitrophenol at 405 nm of 18,500 M^{-1} cm^{-1}. phosphate buffer (50 mM, pH 7.4) was also tested using the same protocol. Standard error at each time point was calculated from a minimum of two repeats.

Transesterification. Hexanol (2 mM) and vinyl acetate (10 mM) in hexane (2 mL) was combined with an aqueous suspension of the CALB (test) or BSA (control) ZIF-8 biocomposite (2 mL) or an air-dried sample in hexane (2 mL) in a 5 mL glass vial. The reaction mix was shaken at 30°C, and aliquots were taken from the hexane and aqueous layer at 1-hour intervals. Lyophilised CALB (2 mg) was used for free enzyme reactions.

4.5.5. Characterisation

Powder X-ray Diffraction. Powder X-ray diffraction (PXRD) data were collected on a Bruker D8 Advanced X-ray powder diffractometer (parallel X-ray, capillary-loaded) using a Cu Kα λ=1.5418 Å radiation source, or Bruker D4-Endeavor diffractometer (flat plate) using Co Kα λ=1.78897 Å depending on sample mass. For the D8, samples were mounted in 0.5 mm glass capillaries and data collected for between 2θ of 2° to 52.94° with Phi rotation at 20 rotations per min at 1-second exposure per step at 5001 steps. For the D4, data was collected over the range 2θ of 2° to 50° and was expressed as Cu radiation using Pow DLL converter (version 2.68.00). The data was processed as per **Chapter 3**.

N_2 Adsorption Isotherms. N_2 (UHP grade, 99.999%) adsorption isotherm measurements were performed on a 3Flex physisorption analyser. The temperature was maintained at 77 K *via* a helium cryostat. The 20:400, and 40:640 CALB@ ZIF-8 samples were washed with ethanol and dried under vacuum in a desiccator for 1 hour. The dried samples were heated under vacuum at 120 °C for 2 hours. The 20:80 and 20:160 CALB@ZIF-8 were washed with ethanol and chloroform and dried under vacuum in a desiccator for 1 hour prior to activation at 80 °C for 3 hours.

Scanning Election Microscopy (SEM). SEM images were collected on either the Philips XL30 or Quanta 450 Field Emission Scanning Electron Microscopes (FESEM). Samples were dry loaded onto carbon tabs on aluminium stages and sputter coated with carbon.

Electron Dispersive X-ray Analysis was collected with an Oxford Instruments Ultim Max 170 EDX attachment on the Quanta 450.

Zeta Potential Measurements. CALB (or FITC-CALB) (1 mg) was dissolved in water or a 160 mM 2-mIM solution. Zeta Potential measurements were recorded on a Malvern ZetaSizer Nano using a disposable folded capillary cell (DTS1070).

Confocal Laser Scanning Microscopy (CLSM). CLSM images were taken on an Olympus FV3000 confocal laser scanning microscope. The FITC-CALB samples were excited at 488 nm, and the fluorescence signal was collected between 495-545 nm.

UV-Visible Absorbance Measurements. Absorbance spectra were recorded at 30°C on an Agilent Cary 60 or an Agilent Cary 5000 UV/Vis spectrophotometer.

Gas Chromatography Analysis. Aliquots were diluted/extracted into ethyl acetate, dried with magnesium sulfate and analysed via Gas Chromatography (Shimadzu, Nexis GC-2030) equipped with a DB-wax column (30.0 m, 0.25 mm, 0.25 mm) and a Flame Ionisation Detector (FID). The column was held at 60°C for 3 minutes and increased at 6°C per minute to 160°C. At the end of each run, the column was heated to 220°C for a burn off. Retention times (hexanol; 7.9 minutes, hexyl acetate; 6.1 minutes, see **Figure S4.21**).

4.6. Conflicts of Interest

There are no conflicts to declare.

4.7. Acknowledgements

This work was supported by the Australian Research Council under the Discovery Projects Scheme (DP170103531). N. K. Maddigan and O.M. Linder-Patton acknowledge an Australian Government Research Training Program Scholarships. The authors acknowledge the facilities, and the scientific and technical assistance of the Australian Microscopy & Microanalysis Research Facility at the Adelaide Microscopy Unit, The University of Adelaide.

4.8. References

1. Benkovic, S. J.; Hammes-Schiffer, S., A perspective on enzyme catalysis. *Science* **2003,** *301* (5637), 1196-1202.

2. Drout, R. J.; Robison, L.; Farha, O. K., Catalytic applications of enzymes encapsulated in metal–organic frameworks. *Coord. Chem. Rev.* **2019,** *381*, 151-160.

3. van Dongen, S. F. M.; Elemans, J. A. A. W.; Rowan, A. E.; Nolte, R. J. M., Processive catalysis. *Angew. Chem. Int. Ed.* **2014,** *53* (43), 11420-11428.

4. Stepankova, V.; Bidmanova, S.; Koudelakova, T.; Prokop, Z.; Chaloupkova, R.; Damborsky, J., Strategies for stabilization of enzymes in organic solvents. *ACS Catal.* **2013,** *3* (12), 2823-2836.

5. Sheldon, R. A.; Brady, D., The limits to biocatalysis: pushing the envelope. *Chem. Commun.* **2018,** *54* (48), 6088-6104.

6. Schmid, A.; Dordick, J. S.; Hauer, B.; Kiener, A.; Wubbolts, M.; Witholt, B., Industrial biocatalysis today and tomorrow. *Nature* **2001,** *409* (6817), 258-268.

7. Bommarius, A. S.; Paye, M. F., Stabilizing biocatalysts. *Chem. Soc. Rev.* **2013,** *42* (15), 6534-6565.

8. Garcia-Galan, C.; Berenguer-Murcia, Á.; Fernandez-Lafuente, R.; Rodrigues, R. C., Potential of different enzyme immobilization strategies to improve enzyme performance. *Adv. Synth. Catal.* **2011,** *353* (16), 2885-2904.

9. Majewski, M. B.; Howarth, A. J.; Li, P.; Wasielewski, M. R.; Hupp, J. T.; Farha, O. K., Enzyme encapsulation in metal–organic frameworks for applications in catalysis. *CrystEngComm.* **2017,** *19* (29), 4082-4091.

10. Gkaniatsou, E.; Sicard, C.; Ricoux, R.; Mahy, J.-P.; Steunou, N.; Serre, C., Metal–organic frameworks: a novel host platform for enzymatic catalysis and detection. *Mater. Horiz.* **2017,** *4* (1), 55-63.

11. Wu, X.; Hou, M.; Ge, J., Metal–organic frameworks and inorganic nanoflowers: a type of emerging inorganic crystal nanocarrier for enzyme immobilization. *Catal. Sci.* **2015,** *5* (12), 5077-5085.

12. Doonan, C.; Riccò, R.; Liang, K.; Bradshaw, D.; Falcaro, P., Metal–organic frameworks at the biointerface: synthetic strategies and applications. *Acc. Chem. Res.* **2017,** *50* (6), 1423-1432.

13. Lian, X.; Fang, Y.; Joseph, E.; Wang, Q.; Li, J.; Banerjee, S.; Lollar, C.; Wang, X.; Zhou, H.-C., Enzyme–MOF (metal–organic framework) composites. *Chem. Soc. Rev.* **2017,** *46* (11), 3386-3401.

14. Chen, Y.; Lykourinou, V.; Vetromile, C.; Hoang, T.; Ming, L.-J.; Larsen, R. W.; Ma, S., How can proteins enter the interior of a MOF? Investigation of cytochrome c translocation into a mof consisting of mesoporous cages with microporous windows. *J. Am. Chem. Soc.* **2012,** *134* (32), 13188-13191.

15. Liu, W.-L.; Lo, S.-H.; Singco, B.; Yang, C.-C.; Huang, H.-Y.; Lin, C.-H., Novel trypsin–FITC@MOF bioreactor efficiently catalyzes protein digestion. *J. Mater. Chem. B.* **2013,** *1* (7), 928-932.

16. Jung, S.; Kim, Y.; Kim, S.-J.; Kwon, T.-H.; Huh, S.; Park, S., Bio-functionalization of metal–organic frameworks by covalent protein conjugation. *Chem. Commun.* **2011,** *47* (10), 2904-2906.

17. Huo, J.; Aguilera-Sigalat, J.; El-Hankari, S.; Bradshaw, D., Magnetic MOF microreactors for recyclable size-selective biocatalysis. *Chem. Sci.* **2015,** *6* (3), 1938-1943.

18. Park, K. S.; Ni, Z.; Côté, A. P.; Choi, J. Y.; Huang, R.; Uribe-Romo, F. J.; Chae, H. K.; O'Keeffe, M.; Yaghi, O. M., Exceptional chemical and thermal stability of zeolitic imidazolate frameworks. *Proc. Natl. Acad. Sci.* **2006,** *103* (27), 10186.

19. Zhang, C.; Gee, J. A.; Sholl, D. S.; Lively, R. P., Crystal-size-dependent structural transitions in nanoporous crystals: adsorption-induced transitions in ZIF-8. *J. Phys. Chem. C.* **2014,** *118* (35), 20727-20733.

20. Liang, K.; Ricco, R.; Doherty, C. M.; Styles, M. J.; Bell, S.; Kirby, N.; Mudie, S.; Haylock, D.; Hill, A. J.; Doonan, C. J.; Falcaro, P., Biomimetic mineralization of metal-organic frameworks as protective coatings for biomacromolecules. *Nat. Commun.* **2015,** *6* (1), 7240.

21. Liang, W.; Ricco, R.; Maddigan, N. K.; Dickinson, R. P.; Xu, H.; Li, Q.; Sumby, C. J.; Bell, S. G.; Falcaro, P.; Doonan, C. J., Control of structure topology and spatial distribution of biomacromolecules in protein@ZIF-8 biocomposites. *Chem. Mater.* **2018,** *30* (3), 1069-1077.

22. Carraro, F.; Velasquez, M.; Astria, E.; Liang, W.; Twight, L.; Parise, C.; Ge, M.; Huang, Z.; Ricco, R.; Zou, X.; villanova, L.; Kappe, C. O.; Doonan, C.; Falcaro, P., Phase dependent encapsulation and release profile of zif-based biocomposites. *Chem. Sci.* **2020,** *11*, 3397-3404.

23. Shi, Q.; Chen, Z.; Song, Z.; Li, J.; Dong, J., Synthesis of ZIF-8 and ZIF-67 by Steam-assisted conversion and an investigation of their tribological behaviors. *Angew. Chem. Int. Ed.* **2011,** *50* (3), 672-675.

24. Velásquez-Hernández, M. d. J.; Ricco, R.; Carraro, F.; Limpoco, F. T.; Linares-Moreau, M.; Leitner, E.; Wiltsche, H.; Rattenberger, J.; Schröttner, H.; Frühwirt, P.; Stadler,

E. M.; Gescheidt, G.; Amenitsch, H.; Doonan, C. J.; Falcaro, P., Degradation of ZIF-8 in phosphate buffered saline media. *CrystEngComm.* **2019,** *21* (31), 4538-4544.

25. Luzuriaga, M. A.; Benjamin, C. E.; Gaertner, M. W.; Lee, H.; Herbert, F. C.; Mallick, S.; Gassensmith, J. J., ZIF-8 degrades in cell media, serum, and some—but not all—common laboratory buffers. *Supramol. Chem.* **2019,** *31* (8), 485-490.

26. Yang, X.; Tang, Q.; Jiang, Y.; Zhang, M.; Wang, M.; Mao, L., Nanoscale ATP-Responsive Zeolitic Imidazole Framework-90 as a General Platform for Cytosolic Protein Delivery and Genome Editing. *J. Am. Chem. Soc.* **2019,** *141* (9), 3782-3786.

27. Liang, W.; Xu, H.; Carraro, F.; Maddigan, N. K.; Li, Q.; Bell, S. G.; Huang, D. M.; Tarzia, A.; Solomon, M. B.; Amenitsch, H.; Vaccari, L.; Sumby, C. J.; Falcaro, P.; Doonan, C. J., Enhanced activity of enzymes encapsulated in hydrophilic metal–organic frameworks. *J. Am. Chem. Soc.* **2019,** *141* (6), 2348-2355.

28. Cui, J.; Feng, Y.; Jia, S., Silica encapsulated catalase@metal-organic framework composite: A highly stable and recyclable biocatalyst. *Chem. Eng. J.* **2018,** *351*, 506-514.

29. Cui, J.; Feng, Y.; Lin, T.; Tan, Z.; Zhong, C.; Jia, S., Mesoporous metal–organic framework with well-defined cruciate flower-like morphology for enzyme immobilization. *ACS Appl. Mater.* **2017,** *9* (12), 10587-10594.

30. Du, Y.; Gao, J.; Liu, H.; Zhou, L.; Ma, L.; He, Y.; Huang, Z.; Jiang, Y., Enzyme@silica nanoflower@metal-organic framework hybrids: A novel type of integrated nanobiocatalysts with improved stability. *Nano. Res.* **2018,** *11* (8), 4380-4389.

31. Cai, X.; Zhang, M.; Wei, W.; Zhang, Y.; Wang, Z.; Zheng, J., The Immobilization of *Candida antarctica* lipase B by ZIF-8 encapsulation and macroporous resin adsorption: preparation and characterizations. *Biotechnol. Lett.* **2020,** *42* (2), 269-276.

32. Wu, X.; Yang, C.; Ge, J., Green synthesis of enzyme/metal-organic framework composites with high stability in protein denaturing solvents. *Bioresoour. Bioprocess.* **2017,** *4* (1), 24.

33. Pitzalis, F.; Carucci, C.; Naseri, M.; Fotouhi, L.; Magner, E.; Salis, A., Lipase encapsulation onto ZIF-8: a comparison between biocatalysts obtained at low and high zinc/2-methylimidazole molar ratio in aqueous medium. *ChemCatChem.* **2018,** *10* (7), 1578-1585.

34. Maddigan, N. K.; Tarzia, A.; Huang, D. M.; Sumby, C. J.; Bell, S. G.; Falcaro, P.; Doonan, C. J., Protein surface functionalisation as a general strategy for facilitating biomimetic mineralisation of ZIF-8. *Chem. Sci.* **2018,** *9* (18), 4217-4223.

35. Rabbani, G.; Ahmad, E.; Khan, M. V.; Ashraf, M. T.; Bhat, R.; Khan, R. H., Impact of structural stability of cold adapted *Candida antarctica* lipase B (CaLB): in relation to pH, chemical and thermal denaturation. *RSC Adv.* **2015,** *5* (26), 20115-20131.

36. Basnayake, S. A.; Su, J.; Zou, X.; Balkus, K. J., Carbonate-based zeolitic imidazolate framework for highly selective CO_2 capture. *Inorg. Chem.* **2015,** *54* (4), 1816-1821.

37. Verploegh, R. J.; Nair, S.; Sholl, D. S., Temperature and loading-dependent diffusion of light hydrocarbons in zif-8 as predicted through fully flexible molecular simulations. *J. Am. Chem. Soc.* **2015,** *137* (50), 15760-15771.

38. Pan, Y.; Li, H.; Farmakes, J.; Xiao, F.; Chen, B.; Ma, S.; Yang, Z., How do enzymes orient when trapped on metal–organic framework (MOF) surfaces? *J. Am. Chem. Soc.* **2018,** *140* (47), 16032-16036.

39. Chen, B.; Miller, M. E.; Gross, R. A., Effects of porous polystyrene resin parameters on *Candida antarctica* lipase b adsorption, distribution, and polyester synthesis activity. *Langmuir* **2007,** *23* (11), 6467-6474.

40. Mei, Y.; Miller, L.; Gao, W.; Gross, R. A., Imaging the distribution and secondary structure of immobilized enzymes using infrared microspectroscopy. *Biomacromolecules* **2003,** *4* (1), 70-74.

41. Ortiz, C.; Ferreira, M. L.; Barbosa, O.; dos Santos, J. C. S.; Rodrigues, R. C.; Berenguer-Murcia, Á.; Briand, L. E.; Fernandez-Lafuente, R., Novozym 435: the “perfect” lipase immobilized biocatalyst? *Catal. Sci.* **2019,** *9* (10), 2380-2420.

42. Linder-Patton, O. M.; de Prinse, T. J.; Furukawa, S.; Bell, S. G.; Sumida, K.; Doonan, C. J.; Sumby, C. J., Influence of nanoscale structuralisation on the catalytic performance of ZIF-8: a cautionary surface catalysis study. *CrystEngComm.* **2018,** *20* (34), 4926-4934.

43. Lozano, P.; De Diego, T.; Sauer, T.; Vaultier, M.; Gmouh, S.; Iborra, J. L., On the importance of the supporting material for activity of immobilized *Candida antarctica* lipase B in ionic liquid/hexane and ionic liquid/supercritical carbon dioxide biphasic media. *J. Supercrit. Fluid* **2007,** *40* (1), 93-100.

44. Park, S.-C.; Chang, W.-J.; Lee, S.-M.; Kim, Y.-J.; Koo, Y.-M., Lipase-catalyzed transesterification in several reaction systems: An application of room temperature lonic liquids for bi-phasic production ofn-butyl acetate. *Biotechnol. Bioproc. E.* **2005,** *10* (1), 99.

45. Shirai, K.; Jackson, R. L., Lipoprotein lipase-catalyzed hydrolysis of p-nitrophenyl butyrate. Interfacial activation by phospholipid vesicles. *J. Biol. Chem.* **1982,** *257* (3), 1253-1258.

4.9. Supporting Information

4.9.1. CALB@ZIF-8 Synthesis

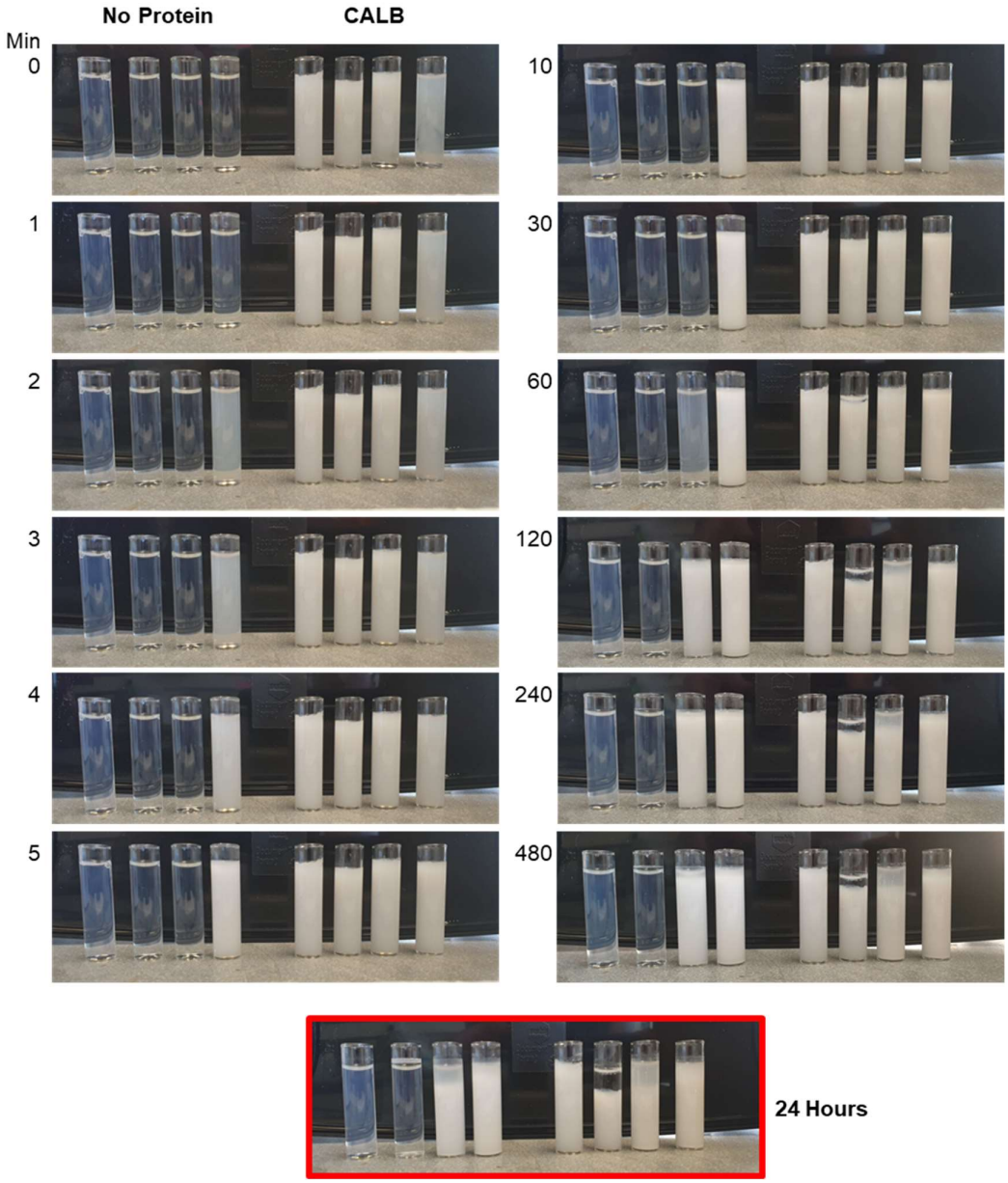

Figure S4.1: Time scale photos to visually inspect the formation of ZIF-8 using each ratio (L-R: 20:80, 20:160, 20:400 and 40:640) after the addition of the Zn^{2+} solution to the 2-mIM solution (t=0). Without the addition of protein, minimal ZIF-8 precipitate formed over the 24-hour timeframe for the low ratio samples whereas noticeable ZIF formation occurs for the 20:400 and 40:640 samples at 60 and 2 minutes, respectively. The addition of CALB accelerates the initial ZIF-8 nucleation, however this appeared to be a slower process for 40:640 compared to 20:80.

4.9.2. CALB Characterisation

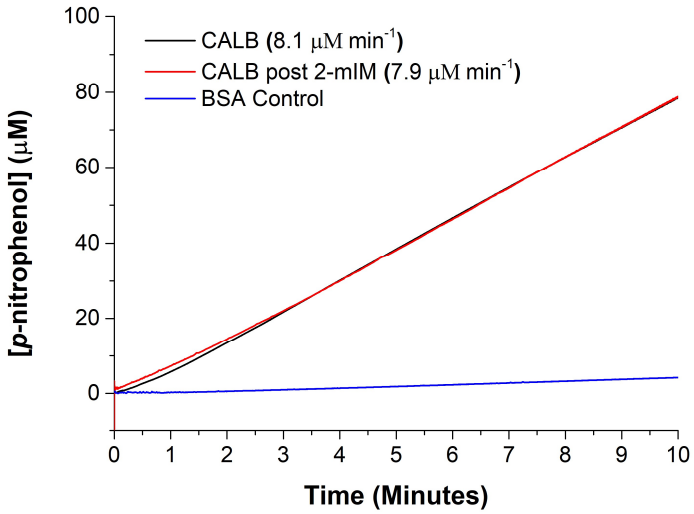

Figure S4.2: Hydrolytic activity of free CALB after exposure to 2-mIM (640 mM). CALB (2 mg) was dissolved in a solution of 2-mIM (1.28 M) and was left at room temperature for 5 minutes to mimic the maximum exposure time to the pH 11 solution. The protein was diluted in tris buffer (50 mM, 7.4) before being exchanged into water using a 10 KDa membrane and centrifugation (3600 rpm, 4°, 4 cycles. The assay was performed in tris (pH 7.4, 50 mM)+ TritonX-100 (0.1%) using 0.6 μM CALB (calculated from CALB molar extinction coefficient, 40,690 M^{-1} cm^{-1} at 280 nm and CALB molecular weight, 33 KDa).[1] *p*-nitrophenyl butyrate, *p*-NPB (0.25 mM) measuring the absorbance of *p*-nitrophenol at 405 nm (18,500 $M^{-1}.cm^{-1}$). Controls of BSA alone and BSA@ZIF-8 (see **Figure S4.9)** show minimal hydrolytic activity, confirming activity is solely from CALB.

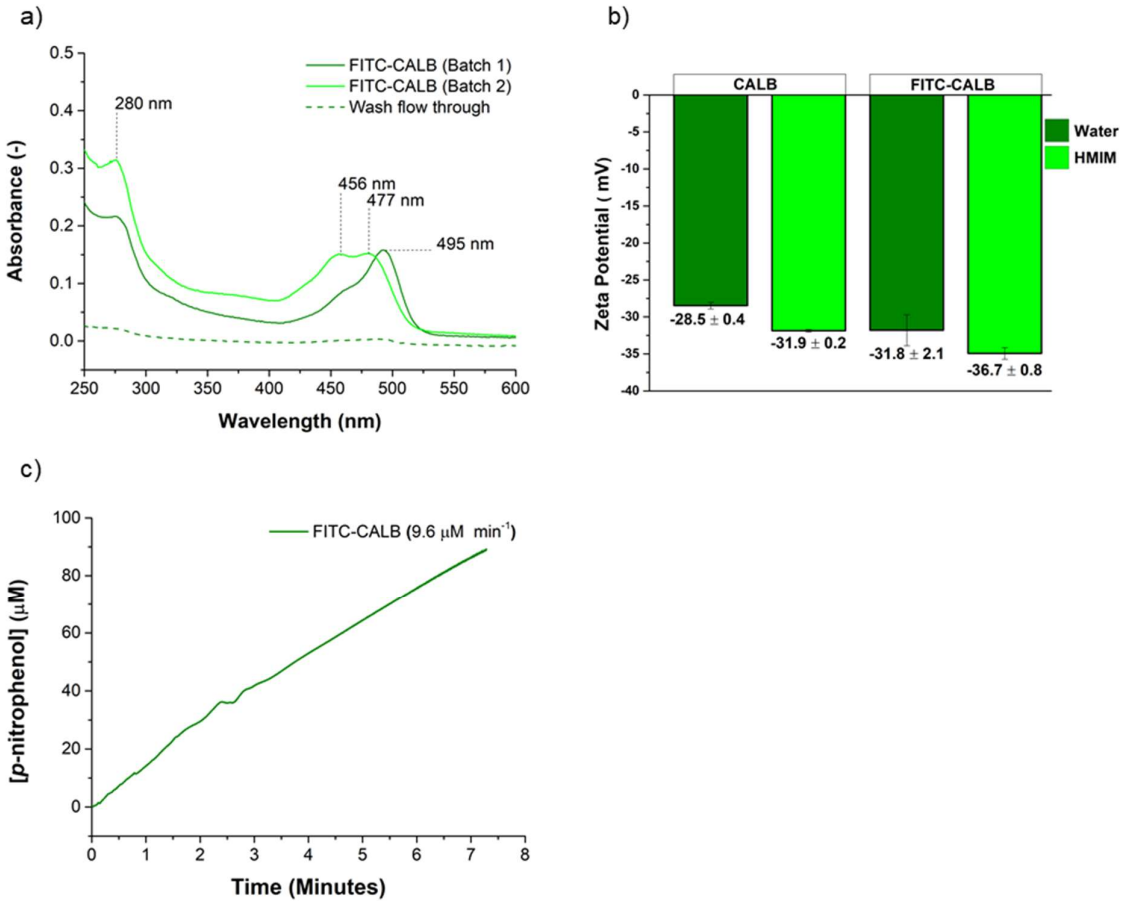

Figure S4.3: (a) Absorbance spectrum of FITC- tagged CALB after tagging for 2 hours (Batch 1) and 16 hours (Batch 2). The peak at 280 nm can be attributed to the protein and the peak(s) at 450-500 nm are from the FITC tag. The shift in absorbance of batch 2 from 495 to 477 nm and increase in the shoulder 456 nm can be attributed to multi tagged enzyme.[2] Prior to use, the FITC-CALB was buffer exchanged using a 10 kDa centrifuge membrane until no significant absorbance was observed in the flow through, ensuring no unbound FITC remained in the protein solution (dashed line). (b) Zeta potential measurements of FITC-CALB showed a slight negative shift compared to the untagged enzyme in both water and 2-mIM (160 mM) solution however it is important to note that the shift may result in changes to the ZIF-8 bio-mineralisation process and enzyme spatial distribution. However, due to the highly negative zeta potential of the unmodified CALB in 2-mIM and the small change in zeta potential upon tagging, minimal changes in biomimetic mineralisation would be expected. (c) FITC tagging was shown to not alter the activity of the enzyme.

4.9.3. CALB@ZIF-8 Encapsulation Efficiency

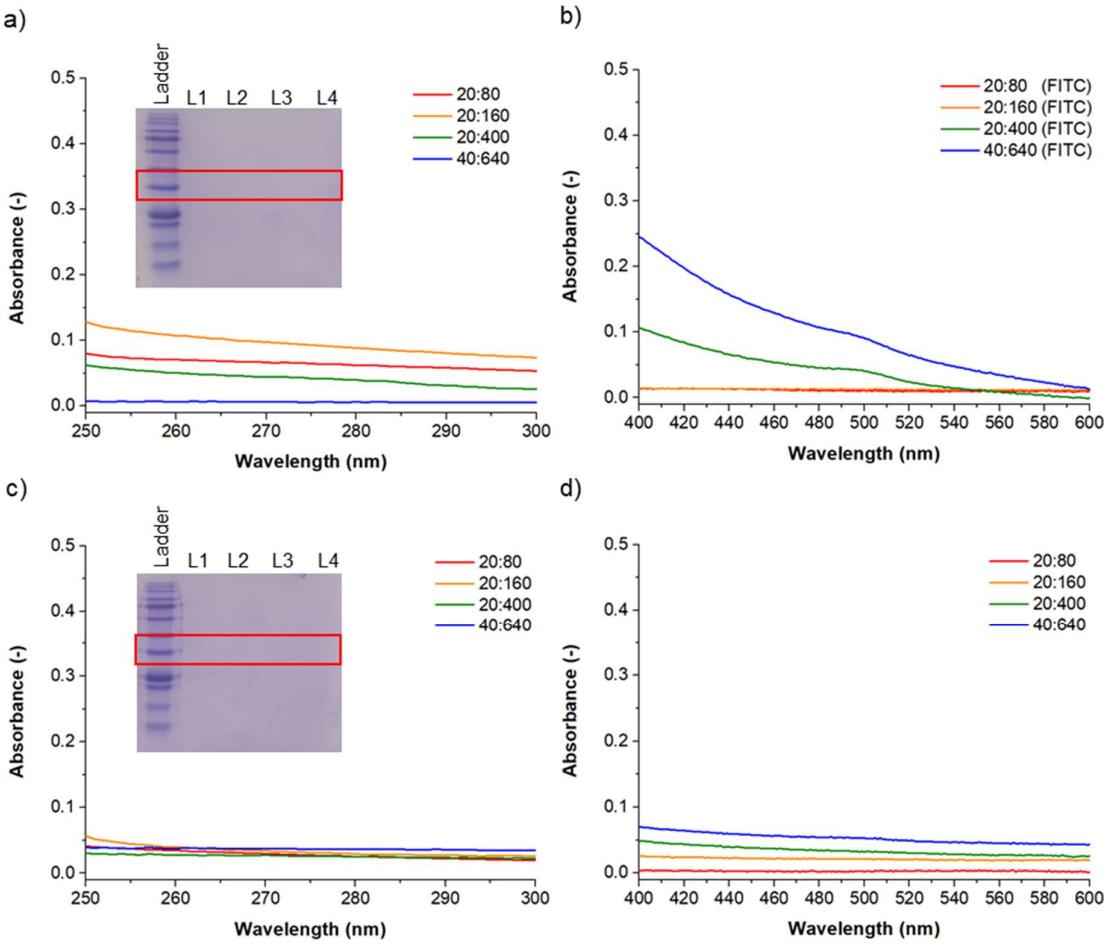

Figure S4.4: (a) Absorbance spectrum of the UV region of the supernatants of non-tagged CALB biocomposites after washing to remove excess 2-mIM (10 kDa membrane with centrifugation). SDS-PAGE (Inset) of the concentrated supernatants suggesting that any protein that may have been present in the supernatants would be lower than the detection limit of the dye (200 ng). L1, L2,L3 and L4 refers to the 20:80, 20:160, 20:400 and 40:640 samples respectively. The ladder lane consists of protein standards of known molecular weight, with the red box encompassing the 30 kDa standard. (b) Absorbance spectrum of the visible region of the supernatants of FITC-CALB biocomposites (before washing) showing a slight shoulder at 500 nm indicating the presence of low quantities of FITC for the 20:400 and 40:640 samples. Each biocomposite was then washed with water and the washings were collected and concentrated as above. (c) CALB and (d) FITC-CALB water washes showed no detectable protein in via absorption spectroscopy nor SDS-PAGE analysis.

4.9.4. CALB@ZIF-8 Activity (Hydrolysis)

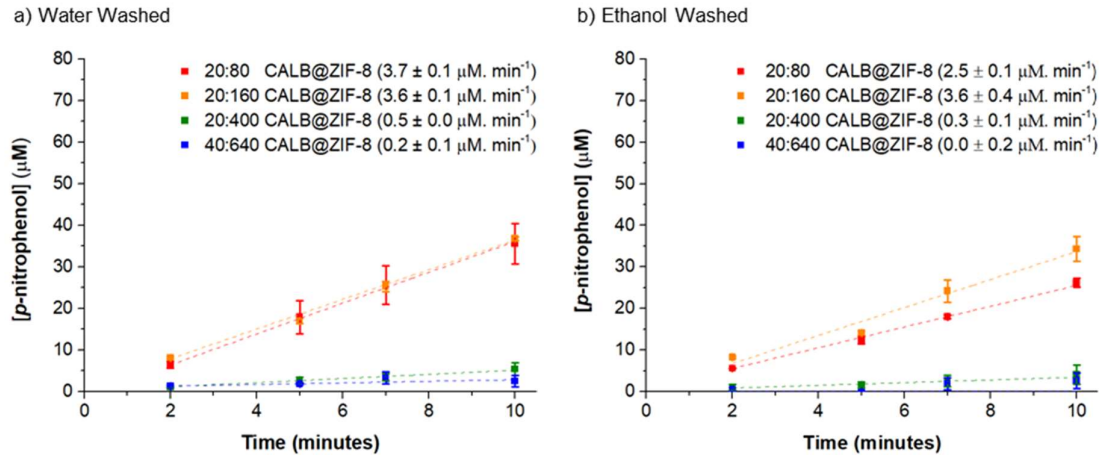

Figure S4.5: Hydrolysis activity of the CALB@ZIF-8 biocomposites using *p*-NPB after (a) two water washes and (b) two additional ethanol washes. All assays were undertaken in tris (50 mM, pH 7.4) + Triton X-100 (0.1%) using 0.6 μM enzyme. Standard error for each time point was generated from a minimum of two repeat assays.

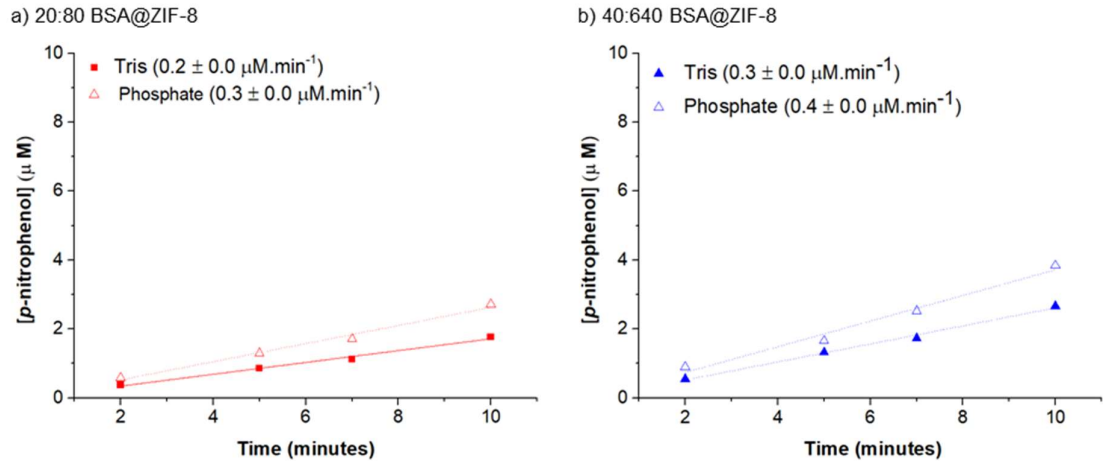

Figure S4.6: Control assays BSA@ZIF-8 biocomposites using *p*-NPB. The 20:80 (a) and 40:640 (b) BSA@ZIF-8 samples were tested to account for particle size effects. Assays were performed after 30 minutes exposure to tris or phosphate buffer, with only low levels of activity being observed.

4.9.5. *Surface Area and Pore Size*

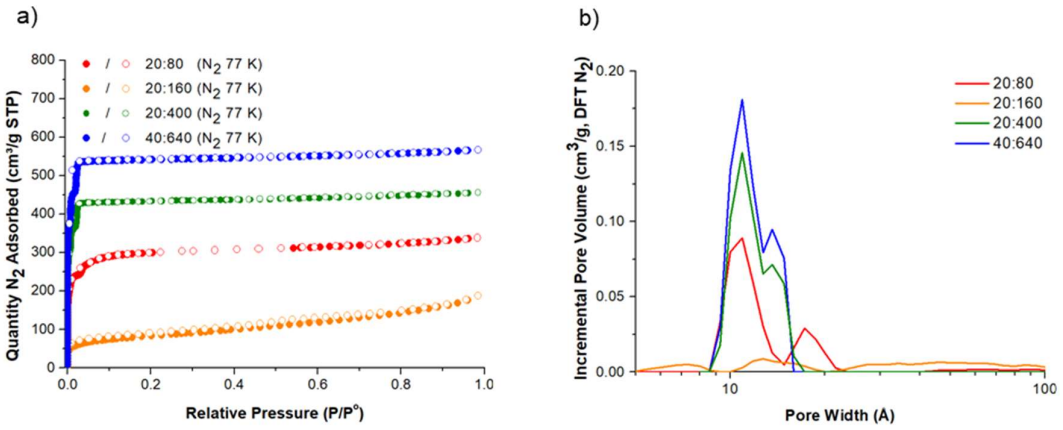

Figure S4.7: (a) N_2 sorption/desorption curves at 77 K giving BET surface areas of 1026 ± 4, 248 ± 2, 1570 ± 11, 1956 ± 20 $m^2.g^{-1}$ for 20:80, 20:160, 20:400, and 40:640 CALB@ZIF-8 respectively. 20:160 CALB@ZIF-8 was not stable to the two activation conditions tested as characterised by PXRD (**Figure S4.8**). (b) Pore Size distribution of each CALB@ZIF-8 preparation. The samples formed from the high 2-mIM:Zn^{2+} ratio (20:400, 40:640) displayed similar pore size distributions, whereas the lowest ratio sample (20:80) possessed a larger pore (~17 Å).

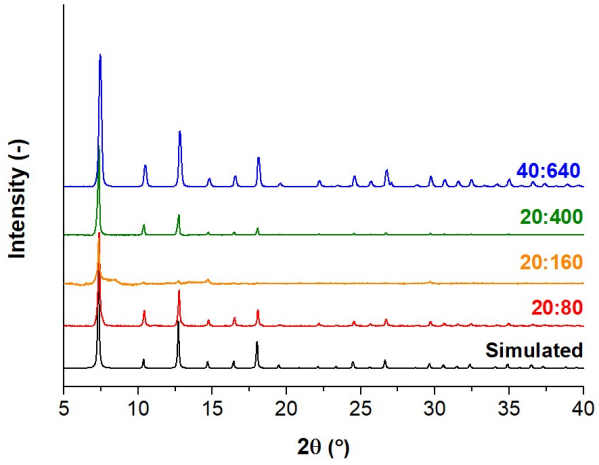

Figure S4.8: PXRD patterns of each CALB@ZIF-8 biocomposite after activation and N_2 sorption/desorption studies. Activation conditions: 20:80 and 20:160 were washed with ethanol and chloroform and dried under vacuum in a desiccator for 1 hour prior to activation at 80 °C for 3 hours. 20:400 and 40:640 were washed with ethanol, dried in a desiccator and activated at 120 °C for 2 hours.

4.9.6. CALB Surface Adsorption

ZIF-8, 1 µm crystals (5 mg, 10mg, 20 mg) were adsorbed with 0.2 mg of CALB (calculated from CALB extinction coefficient/equals 2 mg CALB powder). The total external surface area of each ZIF-8 sample, and an estimated CALB surface coverage was calculated and reported in **Table S4.1**.

Table S4.1: Total surface area of 1 um ZIF-8 crystals, showing the maximum potential CALB surface coverage and the actual CALB surface coverage calculated from unbound enzyme absorbance measurements.

1 µm ZIF-8 Mass (mg)	Surface Area (cm^2)*	CALB Surface Coverage Maximum (%)#	CALB Surface Coverage Calculated (%)+
5	990	60	20
10	1980	30	20
20	3960	15	11

*External surface areas were calculated per methods provided by Linder-Patton *et. al.*[3]

Percentage coverage was calculated assuming 100% immobilisation efficiency. The dimensions of CALB are 30x40x50 Å,[1] was used to calculate the average surface area (SA) of a single side of the enzyme that could adsorb to ZIF-8. This was converted to the average side SA of 0.2 mg of CALB and presented as a percentage of the total ZIF-8 surface area.

+ After the surface adsorption process, the ZIF-8 samples were centrifuged, and the supernatants were analysed for remaining CALB (**Figure S4.10b**). Here it was determined that a greater proportion of CALB was adsorbed when using a larger mass of ZIF-8 material. According to the A_{280} absorbance, the supernatants of the 5 mg, 10 mg and 20 mg ZIF-8 samples contained 0.13 mg (A_{280} :0.14), 0.06 mg (A_{280} :0.06), and 0.05 mg (A_{280} :0.05) respectively which was then used to calculate the surface coverage percentage.

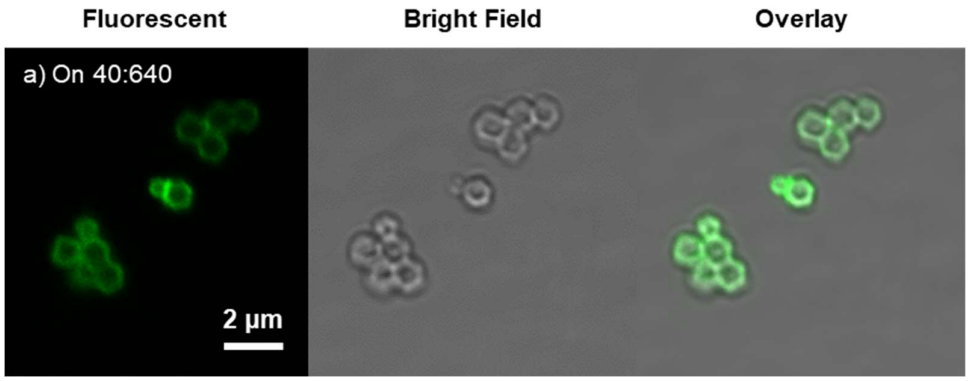

Figure S4.9: CLSM images of FITC-CALB surface bound to pre-synthesised (protein free) 40:640 crystals.

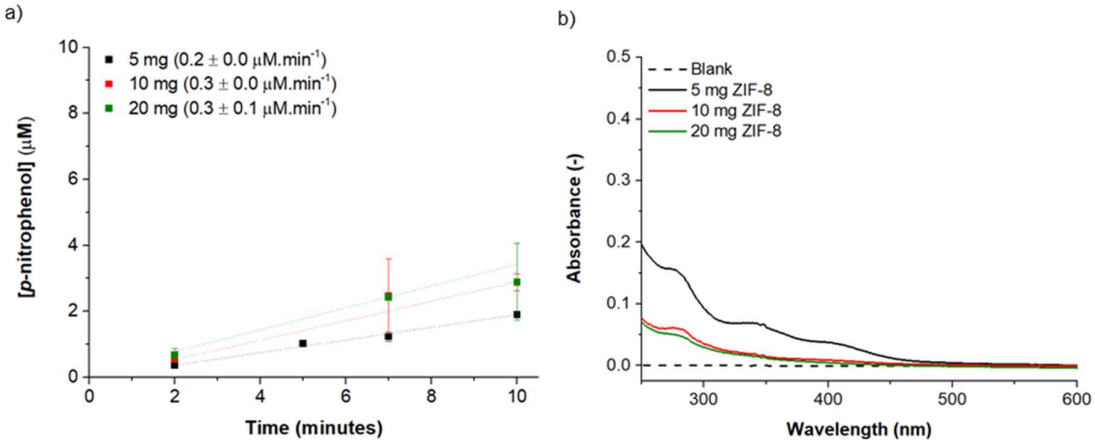

Figure S4.10: a) Hydrolysis assay data of CALB (0.2 mg) surface bound onto 40:640 ZIF-8 (5 mg, 10 mg and 20 mg). Rates are similar to BSA@ZIF-8 controls. b) Absorbance spectrum of the supernatants obtained of each surface bound sample used to calculate surface coverage values in **Table S4.1**. Analysis of the supernatant of the surface only samples, indicated that near 100% adsorption of CALB (and FITC-CALB) was possible, but reduced when the mass of support was decreased.

4.9.7. Buffer Comparison (Hydrolysis)

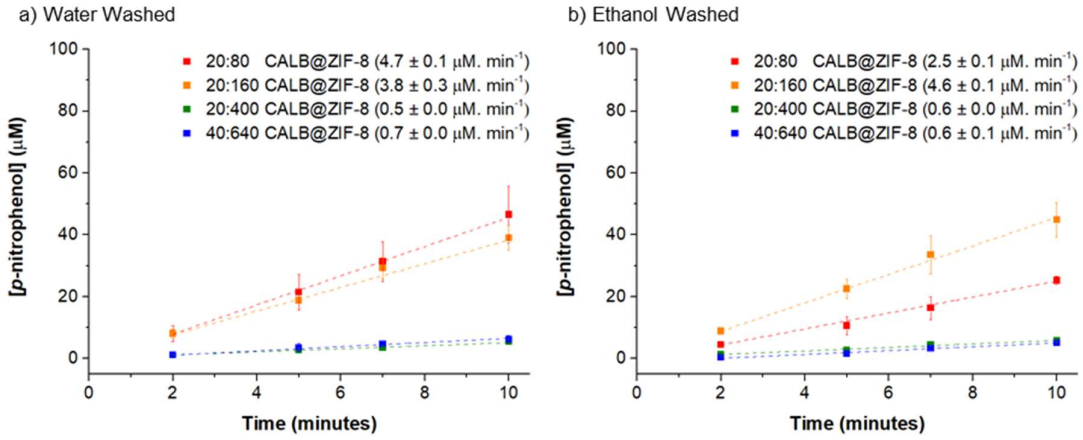

Figure S4.11: Hydrolytic activity of the CALB@ZIF-8 biocomposites in phosphate buffer (50 mM, pH 7.4) + Triton X-100 (0.1%) (a) two water washes and (b) two additional ethanol washes. All assays were undertaken as per the tris assay.

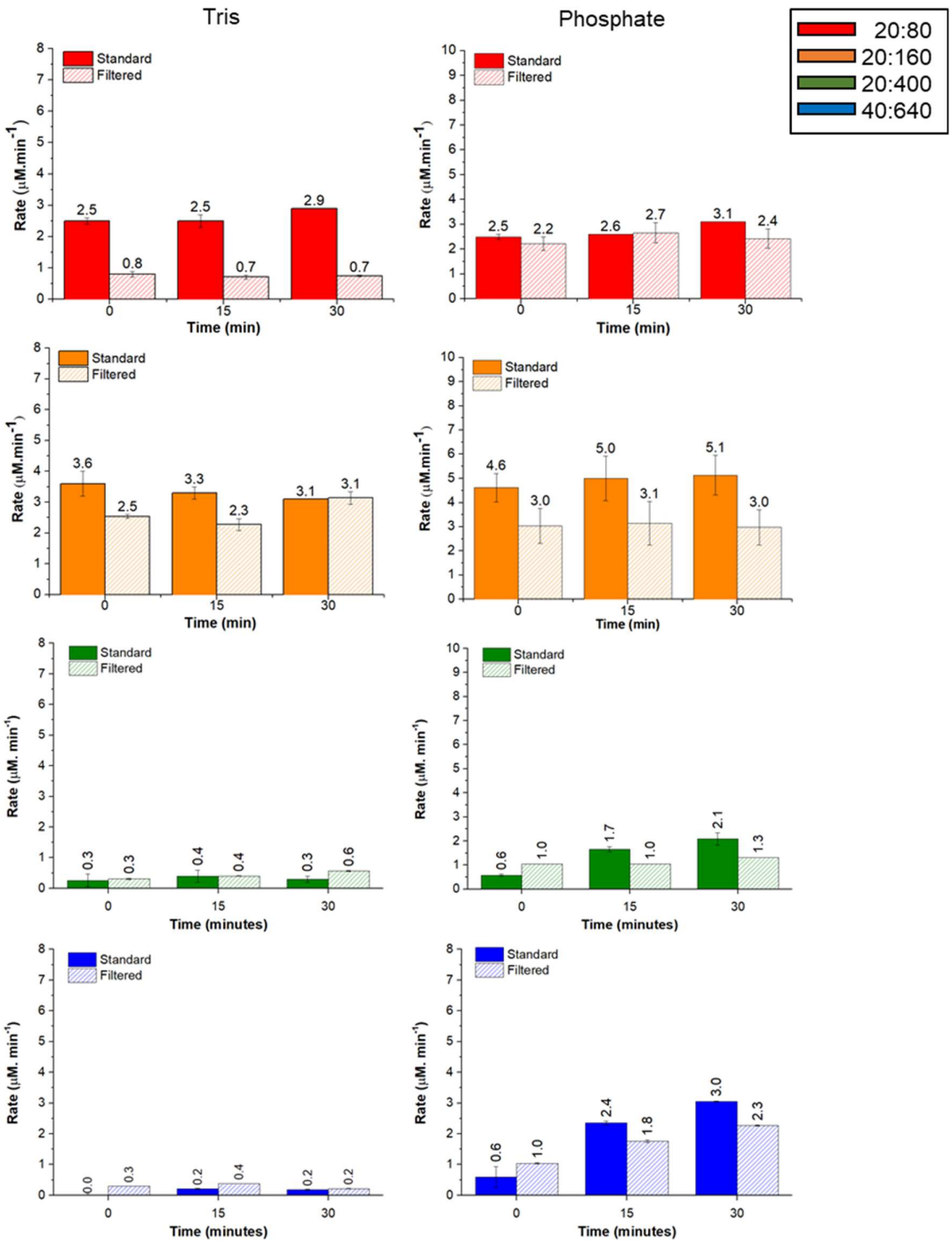

Figure S4.12: Average rates of *p*-NPB production using ethanol washed samples after exposure to tris or phosphate buffer. Both the standard assay conditions, and the filtered biocomposites have been reported.

4.9.8. CALB@ZIF-8 Stability Testing

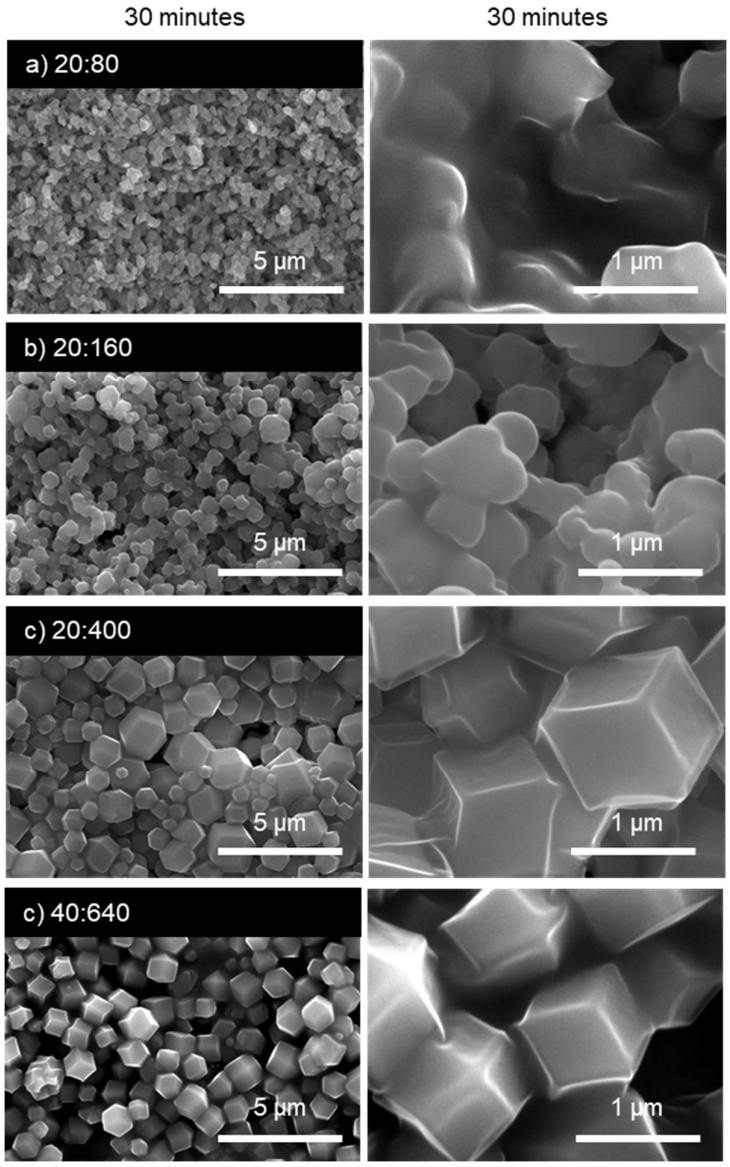

Figure S4.13: SEM images of each CALB@ZIF-8 composite after 30 minutes exposure to tris buffer. Surface charging was more significant on the smaller crystals (a) and (b) due to the greater surface area of the bulk material.

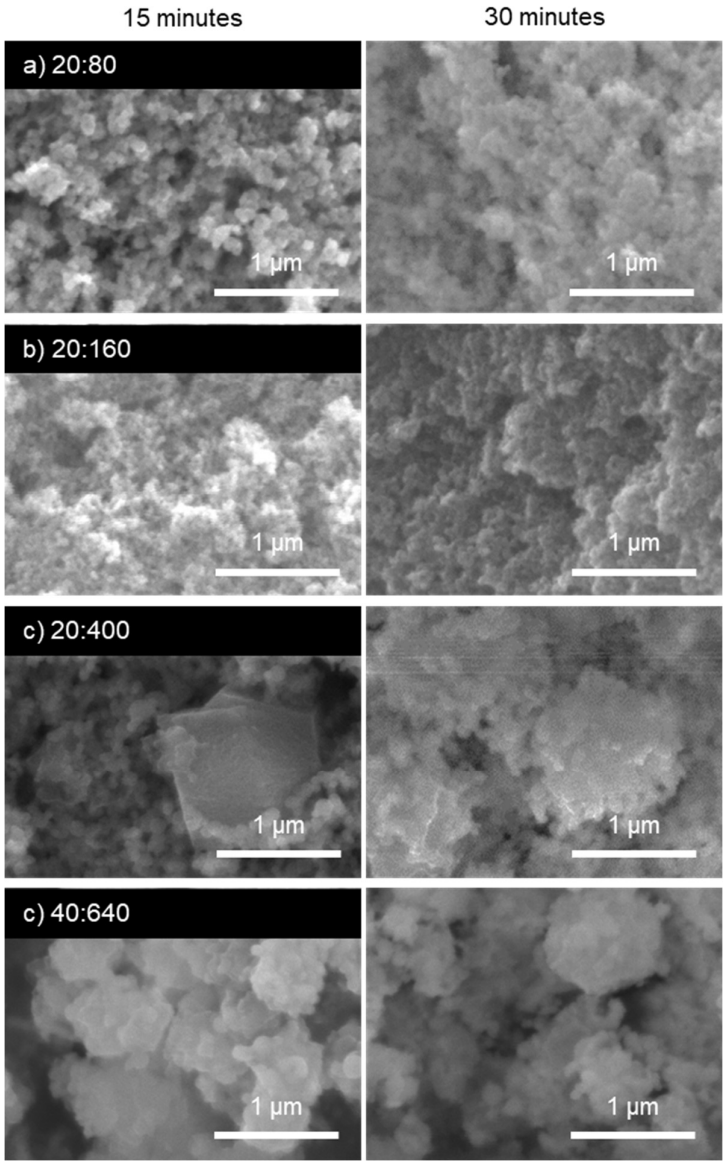

Figure S4.14: SEM images of after 15- and 30-minute exposure to 50 mM phosphate buffer. Size dependant destruction was observed with the 20:80 (a) and 20:160 (b) samples losing all crystallinity, and the larger samples 20:400 (c) and 40:640 (d) retained some structural integrity in conjunction with smaller particle formation. Additional images obtained after 15 minutes, showed that the complete degradation of some crystals had occurred during the shorter exposure time.

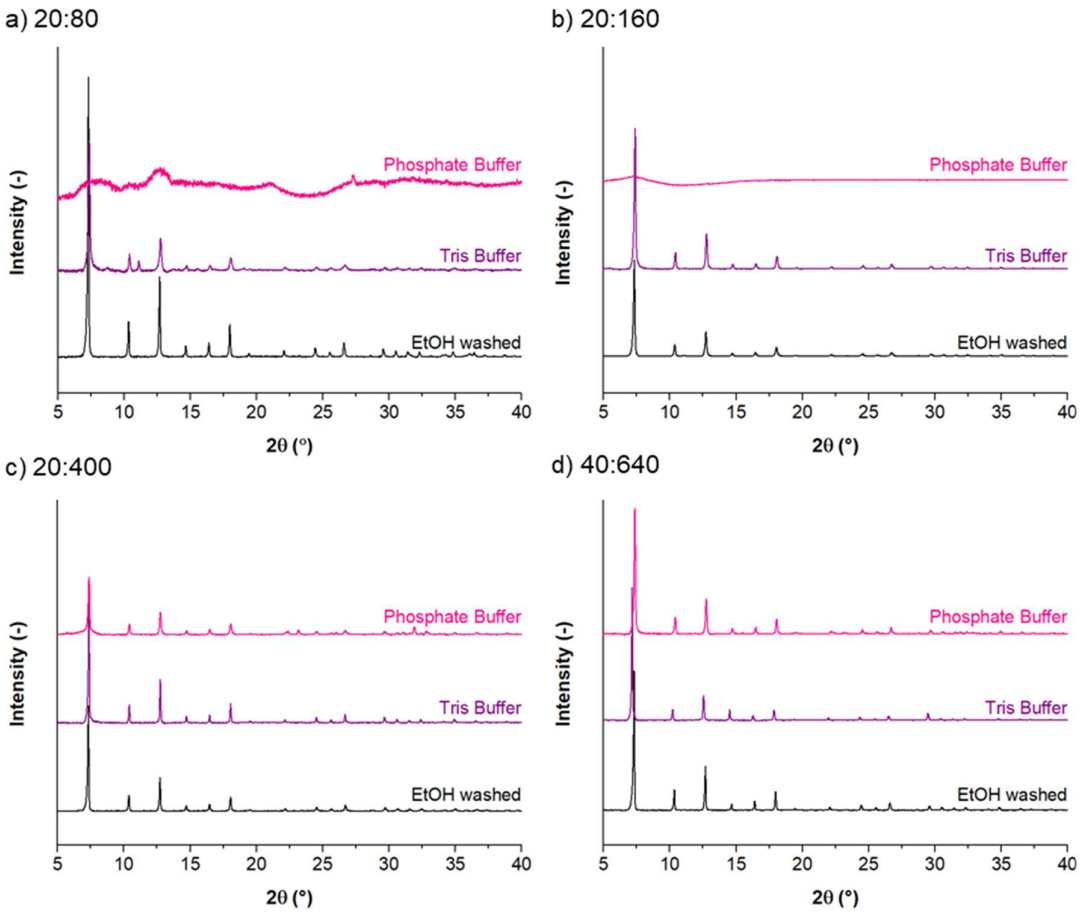

Figure S4.15: PXRD of each CALB@ZIF-8 after 30 minutes exposure to tris or phosphate buffer (50 mM, pH 7.4). All samples retained bulk crystallinity after exposure to tris buffer. Smaller crystals of the(a) 20:80 and (b) 20:160 lost all peak intensity after 30 minutes exposure to phosphate, whereas the larger crystals of the (c) 20:400 and (d) 40:640 retained some crystallinity, further highlighting the size dependant degradation.

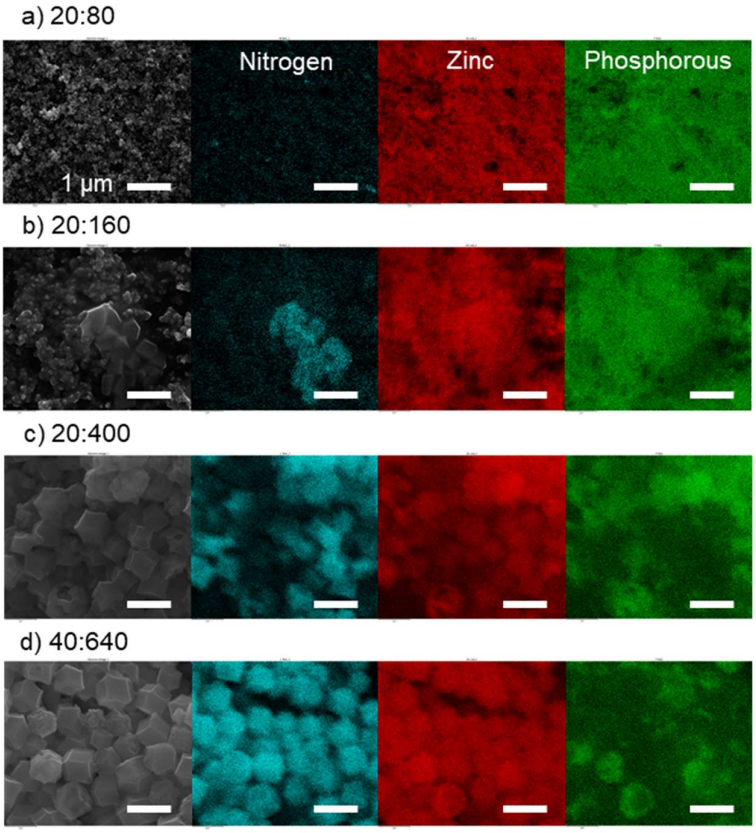

Figure S4.16: SEM-EDX of each ZIF-8 biocomposites further highlighting the size dependence of phosphate buffer degradation. (a) and (b) show complete degradation, highlighted by the full coverage of phosphorous across the entire sample. (c) and (d) show degradation to a lesser extent, observable by SEM and the isolated regions of phosphorous that is concentrated around the surface of the crystals. All samples were washed three times to remove soluble sodium-phosphate salts, so phosphorous content can be mainly attributed to the formation of insoluble zinc-phosphate salts.

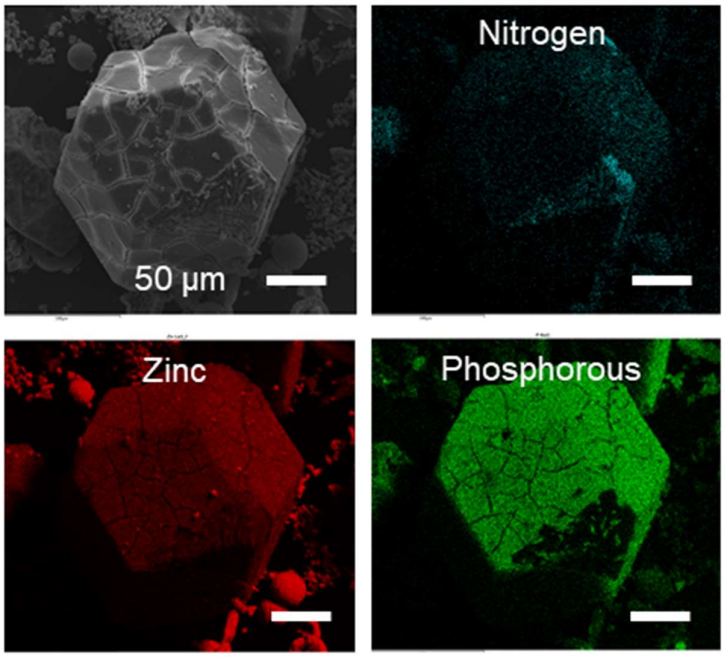

Figure S4.17: SEM-EDX of >100 µm protein free crystals. The sample was washed three times to remove soluble sodium-phosphate salts.

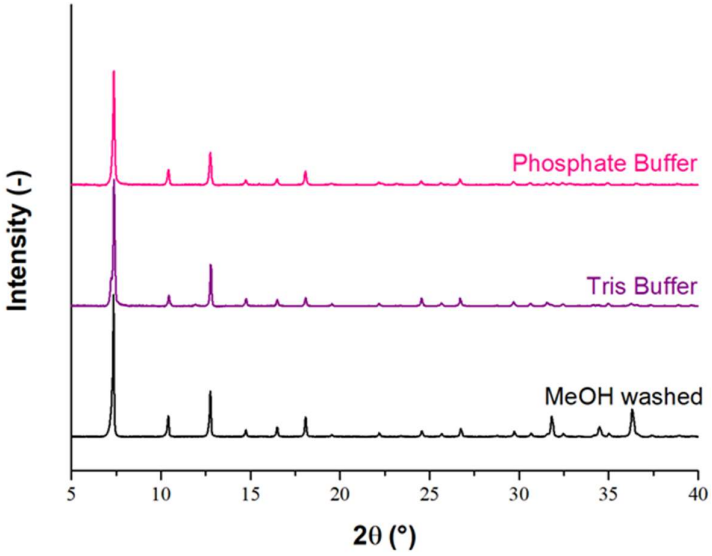

Figure S4.18: PXRD of >100 µm protein free crystals as-synthesised (methanol washed) and post tris and phosphate buffer exposure.

4.9.9. CALB@ZIF-8 Activity (Transesterification)

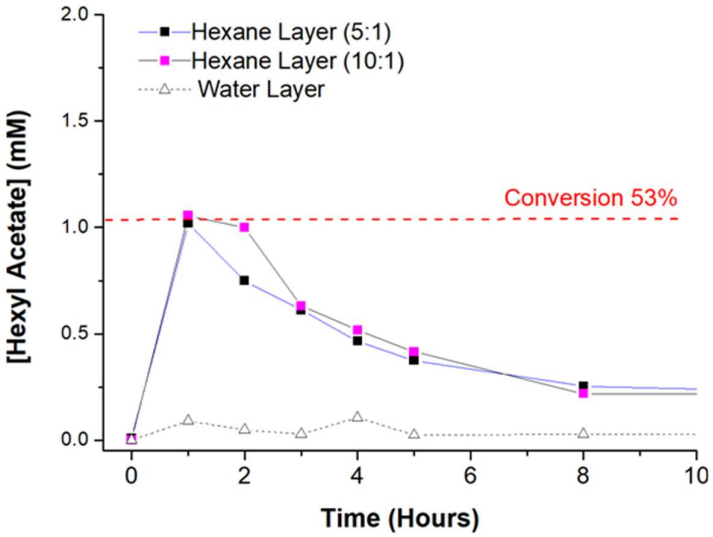

Figure S4.19: Transesterification of vinyl acetate: hexanol (5:1) in 50:50 water: hexane using the free CALB (black). The aqueous layer contained only low levels of hexyl acetate showing that most of the product was being extracted into the organic layer throughout the duration of the reaction. (grey) Increasing the initial vinyl acetate concentration (10:1), did not change the initial production rate or the overall activity trend (pink). In the remaining time points, the concentration of hexyl acetate decreased, correlating with an increase in hexanol production, suggesting that the ester concentration had reached a threshold where hydrolysis of the product was favoured. After 24 hours, the hexyl acetate concentration had decreased to 15%. When in the presence of only hexyl acetate, CALB was shown to hydrolyse 90% of the ester after 5 hours. Reports of 80% ester production have been measured for similar biphasic systems, so it is therefore possible for the percentage conversion to have been higher during the first hour of the reaction.[4] Concentrations refer to the hexane layer of the biphasic system. GC-FID retention times are displayed in **Figure S4.21**.

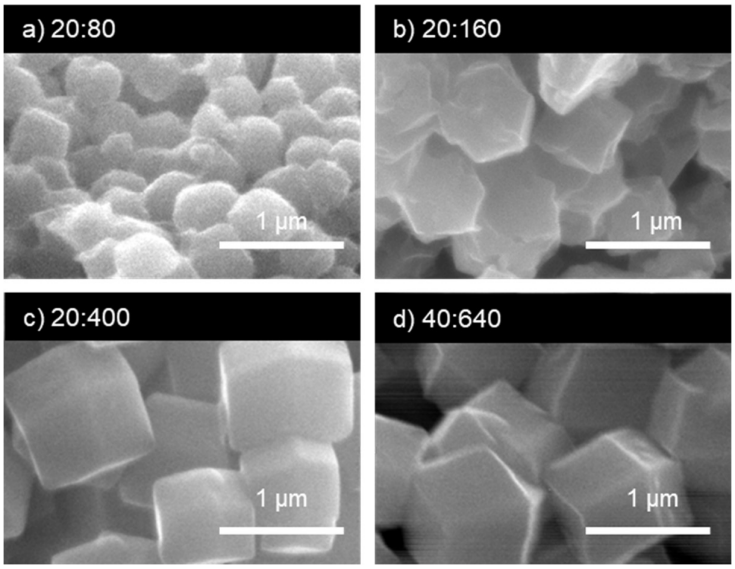

Figure S4.20: SEM images of each CALB@ZIF-8 composite after an 8-hour transesterification reaction with hexanol and vinyl acetate in hexane.

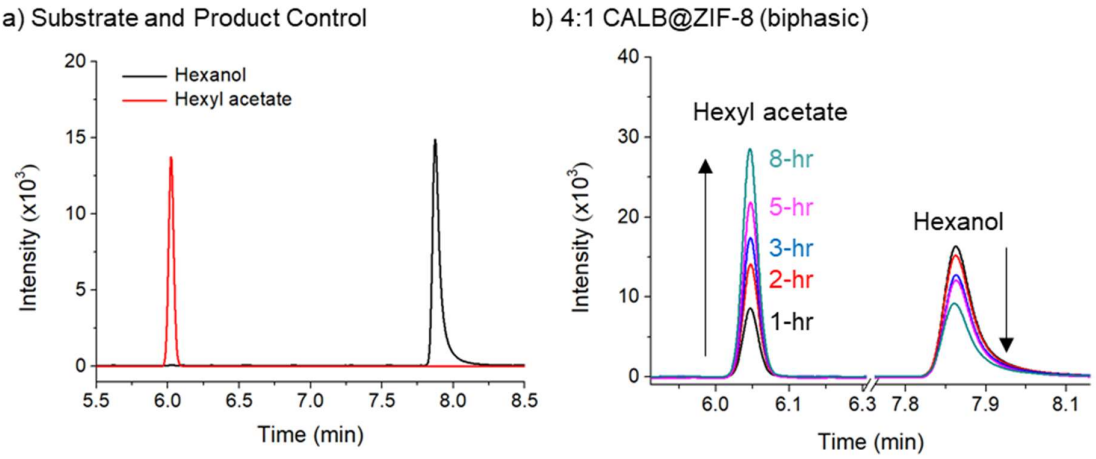

Figure S4.21: a) Hexanol and hexyl acetate GC-FID control traces, with retention times 7.9- and 6.1 minutes respectively. b) Example GC-FID trace of the 4:1 CALB@ZIF-8 biocomposite in the 50:50 (water/hexanol) biphasic system.

4.9.10. Removal of Surface Bound Enzyme

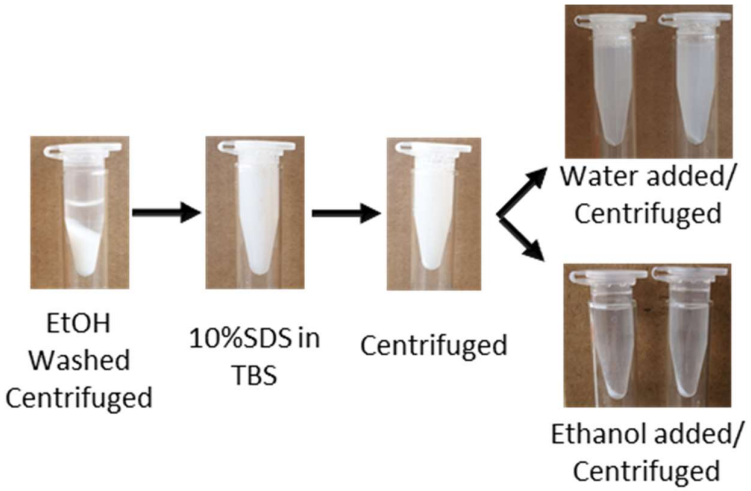

Figure S4.22: Each composite was soaked in a solution of 10% SDS in tris buffered saline (TBS, pH 7.5) for 30 minutes, however after centrifugation, a large proportion of the particles remained dispersed in solution. Liang *et. al.* reported using an ethanol wash to remove excess surfactant,[5] however, as described previously, an ethanol wash lead to a reduction in activity for the 20:80 sample. As no spatial distribution could be obtained from the CLSM images, it would be challenging to distinguish between the removal of surface enzyme via SDS wash and a general loss of activity due to ethanol.

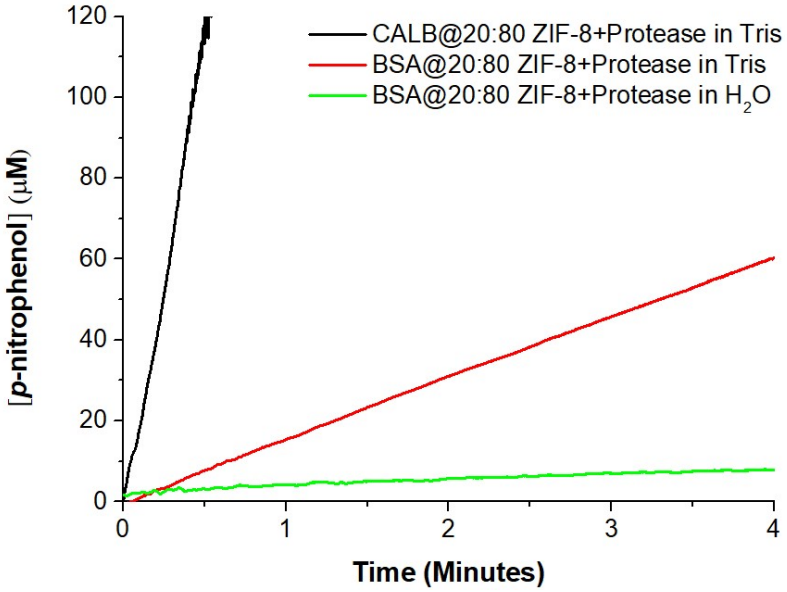

Figure S4.23: A secondary method utilised a proteolytic enzyme (protease from *Bacillus lichenformis*) which has a broad substrate range, capable of cleaving most peptide bonds. This method should lead to denaturation of only surface bound CALB as the pore aperture of ZIF-8 would prevent interaction of the proteolytic enzyme with sub-surface lipase. When tested with the free enzyme and CALB@ZIF-8 it was found that the proteolytic enzyme in tris interfered with the reaction, leading to an increase in the key absorbance at 405 nm, at a rate much faster than expected from the lipase (Black). Similarly, when tested with the BSA@ZIF-8 biocomposites false positive readings were obtained if the protease was not effectively removed (Red) Surface adsorbing of enzymes onto ZIF-8 has also been established in previous literature, so it is not unreasonable to assume that the protease would adhere to the surface and this would need additional steps to remove. Multiple water washes (3x) of the BSA@ZIF-8 sample led to a reduction in activity (Green), suggesting that the protease was being removed however partial loss of the biocomposite occurred after each centrifugation cycle, likely due to the dispersion caused by tris buffer.

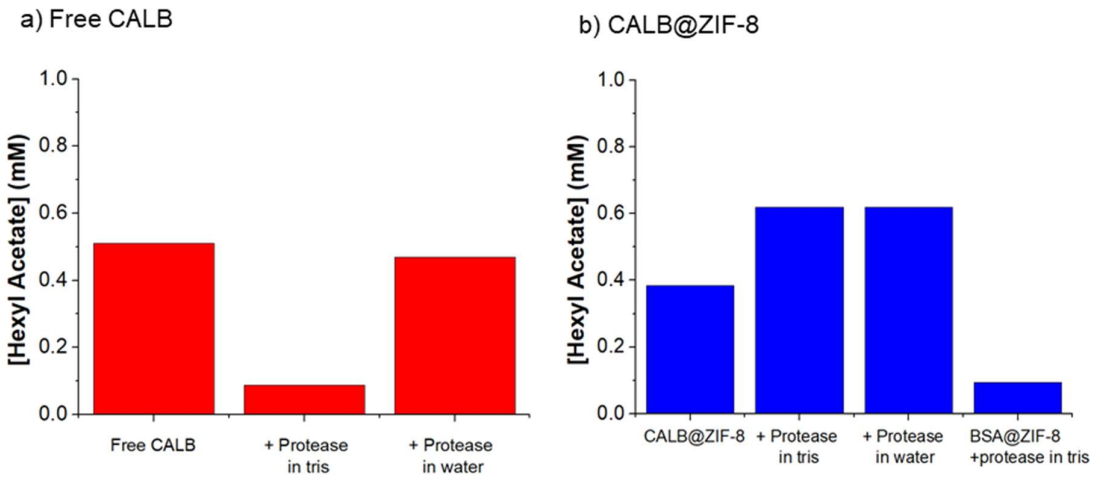

Figure S4.24: The protease was tested for its influence on the transesterification in the biphasic system. First, the protease was shown to not cleave hexyl acetate, so all activity variations arise from the change in CALB. a) The free enzyme, measured at the maximum conversion (1 hour) timepoint, saw a reduction in activity (~85%) when treated with protease in tris buffer, but not in water. b) CALB@ZIF-8 assay, measured at the maximum conversion (8 hour) timepoint. Enhanced activity was observed for the CALB@ZIF-8 sample treated with protease in both tris and water however, minimal interference was noted for the BSA@ZIF-8 (protease treated) control. These findings suggest that activity of CALB@ZIF-8 is due to an increased exposure of the lipase to the substrates, rather than the degradation and release of Zn^{2+} and 2-mIM. As such, this method was not deemed suitable for removing surface bound enzyme for this assay. Attempts using trypsin as the proteolytic enzyme yielded the same result.

Supporting Information 4.9 References

1. Rabbani, G.; Ahmad, E.; Khan, M. V.; Ashraf, M. T.; Bhat, R.; Khan, R. H., Impact of structural stability of cold adapted *Candida antarctica* lipase B (CaLB): in relation to pH, chemical and thermal denaturation. *RSC. Adv.* **2015,** *5* (26), 20115-20131.

2. Hungerford, G.; Benesch, J.; Mano, J. F.; Reis, R. L., Effect of the labelling ratio on the photophysics of fluorescein isothiocyanate (FITC) conjugated to bovine serum albumin. *Photochem. Photobiol.* **2007,** *6* (2), 152-158.

3. Linder-Patton, O. M.; de Prinse, T. J.; Furukawa, S.; Bell, S. G.; Sumida, K.; Doonan, C. J.; Sumby, C. J., Influence of nanoscale structuralisation on the catalytic performance of ZIF-8: a cautionary surface catalysis study. *CrystEngComm.* **2018,** *20* (34), 4926-4934.

4. Park, S.-C.; Chang, W.-J.; Lee, S.-M.; Kim, Y.-J.; Koo, Y.-M., Lipase-catalyzed transesterification in several reaction systems: An application of room temperature lonic liquids for bi-phasic production ofn-butyl acetate. *Biotechnol. Bioproc. E.* **2005,** *10* (1), 99.

5. Liang, W.; Ricco, R.; Maddigan, N. K.; Dickinson, R. P.; Xu, H.; Li, Q.; Sumby, C. J.; Bell, S. G.; Falcaro, P.; Doonan, C. J., Control of structure topology and spatial distribution of biomacromolecules in protein@ZIF-8 biocomposites. *Chem. Mater.* **2018,** *30* (3), 1069-1077.

Chapter 5.

Enantioselective Transesterification with Lipase Immobilised within a Metal-Organic Framework (ZIF-90) and a Hydrogen-bonded Organic Framework (BioHOF-1)

Chapter 5. Enantioselective Transesterification with Lipase Immobilised within a Metal-Organic Framework (ZIF-90) and a Hydrogen-bonded Organic Framework (BioHOF-1)

5.1. Abstract

The immobilisation of enzymes within porous supports has been demonstrated to stabilise the biomacromolecules to non-biological media, extending their activity to reaction conditions that would otherwise cause protein denaturation. The chemistry and porosity of the framework can however alter enzyme activity and careful selection of the immobilisation support is required to maximise activity whilst maintaining biocomposite stability, handling ease, and reusability. We have immobilised *Candida antarctica* lipase B (CALB) into zeolitic imidazolate framework-90 (ZIF-90) and a porous Hydrogen-bonded Organic Framework (BioHOF-1), and have demonstrated that the properties of these frameworks (crystal size, hydrophobicity and pore size) provide enhanced enzyme activity and reusability compared to the hydrophobic framework, zeolitic imidazolate framework-8 (ZIF-8). The reactions catalysed by these new biocomposites maintains the high enantioselectivity (ee. 99%) of the enzyme and stability over an extended reaction period.

5.2. Introduction

The syntheses of enantiopure compounds are an important component of medicinal and organic chemistry. The biological function of many pharmaceuticals is often affected by the stereochemistry of the drug and hence the separation of enantiomers from a racemate is necessary.[1-4] Kinetic resolution of enantiomers utilising a chiral catalyst or reagent and relies on different reactivity to generate an enantiopure product that can be easily separated from the unreacted starting material.[5] Enzymes are chiral catalysts that provide control over substrate accessibility and orientation within an active site, and thus can mediate these reactions with high chemo-, regio- and stereo-selectivity.[6] They function under mild reaction conditions, making them a 'greener' alternate to standard chemical techniques, however their activity can be hindered by high temperature, extreme pH and organic solvents. [7-9] Enzymatic reactions are further complicated during purification, where intricate and expensive processes are required to separate the product from the enzyme catalyst, often denaturing the enzyme and limiting the potential turnover number.[10-11] Enzyme immobilisation techniques can be implemented to generate a heterogeneous enzyme catalyst that can be more easily separated from the reaction mixture prior to product purification.[12] This enables efficient enzyme recycling, thus maximising the overall catalytic output of the enzyme. Enzymes can be immobilised via several methods, including enzyme-enzyme cross-linking, attachment to a solid support, or encapsulation/entrapment within a porous material, all of which will generate biocomposites of varied stability and activity resulting from different enzyme-support interactions.[13-15]

Candida antarctica lipase B (CALB) is an enzyme commonly employed for kinetic resolution experiments with enantiomeric excess (ee) of 99% reported for certain transesterification and hydrolysis reactions.[16-18] Care must be taken, however when selecting an immobilisation support, as a drastic reduction in catalytic rate and change in selectively are possible.[19-22] For example, commercially available Novozym 435 (CALB immobilised onto Lewatit VP OC 1600) hydrolyses 2-O-butyryl-2-phenylacetic acid **(1)** with preference for the *S* ester (ee 99%) but prefers hydrolysis of the *R* ester (99%) of 3-phenylglutaricdimethyl diester **(2)** (**Figure S5.1**).[21] Changing the immobilisation support to Octadecyl-Sepabeads, resulted in an inversion in the preference of **1** (90% *R* ester) but maintained the *R* preference, with lowered selectivity, for **2** (61%, **Figure S5.1**).[21] CALB has also been reported to catalyse reactions with little or no selectivity, however, alterations to reaction solvent, pH and temperature can instigate enzyme conformation changes which improve reactivity and/or selectivity.[23-24] Activity and selectivity can therefore be controlled through judicious selection of the

immobilisation method and conditions; however, predicting this process is challenging for different substrates.[20-21]

Chapter 4 describes the activity of CALB within a metal-organic framework, ZIF-8 (zeolitic imidazolate framework-8) which reported the relationship between enzyme activity and the synthetic conditions used to generate the CALB@ZIF-8 biocomposite**.** Metal-organic frameworks (MOFs) are network solids composed of metal nodes connected via organic links and are noteworthy for their high degree of crystallinity and porosity.[25-26] ZIF-8 is a class of MOF composed of tetrahedral Zn^{2+} nodes and 2-methyl imidazole (2-mIM) links that form a porous sodalite topology.[27] CALB@ZIF-8 was previously examined for a transesterification reaction between vinyl acetate and hexanol where size dependant activity was observed for the biocomposite i.e. small (500 nm) CALB@ZIF-8 biocomposites exhibited higher activity than the larger particles (1 μm). This was attributed to the different formation mechanisms that gave rise to a hierarchical pore structure in the smaller biocomposites. However, other factors such as framework hydrophobicity and average pore size need to be considered as it is well known that these properties can influence enzyme activity retention and substrate diffusion.[28-30] Therefore we sought to examine the immobilisation of CALB on two frameworks, zeolitic imidazolate framework 90 (ZIF-90) and a Hydrogen-bonded Organic Framework (HOF) that have different hydrophilicities and, in the case of the HOF, significantly different pore sizes.

ZIF-90 is a zinc-based, sodalite framework, that replaces the 2-mIM linker of ZIF-8 with 2-imidazole carboxaldehyde (ICA).[31](**Figure S5.2**). This simple change to the organic linker creates a protein@ZIF biocomposite that forms via a co-precipitation method rather than the biomimetic mineralisation process of ZIF-8.[29, 32-33]. Whilst the protein plays an integral role in seeding and accelerating the growth of ZIF-8, the initial formation (first 500 seconds) of ZIF-90 is not strongly influenced by the addition of a protein. The ZIF-90 biocomposite is significantly more hydrophilic than ZIF-8, which results in different enzyme-enzyme and enzyme-support interactions. This, in addition to the distinct formation processes, will likely create CALB@ZIF-90 biocomposites that exhibit different enzyme conformations, spatial distribution and activity.[20] Indeed, recent reports have shown that catalytic activity of catalase is impeded when immobilised onto the hydrophobic ZIF-8 framework but is maintained when immobilised on the more hydrophilic framework of ZIF-90.[29] Similarly, CALB transesterification activity was lost when encapsulated within 1 μm ZIF-8 and only partially retained when surface adsorbed on the framework.

HOFs are porous, metal-free frameworks that form via intermolecular hydrogen bonding of discrete organic ligands.[34-38] Much like the assembly of MOFs, this class of porous material can be assembled in a modular fashion, and with careful ligand selection and tailoring of the synthetic conditions, a vast library of HOF materials of different properties (pore size, shape, stability, permanent porosity) can be constructed.[39] More recently, HOFs have become a target material for biological applications as they can be synthesised in biocompatible conditions of aqueous media, low temperature and minimal acid/base inclusion.[39-40] In particular, the biocompatible assembly of a novel HOF (hereafter termed BioHOF-1), comprising of tetra-amidinium and tetra-carboxylate ligands (**Figure S5.2**), has been developed to encapsulate and stabilise enzymes such as catalase and alcohol oxidase.[30] BioHOF-1 has a pore size of 6.4 Å, which exceeds that of the ZIFs (~3.4 Å), and thus may allow for larger substrates to be accessible to the enzyme. In a recent study, the solution accessible porosity of BioHOF-1 was measured, where it was shown that the fluorescent molecule, fluorescein (size 7 Å) could diffuse homogenously throughout the framework.[30] Additionally, BioHOF-1 is stable to buffers, chelating agents, and mild acidic conditions that would ordinarily lead to complete degradation of ZIFs, and thus increase the potential reaction conditions.[30]

In this study we, synthesised encapsulated CALB biocomposites (CALB@ZIF-90 and CALB@BioHOF-1) and tested them for the transesterification of hexanol and vinyl acetate. We were therefore motivated to understand the effect of the more hydrophilic framework (ZIF-90) and the novel metal free framework (BioHOF-1) on the activity and selectivity of equivalently sized CALB@ZIF-8 particles.

5.3. Results and Discussion

5.3.1. CALB@ZIF-90 Synthesis

The encapsulated CALB biocomposites and their respective protein free samples were synthesised according to procedures reported in the literature for catalase.[29-30] During the screening process for CALB@ZIF-90, a correlation between formation time and particle size was observed. Mixing the precursors (Zn^{2+}, ICA, and CALB) led to instant precipitation, generating ~1 μm particles after 10 minutes (**Figure 5.1a),** but when left for 24 hours the particle size increased to ~2 μm (**Figure 5.1b**)**.** Interestingly, the 10-minute sample contained a mixture of crystal sizes, including crystals of approximately 5 μm in diameter (similar to the protein free control), however these larger crystals were not observed in the 24-hour sample. PXRD of these samples revealed that phase pure crystals were formed after 10 minutes (**Figure 5.2a**)**,** however longer formation times often led to crystallisation of a second phase (**Figure 5.2b**), later determined to be crystallised ligand (**Figure S5.3**).

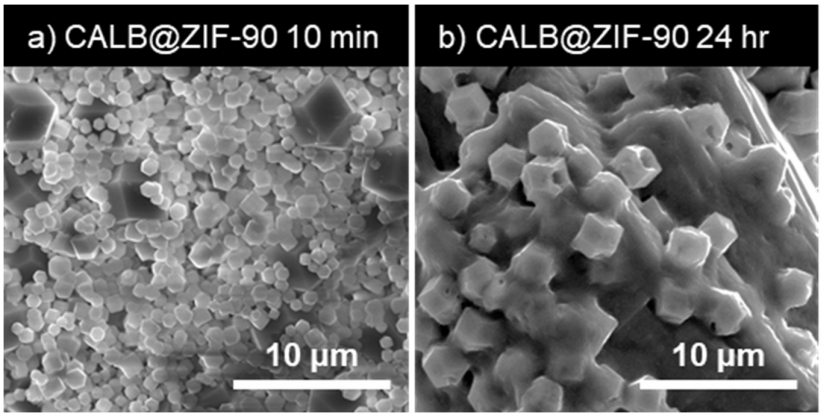

Figure 5.1: Scanning Electron Microscopy (SEM) images of CALB@ZIF-90 biocomposites after 10 minutes of formation versus 24 hours. The predominant particle size of the CALB sample was ~1 μm with some larger crystals (approximate size of protein free ZIF-90, 5μm) also being formed suggesting that the lipase is altering the growth. After 24 hours, the CALB@ZIF-90 were larger in size (2 μm) and showed the presence of ligand like crystals (**Figure S5.3**).

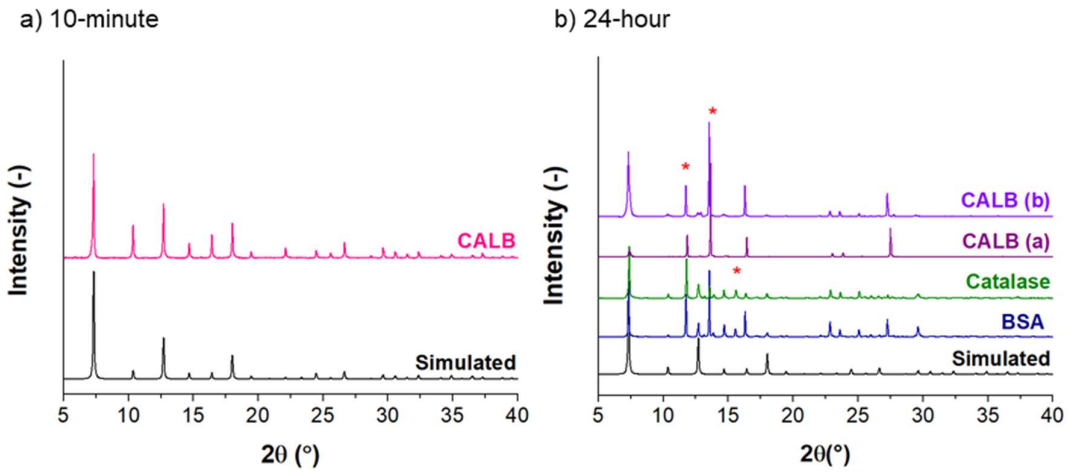

Figure 5.2: PXRD of ZIF-90 biocomposites. a) Phase pure sodalite CALB@ZIF-90 was formed in the initial 10 minutes. b) When left for 24 hours the CALB@ZIF-90, transitioned into multiple phases with peaks in addition to the sodalite pattern appearing at 2θ values (*). Due to variability in the CALB@ZIF-90 samples (repeated twice), BSA, and Catalase, were tested and left to form for 24 hours for comparison. Each additional biocomposite retained sodalite features in addition to the alternative phase observed with CALB.

In the absence of protein, much larger crystals were obtained for ZIF-90 indicating that CALB (and other proteins) were influencing crystal growth. (**Figure 5.3**). Over the course of 24 hours, the protein free ZIF-90 samples transitioned from large (5-10 μm), rhombic dodecahedral crystals of sodalite topology (10 minutes) to a less well-defined structure, consisting of a more densely packed crystal phase (24-hour). With the inclusion of an enzyme such as CALB, ZIF-90 forms smaller crystals after 10 minutes (1 μm) which are resilient to morphological and topological changes, which can be attributed to the influence of CALB on the formation rate of the framework relative to the protein free control. The rapid ZIF-90 formation in the absence of protein may result in significant defects within the crystals, which may have caused the phase transition, from sodalite to a more densely packed phase, over the 24-hour period (**Figure 5.4**).[41] Additionally, during the imaging process, it was noted that the larger rhombic dodecahedral crystals of the control (**Figure 5.3a-c**) were susceptible to degradation and loss of edge definition by the electron source of the SEM (10 keV). In the presence of CALB, ZIF-90 forms more slowly, potentially allowing for more self-correction during framework self-assembly, thereby forming a more stable sodalite composite. The slower formation did however lead to competitive crystallisation of the ligand which could not be removed using standard water wash procedures.

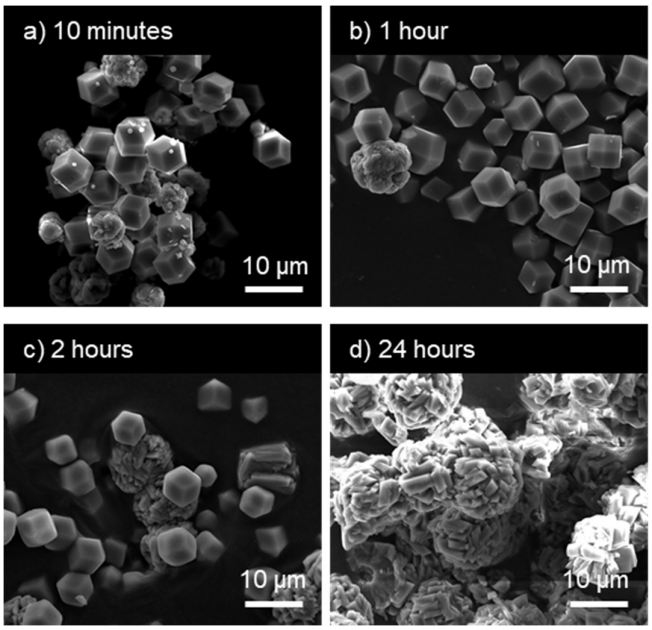

Figure 5.3: SEM images of time dependent formation of protein free ZIF-90 crystals. After the initial mixing of precursors, the protein free ZIF-90 sample was left for (a) 10 minutes, (b) 1, (c) 2 and (d) 24 hours.

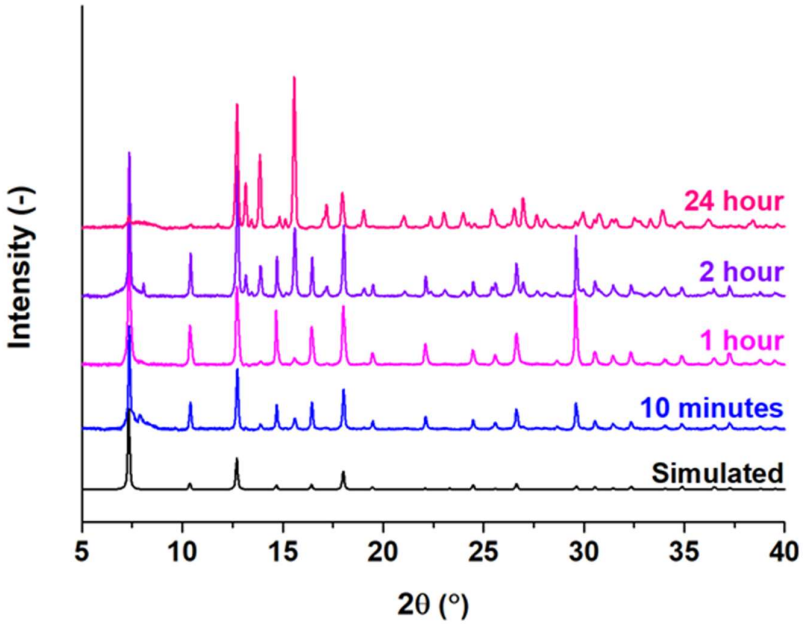

Figure 5.4: PXRD of the protein free ZIF-90 formation at different time points. Monitoring via PXRD highlighted a change in powder pattern that lead to a complete change in topology

after 24 hours. Peaks began appearing after 10 minutes at 13.2, 13.8 15.6 and 17.2**,** which further increased in intensity relative to the 7.4 peak at the subsequent time points.

5.3.2. Considerations for ZIF-90 Biocomposite Analysis

To enable direct comparison of CALB biocomposites, it is essential to have phase pure ZIF-90 samples with consistent crystal morphology to minimise the variability in the enzyme - support interaction. For both CALB@ZIF-90 and protein free ZIF-90, sample uniformity was greatest for the 10-minute synthetic conditions. Due to the inconsistencies of the 24-hour samples (morphology, topology, and ligand crystallisation), there is greater variability in the support surfaces and thus possible interactions with the enzyme. As such, initial studies focussed on comparing the CALB@ZIF-90 (10-minute) to CALB adsorbed on the surface of the protein free ZIF-90 (10-minute).

5.3.3. Spatial Distribution Analysis with ZIF-90 Biocomposites

Prior to activity testing, the spatial distribution and immobilisation efficiency of the 10-minute samples was determined using Fluorescein isothiocyanate (FITC) tagged CALB. A direct comparison was made between CALB@ZIF-90 (10-minute) with a sample of ZIF-90 (10-minute) to which FITC-CALB had been adsorbed to the surface (CALB on ZIF-90). Fluorescence of FITC-CALB was observed across the whole CALB@ZIF-90 crystal showing that the FITC tagged enzyme is colocalising with the ZIF-90 (**Figure 5.5a**). There is an increase in fluorescence intensity around the edges of the crystals suggesting that there is a mixture of surface bound, and sub-surface (or encapsulated enzyme). Whereas for the surface adsorbed sample, CALB on ZIF-90, fluorescence intensity was observed at only the exterior of the crystals (**Figure 5.5b**). No absorbance peak of FITC (495 nm) was observed in the supernatants of each biocomposite, which is indicative of complete loading of the FITC-CALB onto the support for both the co-precipitation and surface adsorbed samples (**Figure S5.4**).

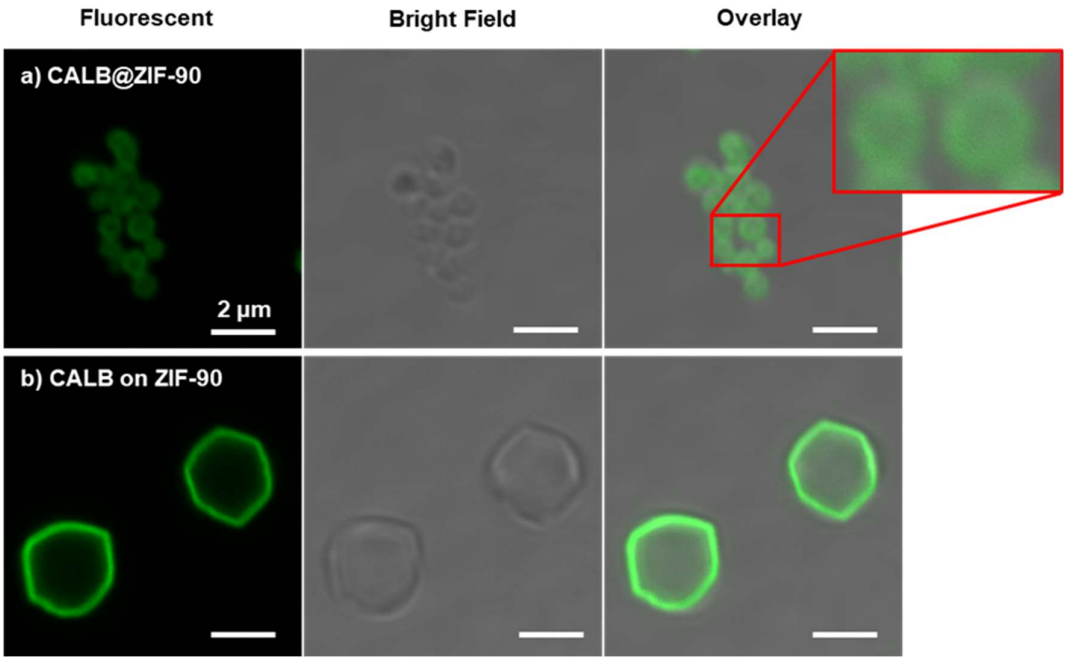

Figure 5.5: Confocal Laser Scanning Microscopy (CLSM) images of CALB@ZIF-90 and CALB on ZIF-90. Fluorescein isothiocyanate (FITC) tagged enzyme (2 mg CALB) was used for both encapsulation and surface adsorption. The FITC-CALB sample was washed thoroughly using a 10 KDa membrane with centrifugation until no absorbance from the tag remained in the flow through, ensuring that the only FITC in the biocomposites was from tagged CALB.

5.3.4. CALB@ZIF-90 Activity (Hydrolysis)

The activity of CALB@ZIF-90 was measured via the hydrolysis of *p*-nitrophenyl butyrate (*p*-NPB), and transesterification between hexanol and vinyl acetate (**Figure 5.6**). The reaction conditions, including substrate and CALB concentrations (based on FITC-CALB data, **Figure S5.4**) were consistent with those reported for ZIF-8 biocomposites (**Chapter 4**) to allow for a direct comparison of framework properties.

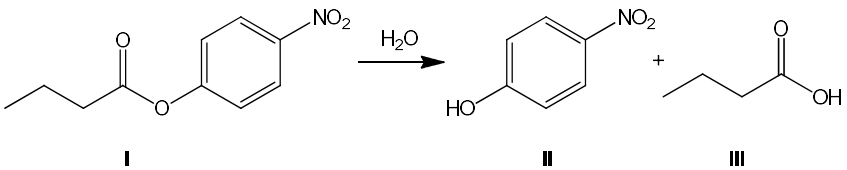

Figure 5.6: Hydrolysis Reaction Scheme. *p*-nitrophenyl butyrate (*p*-NPB) **I** is hydrolysed, generating *p*-nitrophenol (*p*-NP) **II** and a butyric acid **III**. Assays were measured in tris buffer (50 mM, pH 7.4) as ZIF-90 have been proven to be stable to these conditions.[29]

For ZIF-8, the size of the crystals was shown to significantly impact the catalytic output of the biocomposite (**Chapter 4**). Hence, for direct comparison of ZIF-8 and ZIF-90 it is important to minimise particle size variation between biocomposite samples. As such, the CALB@ZIF-90 (10-minute sample) was tested as the mean particle size was ~1 µm and most closely resembled the inactive, 1 µm ZIF-8 (Zn^{2+}:2-mIM; 40:640 mM) biocomposite. In contrast to the ZIF-8 biocomposites, the CALB@ZIF-90 (10-minute) was active, with respective rates of *p*-NPB hydrolysis of 0.3 ± 0.1 µM.min^{-1} (**Chapter 4**) and 1.0 ± 0.0 µM.min^{-1} (**Figure 5.7a**). The enhanced rate highlights that the more hydrophilic framework immobilises CALB in an active conformation with a spatial distribution within the framework that is substrate accessible.

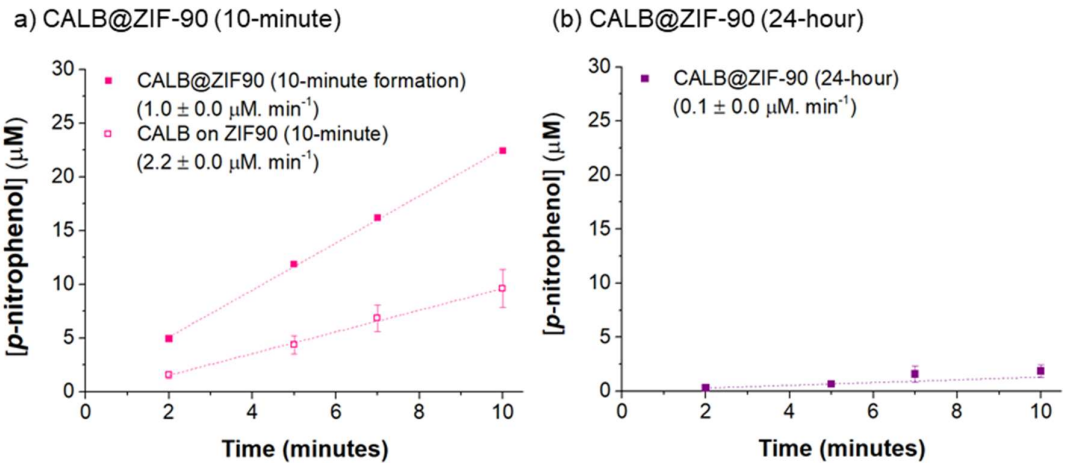

Figure 5.7: Hydrolytic activity of ZIF-90 biocomposites in tris buffer (50 mM, pH 7.4)+Triton X-100 (0.1%). (a) CALB@ZIF-90 (10-minute) was more active than the equivalently sized CALB@ZIF-8 (0.2 ± 0.1 µM.min^{-1}). It is, however, slower than the smaller, 4:1 CALB@ZIF-8 biocomposite (3.7 ± 0.1 µM.min^{-1}). Adsorbing CALB onto the surface of the 10-minute ZIF-90 increased the activity (~2x), whereas activity for CALB on ZIF-8 remained low. For (b) CALB@ZIF-90 (24-hour), activity was depleted to background hydrolysis rates (**Figure S5.5**). All samples were tested after three water washes to remove excess precursors and unbound and loosely bound enzyme.

To assess the effect of diffusion constraints and potential defects within the crystal, CALB was immobilised onto the surface of ZIF-90 (10-minute). A significant enhancement of activity of CALB on ZIF-90 (2.2 ± 0.0 µM.min^{-1}) relative to the CALB@ZIF-90 biocomposite was observed (**Figure 5.7a**). CLSM images, and the absorbance spectrum of the supernatants of both CALB on ZIF-90 and CALB@ZIF90 confirm that CALB is being immobilised on both

supports with ~100% efficiency (**Figure 5.5, Figure S5.4**). As the enzyme loading is equal, this suggests that the activity of the CALB@ZIF-90 sample is being hindered by the encapsulation process, or by substrate diffusion restraints to the embedded enzyme. However, both the encapsulated and surface adsorbed samples were significantly more active than the CALB@ZIF-8 and CALB on ZIF-8 composite of equivalent size, indicating that the interactions on ZIF-90 is more favourable than on the more hydrophobic, ZIF-8 framework.

Next, the effect of formation time and particle size was determined for CALB@ZIF-90 by comparing the rate of hydrolysis of the 10-minute (1 μm) and 24-hour (2 μm) samples (**Figure 5.7b**). The rate of hydrolysis with CALB@ZIF-90 (10-minute) sample was approximately 10 times faster than the CALB@ZIF-90 sample (24-hour). The CALB@ZIF-90 24-hour sample had an activity similar to the background hydrolysis of BSA@ZIF-90 (10-minute) (**Figure S5.5**). Whilst, the presence of crystalline ligand (**Figure S5.3**), complicated the assessment of the CALB@ZIF-90 24-hour sample, the loss of activity suggests that longer formation times are not favourable for the immobilisation of CALB.

5.3.5. CALB@ZIF-90 Pore Size Analysis

Activity, in the 24-hour sample may be being inhibited by increased encapsulation (larger crystal sizes) or pore blockage caused by ligand crystallisation. Additionally, FITC diffusion experiments suggested that, based off of size alone, substrate (*p*-NPB) diffusion would be unfavourable in perfect ZIF-90 crystals,[30] so the activity that was measured for CALB@ZIF-90 (10-minutes) may indicate the presence of crystal defects or a higher proportion of surface bound enzyme. Analysis of the BET surface areas, by performing 77 K N_2 adsorption isotherms, revealed that the smaller, faster forming CALB@ZIF-90 (10-minute) exhibited a larger surface area (1051 ± 0 $m^2.g^{-1}$) than the CALB@ZIF-90 (24-hour) sample (623 ± 0 $m^2.g^{-1}$). This observation was likely due to ligand crystallisation in the 24-hour sample contributing to sample mass, and thus lower N_2 adsorption (**Figure S5.6a**). Additionally, similar pore size distribution between the two different sample preparations (calculated via DFT N_2 model) (**Figure S5.6b**), suggests that the activity was not due to the differences in porosity of the two samples.

5.3.6. CALB@ZIF-90 Activity (Transesterification)

Next, we investigated the range of CALB@ZIF-90 reactions by testing the activity and stability of the biocomposite to the transesterification conditions (**Figure 5.8**). Transesterification yields can be greatly enhanced in organic solvents by lowering the water content of the reaction, thus minimising the product hydrolysis that would arise in aqueous media.

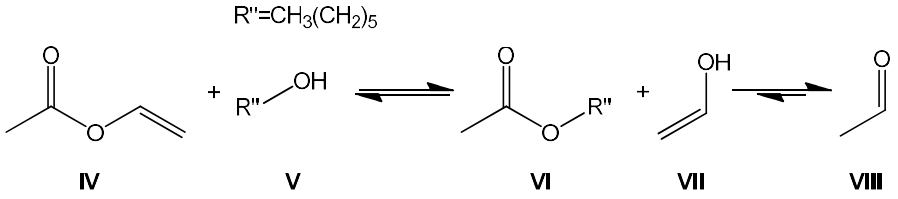

Figure 5.8: The transesterification of vinyl acetate **IV** with hexanol **V** to generate hexyl acetate **VI** and vinyl alcohol **VII.** Vinyl alcohol tautomerises to acetaldehyde **VIII**, inhibiting the reverse reaction. Hexyl acetate **VI** can hydrolyse to form acetic acid and hexanol **V** in the presence of water.

In **Chapter 4**, it was shown that the 1 µm CALB@ZIF-8 (and CALB on ZIF-8) samples are not active for the transesterification reaction between hexanol and vinyl acetate, and thus we were motivated to determine whether the hydrophilic support of ZIF-90 would result in activity. CALB@ZIF-90 (10 min) was active at a similar initial rate to CALB on ZIF-90, leading to a maximum measured conversion after 8 hours of 80- and 90 % respectively (**Figure 5.9**).

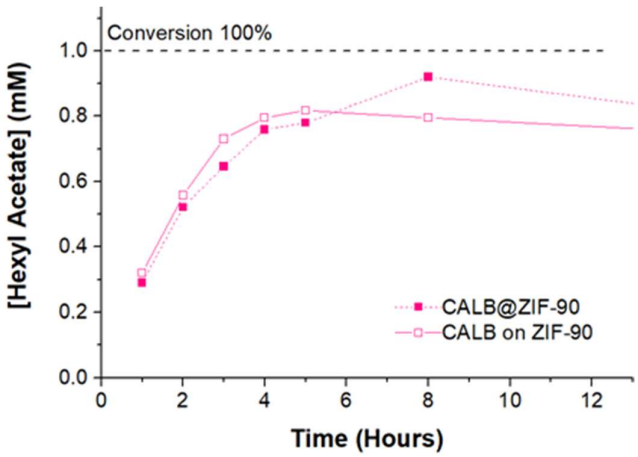

Figure 5.9: Transesterification of hexanol and vinyl acetate by CALB@ZIF-90 and CALB on ZIF-90 (both 10-minute).

The similarities between encapsulated and surface bound samples suggest that enzyme activity is not limited by substrate diffusion and could result from CALB that is substrate accessible (surface bound or sub-surface). CLSM suggested that some surface bound enzyme was present on the CALB@ZIF-90 (10-minute) sample (**Figure 5.5**) which may be responsible for the observed transesterification activity. Alternatively, the substrate shape and size (hexanol; 5.37 Å) and reaction time (hours) may well allow for better substrate transfer compared to the hydrolysis reaction (minutes, *p*-NPB; 6.57Å). The levels of background hydrolysis of *p*-NPB by the MOF control, however, prevented extending the reaction time to further test this theory. In either case, CALB@ZIF-90 was active whereas CALB@ZIF-8 (equivalent size) was not, despite similar enzyme loadings, further highlighting the advantage of the ZIF-90 framework. SEM and PXRD after transesterification showed no noticeable change to the crystal structure after the reaction (**Figure 5.10, Figure S5.7**).

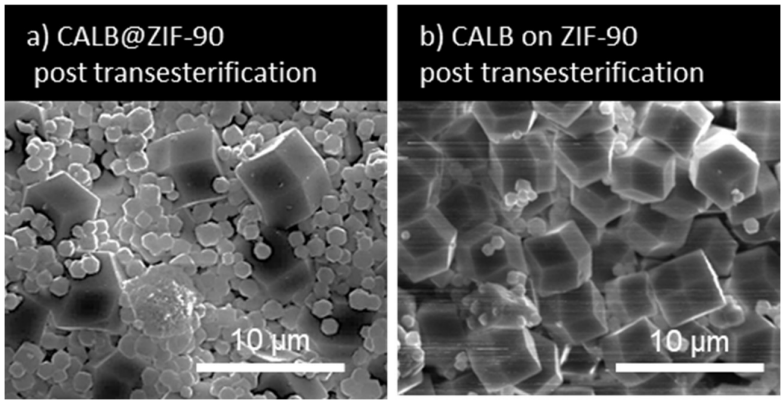

Figure 5.10: SEM of the (a) CALB CALB@ZIF-90 and (b) CALB on ZIF-90 (10-minute) after a 24-hour transesterification reaction in 100% hexane.

5.3.7. CALB@BioHOF-1 Synthesis

After establishing the impact of the framework (ZIF-90 versus ZIF-8), we proceeded to immobilise CALB using the chemically and structurally different BioHOF-1 framework. The metal-free, hydrogen-bonded framework retained the activity of enzymes that were not active within ZIF-8 (catalase, alcohol oxidase) so we were motivated to apply the BioHOF-1 immobilisation method to CALB. Unlike ZIF-8, BioHOF-1 is stable to both tris and phosphate buffers and thus will allow for activity screening in buffered media without the risk of support degradation.

The synthesis of the protein free BioHOF-1 was confirmed by PXRD and SEM (**Figure 5.11a, 5.12**) and upon the addition of a control protein (BSA), no significant changes to the crystallinity or morphology where observed (**Figure 5.11b, 5.12**). Interestingly when synthesised using CALB, the HOF showed a significant reduction in crystallinity evidenced by a broadening of the peaks in the powder pattern (**Figure 5.12**). This coincided with a change in morphology via SEM where the CALB@HOF crystals became shorter and more rounded at the edges (**Figure 11c**). Additional small crystallites (or aggregates) less than 1 μm in size, were also present in the CALB sample that may be responsible for the peak broadening in the PXRD pattern. This observation was consistent across multiple batches indicating that either the CALB enzyme, or additives within the lyophilised powder were changing how the HOF was being formed. Different enzyme types (i.e. surface chemistry) and preparations (lyophilisation and purification), as well as the concentration used may be responsible for the observed changes, however this phenomenon is not well understood. Catalase and alcohol oxidase, both generate rod shaped crystals, however their thickness and length varied between samples.[30]

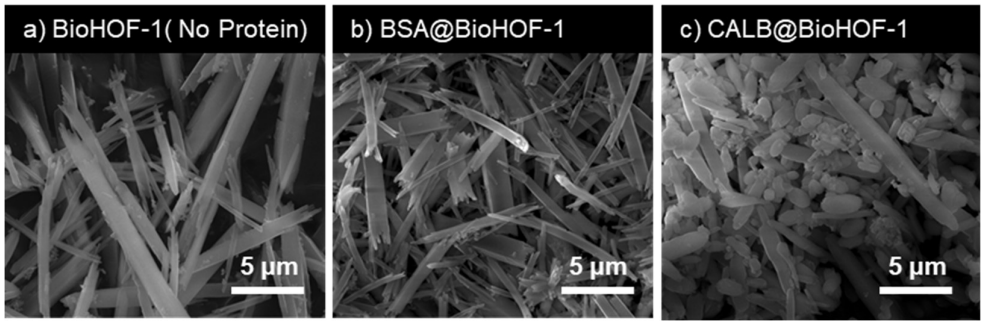

Figure 5.11: SEM of as-synthesised BioHOF-1 made without protein, with BSA (2 mg), and with CALB (2 mg). The choice of protein appears to alter the crystal size and morphology with respect to the as-synthesised protein free sample.

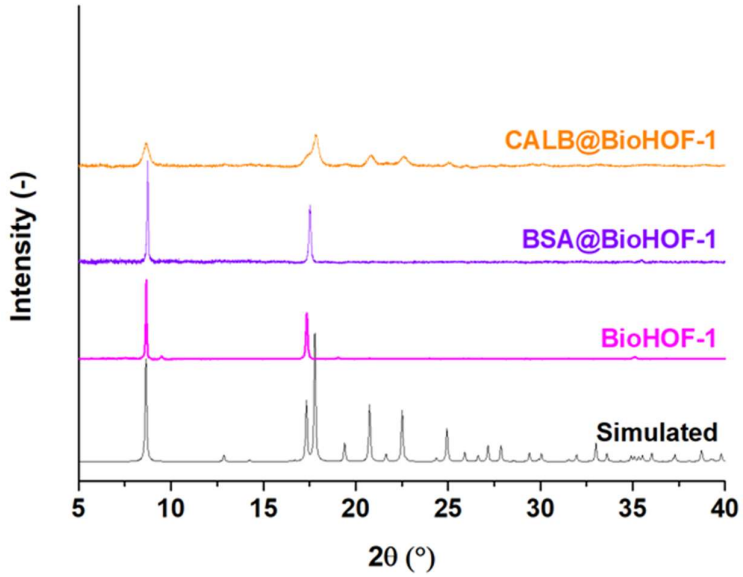

Figure 5.12: As-synthesised PXRD pattern of BioHOF-1 made in the presence of CALB, BSA, or no protein. The additional peaks in the simulated pattern will appear in the synthesised samples upon manual grinding, as the effects of preferred orientation are overcome.[30] Peak broadening and reduced intensity of CALB@BioHOF-1 was an element of all CALB@BioHOF-1 synthetic attempts and can be attributed to the formation of small crystalline aggregates (**Figure 5.11**). The simulated powder pattern was generated form single crystal X-ray diffraction data of the protein free BioHOF-1.[39]

To investigate the morphological change, a lower concentration of FITC-CALB (1 mg per sample) that had been washed to remove excess salts was used for fluorescent mapping of the crystals (Confocal Laser Scanning Microscopy, CLSM). Despite the change in enzyme concentration and the buffer exchange, CLSM images showed that the rounded crystals remained the dominant morphology (**Figure 5.13a**). Fluorescence was observed across all of the crystals, with its central location indicating encapsulation; however according to reports in the literature, low levels of surface bound enzyme are also expected.[30] Again, no FITC absorbance was observed in the supernatant of the framework, indicating full CALB immobilisation (**Figure S5.8**). FITC-CALB combined with the pre-synthesised HOF sample confirmed that adsorption of CALB on the HOF external surface was also possible (**Figure 5.13b**).

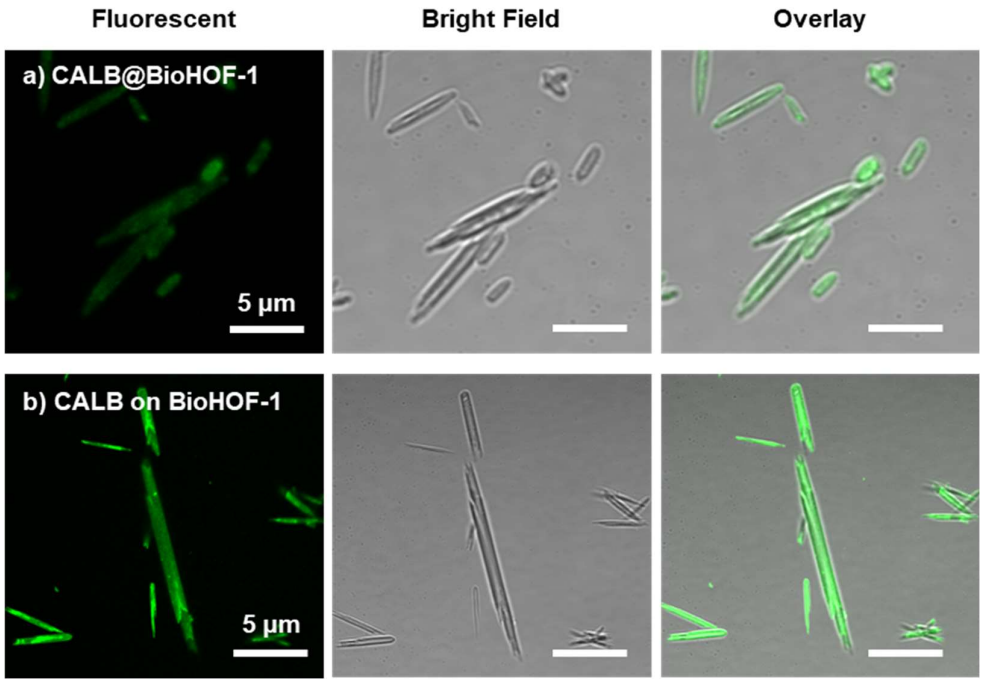

Figure 5.13: Confocal Laser Scanning Microscopy (CLSM) images of CALB@BioHOF-1 (a) and CALB on BioHOF-1. (b) Fluorescein isothiocyanate (FITC) tagged enzyme (1 mg CALB) was used for both encapsulation and surface adsorption. The CALB@BioHOF-1 sample (1 mg enzyme) retained the same morphology and crystallinity as the standard CALB@BioHOF-1 preparation (2 mg enzyme).

5.3.8. CALB@BioHOF-1 Activity (Hydrolysis)

The reported pore aperture of BioHOF-1 is 6.4 Å which may restrict the diffusion of large substrates such as the *p*-nitrophenyl esters (*p*-NPB, 6.5 Å) used in the lipase hydrolysis assay. Whilst the flexibility of the BioHOF-1 framework allows for diffusion of molecules (fluorescein) much larger than *p*-NPB, the short time scale of the hydrolysis reaction (10 minutes, due to the background hydrolysis in the buffer) may not allow sufficient transfer of the substrate through the pores. This was confirmed during the testing process, when the CALB@BioHOF-1 composite only catalysed background level *p*-NPB hydrolysis in tris and phosphate buffer (**Figure 5.14a, S5.9**). The activity however was increased ~7-fold when CALB was surface adsorbed only (**Figure 5.14b**) implying that the process of immobilisation on the surface of BioHOF-1 was not causing enzyme deactivation, and therefore the CALB@BioHOF-1 samples are likely to consist primarily encapsulated rather than surface bound enzyme.

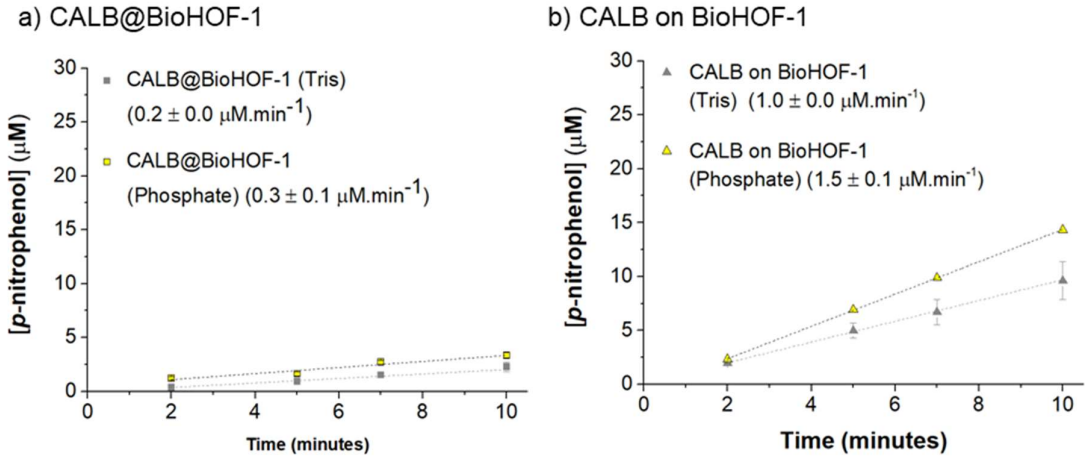

Figure 5.14: Hydrolytic activity of the BioHOF-1 composites in tris buffer and phosphate buffer (50 mM, pH 7.4) + Triton X-100. (a) CALB@BioHOF-1 was only slightly more active than the BSA@BioHOF-1 control (0.0 ± 0.0 μM. min^{-1}, **Figure S5.9**). However, when adsorbed onto the surface of the crystals (b) CALB on BioHOF-1 was capable of *p*-NPB hydrolysis. In both cases, activity was slightly higher in the phosphate Buffer which is expected based on free enzyme activity being faster in phosphate buffer. There was no evidence in this study, nor those reported previously, for buffer mediated BioHOF-1 degradation. All samples were tested after three water washes to remove excess precursors and unbound and loosely bound enzyme.

5.3.9. CALB@BioHOF-1 Activity (Transesterification)

Next, CALB@BioHOF-1 (and CALB on BioHOF-1) was tested for the transesterification of hexanol and vinyl acetate. The initial rate of CALB@BioHOF-1 was slower than CALB@ZIF-90 (10-minute) however a greater maximum conversion of 97%, compared to 80%, was reached after 12 hours (**Figure 5.15**). The surface adsorbed CALB on BioHOF-1 reached 100% conversion in the hexane solvent at a rate faster than the encapsulated enzyme equivalent, suggesting that there were diffusion constraints in the encapsulated sample. The framework topology and crystal size/morphology of the as-synthesised CALB@BioHOF-1 and CALB on BioHOF-1 samples, post-transesterification (100% hexane) were consistent with the pre-assay samples, as determine by PXRD and SEM analysis (**Figure 5.16, S5.10**). Due to the high activity of CALB@BioHOF-1 in hexane, and the promising substrate accessibility of BioHOF-1 relative to the ZIF materials, this sample was examined for its reusability. Here, CALB@BioHOF-1 could be reused to maximum conversion (~97%) for 5 cycles without loss in activity (**Figure 5.17**).

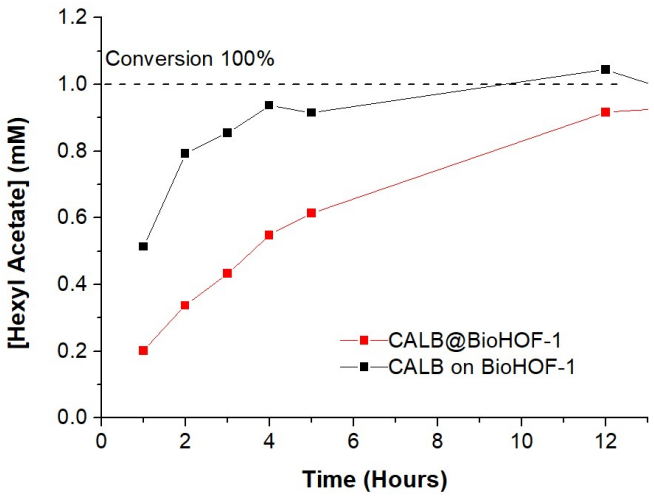

Figure 5.15: Transesterification of hexanol and vinyl acetate by CALB@BIOHOF-1 (red) and CALB on BioHOF-1 (black).

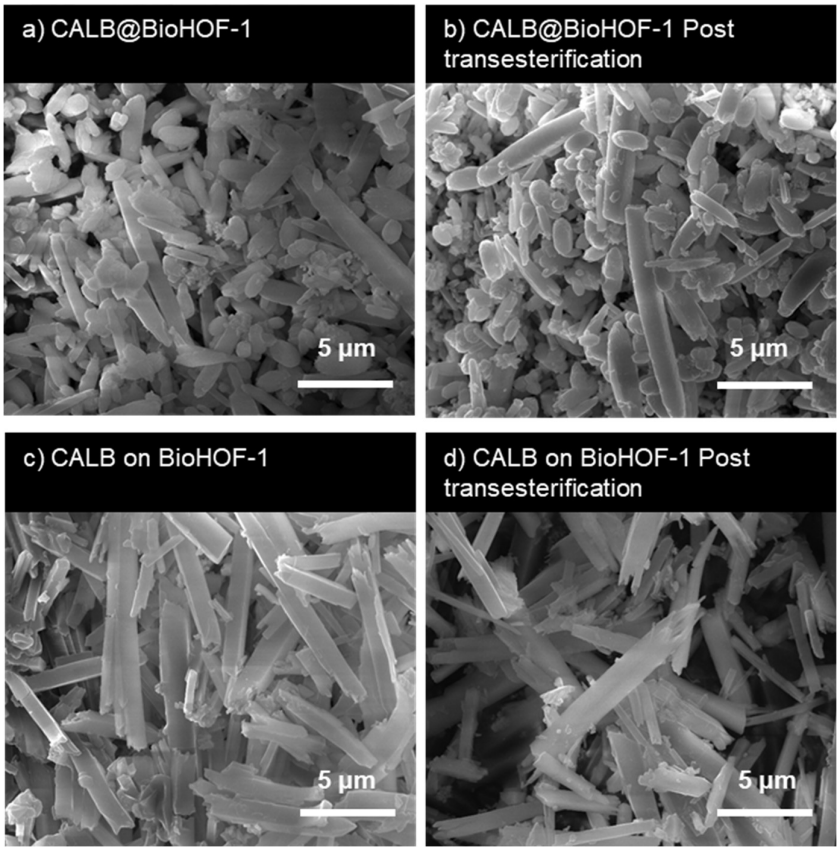

Figure 5.16: SEM images of (a, b) CALB@BioHOF-1 and (c, d) CALB on BioHOF-1 as-synthesised and post transesterification.

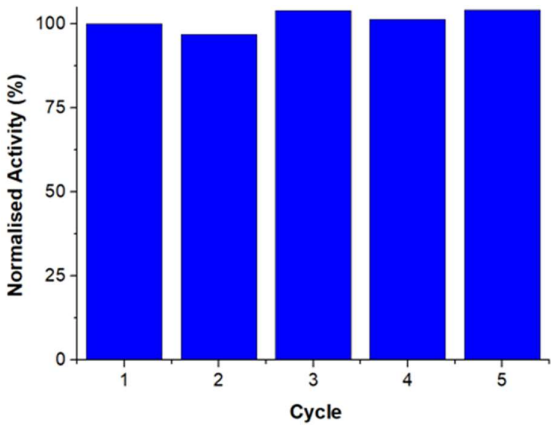

Figure 5.17: Activity of the CALB@BioHOF-1 after multiple cycles (normalised to the first cycle). After each cycle, the hexane was removed, and the sample was washed three times with fresh hexane to remove reactant/ product from the previous reaction. Activity was maintained after each 16-hour cycle, with the first cycle equalling 96% conversion.

5.3.10. Enantioselective Transesterification

The enantioselectivity of the CALB@ZIF-90 (10-minute) and CALB@BioHOF-1 samples were then determined for the transesterification of (*R/S*)-1-phenylethanol (1-PE) using the same concentrations and solvents as the hexanol/vinyl acetate assay (**Figure 5.18-19**). Novozym435, tested as a control, selectively converts (*R*)-1-PE into (*R*)-1-phenylethyl acetate (1-PEA) reaching 60% (*R*) production after 24 hours (**Figure S5.11-12, Table S5.1**). In the subsequent time-points, however, Novozym435 began hydrolysing the ester (**XI)** in hexane, reducing the product to 19% after 5 days.

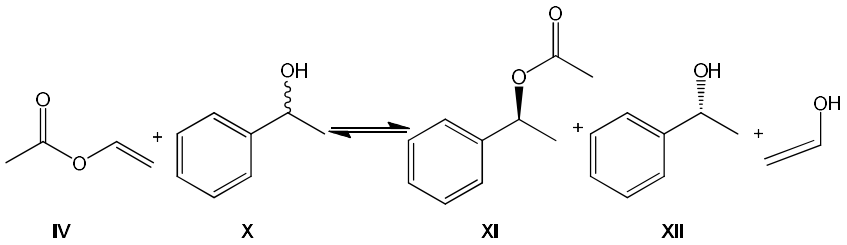

Figure 5.18: Enantioselective transesterification reaction scheme. In the presence of (*R/S*)-1-phenylethanol **X**, CALB enantioselectivity esterifies the *R* isomer to yield (*R*)-1-phenylethyl acetate **XI** and (*S*)-1-phenylethanol **XII**.

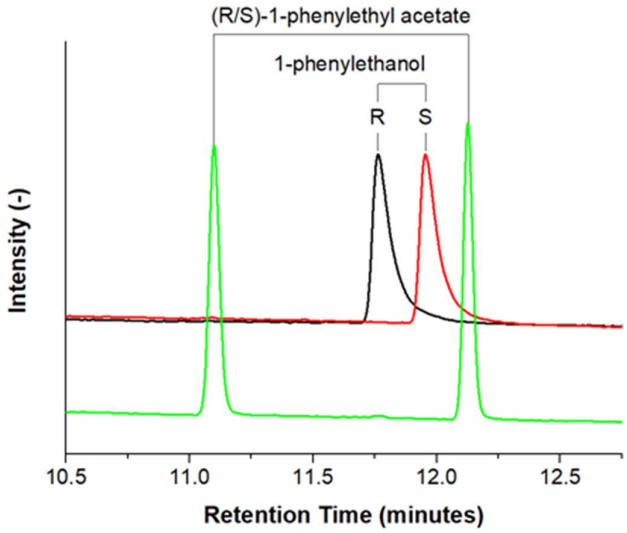

Figure 5.19: Gas chromatogram of chiral column separation of substrate and product standards. The retention times of (*R*)-1-phenylethanol, and (*S*)-1-phenylethanol were 11.7-and 11.9 minutes respectively. The retention times of (*R/S*)-1-phenylethyl acetate was 11.3 and 12.1 minutes.

Immobilising CALB within ZIF-90 an BioHOF-1 led to a reduction in rate, however the enantioselectivity was maintained, with no (*S*)-PEA appearing for any samples during the 5-day reaction (**Figure 5.20-21, Table S5.1**).

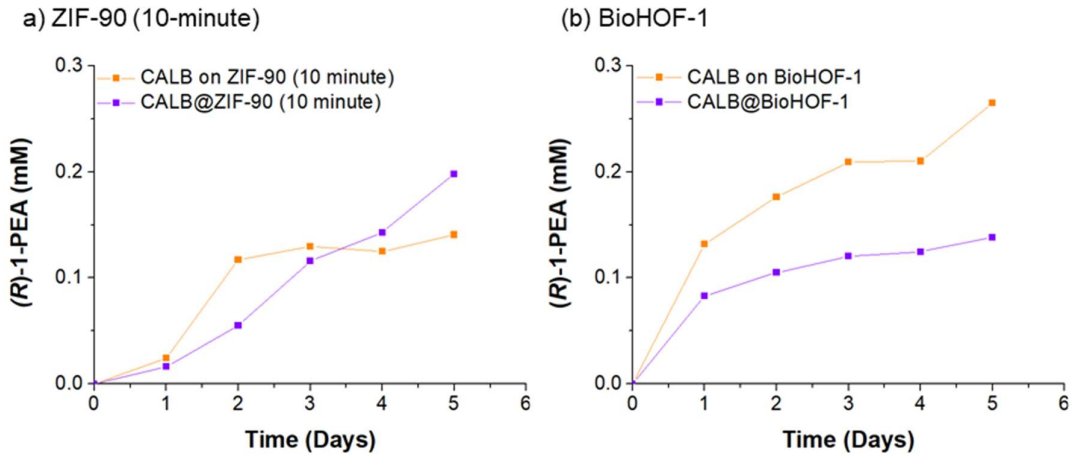

Figure 5.20: Concentration of (*R*)-1-phenylethyl acetate generated by CALB@ZIF-90 (10-minute) and CALB@BioHOF-1, and their surface adsorbed counterparts, over a 5-day reaction. Percent conversions are tabulated in **Table S5.1**.

1-Phenylethanol (6.86 Å) is of a similar size to *p*-NPB (6.5 Å), and therefore substrate diffusion through the framework is expected to be slow. However, as the enantioselective transesterification reaction was monitored for 5 days, there was sufficient time for the substrate to diffuse and reach the enzyme. Using the ZIF-90 framework, the encapsulated enzyme was more active than the surface bound variant, indicating encapsulation process was better for long term stability and that there is likely to be sub-surface enzyme that is protected but still accessible to the substrate. For the BioHOF-1 framework, the surface bound CALB was more active, highlighting potential diffusion restrictions of the encapsulated sample, and that the BioHOF-1 is a better candidate for stabilising enzymes in long term reactions.

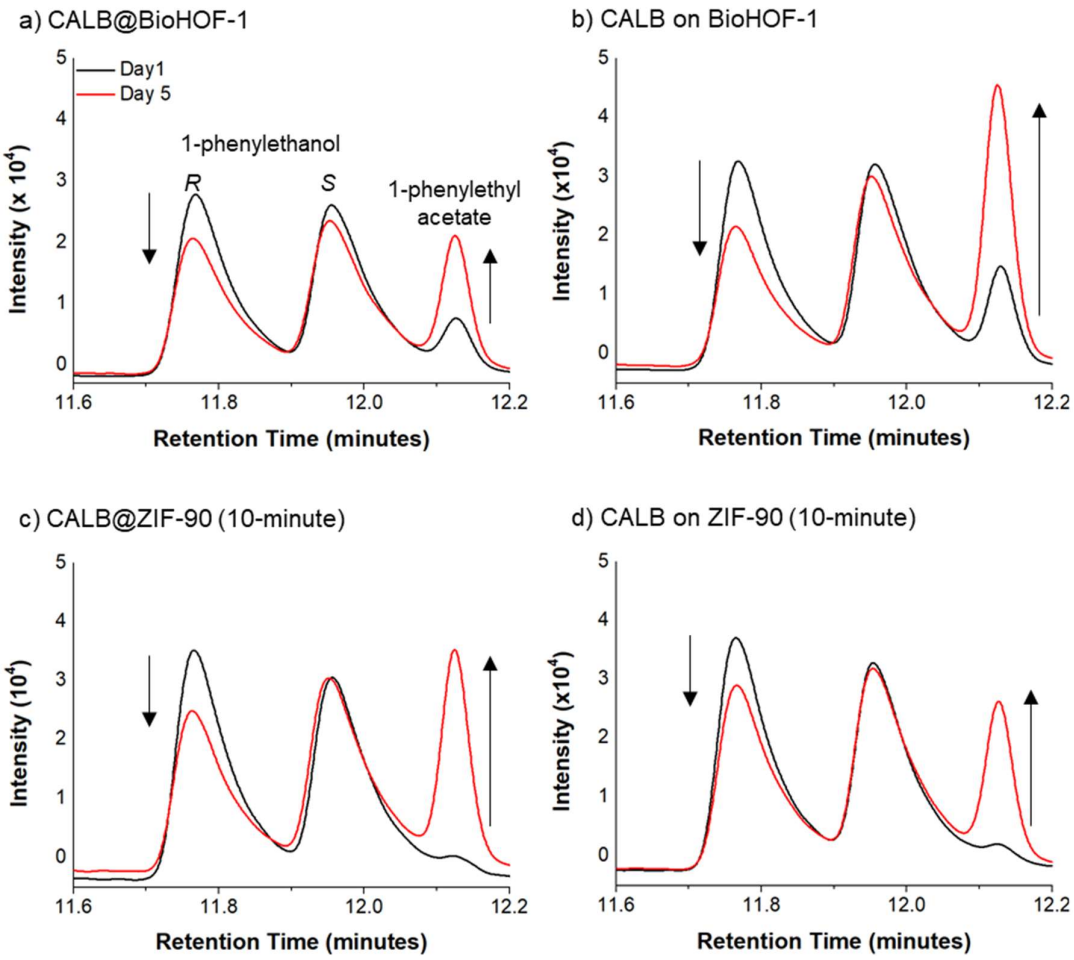

Figure 5.21: Gas chromatogram of chiral column separation of (*R*/*S*)-1-phenylethanol transesterification. No (*S*)-1-phenylethyl acetate was produced (retention time; 11.2 minutes).

5.4. Conclusion

CALB was immobilised for the first time into ZIF-90 and BioHOF-1 via one-pot synthesis in each case. The activity of CALB@ZIF-90 was determined to be dependent on the formation time of the composite. A 10-minute synthesis time generated 1 μm crystals that were active to hydrolysis and transesterification reactions, whereas the 24-hour synthesis formed 2 μm crystals and saw a significant reduction in catalytic output. This can be attributed to the degree of encapsulation of the different sample preparations, with the smaller CALB@ZIF-90 crystals containing a higher proportion of surface bound or sub surface crystals compared to the larger crystals that consistently encapsulate enzyme in the literature.[29] Additionally, longer formation times lead to ligand crystallisation which is not removed by water washes, which may contribute to pore blockage that reduced activity of the larger samples. CALB@BioHOF-1 was not active for the hydrolysis reaction due to the larger substrate size and the short reaction time that was not complementary to diffusion. CALB@ZIF-90 (10-minute) demonstrated enhanced activity over CALB@ZIF-8 (similar sized) biocomposites for the transesterification of hexanol and vinyl acetate in hexane. CALB encapsulated within or surface bound to ZIF-8 were not active indicating that the activity of the ZIF-90 framework must be affording more favourable interactions with CALB. CALB@BioHOF-1 was also stable and active to transesterification in hexane and could be reused for 5 cycles with minimal loss in activity. Additionally, the enantioselectivity of the CALB biocomposites studied were unaltered, relative to Novozym435, maintaining selectivity (*R*, ee: 99%) over a 5-day reaction.

5.5. Experimental

5.5.1. Materials

Lipase B from *Candida antarctica* (CALB) recombinant from *Aspergillus oryzae* (Product Code 62288, 9 $U.mg^{-1}$) was purchased from Merck as a lyophilised powder and used without purification. Novozym435 (Product Code 1002850352, 5000 $U.g^{-1}$) as lipase immobilised on macroporous acrylic resin was purchased from Merck and used as is. The BioHOF-1 tetrahedral amidinium and carboxylate ligand precursors were supplied by Dr. Nicholas White of Australian National University.[40] All other chemicals were purchased from commercial sources and used as received. Ultra-pure Milli-Q (MQ) with resistivity of >18 MΩ cm^{-1} (Merck Millipore purification system) was used for all syntheses, wash protocols and buffer preparations.

5.5.2. Fluorescein Tagged CALB

CALB was tagged using fluorescein isothiocyanate (FITC) as per previously reported protocols. Detailed protocols can be found in the experimental for **Chapter 4**.

5.5.3. Biocomposite Syntheses

BioHOF-1 Protein Free Synthesis. HOF synthesis was adapted from literature reported for enzymes, catalase and alcohol oxidase. Structures are shown in **Figure S5.2**. Ligand 3 (amidinium) (4 mg) was dissolved in water (1 mL). Ligand 4 (carboxylate) (3 mg) was added to water (0.95 mL) and dissolved with the addition of a 1% ammonia solution (~50 μL). Under gentle stirring, the carboxylate solution was added dropwise to the amidinium solution over the course of 15 minutes. The resulting suspension was left to stir for an additional hour to ensure complete HOF formation, after which the product was collected by centrifugation and washed three times with MQ water.

Protein@ZIF-90 Synthesis. A similar method was used for protein encapsulation, where a protein solution (2 mg, 0.25 mL) combined Ligand A solution (4 mg, 0.75 mL).

Protein Free Synthesis. 62 mg ICA dissolved in 3.8 mL MQ water at elevated temperature (approximately 80 degrees) with rapid stirring. The solution was cooled to 30°C prior to use as cooling the ligand below 30°C leads to precipitation of the ligand that cannot be fully separated from the ZIF-90 crystals. Zinc nitrate hexahydrate (47 mg) dissolved in 200 μL MQ water was added and quickly mixed into the ICA solution. The resulting suspension was left undisturbed for 10 minutes before collection via centrifugation (6000 rpm, 5 minutes). Leaving the product to form for a longer timeframe initially leads to a loss of crystal definition

followed by a complete collapse in crystal structure. The product was washed three times with water to remove excess precursors.

Protein@ZIF-90 Synthesis. A similar method was used for protein encapsulation, where the protein (powder or solution was added to the ICA solution (upon reaching 30 degrees). After the addition of Zn^{2+}, the resulting precipitate was collected after 10 minutes or 24 hours.

Surface Adsorbed Biocomposites. CALB or FITC-CALB (2 mg) in water 0.5 mL was gently shaken for 4 hours with the protein free BioHOF-1 or ZIF-90. The sample was washed twice with water to remove loosely bound CALB prior to use.

5.5.4. Activity Determination

Hydrolysis: The hydrolysis of *p*-nitrophenyl butyrate (*p*-NPB) assay was adapted from literature procedures and is outlined in **Chapter 4**.[42-43]

Transesterification: Hexanol or (*R/S*)-1-phenylethanol (2 mM) and vinyl acetate (10 mM) in hexane (2 mL) was combined with an air-dried biocomposite in hexane (2 mL) in a 5 mL glass vial. The reaction mix was shaken at 30°C, and aliquots were taken from the hexane at 1-hour intervals.

5.5.5. Characterisation

Powder X-ray Diffraction (PXRD), Scanning Electron Microscopy (SEM) and UV-Visible Absorbance Measurements. All instrument descriptions and characterisation protocols are described in **Chapter 4** and were used without modification.

N_2 Adsorption Isotherms. N_2 (UHP grade, 99.999%) adsorption isotherm measurements were performed on a 3Flex physisorption analyser. The temperature was maintained at 77 K via a helium cryostat. The samples were washed with ethanol and dried under vacuum in a desiccator for 1-hour. The dried samples were heated under vacuum at 120 °C for 2 hours.

Gas Chromatography Analysis. Aliquots were diluted/extracted into ethyl acetate, dried with magnesium sulphate and analysed via Gas Chromatography (Shimadzu, Nexis GC-2030) equipped with a DB-wax column (30.0 m, 0.25 mm, 0.25 mm) and a Flame Ionisation detector (FID). The column was held at 60 °C for 3 minutes and increased at 6 °C per minute to 160 °C. At the end of each run, the column was heated to 220 °C for a burn off. For separation of enantiomers the samples were analysed by Gas chromatography (Shimadzu GC-2010)

equipped with a chiral Restek-BDEXse column (30.0 m, 0.32 mm, 0.25 μm) and a Barrier Ionisation Discharge (BID) detector. The column was held at 80 °C for 3 minutes and increased at 5 °C per minute to 140 °C. At the end of each run, the column was heated to 220 °C for a burn off. Retention times are as follows. Hexanol; 7.9 min and hexyl acetate; 6.1 min, see **Chapter 4**, **Figure S4.21**. (*R*)-1-phenylethanol; 11.7 min, (*S*)-1-phenylethanol; 11.9 min, (*R*)-1-phenylethyl acetate 12.1 min, see **Figure 5.18**.

5.6. Acknowledgements

N. K. Maddigan acknowledges O.M. Linder-Patton for his technical assistance and Dr. N. White for supplying the BioHOF-1 building units.

5.7. References

1. Nguyen, L. A.; He, H.; Pham-Huy, C., Chiral drugs: an overview. *Int. J. Biomed. Sci.* **2006,** *2* (2), 85-100.

2. Patel, R. N., Synthesis of chiral pharmaceutical intermediates by biocatalysis. *Coord. Chem. Rev.* **2008,** *252* (5), 659-701.

3. Pollard, D. J.; Woodley, J. M., Biocatalysis for pharmaceutical intermediates: the future is now. *Trends Biotechnol.* **2007,** *25* (2), 66-73.

4. Straathof, A. J. J.; Panke, S.; Schmid, A., The production of fine chemicals by biotransformations. *Curr. Opin. Biotech.* **2002,** *13* (6), 548-556.

5. Robinson, D. E. J. E.; Bull, S. D., Kinetic resolution strategies using non-enzymatic catalysts. *Tetrahedron: Asymmetry* **2003,** *14* (11), 1407-1446.

6. Benkovic, S. J.; Hammes-Schiffer, S., A perspective on enzyme catalysis. *Science* **2003,** *301* (5637), 1196-1202.

7. Sheldon, R. A.; Brady, D., The limits to biocatalysis: pushing the envelope. *Chem. Commun.* **2018,** *54* (48), 6088-6104.

8. Iyer, P. V.; Ananthanarayan, L., Enzyme stability and stabilization—Aqueous and non-aqueous environment. *Process Biochem.* **2008,** *43* (10), 1019-1032.

9. Stepankova, V.; Bidmanova, S.; Koudelakova, T.; Prokop, Z.; Chaloupkova, R.; Damborsky, J., Strategies for stabilization of enzymes in organic solvents. *ACS Catal.* **2013,** *3* (12), 2823-2836.

10. Hartmann, M., Ordered mesoporous materials for bioadsorption and biocatalysis. *Chem. Mater.* **2005,** *17* (18), 4577-4593.

11. Hartmann, M.; Jung, D., Biocatalysis with enzymes immobilized on mesoporous hosts: the status quo and future trends. *J. Mater. Chem.* **2010,** *20* (5), 844-857.

12. Xie, T.; Wang, A.; Huang, L.; Li, H.; Chen, Z.; Wang, Q.; Yin, X., Recent advance in the support and technology used in enzyme immobilization. *Afr. J. Biotechnol.* **2009,** *8* (19), 4724-4733.

13. Hoarau, M.; Badieyan, S.; Marsh, E. N. G., Immobilized enzymes: understanding enzyme – surface interactions at the molecular level. *Org. Biomol. Chem.* **2017,** *15* (45), 9539-9551.

14. Mohamad, N. R.; Marzuki, N. H. C.; Buang, N. A.; Huyop, F.; Wahab, R. A., An overview of technologies for immobilization of enzymes and surface analysis techniques for immobilized enzymes. *Biotechnol. Biotechnol. Equip.* **2015,** *29* (2), 205-220.

15. Hanefeld, U.; Gardossi, L.; Magner, E., Understanding enzyme immobilisation. *Chem. Soc. Rev* **2009,** *38* (2), 453-468.

16. Kamble, M. P.; Yadav, G. D., Kinetic resolution of (*R,S*)-α-tetralol by immobilized C*andida antarctica* lipase B: comparison of packed-bed over stirred-tank batch bioreactor. *Ind. Eng. Chem.* **2017,** *56* (7), 1750-1757.

17. Łukowska-Chojnacka, E.; Kowalkowska, A.; Napiórkowska, A., Lipase-catalyzed kinetic resolution of novel antitubercular benzoxazole derivatives. *Chirality* **2018,** *30* (4), 457-468.

18. Listunov, D.; Joly, E.; Duhayon, C.; Saffon-Merceron, N.; Fabing, I.; Génisson, Y.; Maraval, V.; Chauvin, R., Methinylogation approach in chiral pharmacophore design: from alkynyl- to allenyl-carbinol warheads against tumor cells. *ChemMedChem.* **2018,** *13* (16), 1711-1722.

19. Barbosa, O.; Ariza, C.; Ortiz, C.; Torres, R., Kinetic resolution of (*R/S*)-propranolol (1-isopropylamino-3-(1-naphtoxy)-2-propanolol) catalyzed by immobilized preparations of *Candida antarctica* lipase B (CAL-B). *New Biotechnol.* **2010,** *27* (6), 844-850.

20. Ortiz, C.; Ferreira, M. L.; Barbosa, O.; dos Santos, J. C. S.; Rodrigues, R. C.; Berenguer-Murcia, Á.; Briand, L. E.; Fernandez-Lafuente, R., Novozym 435: the "perfect" lipase immobilized biocatalyst? *Catal. Sci.* **2019,** *9* (10), 2380-2420.

21. Cabrera, Z.; Fernandez-Lorente, G.; Fernandez-Lafuente, R.; Palomo, J. M.; Guisan, J. M., Novozym 435 displays very different selectivity compared to lipase from *Candida antarctica* B adsorbed on other hydrophobic supports. *J. Mol. Catal. B. Enzym.* **2009,** *57* (1), 171-176.

22. Fernandez-Lorente, G.; Cabrera, Z.; Godoy, C.; Fernandez-Lafuente, R.; Palomo, J. M.; Guisan, J. M., Interfacially activated lipases against hydrophobic supports: Effect of the support nature on the biocatalytic properties. *Process. Biochem.* **2008,** *43* (10), 1061-1067.

23. Torres, R.; Ortiz, C.; Pessela, B. C. C.; Palomo, J. M.; Mateo, C.; Guisán, J. M.; Fernández-Lafuente, R., Improvement of the enantioselectivity of lipase (fraction B) from *Candida antarctica* via adsorpiton on polyethylenimine-agarose under different experimental conditions. *Enzyme Microb. Technol.* **2006,** *39* (2), 167-171.

24. Palomo, J. M.; Fernández-Lorente, G.; Mateo, C.; Fuentes, M.; Fernández-Lafuente, R.; Guisan, J. M., Modulation of the enantioselectivity of *Candida antarctica* B lipase via conformational engineering. Kinetic resolution of (±)-α-hydroxy-phenylacetic acid derivatives. *Tetrahedron: Asymmetry* **2002,** *13* (12), 1337-1345.

25. Furukawa, H.; Cordova, K. E.; O'Keeffe, M.; Yaghi, O. M., The chemistry and applications of metal-organic frameworks. *Science* **2013,** *341* (6149), 1230444.

26. Kitagawa, S., Porous crystalline materials: closing remarks. *Faraday Discuss.* **2017,** *201* (0), 395-404.

27. Park, K. S.; Ni, Z.; Côté, A. P.; Choi, J. Y.; Huang, R.; Uribe-Romo, F. J.; Chae, H. K.; O'Keeffe, M.; Yaghi, O. M., Exceptional chemical and thermal stability of zeolitic imidazolate frameworks. *Proc. Natl. Acad. Sci.* **2006,** *103* (27), 10186.

28. Liang, W.; Ricco, R.; Maddigan, N. K.; Dickinson, R. P.; Xu, H.; Li, Q.; Sumby, C. J.; Bell, S. G.; Falcaro, P.; Doonan, C. J., Control of structure topology and spatial distribution of biomacromolecules in protein@ZIF-8 biocomposites. *Chem. Mater.* **2018,** *30* (3), 1069-1077.

29. Liang, W.; Xu, H.; Carraro, F.; Maddigan, N. K.; Li, Q.; Bell, S. G.; Huang, D. M.; Tarzia, A.; Solomon, M. B.; Amenitsch, H.; Vaccari, L.; Sumby, C. J.; Falcaro, P.; Doonan, C. J., Enhanced activity of enzymes encapsulated in hydrophilic metal–organic frameworks. *J. Am. Chem. Soc.* **2019,** *141* (6), 2348-2355.

30. Liang, W.; Carraro, F.; Solomon, M. B.; Bell, S. G.; Amenitsch, H.; Sumby, C. J.; White, N. G.; Falcaro, P.; Doonan, C. J., Enzyme encapsulation in a porous hydrogen-bonded organic framework. *J. Am. Chem. Soc.* **2019,** *141* (36), 14298-14305.

31. Morris, W.; Doonan, C. J.; Furukawa, H.; Banerjee, R.; Yaghi, O. M., Crystals as molecules: postsynthesis covalent functionalization of zeolitic imidazolate frameworks. *J. Am. Chem. Soc.* **2008,** *130* (38), 12626-12627.

32. Liao, F.-S.; Lo, W.-S.; Hsu, Y.-S.; Wu, C.-C.; Wang, S.-C.; Shieh, F.-K.; Morabito, J. V.; Chou, L.-Y.; Wu, K. C. W.; Tsung, C.-K., Shielding against unfolding by embedding enzymes in metal–organic frameworks via a de novo approach. *J. Am. Chem. Soc.* **2017,** *139* (19), 6530-6533.

33. Shieh, F.-K.; Wang, S.-C.; Yen, C.-I.; Wu, C.-C.; Dutta, S.; Chou, L.-Y.; Morabito, J. V.; Hu, P.; Hsu, M.-H.; Wu, K. C. W.; Tsung, C.-K., Imparting functionality to biocatalysts via embedding enzymes into nanoporous materials by a de novo approach: size-selective sheltering of catalase in metal–organic framework microcrystals. *J. Am. Chem. Soc.* **2015,** *137* (13), 4276-4279.

34. Simard, M.; Su, D.; Wuest, J. D., Use of hydrogen bonds to control molecular aggregation. Self-assembly of three-dimensional networks with large chambers. *J. Am. Chem. Soc.* **1991,** *113* (12), 4696-4698.

35. Russell, V. A.; Evans, C. C.; Li, W.; Ward, M. D., Nanoporous molecular sandwiches: pillared two-dimensional hydrogen-bonded networks with adjustable porosity. *Science* **1997,** *276* (5312), 575.

36. Luo, J.; Wang, J.-W.; Zhang, J.-H.; Lai, S.; Zhong, D.-C., Hydrogen-bonded organic frameworks: design, structures and potential applications. *CrystEngComm.* **2018,** *20* (39), 5884-5898.

37. Lin, R.-B.; He, Y.; Li, P.; Wang, H.; Zhou, W.; Chen, B., Multifunctional porous hydrogen-bonded organic framework materials. *Chem. Soc. Rev.* **2019,** *48* (5), 1362-1389.

38. Hisaki, I.; Xin, C.; Takahashi, K.; Nakamura, T., Designing hydrogen-bonded organic frameworks (hofs) with permanent porosity. *Angew. Chem. Int. Ed.* **2019,** *58* (33), 11160-11170.

39. Boer, S. A.; Morshedi, M.; Tarzia, A.; Doonan, C. J.; White, N. G., Molecular tectonics: a node-and-linker building block approach to a family of hydrogen-bonded frameworks. *Chem. Eur. J.* **2019,** *25* (42), 10006-10012.

40. Morshedi, M.; Thomas, M.; Tarzia, A.; Doonan, C. J.; White, N. G., Supramolecular anion recognition in water: synthesis of hydrogen-bonded supramolecular frameworks. *Chem. Sci.* **2017,** *8* (4), 3019-3025.

41. Chaemchuen, S.; Luo, Z.; Zhou, K.; Mousavi, B.; Phatanasri, S.; Jaroniec, M.; Verpoort, F., Defect formation in metal–organic frameworks initiated by the crystal growth-rate and effect on catalytic performance. *J. Catal.* **2017,** *354*, 84-91.

42. Quinn, D. M.; Shirai, K.; Jackson, R. L.; Harmony, J. A. K., Lipoprotein lipase-catalyzed hydrolysis of water-soluble p-nitrophenyl esters. Inhibition by apolipoprotein C-II. *Biochemistry* **1982,** *21* (26), 6872-6879.

43. Shirai, K.; Jackson, R. L., Lipoprotein lipase-catalyzed hydrolysis of p-nitrophenyl butyrate. Interfacial activation by phospholipid vesicles. *J. Biol. Chem.* **1982,** *257* (3), 1253-1258.

5.8. Supporting Information

5.8.1. CALB background information

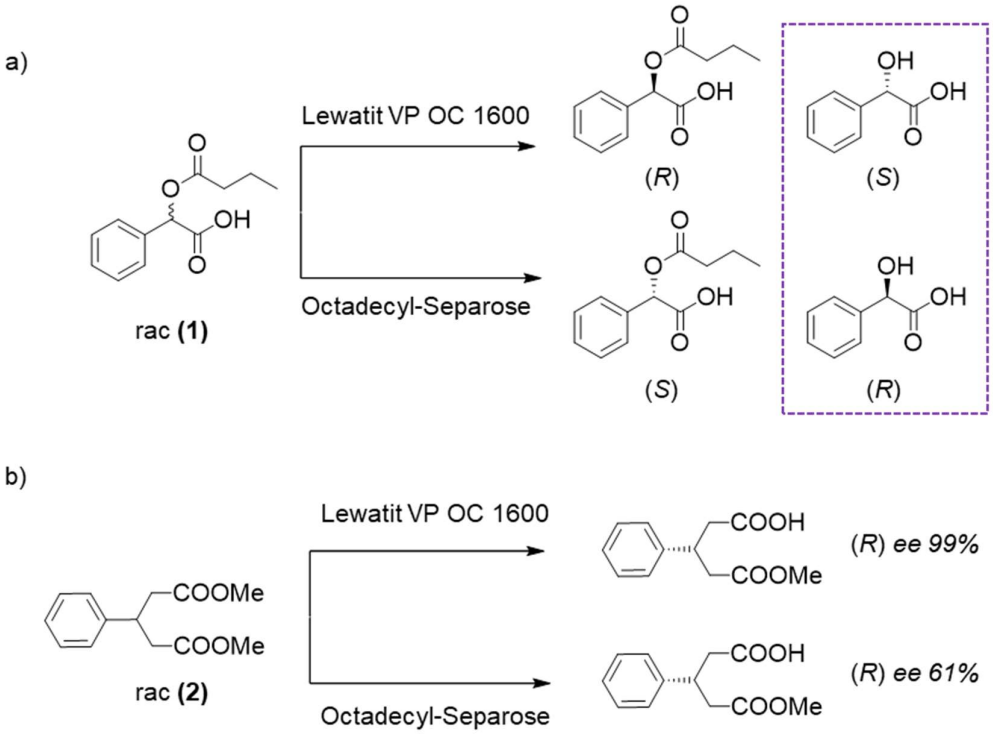

Figure S5.1: Enantioselective hydrolysis reactions of a) 2-O-butyryl-2-phenylacetic acid and b) 3-phenylglutaricdimethyl diester. Changing the support from Lewatit VP OC 1600 to Octadecyl Separose results in an inversion of enantioselectivity of **1** (*S* to *R*) but reduces the *R* preference of **2** (99-to 61%).[1]

5.8.2. Biocomposite building units

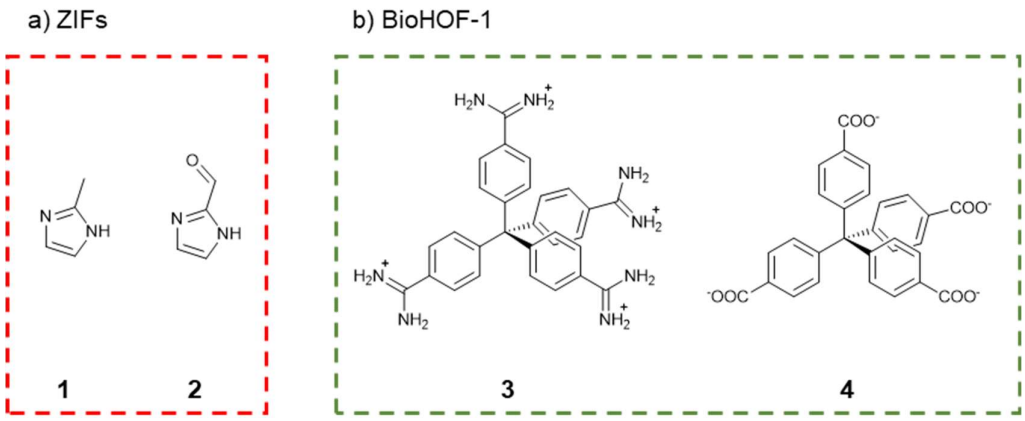

Figure S5.2: The structure of the ligands used in the synthesis of the ZIF materials (a) and BioHOF-1 (b). ZIF-8 is formed from zinc acetate dihydrate, $Zn(CH_3COO^-)_2 \cdot H_2O$ and 2-methyl imidazole, 2-mIM (**1**). ZIF-90 is formed from zinc nitrate hexahydrate, $Zn(NO_3)_2 \cdot 6H_2O$ and imidazole-2-carboxaldehyde, ICA (**2**). BioHOF-1 is synthesised from poly- amidinium (**3**) and poly-carboxylate (**4**) tectons. Two CALB@ZIF-8 preparations are referred to in this work. Large (1 µm) crystals formed using a Zn^{2+}:2-mIM ratio of 40:640 mM was used for direct activity comparison to equally sized ZIF-90 samples. Smaller (500 nm) crystals formed using a ratio of 20:80 mM were used for enantioselectivity testing (**Figure S5.13**).

5.8.3. ZIF-90 Characterisation

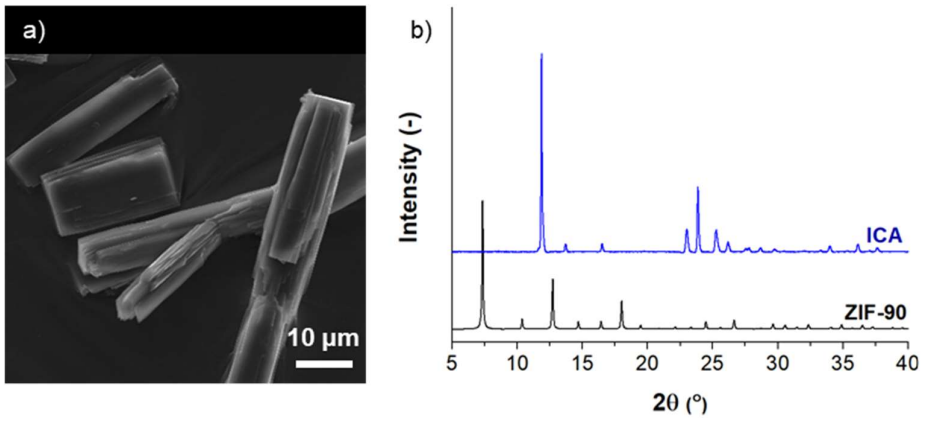

Figure S5.3: a) SEM and b) PXRD pattern of the ICA ligand. Repeating the 24-hour ZIF-90 protocol with ICA but no zinc source led to crystallisation of the ligand, generating a PXRD pattern with a major peak at 2θ value of 12°. This peak appeared in all 24-hour protein@ZIF-90 samples (**Figure 5.2b**), and a similarly shaped crystal was observed in the CALB@ZIF-90 SEM images (**Figure 5.1b**). Due to the low solubility of the ICA ligand in water at room temperature standard washing protocols (water) are not sufficient for removing excess ligand from the ZIF-90 crystals.

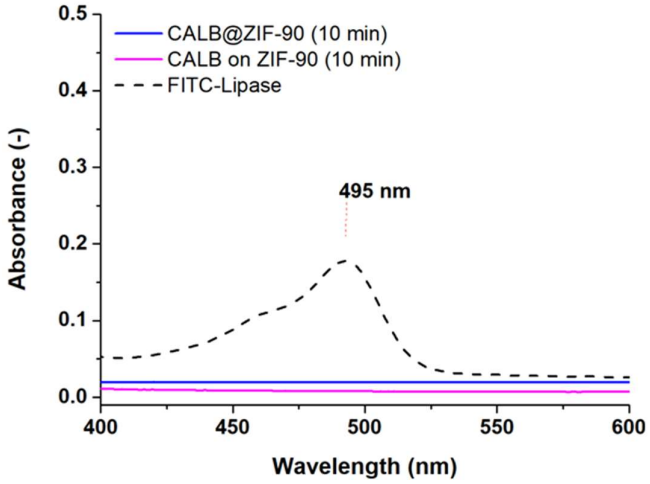

Figure S5.4: Absorbance spectrum of the supernatants of FITC-CALB@ZIF-90 (10-minute) before washing. No absorbance peak was observed at 495 nm (corresponding to FITC) indicating no FITC or FITC-CALB was left in solution. The absorbance of the FITC-CALB is shown as a dotted reference line. Traces are offset on the y axis for clarity.

5.8.4. ZIF-90 hydrolysis controls

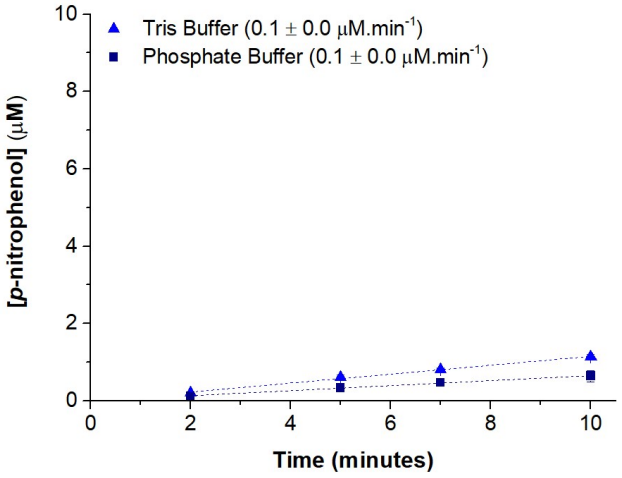

Figure S5.5: Control assays BSA@ZIF-90 (10-minute) in tris and phosphate buffer. Assays were performed after 0- and 30-minutes exposure to each buffer and are reported as the mean and standard error. Low levels of background hydrolysis was reported for each buffer with the small standard error range indicating that incubation time was not impacting the rate.

5.8.5. CALB@ZIF-90 N_2 sorption analysis

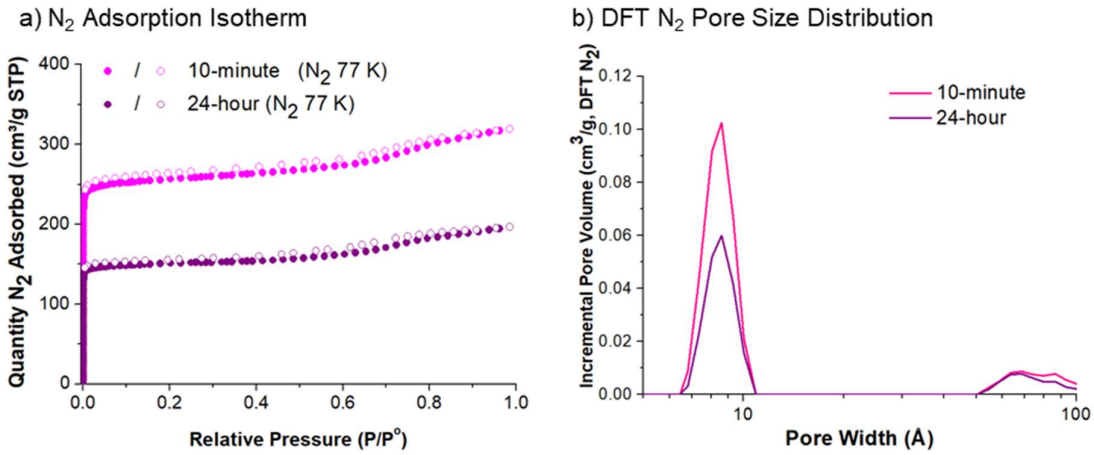

Figure S5.6: N_2 sorption/desorption curves at 77 K giving BET surface areas of 1051 ± 1 and 623 ± 0 $m^2.g^{-1}$ respectively for the 10-minute and 24-hour CALB@ZIF-90. (b) Pore size distribution of each CALB@ZIF-8 preparation indicate a similar pore size for both samples.

5.8.6. CALB@ZIF-90 stability characterisation

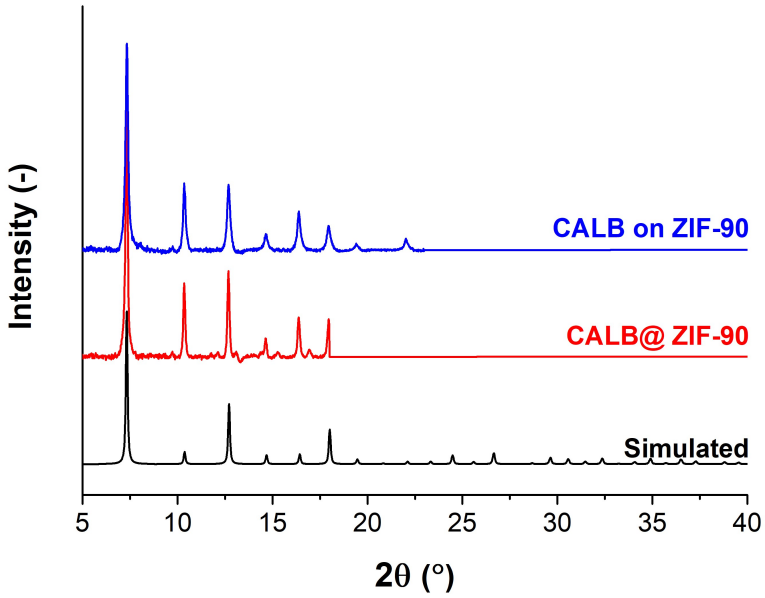

Figure: S5.7: PXRD patterns of the CALB@ZIF-90 and CALB on ZIF-90 (10-minute) after 24 hours transesterification in 100% hexane.

5.8.7. BIOHOF-1 characterisation

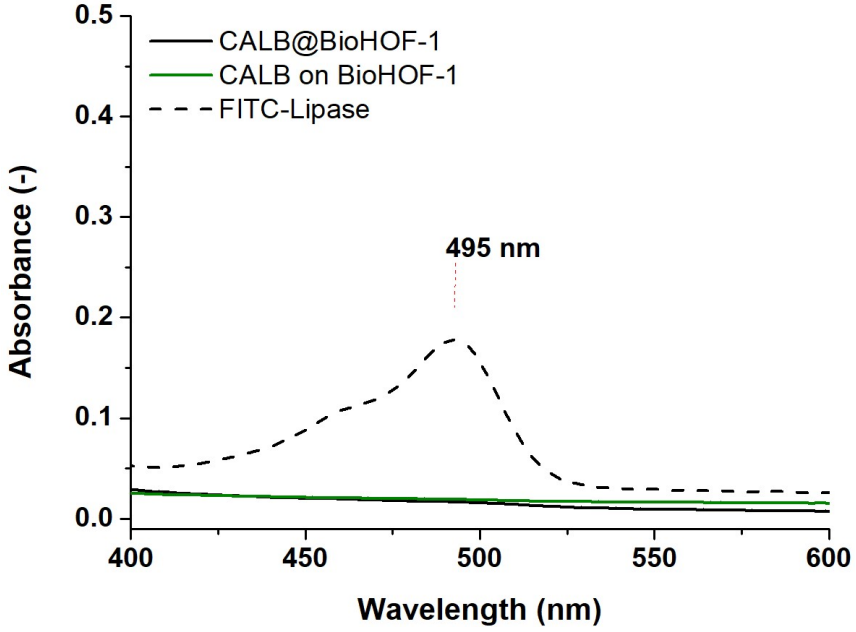

Figure S5.8: Absorbance spectrum of the supernatants of FITC-CALB@BioHOF-1 before washing. No absorbance peak was observed at 495 nm (corresponding to FITC) indicating no FITC or FITC-CALB was left in solution. The absorbance of the FITC-CALB is shown as a dotted reference line. Traces are offset on the y axis for clarity.

5.8.8. BioHOF-1 hydrolysis controls

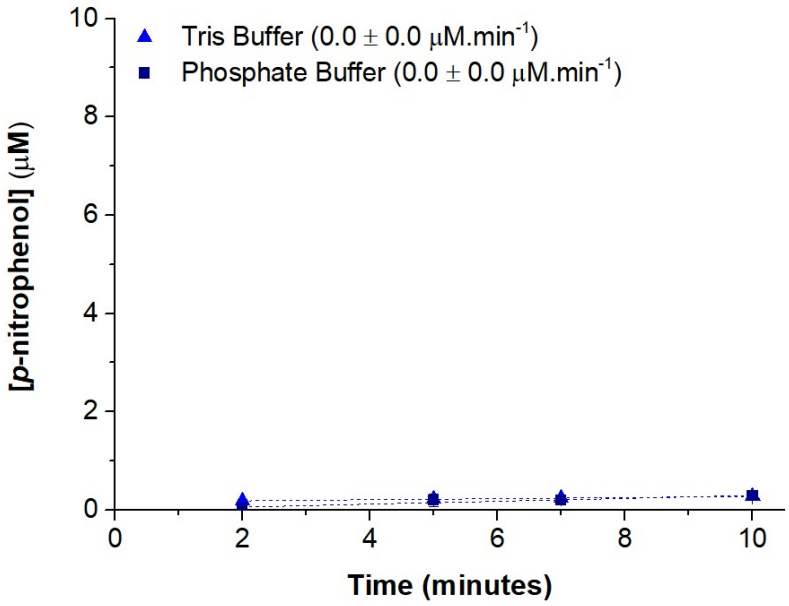

Figure S5.9: Control assays BSA@BioHOF-1 in tris and phosphate buffer. Assays were performed after 0- and 30-minutes exposure to each buffer and are reported as the mean and standard error. Low background hydrolysis was reported for each buffer with the small standard error range indicating that incubation time was not impacting the rate.

5.8.9. BioHOF-1 stability testing

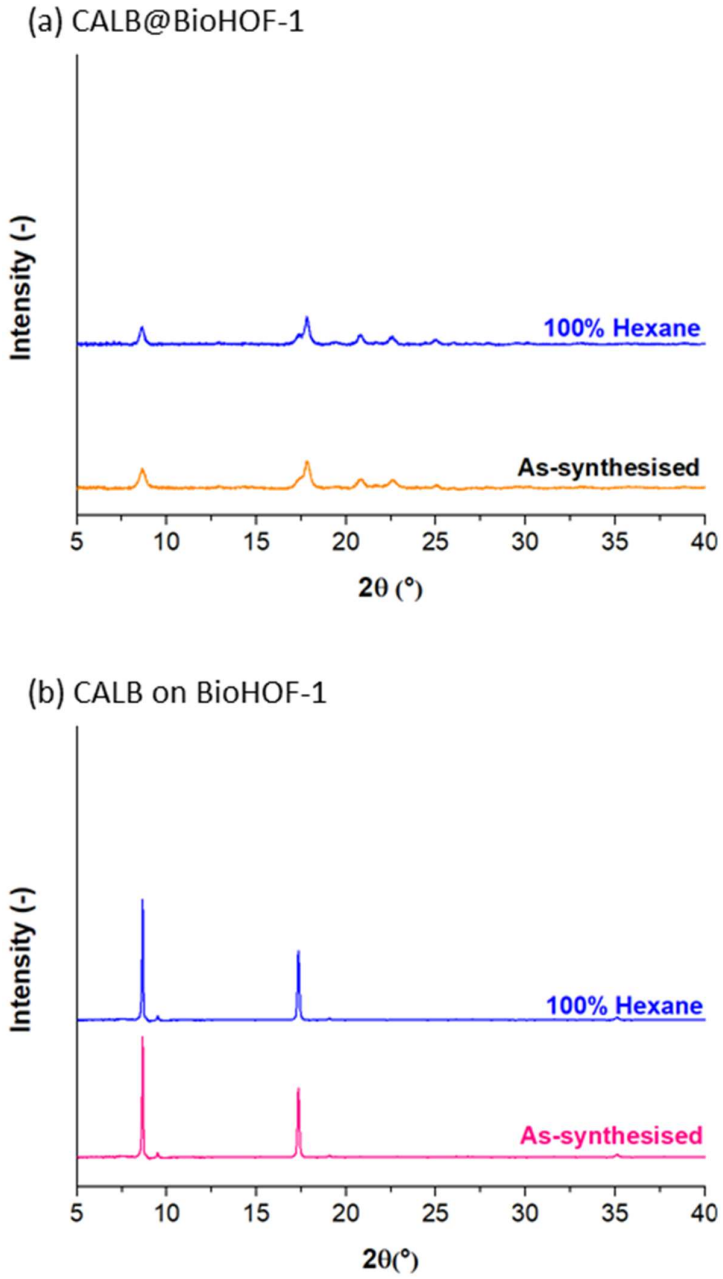

Figure S5.10: PXRD of CALB@BioHOF-1 (a) and CALB on BioHOF-1 (b) as-synthesised and post transesterification.

5.8.10. Enantioselective transesterification

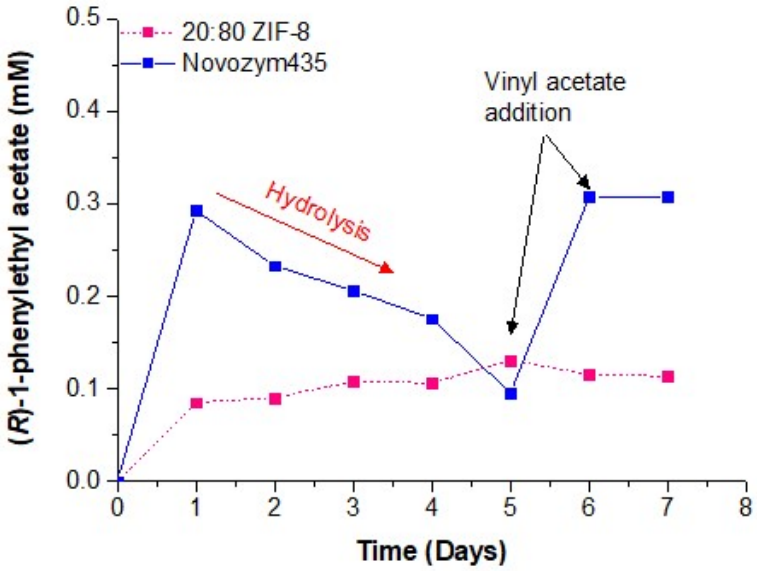

Figure S5.11: Concentration of (*R*)-1-phenylethyl acetate generated by Novozym435 and CALB@ZIF-8 (20:80 mM) over a 7-day reaction. Novozym435 was the most active biocomposite, yielding 60% of the *R*-ester after 24 hours. In the remaining timepoints, the ester concentration was reduced due to ester hydrolysis to 19 %. Vinyl acetate addition after day 5 pushed the reaction towards hexyl acetate production again, however a maximum production of 62% was possible, with further addition on day 6 not increasing it further. CALB@ZIF-8 yielded approximately 25% (*R*)-1-phenylethyl acetate and did not increase further upon vinyl acetate addition, suggesting that the biocomposite was being deactivated.

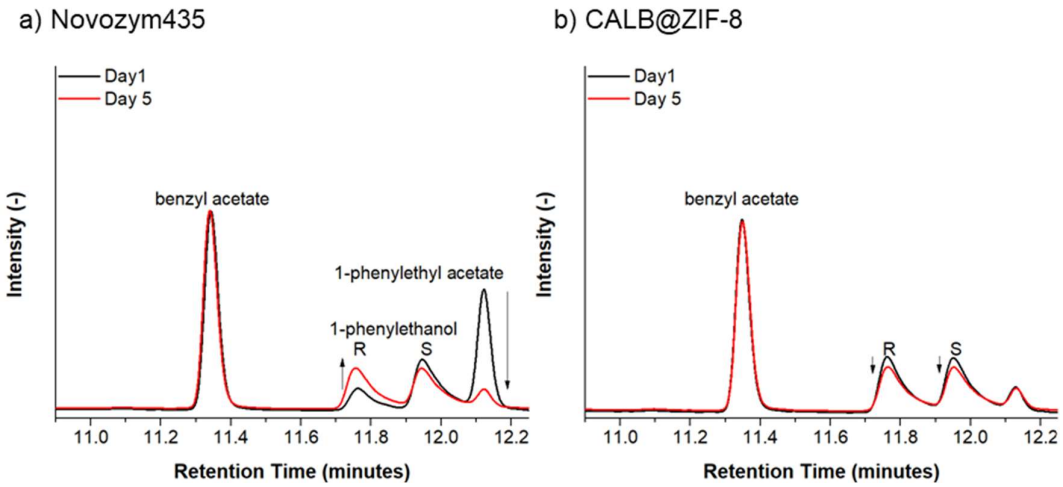

Figure S5.12: Gas chromatogram of chiral column separation of 1-phenylethanol transesterification.Novozym435 saw an initial increase in peak area at 12.1 minutes and reduction at 11.7 minutes, due to the production of (*R*)-1-phenylethyl acetate and consumption of (*R*)-1-phenylethanol (day 1, black trace). In the following days the ester peak reduced, and the *R* alcohol increased due to product hydrolysis (day 5, red). CALB@ZIF-8 (20:80 mM) generated a small *R*- ester peak on day 1 which did not increase significantly at day 5. The *R* and *S* alcohol peaks did reduce slightly, potentially due to adherence of the alcohols to the ZIF surface. There is no peak at 11.3 minutes indicating that no (*S*)-1-phenylethyl acetate was being produced.

Table S5.1: Comparison of CALB percentage yields of hexyl acetate and (R)-1-phenylethyl acetate of CALB@BioHOF-1, CALB@ZIF-90 (10-minute) and their surface bound equivalents. CALB@ZIF-8 (20:80 mM) and Novozym435 are included for comparison.

(*R*/*S*)-1-Phenylethanol

Support	% Conversion		*ee*
	Day 1	Day 5	
CALB@BioHOF-1	16	28	>99
CALB on BioHOF-1	26	53	>99
CALB@ZIF-90 (10-minute)	3	40	>99
CALB on ZIF-90 (10-minute)	4	28	>99
CALB@ZIF-8 (20:80 mM)	17	26	>99
Novozym435	58	19	>99

Supporting Information 5.8 References

1. Cabrera, Z.; Fernandez-Lorente, G.; Fernandez-Lafuente, R.; Palomo, J. M.; Guisan, J. M., Novozym 435 displays very different selectivity compared to lipase from *Candida antarctica* B adsorbed on other hydrophobic supports. *J. Mol. Catal. B. Enzym.* **2009,** *57* (1), 171-176

.

Chapter 6.

Enhanced Stability and Activity of a Haloalkane Dehalogenase Immobilised in a Hydrogen-bonded Organic Framework (Compared to Metal-Organic Frameworks)

Chapter 6. Enhanced Stability and Activity of a Haloalkane Dehalogenase Immobilised in a Hydrogen-bonded Organic Framework (Compared to Metal-Organic Frameworks)

6.1. Abstract

The encapsulation of enzymes within porous materials is a rapidly developing area of research that is focussed on the immobilisation of biomacromolecules to enhance their activity, stability, and reusability. Recombinant protein expression enables the creation of extensive libraries of enzymes to fully capitalise on this by creating novel biocomposites with a broad range of applications. Here we describe the expression and purification of a haloalkane dehalogenase enzyme, LinB and demonstrate, for the first time, its immobilisation within zeolitic imidazolate frameworks, ZIF-8 and ZIF-90, and a porous hydrogen bonded organic framework, BioHOF-1. The activity of LinB immobilised within BioHOF-1 (LinB@BioHOF-1) was comparable to the free enzyme, reaching 75- and 98% single step dehalogenation of alkyl halides, 1,2-dibromoethane and 1,3-dibromopropane respectively. The LinB@BioHOF-1 composite displayed enhanced reusability and thermal stability relative to the free enzyme, whereas ZIF immobilisation afforded biocomposites that were either inactive or unstable to the reaction conditions. These findings highlight a general strategy for enzyme immobilisation in porous materials, demonstrating that BioHOF-1 can accommodate enzymes which are not active or stabilised in ZIF materials.

6.2. Introduction

Haloalkane dehalogenases, HLDs (EC 3.8.1.5) are a family of microbial enzymes that share structural similarities with α/β hydrolase enzymes (esterases, lipases etc).[1] HLDs function via a hydrolytic mechanism, and target the cleavage of carbon-halogen bonds, to yield the corresponding alcohol and free halide. The reaction is catalysed by a triad of amino acids (Aspartate; Asp, Histidine; His, and Aspartate or Glutamate; Glu), initiated via nucleophilic attack of an Asp residue onto the substrate, followed by hydrolysis of the enzyme bound intermediate (**Figure 6.1**).[2-4]

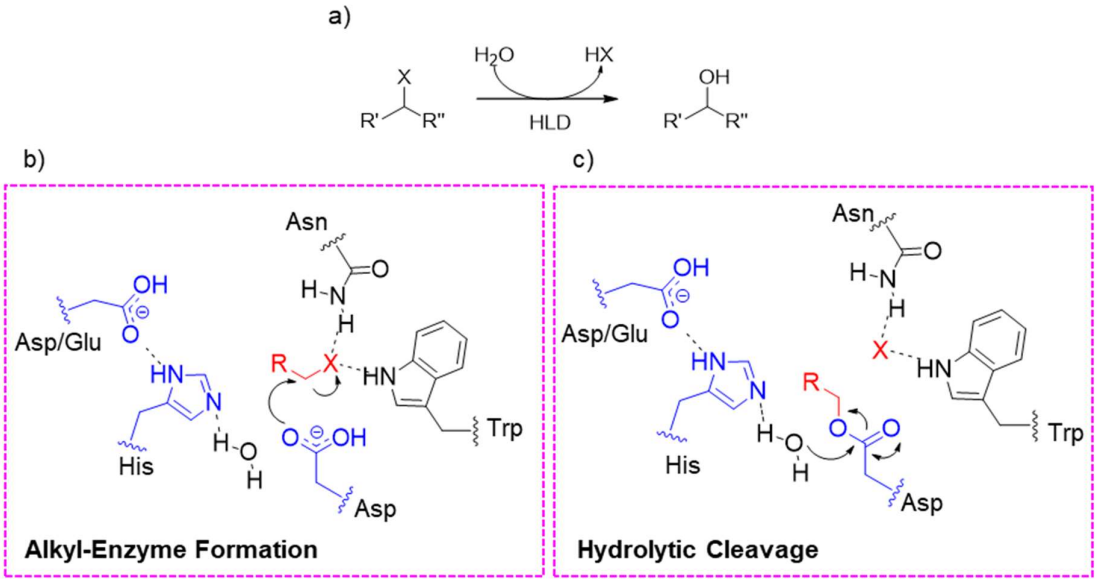

Figure 6.1: (a) General reaction mechanism of haloalkane dehalogenases (HLDs). (b-c) Simplified HLD active site mechanism of the dehalogenation reaction.[2-4] The catalytic triad (Asp-His-Asp/Glu) are depicted in blue. The first step (b) involves the formation of an alkyl-enzyme intermediate via an S_N2 attack of the substrate by the acidic Asp residue. This is followed the cleavage of the alkyl-enzyme intermediate (c) by an active site water molecule. The His residue activates the water molecule and is itself stabilised the third catalytic residue (Asp/Glu). Additional residues (Asn, Trp) are shown in black and position and stabilise the halide.

The reaction proceeds with water as the only external cofactor,[1, 5] making HLDs a relatively simple enzyme to employ for biotechnological purposes.[1, 6] HLDs are useful for biosynthesis, being favoured for their enantioselectivity and kinetic resolution of alcohols.[7-9] Additionally, their ability to break down toxic halogen containing compounds make HLDs an attractive system for the bio-remediation of environmental contaminants.[8, 10-12]

One such HLD is LinB from the bacterial species *Sphingobium japonicium* (formerly *Sphingomonas paucimobilis*) UT26.[13] Within this bacterial strain, LinB is one of 15 proteins involved in the metabolism of insecticide, γ-hexachlorocyclohexane (lindane) to benzene-1-4-diol, and is responsible for the second and third dehalogenation steps of this compound (**Figure S6.1**).[13-15] LinB has a large active site relative to other HLDs and as such accepts a broad range of substrates including bromo-, chloro- and iodo-alkanes.[4, 16-17] LinB maintains activity over a broad pH range (7.5-10.5), and mildly elevated temperatures (30-50°C), however in order to apply LinB for the aforementioned purposes, there is a need to increase its stability, reusability and longevity, to a wider variety of environmental conditions and substrates.[7, 18]

HLD immobilisation is of interest as this affords a heterogeneous biocatalyst that can be utilised at elevated temperatures enabling catalysis of volatile substrates at a solid to gas interface.[19] The process of immobilisation involves the attachment of the enzyme to a solid support, which enhances structural stability and reusability. This has allowed the application of various HLD enzymes for the sensing and bioremediation of airborne pollutants.[20] Nevertheless, while, many immobilisation strategies (cross-linking, covalent attachment, and entrapment within mesoporous materials) have been tested in a research setting,[21-22] there has been limited reports of the commercial application of immobilised LinB.[7] As such, there is a need to develop new methods of immobilisation for LinB. Post synthetic entrapment within mesoporous materials, provides control over substrate diffusion and the enzyme's microenvironment, however there is a high potential for enzyme leaching as the pore size must be larger than the size of the enzyme.[23] An alternative to entrapment, is encapsulation within a microporous material, which can be synthesised around the enzyme in processes termed 'biomimetic mineralisation'[24] or 'co-precipitation'.[25] In these cases the of pore apertures of the microporous network are smaller than the enzyme thus leaching is hindered but diffusion of small substrates is sustained.[26-28]

Metal-Organic Frameworks (MOFs) and Hydrogen-bonded Organic Frameworks (HOFs) are two classes of porous materials that can be utilised for enzyme immobilisation. They are synthesised via a modular approach, that allows for control of the frameworks hydrophobicity, pore size, topology, particle size and morphology.[29-30] Zeolitic-imidazolate frameworks (ZIFs) are porous materials constructed from tetrahedral Zn^{2+} nodes linked via imidazolate organic units. ZIF-8 is synthesised from Zn^{2+} and 2-methyl imidazole (2-mIM) and is known to form a number of crystalline topologies. With respect to the formation of enzyme@ZIF-8 biocomposites the topology (and also particle size) can be controlled through

judicious selection of precursor concentrations.[31] This is noteworthy, as topology and particle size lead to enzyme biocomposites of distinct activity and stability. Employing imidazole-2-carboxaldehdye (ICA) as the organic link, generates ZIF-90, a topologically identical material to ZIF-8.[32] However, the aldehyde group renders the ZIF-90 framework more hydrophilic than ZIF-8. Indeed, this proved advantageous for enzymes that exhibit unfavourable conformational changes upon immobilisation on hydrophobic supports.[33] Similar trends were observed for CALB (*Candida antarctica* Lipase B) in **Chapter 5**, thus highlighting the potential influences of framework chemistry on enzyme activity.

More recently, the Hydrogen-bonded Organic Framework (BioHOF-1), has been demonstrated to encapsulate enzymes in a metal-free framework.[34] BioHOF-1 is synthesised from tetra-amidinium and tetra-carboxylate components, to yield an extended network that has a larger pore aperture (6.4 Å) than both the ZIF materials studied (~3.4 Å), potentially allowing for a larger range of substrates to be utilised.[35-37] BioHOF-1 was selected as a complementary candidate for LinB immobilisation as it retains water within its framework, making it more compatible for enzymes such as LinB that require water as cofactor.[34, 38] Each of the aforementioned frameworks, ZIF-8, ZIF-90 and BioHOF-1, form in aqueous, room temperature conditions, via protocols that that can initiate immobilisation without the need for additional precipitants or enzyme modification steps. As LinB has yet to be immobilised within these porous materials, we were motivated to synthesise biocomposites of each, hereafter known as LinB@ZIF-8, LinB@ZIF-90 and LinB@BioHOF-1, to ascertain if they can preserve the activity of LinB for the dehalogenation of 1,2-dibromoethane and 1,3-dibromopropane.

6.3. Results and Discussion

The proteins studied for ZIF and BioHOF-1 immobilisation are often obtained from commercial sources as lyophilised powders and have the potential to contain undisclosed buffer salts and stabilising agents from the lyophilisation process. Alternatively, proteins can be expressed recombinantly prior to immobilisation, which allows greater control over handling and purification.[39] Additional benefits to this process include the ability to modify the sequence from which the protein is translated, enabling the incorporation of tag sequences for purification, as well as mutations to expand substrate recognition. In this study, a histidine tagged-LinB protein was expressed in *Escherichia coli* and purified using nickel column chromatography to yield a highly active and pure enzyme (**Figure 6.2, S6.2-S6.3**).

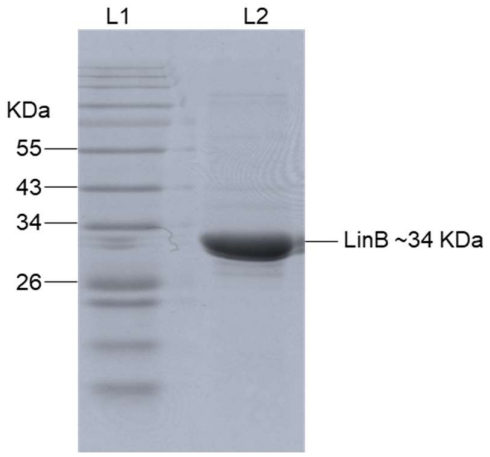

Figure 6.2: SDS-PAGE (Poly Acrylamide Gel Electrophoresis) analysis of purified LinB (MW: 34 KDa). L1: Protein MW Standard, L2: Purified LinB. The purified LinB fraction was concentrated via ultra-filtration and analysed via SDS PAGE (12% acrylamide) to determine the enzymes purity. A single intense band between the 26-34 KDa marker indicates successful expression and purification of LinB.

The activity of LinB (free enzyme) was determined using 1,2-dibromoethane (1,2-DBE) and 1,3-dibromopropane (1,3-DBP), as these alkyl halides are known to be rapidly dehalogenated by LinB to yield products of 2-bromoethanol and 3-bromopropan-1-ol respectively (**Figure 6.3**).[13] The bromo-alcohol product can be dehalogenated further to produce the diol products (ethane-1,2-diol, and propane-1,3-diol) however this process is less favourable and often requires significant depletion of the first product.[40-41] As the dehalogenation reaction only requires water as a cofactor, activity can be monitored directly

via gas chromatography, enabling simultaneous measurement of both the substrate and the first dehalogenation product.

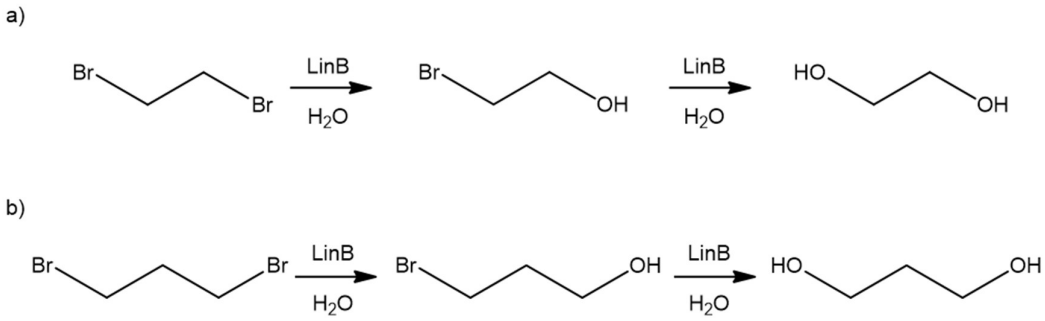

Figure 6.3: (a) The dehalogenation of 1,2-dibromoethane to 2-bromoethanol, which can be dehalogenated further to form ethan-1,2-diol. (b) The dehalogenation of 1,3-dibromopropane to 3-bromopropan-1-ol, followed by propane-1,3-diol.

It was established that for free LinB, that maximum substrate conversion to the bromo-alcohol products occurred within the first 16 hours for both substrates, but between 16- to 24-hours there was a noticeable decrease in the product concentration, suggesting conversion to the diol product was occurring (**Figure 6.4, Table 6.1**). However, due to the increased hydrophilicity of the diol products, they were not extracted out of the buffer solution and thus could not be directly accounted for in this reaction.

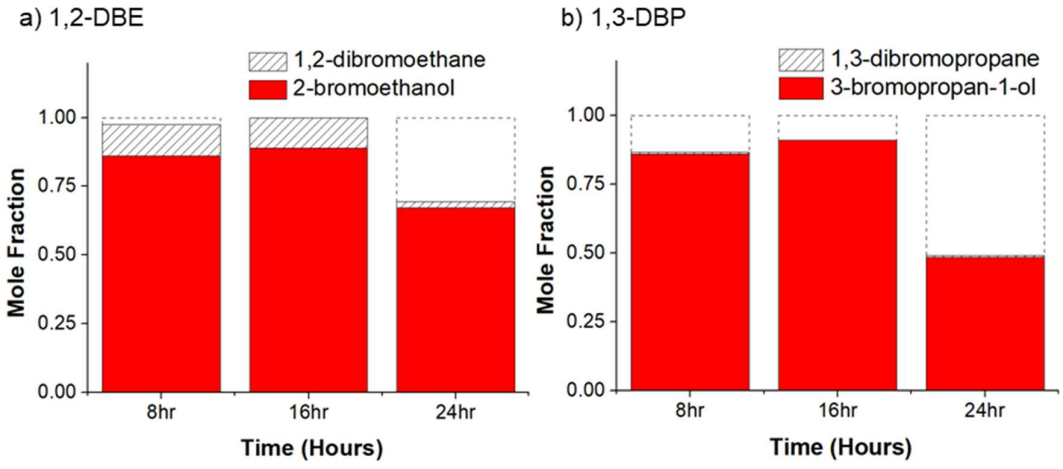

Figure 6.4: Free LinB enzyme conversion of the 1,2-DBE to 2-bromoethanol and 1,3-DBP to 3-bromopropan-1-ol reactions. The substrate and first product (the haloalcohol) concentrations were calculated from separate calibration curves at times, t = 8-, 16- and 24-hours and are reported as a mole fraction of the reaction. Red, black stripes and white segments account for substrate, product, and remaining mole fraction, respectively.

Table 6.1: Quantitative analysis for the mole fraction data showing the percent production of 2-bromoethanol and 3-bromo-1-propanol.

Time	2-bromoethanol (%)	3-bromopropan-1-ol (%)
8 hr	86	86
16 hr	89	91
24 hr	67	48

To investigate the observed reduction in concentration during the free enzyme testing, substrate and product volatility studies were undertaken. The substrate and product controls (1 mM) in tris (50 mM pH 8) were shaken at room temperature for 8-,16- and 24- hours and the concentrations were quantified via GC-FID analysis (**Figure S6.4-S6.5, Table S6.1**). 1,2-DBE and 1,3-DBP were both susceptible to significant evaporation due to their volatility, however the bromo-alcohol controls remained unchanged, confirming that product depletion was not due to evaporation. These experiments provided convincing evidence that the observed decrease between 16- and 24- hours is likely due to conversion to the secondary diol products by the enzyme. Furthermore, in a control reaction, the free LinB could convert 2-bromoethanol to the diol product, as shown by a reduction in the concentration of 2-bromoethanol (0.79 mM) relative to a control (1.1 mM, in the absence of the enzyme) (**Figure S6.6**). As such, we opted to analyse 8-hour reactions to minimise product loss that was prevalent at later timepoints due to the conversion to the diol product that could not be easily quantified.

We then proceeded to investigate the impact of the immobilisation strategy on enzyme activity using the different encapsulation protocols reported for ZIF-8, ZIF-90 and BioHOF-1. The study in **Chapter 4** using CALB@ZIF-8 (CALB: *Candida antarctica* Lipase B) demonstrated that changing the synthetic conditions yields biocomposites of vastly different particle size, pore structure and activity and we were interested in seeing if this trend extended to the LinB system. As such, two preparations of LinB@ZIF-8 were synthesised by changing the Zn^{2+}:2-mIM ratios from 20:80 to 40:640 mM and analysed by SEM (**Figure 6.5a-b**). After 16 hours, these conditions generated particle sizes of 500 nm and 1 μm respectively, consistent with samples synthesised with proteins of low surface charge. Histidine tagged LinB has an isoelectric point of 5.5 and induced ZIF-8 formation via biomimetic mineralisation at low precursor ratios. The crystallinity of all biocomposites was confirmed to match their respective simulated powder diffraction patterns (**Figure S6.7**).

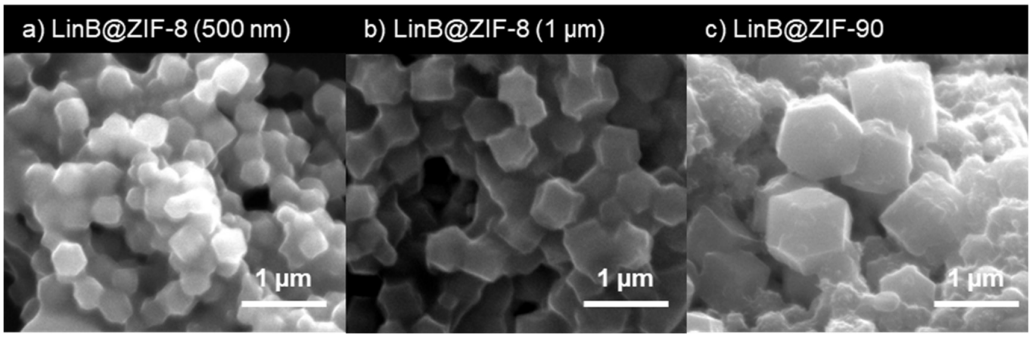

Figure 6.5: SEM of LinB ZIF biocomposites, (a) 500 nm ZIF-8, (b) 1 µm and (c) ZIF-90. The ZIF-8 control does not form under the same conditions used for the 500 nm sample, whilst the conditions for the 1 µm composite generates crystals of the same morphology and size when synthesised without the protein. The inclusion of LinB into the ZIF-90 crystals yield crystals ranging from 500 nm to 1 µm, compared to 2-5 µm in the protein free samples. No 5 µm crystals were observed (compared to the CALB@ZIF-90, **Chapter 5, Figure 5.1**) indicating that the CALB and LinB are influencing the formation in different ways. Further investigation is therefore required.

LinB@ZIF-90 was synthesised to compare the effect on enzyme activity of a more hydrophilic framework, as well as the impact of synthetic conditions (ligand, pH) and a different microenvironment relative to ZIF-8. In the synthesis of ZIF based biocomposites, the enzyme is usually dissolved with the ligand rather than the Zn^{2+} solution to favour enzyme dissolution. It is important to account for the enzyme exposure to the different ligands as the ICA solution for ZIF-90 has an approximate pH range of 6-7 whereas the 2-mIM for ZIF-8 can easily exceed pH 11. These distinct synthesis conditions would likely impact the conformation of LinB during immobilisation. The LinB@ZIF-90 material was collected after 10 minutes (formation time) to prevent the crystallisation of ligand which has been observed for CALB in **Chapter 5**. As previously observed, the LinB@ZIF-90 biocomposite comprised of two approximate particle sizes in the one (500 nm and 1 µm, **Figure 6.5c**), which would afford different enzyme to crystal loading and could impact activity. In contrast, the LinB@BioHOF-1 biocomposites were uniformly sized with well-defined crystal edges with topology and morphology matching the enzyme free BioHOF-1 control (**Figure 6.6, S6.8**) This framework has demonstrated promise for enzyme encapsulation due to its pore size, and broader pH stability (see also **Chapter 5**) making it an ideal candidate for testing the substrate range of LinB. Additionally, the pH of the tetra amidinium solution in which the enzyme is dissolved is approximately 6, thus avoiding the extreme basic conditions that occur during ZIF-8 formation.

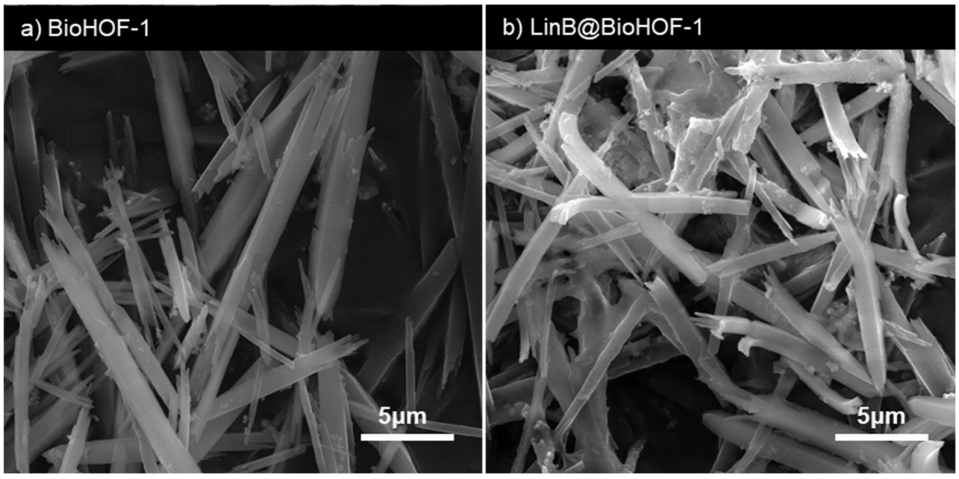

Figure 6.6: SEM of as-synthesised BioHOF-1 made (a) without protein or (b) with LinB (2 mg). Crystal size and shape were unaltered upon the addition of LinB.

After establishing appropriate reaction conditions, we proceeded to investigate the relationship between immobilisation and enzyme activity. Each LinB biocomposite was examined for the dehalogenation of 1,2-DBE and 1,3-DBP and were directly compared to the free enzyme activity after 8 hours (**Figure 6.7**). LinB@BioHOF-1 was the most active biocomposite for both 1,2-DBE and 1,3-DBP, reaching conversions of 75% and 98%, respectively, compared to the 86% conversions reported for free enzyme. This result implies that LinB@BioHOF-1 was retaining the enzyme's active conformation upon immobilisation and was not being restricted by substrate diffusion. In comparison, when tested for the dehalogenation of 1,2-DBE the ZIF-8 samples (500 nm and 1 µm) demonstrated no conversion (<1% and not detected) whilst ZIF-90 was only slightly active with a yield of 11%. The slow production of the ZIF-90 material, and the lack of activity in the ZIF-8 samples suggest that the ligand pH and framework hydrophobicity do not solely contribute to the loss of activity observed and another factor such as substrate diffusion, or the combined effect of these three parameters was causing activity loss. Interestingly, changing the substrate to 1,3-DBP resulted in a significant increase in activity for LinB@ZIF-8 (500 nm) and ZIF-90 biocomposites with conversion to 3-bromopropan-1-ol reaching 54% and 97%. LinB@ZIF-8 (1 µm) remained practically inactive, with only 2% product being detected after 8 hours. These results indicate that activity is substrate dependent and influenced by the method of ZIF-8 formation.

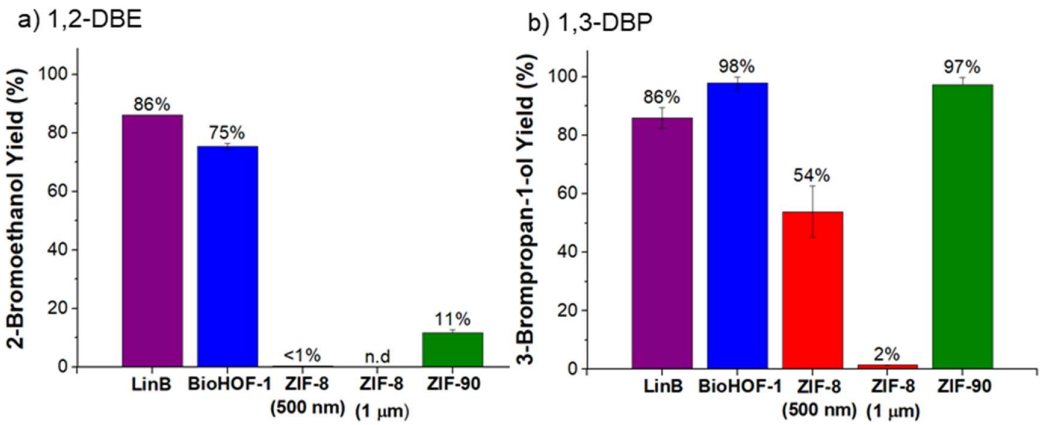

Figure 6.7: Percentage yield of (a) 2-bromoethanol and (b) 3-bromo-1-propanol in the first dehalogenation step of 1,2-DBE or 1,3-DBP. Values were calculated from a GC calibration curve of 2-bromoethanol and 3-bromo-1-propanol and are relative to the maximum production of 1 mM. The ZIF-8 samples displayed were made using Zn^{2+}:2-mIM ratios of 20:80 mM (500 nm) and 40:640 mM (1 μm). Additional ZIF-8 samples gave similar results for 1,2-DBE with 20:160 mM (~700 nm) yielding < 1%, and 20:400 mM (~1 μm) showing no detectable (n.d) product after 8- and 16- hours (**Table S6.2-S3**). A second ZIF-90 sample yielded 5% after 8 hours. For 1,3-DBP, the additional ZIF-8 (700 nm and 1 μm) samples produced 36% and < 1% respectively whilst ZIF-90 reached 85% conversion.

To further understand the activity of the LinB materials for different substrates, the biocomposites were analysed post reaction via SEM and PXRD to visualise the structural stability of each sample. The crystallinity and morphology of LinB@BioHOF-1 remained unchanged for both substrates demonstrating the high compatibility of the BioHOF-1 materials for enzyme catalysis (**Figure 6.8a, S6.9**). After exposure to 1,3-DBP, the surface of the small ZIF-8 crystals was noticeably damaged, however the bulk crystallinity was retained (**Figure 6.8b, S6.10**). This would expose the immobilised enzyme to the substrate or cause the enzyme to leach into solution. The larger LinB@ZIF-8 appeared to be less susceptible to degradation, with the bulk material remaining visually unchanged in the SEM images (**Figure 6.8c, S6.11**). Adsorption of tris onto the ZIFs may have masked etching of the crystals and surface degradation, however there is a clear distinction between the ZIF-8 (500 nm) samples after exposure to each alkyl-halide highlighting potential particle size or morphological dependent substrate effects. We have previously reported size dependant, ZIF-8 surface instability towards hydrophobic substrates containing polar functional groups, which was more prominent on smaller ZIF samples.[42] It is therefore likely that degradation was influenced by the size of

the ZIF-8 particles and the hydrophobicity of the substrates suggesting that ZIF-8 biocomposites would not be suitable for applications with even larger compounds. LinB@ZIF-90, which consisted of both large (1 µm) and small (500 nm) particles was also susceptible to degradation by 1,3-DBP, with the smaller particles degrading completely after 8 hours (**Figure 6.8d, S6.12**). This supports the size dependent degradation of ZIF-8 and suggests that the smaller particles contained the majority of the LinB enzyme as product formation reached a conversion similar to the free enzyme. Forming ZIF-90 without a protein yields 1-2 µm crystals which are also observed in the LinB samples potentially indicating two separate mechanisms of ZIF-90 formation (protein free vs protein containing crystals).

For the 1,2-DBE assay, where biocomposite degradation was not significant, the variation in activity between the BioHOF-1 and ZIF materials may be explained by their porosity and ability to accommodate each substrate. The crystallographic pore aperture of the BioHOF-1 (6.4 Å) is also significantly larger than the ZIFs (~3.4 Å) and would best favour diffusion of the target alkyl halide substrates. Indeed, in a diffusion study by Liang *et. al.* the porosity of BioHOF-1 enabled the solution phase uptake of fluorescein (7 Å), implying structural flexibility of the framework that allows diffusion of compounds that are the larger that the solid-state aperture.[34] BioHOF-1 could therefore allow the diffusion of both di-brominated alkyl halides (1,2-DBE, 4.89 Å and 1,3-DBP, 5.58 Å) whereas activity was only regenerated upon crystal degradation of the ZIF materials. Diffusion of these substrates may be possible for the ZIFs (aperture ~3.4 Å), as framework flexibility allows for diffusion of substrates up to ~5 Å,[43] however the diffusion of these compounds is restricted and quite slow. Analysing the activity results for 1,2-DBE suggest that diffusion was either slow or not occurring.

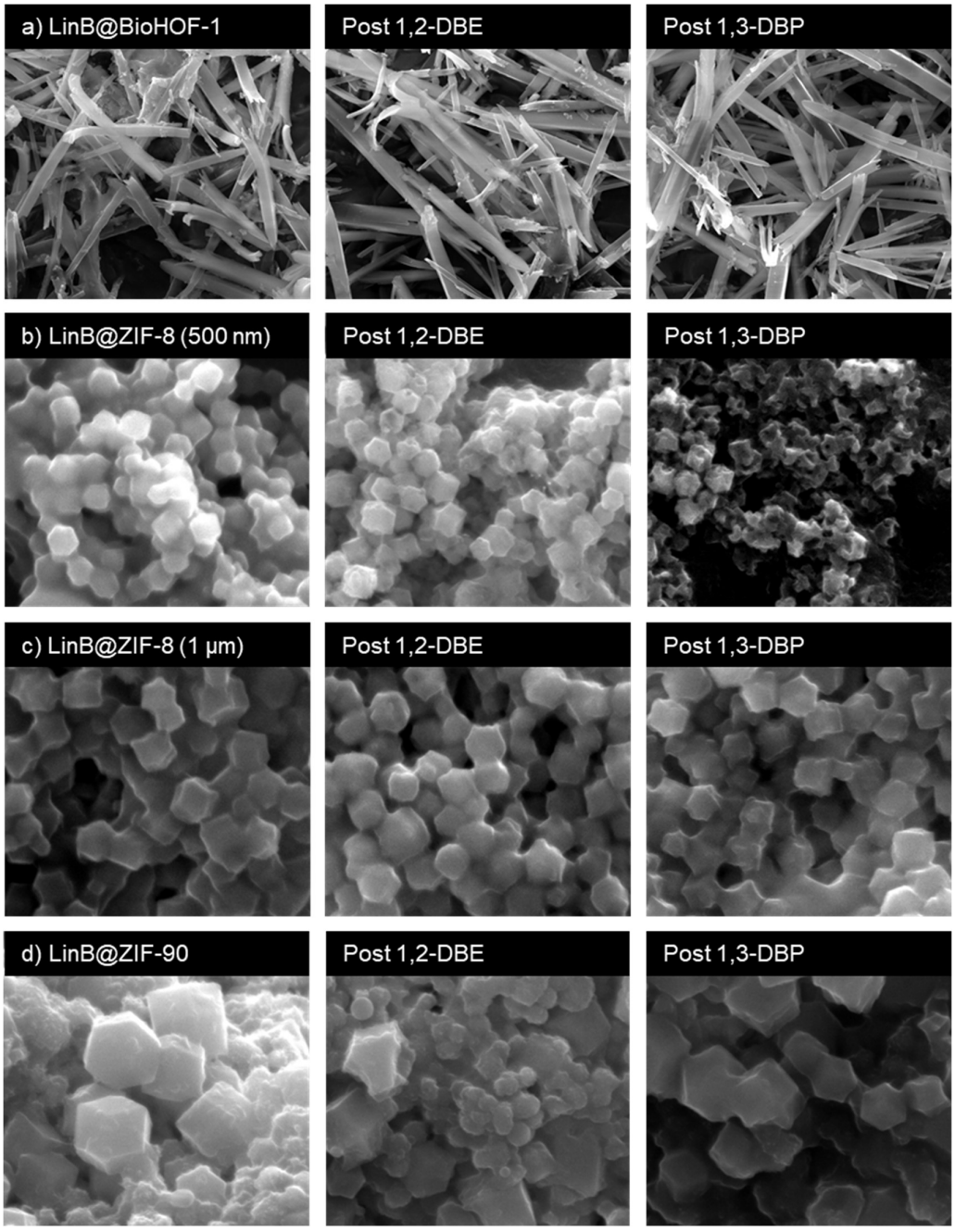

Figure 6.8: SEM images of each biocomposite after reaction with 1,2-DBE, and 1,3-DBP. a) LinB@BioHOF-1 remained unchanged after both reactions. b) LinB@ZIF-8 (500 nm) appeared to be relatively unchanged (mild degradation was possible) after reaction with 1,2-DBE, however, was substantially degraded after reaction with 1,3-DBP. c) Minimal sample variation was observed for LinB@ZIF-8 (1 µm). d) The as-synthesised LinB@ZIF-90 possessed large and small crystals, which were unchanged after reaction with 1,2-DBE. Exposure to 1,3-DBP caused complete loss/degradation of the small crystals.

When analysing the composition of reaction mixtures at 8 hours there was a noticeable discrepancy between the actual and expected concentrations of the substrate and bromo-alcohol products (**Figure S6.13**). When using porous materials, substrate/product adsorption to the support surface or within the pores is possible so care must be taken when analysing the reaction progress, as the support chemistry may influence the concentrations of substrates/ products in solution[43]. To account for this, biocomposite controls made with BSA were shaken with 1 mM 1,2-DBE or 1,3-DBP for 8 hours and the reaction composition was analysed (**Figure S6.14a-b**). No product was detected in each control reaction however the substrate concentration was affected by the different support materials. In particular, the large ZIF-8 crystals saw a reduction in 1,2-DBE by 70% and 1,3-DBP by 90%, whereas the small ZIF-8 particles, ZIF-90 and BioHOF-1 support had a considerably reduced affinity for adsorption of either alkyl halide (**Figure S6.14a-b**). The differences between the large and small ZIF-8 samples implies that there are structural or surface chemistry differences that arise from the different formation mechanisms, which need to be explored further. ZIF-90 demonstrated minimal substrate adsorption, but low activity, whereas BioHOF-1 was favourable for both attributes. Each bromo-alcohol product was also tested, and no adsorption was observed for any of the biocomposites meaning that the reported conversion percentages (calculated from product calibrations) were not been impacted by adsorption effects (**Figure S6.14c-d**). These results highlight how porous materials may affect the substrate and product composition in solution, and the care that is required when analysing and interpreting different reaction types.

The above data confirmed that BioHOF-1 was the best immobilisation support for LinB maintaining similar activity to the free enzyme whilst being stable to both substrates. As such, LinB@BioHOF-1 was examined further to demonstrate the reusability and protective capacity of the support. Under the same conditions for 1,2-DBP, LinB@BioHOF-1 could be reused for 5 cycles, maintaining activity (98% conversion) after each 8-hour reaction (**Figure 6.9**). Heating the free LinB at 60 °C for 30 minutes in solution, led to aggregation and precipitation of the enzyme, (**Figure 6.10**) and a corresponding loss of activity. LinB@BioHOF-1, however, retained activity post heat treatment, demonstrating the capacity of the framework to stabilise the enzyme in an active conformation to elevated temperatures (**Figure 6.11a**). Additionally, LinB@BioHOF-1 dried at ambient temperature and pressure, maintained full activity relative to the fully solvated composite and could be heated without any activity depletion (**Figure 6.11b**). These findings demonstrate that the process of LinB immobilisation in BioHOF-1 can stabilise the enzyme to thermal conditions that would otherwise inactivate the enzyme. As such

BioHOF-1 is a suitable support porous material to investigate LinB catalysis under non-physiological conditions.

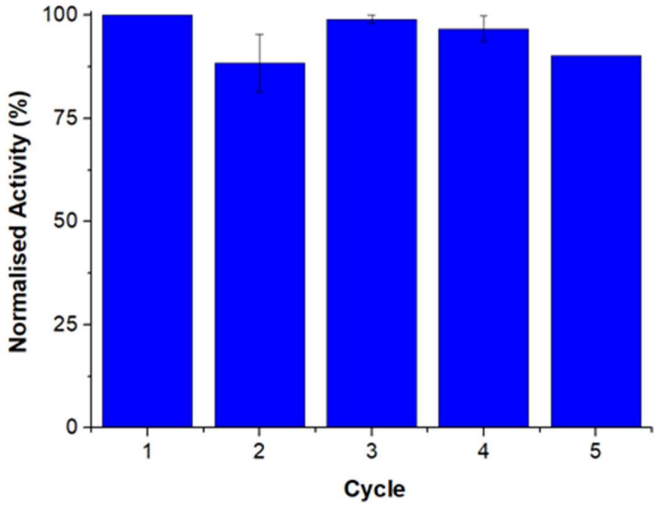

Figure S6.9: Recycling study using LinB@BioHOF-1 and 1,2-DBP. Percent conversion has been normalised relative to the first cycle. Minimal variation in activity was observed in each successive reaction cycle.

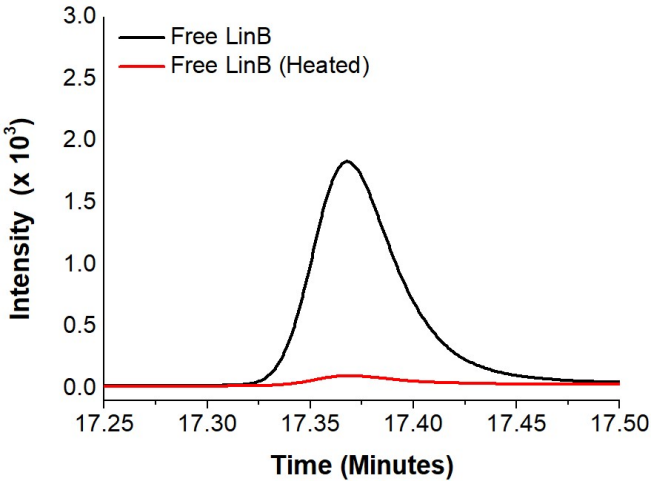

Figure 6.10: GC trace of the free enzyme after an 8-hour reaction with 1,2-DBE to yield 2-bromoethanol (retention time:17.35 min) and the corresponding GC trace after the thermal treatment of LinB. The GC traces were normalised relative the internal standard (1-bromodecane, retention time 15.4 min). Inset: The free LinB sample in water after heating at 60 °C for 30 minutes.

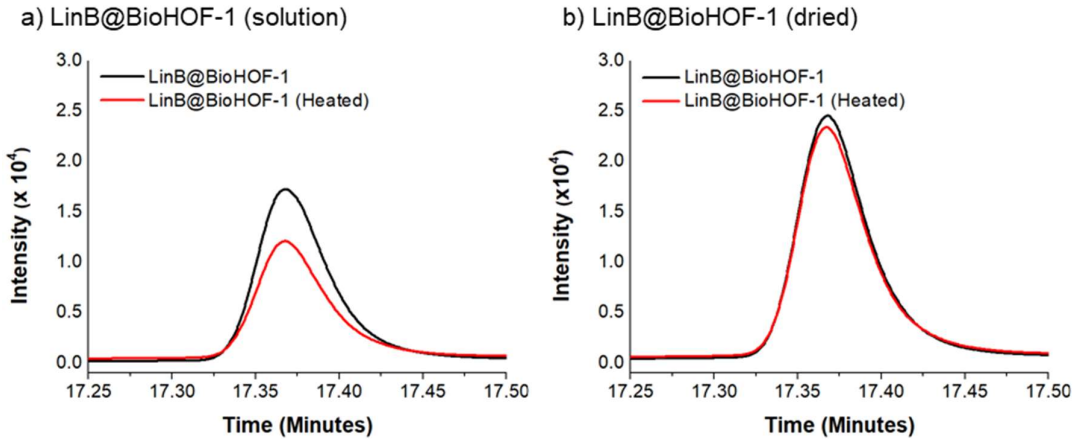

Figure 6.11: GC traces of the 1,2-DBE assay using LinB@BioHOF-1 before and after heat treatment at 60 °C for 30 minutes, whilst in (a) solution or (b) dried under ambient temperature and pressure. GC traces were normalised as per **Figure 6.10**.

6.4. Conclusions

LinB was recombinantly expressed and purified with the aid of a genetically incorporated histidine tag and subsequently immobilised in ZIF-8, ZIF-90 and BioHOF-1. BioHOF-1 was the most compatible framework for LinB, maintaining high levels of activity and stability for dehalogenation of 1,2-dibromoethane and 1,3-dibromopropane whereas activity was significantly or completely reduced upon immobilisation in ZIF-90 and ZIF-8 particles. The clear distinction between the BioHOF-1 and the ZIF-8/90 frameworks, suggests that the pore size of BioHOF-1 is large enough to allow free substrate diffusion, whilst the smaller pores of the ZIFs is too restrictive. The encapsulation process may also lead to varied enzyme activity due to changes in microenvironment of the enzyme, with formation of LinB@BioHOF-1 yielding uniform crystals that retained activity and stability to both reaction conditions. In contrast, the ZIF materials comprised of greater particle size variability, that complicated characterisation and interpretation of activity. The crystallinity, morphology and surface texture of LinB@BioHOF-1 crystals was fully maintained during each alkyl halide reaction and could be reused for multiple cycles and heated without activity reduction whereas each ZIF material was partially degraded under the same reaction conditions. LinB@BioHOF-1 could be synthesised according to procedures reported for different enzymes, forming structurally identical biocomposites without enzyme surface modification steps or optimisation of synthetic protocols. The general approach to immobilisation, in combination with its large pore size relative to the ZIF materials, make BioHOF-1 an excellent candidate to create novel biocomposites with interesting applications.

6.5. Experimental

6.4.1. Expression and Purification

General DNA and microbiological experiments were carried out according to standard protocols, outlined in the Supporting Information.

6.4.2. Biocomposite Synthesis

LinB@ZIF-8, LinB@ZIF-90, LinB@BioHOF-1 and their surface adsorbed equivalents were synthesised according to previously reported protocols,[33-34] and are outlined further in **Chapter 5.** The LinB enzyme was stored in glycerol at -20 °C prior to use and was exchanged into ultra-pure water using a 10 KDa membrane and centrifugation (3400 rpm 4 x 15 minutes, 4°C). Each biocomposite was washed and made up to 1 mL in MQ water (LinB concentration: 2 $mg.ml^{-1}$)

6.4.3. Dehalogenation Reaction

The LinB protein was washed via ultrafiltration to remove glycerol and exchanged into water prior to assay testing. For each reaction, the LinB concentration was set at 0.4 $mg.ml^{-1}$ in tris (50 mM, pH 8) with an initial substrate concentration of 1 mM. 1,3- dibromopropane, or 1,2-dibromoethane (10 µL, 100 mM) was added to tris buffer (790 µL, 50 mM, pH 8) containing the LinB biocomposite (200 µL). Aliquots were taken at 8-, 16- and 24-hours and extracted into cold ethyl acetate containing internal standard (bromodecane).

6.4.4. Characterisation

PXRD and SEM. Characterisation is outlined in **Chapters 2 and 3**.

Gas Chromatography Analysis. Aliquots were extracted into ethyl acetate, dried with magnesium sulfate and analysed via Gas Chromatography (Shimadzu, Nexis GC-2030) equipped with a DB-wax column (30.0 m, 0.25 mm, 0.25 mm) and a Flame Ionisation detector (FID). The column was held at 40°C for 5 minutes and increased at 8°C per minute to 120°C. At the end of each run, the column was heated to 220°C for a burn off for 3-minutes.

6.6. Acknowledgements

N. K. Maddigan acknowledges O.M. Linder-Patton for his technical assistance and Dr. N. White for supplying the BioHOF-1 building units.

6.7. References

1. Janssen, D. B., Evolving haloalkane dehalogenases. *Curr. Opin. Biotech.* **2004,** *8* (2), 150-159.

2. Verschueren, K. H. G.; Seljée, F.; Rozeboom, H. J.; Kalk, K. H.; Dijkstra, B. W., Crystallographic analysis of the catalytic mechanism of haloalkane dehalogenase. *Nature* **1993,** *363* (6431), 693-698.

3. Pries, F.; Kingma, J.; Krooshof, G. H.; Jeronimus-Stratingh, C. M.; Bruins, A. P.; Janssen, D. B., Histidine 289 is essential for hydrolysis of the alkyl-enzyme intermediate of haloalkane dehalogenase. *J. Biol. Chem.* **1995,** *270* (18), 10405-10411.

4. Damborský, J.; Koča, J., Analysis of the reaction mechanism and substrate specificity of haloalkane dehalogenases by sequential and structural comparisons. *Protein Eng. Des. Sel.* **1999,** *12* (11), 989-998.

5. Negri, A.; Marco, E.; Damborsky, J.; Gago, F., Stepwise dissection and visualization of the catalytic mechanism of haloalkane dehalogenase LinB using molecular dynamics simulations and computer graphics. *J. Mol. Graphics Model.* **2007,** *26* (3), 643-651.

6. Fetzner, S.; Lingens, F., Bacterial dehalogenases: biochemistry, genetics, and biotechnological applications. *Microbiol. Rev.* **1994,** *58* (4), 641.

7. Koudelakova, T.; Bidmanova, S.; Dvorak, P.; Pavelka, A.; Chaloupkova, R.; Prokop, Z.; Damborsky, J., Haloalkane dehalogenases: Biotechnological applications. *Biotech.* **2013,** *8* (1), 32-45.

8. Swanson, P. E., Dehalogenases applied to industrial-scale biocatalysis. *Curr. Opin. Biotech.* **1999,** *10* (4), 365-369.

9. Prokop, Z.; Sato, Y.; Brezovsky, J.; Mozga, T.; Chaloupkova, R.; Koudelakova, T.; Jerabek, P.; Stepankova, V.; Natsume, R.; van Leeuwen, J. G. E.; Janssen, D. B.; Florian, J.; Nagata, Y.; Senda, T.; Damborsky, J., Enantioselectivity of haloalkane dehalogenases and its modulation by surface loop engineering. *Angew. Chem. Int. Ed.* **2010,** *49* (35), 6111-6115.

10. Stucki, G.; Thueer, M., Experiences of a large-scale application of 1,2-dichloroethane degrading microorganisms for groundwater treatment. *Environ. Sci. Technol.* **1995,** *29* (9), 2339-2345.

11. Lal, R.; Pandey, G.; Sharma, P.; Kumari, K.; Malhotra, S.; Pandey, R.; Raina, V.; Kohler, H.-P. E.; Holliger, C.; Jackson, C.; Oakeshott, J. G., Biochemistry of microbial degradation of hexachlorocyclohexane and prospects for bioremediation. *Microbiol. Mol. Biol. Rev.* **2010,** *74* (1), 58.

12. Mena-Benitez, G. L.; Gandia-Herrero, F.; Graham, S.; Larson, T. R.; McQueen-Mason, S. J.; French, C. E.; Rylott, E. L.; Bruce, N. C., Engineering a catabolic pathway in plants for the degradation of 1,2-dichloroethane. *Plant. Physiol.* **2008,** *147* (3), 1192.

13. Nagata, Y.; Miyauchi, K.; Damborsky, J.; Manova, K.; Ansorgova, A.; Takagi, M., Purification and characterization of a haloalkane dehalogenase of a new substrate class from a gamma-hexachlorocyclohexane-degrading bacterium, *Sphingomonas paucimobilis* UT26. *Appl. Environ. Microbiol.* **1997,** *63* (9), 3707.

14. Nagata, Y.; Miyauchi, K.; Takagi, M., Complete analysis of genes and enzymes for γ-hexachlorocyclohexane degradation in *Sphingomonas paucimobilis* UT26. *J. Ind. Microbiol. Biotechnol.* **1999,** *23* (4), 380-390.

15. Nagata, Y.; Endo, R.; Ito, M.; Ohtsubo, Y.; Tsuda, M., Aerobic degradation of lindane (γ-hexachlorocyclohexane) in bacteria and its biochemical and molecular basis. *Appl. Microbiol. Biotechnol.* **2007,** *76* (4), 741-752.

16. Kmunícek, J.; Hynková, K.; Jedlicka, T.; Nagata, Y.; Negri, A.; Gago, F.; Wade, R. C.; Damborský, J., Quantitative analysis of substrate specificity of haloalkane dehalogenase LinB from *Sphingomonas paucimobilis* UT26. *Biochemistry* **2005,** *44* (9), 3390-3401.

17. Damborský, J.; Rorije, E.; Jesenská, A.; Nagata, Y.; Klopman, G.; Peijnenburg, W. J. G. M., Structure–specificity relationships for haloalkane dehalogenases. *Environ. Toxicol. Chem.* **2001,** *20* (12), 2681-2689.

18. Jesenská, A.; Bartoš, M.; Czerneková, V.; Rychlík, I.; Pavlík, I.; Damborský, J., Cloning and expression of the haloalkane dehalogenase gene from *Mycobacterium avium*, N85 and preliminary characterization of DhmA. *Appl. Environ. Microbiol.* **2002,** *68* (8), 3724.

19. Lamare, S.; Legoy, M. D., Working at controlled water activity in a continuous process: The gas/solid system as a solution. *Biotechnol. Bioeng.* **1995,** *45* (5), 387-397.

20. Dravis, B. C.; LeJeune, K. E.; Hetro, A. D.; Russell, A. J., Enzymatic dehalogenation of gas phase substrates with haloalkane dehalogenase. *Biotechnol. Bioeng.* **2000,** *69* (3), 235-241.

21. Nevolova, S.; Damborský, J.; Prokop, Z., immobilization of haloalkane dehalogenase linb from *Sphingobium japonicum* UT26 for biotechnological applications. *Biocatal. Biotransfor.* **2013,** *02*.

22. Badieyan, S.; Wang, Q.; Zou, X.; Li, Y.; Herron, M.; Abbott, N. L.; Chen, Z.; Marsh, E. N. G., Engineered surface-immobilized enzyme that retains high levels of catalytic activity in air. *J. Am. Chem. Soc.* **2017,** *139* (8), 2872-2875.

23. Sheldon, R. A.; van Pelt, S., Enzyme immobilisation in biocatalysis: why, what and how. *Chem. Soc. Rev.* **2013,** *42* (15), 6223-6235.

24. Liang, K.; Ricco, R.; Doherty, C. M.; Styles, M. J.; Bell, S.; Kirby, N.; Mudie, S.; Haylock, D.; Hill, A. J.; Doonan, C. J.; Falcaro, P., Biomimetic mineralization of metal-organic frameworks as protective coatings for biomacromolecules. *Nat. Commun.* **2015,** *6* (1), 7240.

25. Lyu, F.; Zhang, Y.; Zare, R. N.; Ge, J.; Liu, Z., One-pot synthesis of protein-embedded metal–organic frameworks with enhanced biological activities. *Nano. Lett.* **2014,** *14* (10), 5761-5765.

26. Doonan, C.; Riccò, R.; Liang, K.; Bradshaw, D.; Falcaro, P., Metal–organic frameworks at the biointerface: synthetic strategies and applications. *Acc. Chem. Res.* **2017,** *50* (6), 1423-1432.

27. Drout, R. J.; Robison, L.; Farha, O. K., Catalytic applications of enzymes encapsulated in metal–organic frameworks. *Coord. Chem. Rev.* **2019,** *381*, 151-160.

28. Lian, X.; Fang, Y.; Joseph, E.; Wang, Q.; Li, J.; Banerjee, S.; Lollar, C.; Wang, X.; Zhou, H.-C., Enzyme–MOF (metal–organic framework) composites. *Chem. Soc. Rev.* **2017,** *46* (11), 3386-3401.

29. Furukawa, H.; Cordova, K. E.; O'Keeffe, M.; Yaghi, O. M., The chemistry and applications of metal-organic frameworks. *Science* **2013,** *341* (6149), 1230444.

30. Boer, S. A.; Morshedi, M.; Tarzia, A.; Doonan, C. J.; White, N. G., Molecular tectonics: a node-and-linker building block approach to a family of hydrogen-bonded frameworks. *Chem. Eur. J.* **2019,** *25* (42), 10006-10012.

31. Park, K. S.; Ni, Z.; Côté, A. P.; Choi, J. Y.; Huang, R.; Uribe-Romo, F. J.; Chae, H. K.; O'Keeffe, M.; Yaghi, O. M., Exceptional chemical and thermal stability of zeolitic imidazolate frameworks. *Proc. Natl. Acad. Sci.* **2006,** *103* (27), 10186.

32. Morris, W.; Doonan, C. J.; Furukawa, H.; Banerjee, R.; Yaghi, O. M., Crystals as molecules: postsynthesis covalent functionalization of zeolitic imidazolate frameworks. *J. Am. Chem. Soc.* **2008,** *130* (38), 12626-12627.

33. Liang, W.; Xu, H.; Carraro, F.; Maddigan, N. K.; Li, Q.; Bell, S. G.; Huang, D. M.; Tarzia, A.; Solomon, M. B.; Amenitsch, H.; Vaccari, L.; Sumby, C. J.; Falcaro, P.; Doonan, C. J., Enhanced activity of enzymes encapsulated in hydrophilic metal–organic frameworks. *J. Am. Chem. Soc.* **2019,** *141* (6), 2348-2355.

34. Liang, W.; Carraro, F.; Solomon, M. B.; Bell, S. G.; Amenitsch, H.; Sumby, C. J.; White, N. G.; Falcaro, P.; Doonan, C. J., Enzyme encapsulation in a porous hydrogen-bonded organic framework. *J. Am. Chem. Soc.* **2019,** *141* (36), 14298-14305.

35. Russell, V. A.; Evans, C. C.; Li, W.; Ward, M. D., Nanoporous molecular sandwiches: pillared two-dimensional hydrogen-bonded networks with adjustable porosity. *Science* **1997,** *276* (5312), 575.

36. Luo, J.; Wang, J.-W.; Zhang, J.-H.; Lai, S.; Zhong, D.-C., Hydrogen-bonded organic frameworks: design, structures and potential applications. *CrystEngComm.* **2018,** *20* (39), 5884-5898.

37. Simard, M.; Su, D.; Wuest, J. D., Use of hydrogen bonds to control molecular aggregation. Self-assembly of three-dimensional networks with large chambers. *J. Am. Chem. Soc.* **1991,** *113* (12), 4696-4698.

38. Morshedi, M.; Thomas, M.; Tarzia, A.; Doonan, C. J.; White, N. G., Supramolecular anion recognition in water: synthesis of hydrogen-bonded supramolecular frameworks. *Chem. Sci.* **2017,** *8* (4), 3019-3025.

39. Wang, Y.; Ryu, B. H.; Yoo, W.; Lee, C. W.; Kim, K. K.; Lee, J. H.; Kim, T. D., Identification, characterization, immobilization, and mutational analysis of a novel acetylesterase with industrial potential (LaAcE) from *Lactobacillus acidophilus*. *Biochim. Biophys. Acta.* **2018,** *1862* (1), 197-210.

40. Biedermannová, L.; Prokop, Z.; Gora, A.; Chovancová, E.; Kovács, M.; Damborský, J.; Wade, R. C., A single mutation in a tunnel to the active site changes the mechanism and kinetics of product release in haloalkane dehalogenase LinB. *J. Biol. Chem.* **2012,** *287* (34), 29062-29074.

41. Buryska, T.; Babkova, P.; Vavra, O.; Damborsky, J.; Prokop, Z., A haloalkane dehalogenase from a marine microbial consortium possessing exceptionally broad substrate specificity. *Appl. Environ. Microbiol.* **2018,** *84* (2), e01684-17.

42. Linder-Patton, O. M.; de Prinse, T. J.; Furukawa, S.; Bell, S. G.; Sumida, K.; Doonan, C. J.; Sumby, C. J., Influence of nanoscale structuralisation on the catalytic performance of ZIF-8: a cautionary surface catalysis study. *CrystEngComm.* **2018,** *20* (34), 4926-4934.

43. Verploegh, R. J.; Nair, S.; Sholl, D. S., Temperature and loading-dependent diffusion of light hydrocarbons in ZIF-8 as predicted through fully flexible molecular simulations. *J. Am. Chem. Soc.* **2015,** *137* (50), 15760-15771.

6.8. Supporting Information

6.8.1. LinB biological function

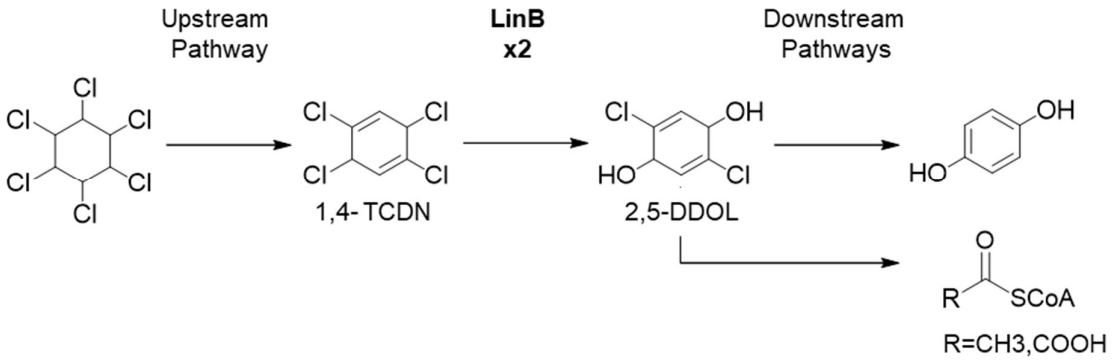

Figure S6.1: Metabolism of γ-hexachlorocyclohexane (lindane) to benzene-1-4-diol. The upstream pathway is a multistep dehalogenation catalysed by LinA. LinB acts on 1,3,4,6-tetrachloro-1,4-cyclohexadiene (1,4- TCDN) converting it into 2,5-dichloro-2,5-cyclohexadiene-1,4-diol (2,5-DDOL) in a 2-step process. The downstream reactions are multi enzyme processes can either produce benzene-1,4-diol or smaller metabolites (e.g. succinyl-CoA; R=COOH, or acetyl-coA; R=CH_3 that can enter the citric acid cycle for energy production. This figure has been adapted from Nagata *et. al.*[1]

6.8.2. LinB gene and pET28a(+)

The *linB* gene was purchased from Genscript within the pET-28a(+) vector (Merck-Millipore). WT LinB (Uniprot: Q6VQX3, Genbank: AY331259).

Genscript linB (A141C mutant) synthetic gene to be cloned into pET28a(+). An additional 6x histidine (6x His) tag sequence at the C-terminal to aid in purification steps. A sequence mutation at codon 141 (GCG to TGC) was introduced to replace an alanine with a cysteine residue. Cysteine residues are often targeted for site selective immobilisation so was included for potential extension to different immobilisation methods.[2] The position of the incorporated cysteine residue was based on a study by Badieyan *et. al*. in 2017 which showed the high retention of activity upon immobilisation via this site.[3] The gene sequence was codon optimised, which replaces uncommon codons of the gene with a redundant codon that is more frequently occurring in the expression system (*Escherichia coli*). This process does not alter the amino acid sequence but is designed to improve translation efficiency into the protein.

Start and stop codons are in bold, restriction sites NdeI at the 5' end and KpnI and HindIII at the 3' end are underlined, the A141C codon change is in red, and the 6 x His tag is in italics.

CAT**ATG**AGCCTGGGCGCGAAACCGTTTGGCGAGAAAAAGTTTATTGAAATTAAA
GGTCGTCGTATGGCGTATATTGATGAGGGCACCGGCGATCCGATTCTGTTCCAGC
ACGGTAACCCGACCAGCAGCTACCTGTGGCGTAACATTATGCCGCACTGCGCGG
GTCTGGGCCGTCTGATTGCGTGCGACCTGATTGGTATGGGCGACAGCGATAAGCT
GGATCCGAGCGGTCCGGAGCGTTACACCTATGCGGAACACCGTGACTACCTGGA
TGCGCTGTGGGAGGCGCTGGACCTGGGCGATCGTGTGGTTCTGGTGGTTCACGAC
TGGGGTAGCGTGCTGGGCTTCGATTGGGCGCGTCGTCACCGTGAGCGTGTGCAG
GGTATTGCGTATATGGAAGCGGTTACCATGCCGCTGGAGTGGTGCGACTTTCCGG
AACAAGACCGTGACCTGTTCCAGGCGTTTCGTAGCCAAGCGGGCGAGGAACTGG
TGCTGCAGGATAACGTGTTCGTTGAACAAGTTCTGCCGGGCCTGATCCTGCGTCC
GCTGAGCGAGGCGGAAATGGCGGCGTACCGTGAGCCGTTTCTGGCGGCGGGTGA
AGCGCGTCGTCCGACCCTGAGCTGGCCGCGTCAAATTCCGATTGCGGGCACCCCG
GCGGATGTGGTTGCGATTGCGCGTGATTATGCGGGTTGGCTGAGCGAGAGCCCG
ATCCCGAAACTGTTCATTAACGCGGAACCGGGTCACCTGACCACCGGTCGTATCC
GTGACTTTTGCCGTACCTGGCCGAACCAGACCGAGATCACCGTTGCGGGTGCGCA
CTTTATTCAAGAGGACAGCCCGGATGAAATCGGCGCGGCGATTGCGGCGTTTGTT
CGTCGTCTGCGTCCGGCG*CATCACCATCACCACCAC***TAATAA**GGTACCAAGCTT

pET28a(+) Vector: pET-28a(+) is a 5.4 kilobase standard expression (Merck Millipore) vector containing a kanamycin resistance gene (for selection purposes), a lac operon and the 5' NdeI and 3' HindIII restriction site (for cloning purposes).

DNA replication: The pET-28a(+)(*linB*) vector was transformed into competent *E.coli* strain DH5-α via standard methods to increase the concentration of DNA. Successfully transformed cells were cultured in Luria Broth (LB) containing kanamycin (30 $\mu g.mL^{-1}$) for 6 hours (37°C, 100 rpm) and the pET-28a(+)(linB) DNA was extracted and purified using a Promega Magic miniprep kit. The presence of the LinB gene was confirmed via gel electrophoresis after digestion with HindIII and NdeI restriction site enzymes (**Figure S6.1**).

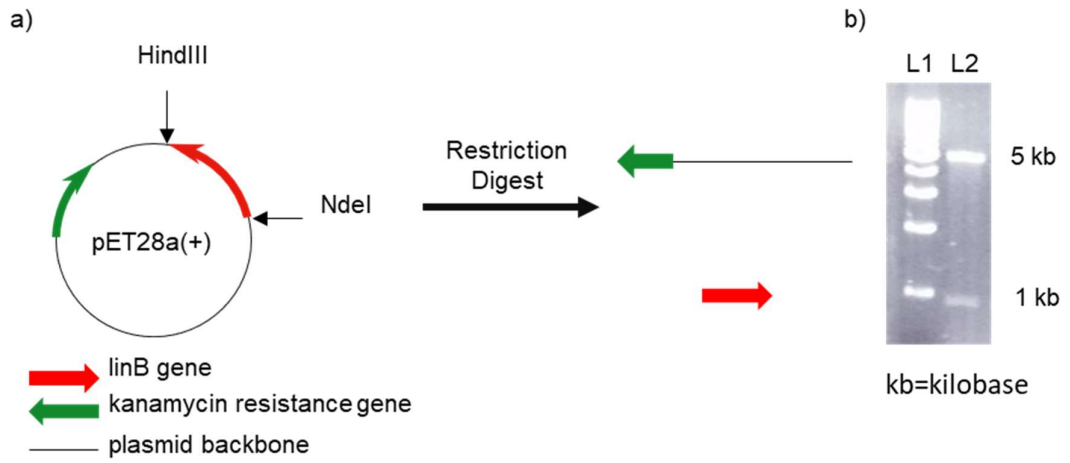

Figure S6.2: (a) The *linB* gene cloned into the pET28a(+) plasmid flanked by a 5' NdeI and 3' HindIII restriction sites. (b) Electrophoresis gel of the *linB*-pET28a(+) replication product after restriction digest with NdeI and HindIII showing the correct *linB* fragment size (906 bp) and pET-28a(+) backbone (5.4 kbp). L1: DNA size marker lane, L2: Digested *linB*-pET28a(+).

6.8.3. Protein Expression and Purification

Final Amino Acid Sequence. The 6 x His tag is in italics and the A141C mutation highlighted in yellow. The molecular weight (MW) expected from the sequence is 34,084 Da with an isoelectric point of 5.54 and Molar Extinction of 56170 $M^{-1}.cm^{-1}$ Coefficient(ExPASy Bioinformatics Resource Portal).[4] For comparison, without the His tag the MW (33,261 Da) and isoelectric point (5.1) are not significantly altered.

MSLGAKPFGEKKFIEIKGRRMAYIDEGTGDPILFQHGNPTSSYLWRNIMPHCAGLGR
LIACDLIGMGDSDKLDPSGPERYTYAEHRDYLDALWEALDLGDRVVLVVHDWGSV
LGFDWARRHRERVQGIAYMEAVTMPLEWCDFPEQDRDLFQAFRSQAGEELVLQDN
VFVEQVLPGLILRPLSEAEMAAYREPFLAAGEARRPTLSWPRQIPIAGTPADVVAIAR
DYAGWLSESPIPKLFINAEPGHLTTGRIRDFCRTWPNQTEITVAGAHFIQEDSPDEIGA
AIAAFVRRLRPA*HHHHHH*

Expression: The pET-28a(+)(linB) was transformed into competent *Escherichia coli* strain BL21 (DE3) for protein expression. The cells were cultured in LB (2 litres) with kanamycin (30 $\mu g.mL^{-1}$) for 8 hours to increase the cell density (37°C, 100 rpm). The culture was cooled to 20°C and protein expression was induced with the addition of IPTG (0.1 mM). The culture was grown for a further 20 hours and the cells were harvested by centrifugation

(4000 g, 10 min, 4°C). The cell pellet was resuspended in phosphate buffer (50 mM, pH 7.4), placed on ice, and lysed by sonication (25 cycles at 20:40 seconds on:off, 70 %, 19 mm probe, Sonics Vibra-Cell). The lysed cells were centrifuged (40,000 g, 10 min, 4°C) to separate the protein from cell debris.

Purification: The protein solution was loaded onto a HisTrap Crude FF column (GE Life Science, 5 mL) pre-equilibrated with binding buffer (50 mM tris, pH 7.4, 300 mM NaCl, 20 mM imidazole, 1 mM dithiothreitol). The column was washed with 5 column volumes of Binding Buffer to remove non-His tagged proteins, and the LinB protein was eluted with 2 column volumes of elution buffer (50 mM tris, pH 7.4, 300 mM NaCl, 300 mM imidazole, 1 mM dithiothreitol). The protein was concentrated and exchanged into phosphate buffer (50 mM, pH 7.4) via ultra-filtration (4x, 10 KDa, 4000 rpm) and combined with an equal volume of 80% glycerol. The protein was filtered through a 0.22 µm syringe filter and stored at -20°C. LinB protein concentration and purity was determined by Bradford Assay (**Figure S6.3**) and SDS-PAGE (**Figure 6.2**) respectively. Prior to use, the protein was exchanged into water and concentrated by ultra-filtration (4x, 10 KDa, 4000 rpm).

Bradford Assay: A Bradford Assay was performed to calculate the LinB concentration as per the Sigma Aldrich Protocol.[5] All BSA protein standards and the LinB sample were made up in sodium phosphate buffer (50 mM, pH 7.4) and the absorbance of the protein-coomassie (dye) complex was measure at 595 nm. The concentration of BSA (MW: 66,400 $g.mol^{-1}$) was calculated using the extinction coefficient of 43,824 $M^{-1}.cm^{-1}$ at 280 nm. According to the Bradford calibration curve (**Figure S6.3**) a 2 L broth expression yielded approximately 73 ± 5 mg of purified LinB. The theoretical extinction coefficient of LinB (56,170 $M^{-1}.cm^{-1}$ @ 280 nm) was used to cross check concentrations prior to usage.

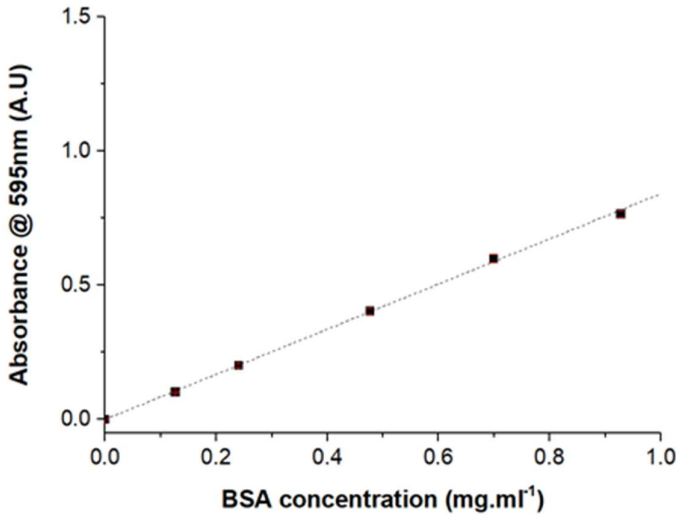

Figure S6.3: Bradford assay calibration curve using Bovine Serum Albumin (BSA). Duplicate calibrations were made with absorbance values measured after 15 minutes with the standard error for each BSA concentration shown in red.

6.8.4. Substrate/product controls.

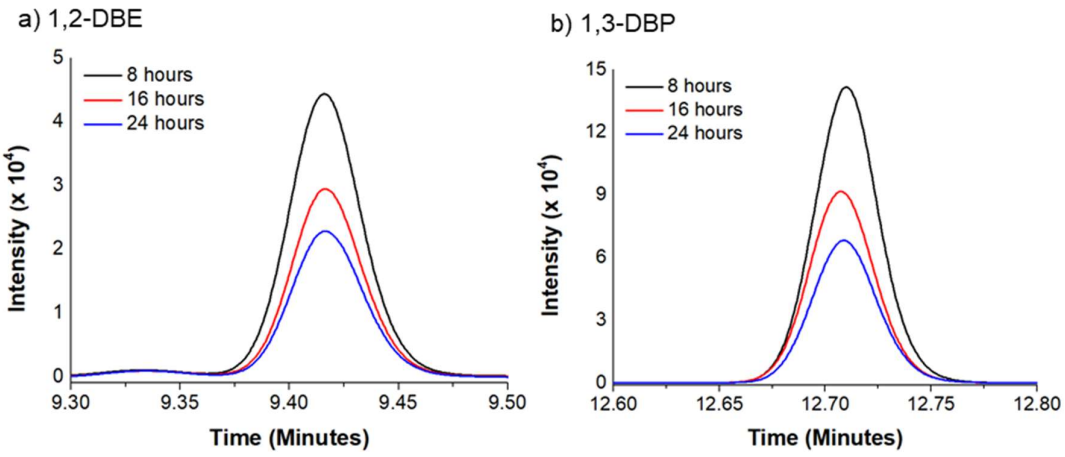

Figure S6.4: GC calibration of 1,2-DBE (left) and 1,3-DBP (adjusted for internal standard variability) from which the time dependant reduction in concentration was calculated from.

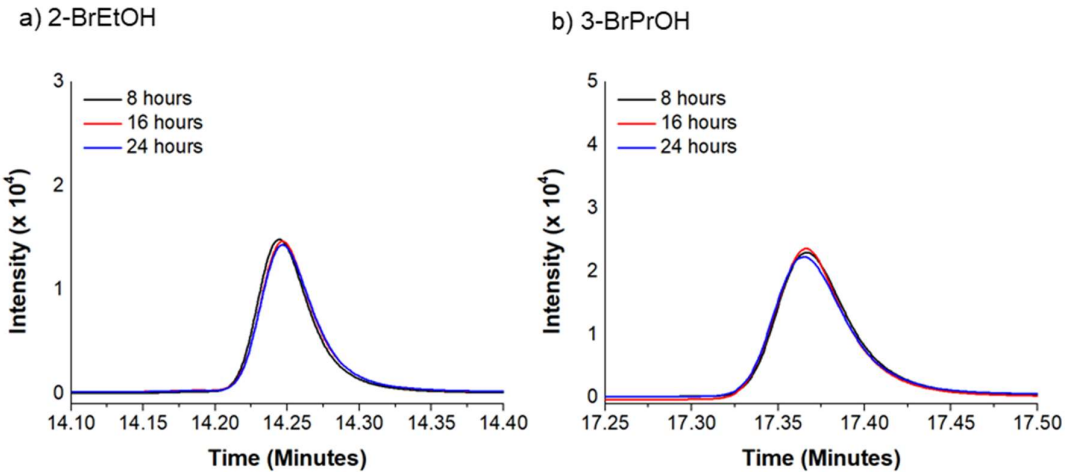

Figure S6.5: GC calibration of 2-bromoethanol and 3-bromo-1-propanol (adjusted for internal standard variability). No significant reduction in concentration was observed over the 24-hour period.

Table S6.1: The concentration of the 1 mM 1,2-DBE, 1,3-DBP, BrEtOH, and BrPrOH controls as calculated from a time=0 substrate and product calibration curve.

	Concentration (mM)			
Time (hours)	**1,2-DBE**	**BrEtOH**	**1,3-DBP**	**BrPrOH**
0	1	1	1	1
8	0.99	1	0.98	1
16	0.70	0.89	0.71	0.98
24	0.53	0.88	0.52	0.82

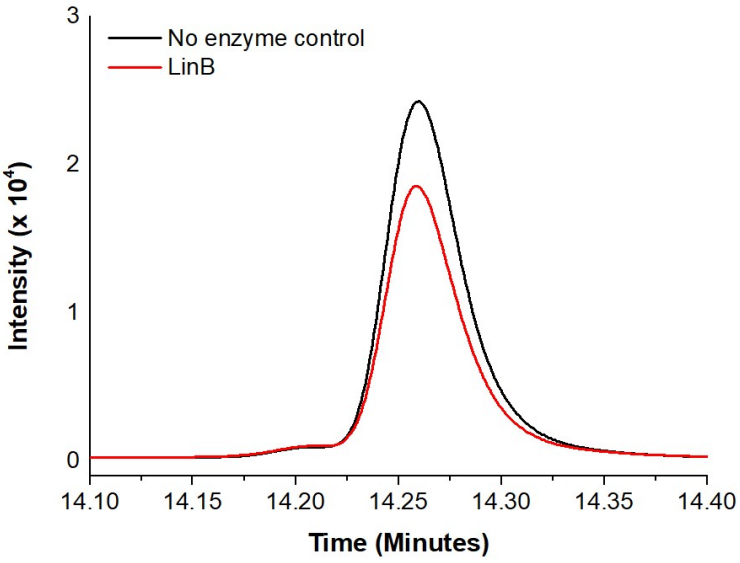

Figure S6.6: GC traces of 2-bromoethanol after 8 hours without LinB (black) and with free enzyme showing consumption of the first bromo-alcohol product.

6.8.5. Biocomposite formation.

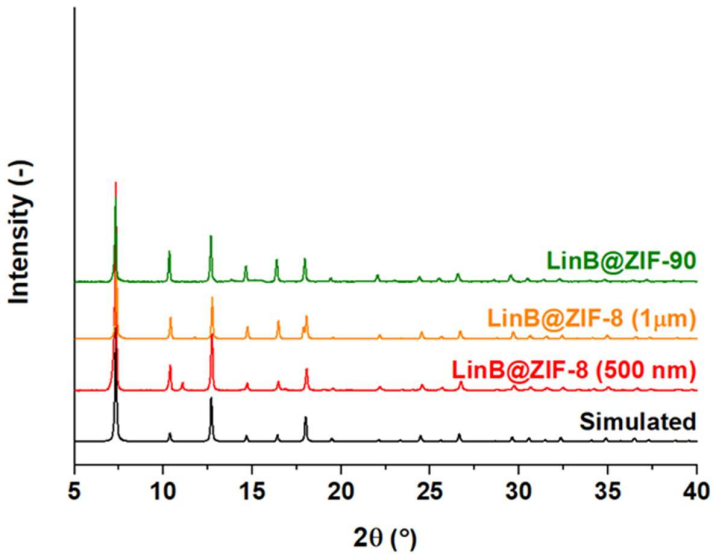

Figure S6.7: As-synthesised PXRD pattern of ZIF-8 (500 nm), ZIF-90 (1 μm) and ZIF-90 made in the presence LinB.

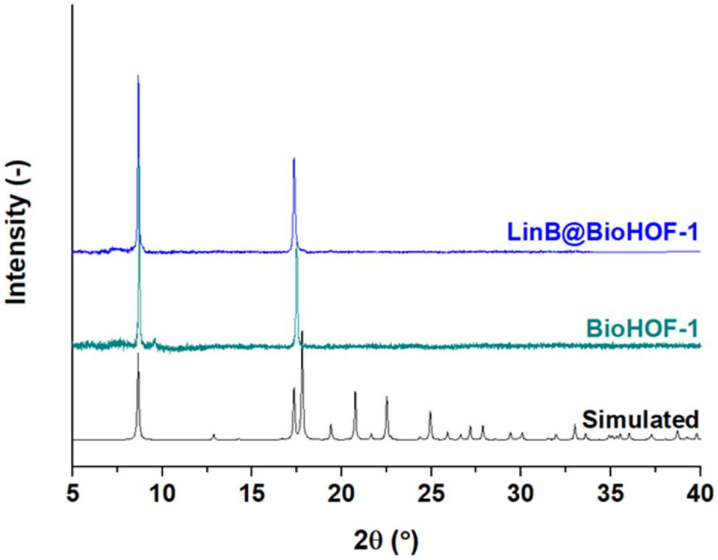

Figure S6.8: As-synthesised PXRD pattern of BioHOF-1 made in the presence LinB or no protein. Additional peaks will appear upon grinding the sample, as the effects of preferred orientation are overcome.[6] The simulated powder pattern was generated form single crystal X-ray diffraction data of the protein free Bio-HOF-1.[7]

6.8.6. Biocomposite activity testing.

Table S6.2: Percentage conversion of the 1,2-DBE to 2-bromoethanol by free LinB, LinB@BioHOF-1, LinB@ZIF-8 (500 nm), LinB@ZIF-8 (1 µm) and LinB@ZIF-90 When allowed to react for 16 hours, both the free LinB and LinB@BioHOF-1 reached 93% conversion, whilst all ZIFs were susceptible to substrate loss without further product formation.

Time	Free	BioHOF-1	ZIF-8 (500 nm)	ZIF-8 (1 µm)	ZIF-90
8 hr	86	75	<1	n.d	11
16 hr	93	94	1	n.d	14
24 hr	67	76	3	n.d	10

Table S6.3: Percentage conversion of the 1,3-DBP to 3-bromopropan-1-ol by free LinB, LinB@BioHOF-1, LinB@ZIF-8 (500 nm), LinB@ZIF-8 (1 µm) and LinB@ZIF-90.

Time	Free	BioHOF-1	ZIF-8 (500 nm)	ZIF-8 (1 µm)	ZIF-90
8 hr	86	97	54	2	97
16 hr	90	85	67	1	100
24 hr	48	58	80	2	92

6.8.7. Post assay characterisation.

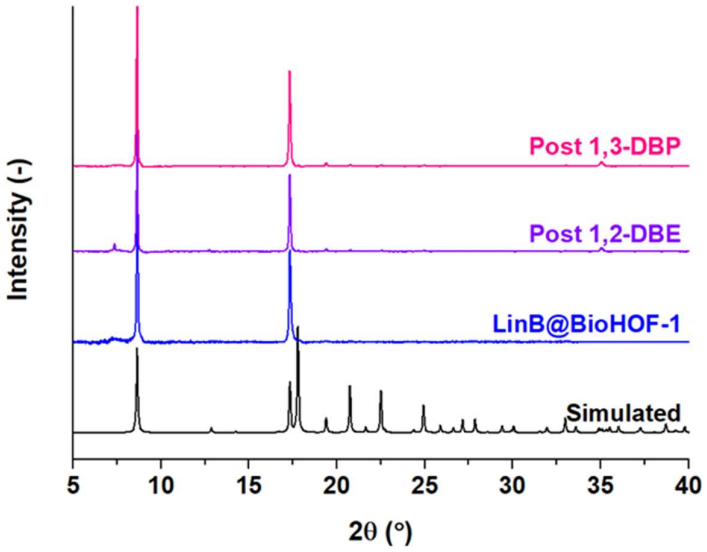

Figure S6.9: PXRD of the LinB@BioHOF-1 composite post assay with 1,2-DBE, and 1,3-DBP. No changes to crystallinity were observed post catalysis.

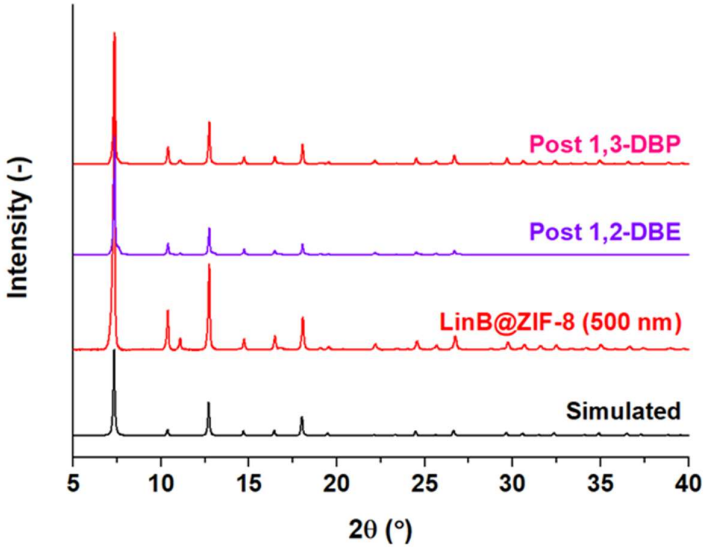

Figure S6.10: PXRD of the LinB@ZIF-8 (500 nm) composite post assay with 1,2-DBE, and 1,3-DBP. Despite the degradation, no changes to bulk crystallinity were observed post catalysis.

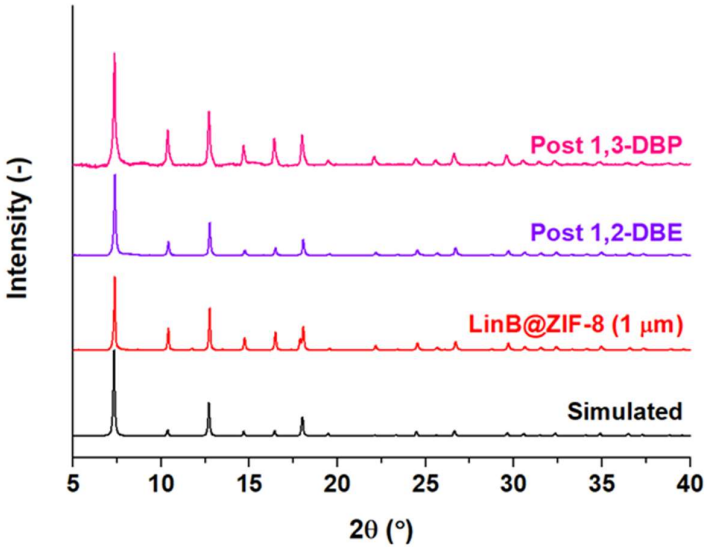

Figure S6.11: PXRD of the LinB@ZIF-8 (1 μm) composite post assay with 1,2-DBE, and 1,3-DBP. No changes to bulk crystallinity were observed post catalysis.

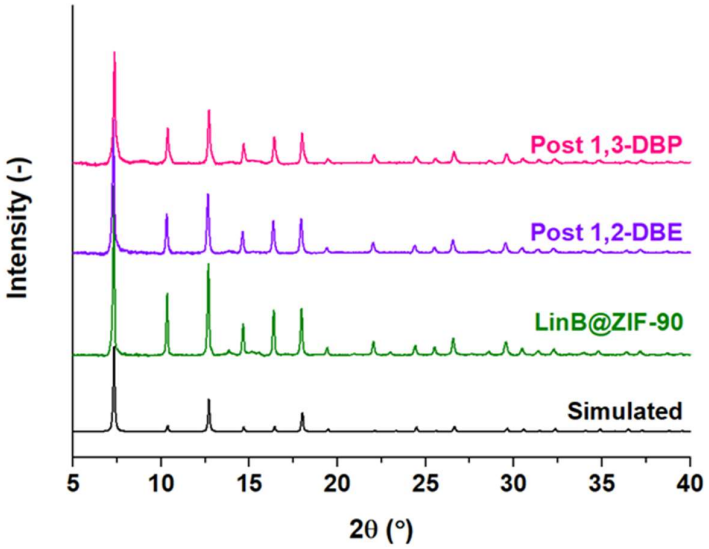

Figure S6.12: PXRD of the LinB@ZIF-90 composite post assay with 1,2-DBE, and 1,3-DBP. Despite the degradation, no changes to bulk crystallinity were observed post catalysis.

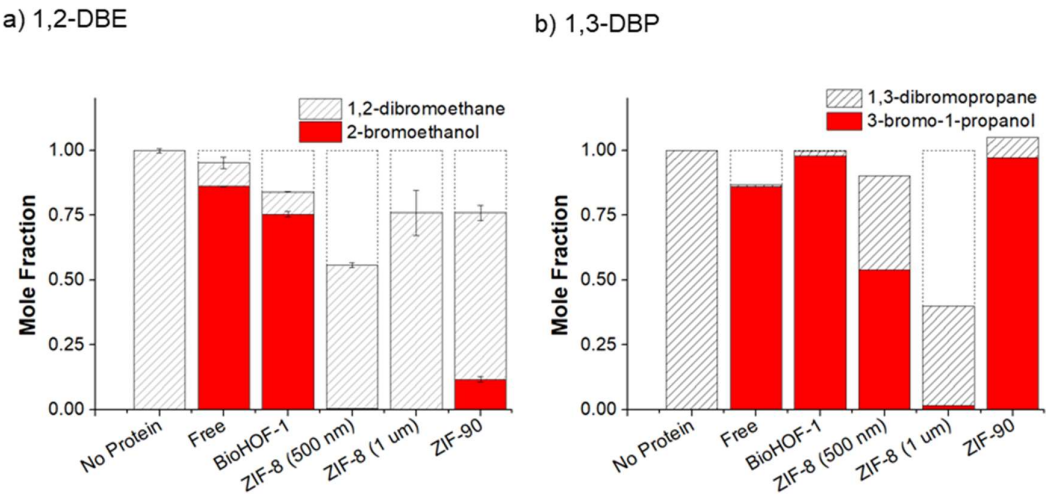

Figure S6.13: Mole fraction of the reaction mixture using free LinB and each biocomposite after an 8-hour reaction with (a) 1,2-DBE and (b) 1,3-DBP. The substrate (stripes) and first products (solid red) concentrations were calculated from calibration curves whilst the white dashed segment represents substrate and/or product that was unaccounted for.

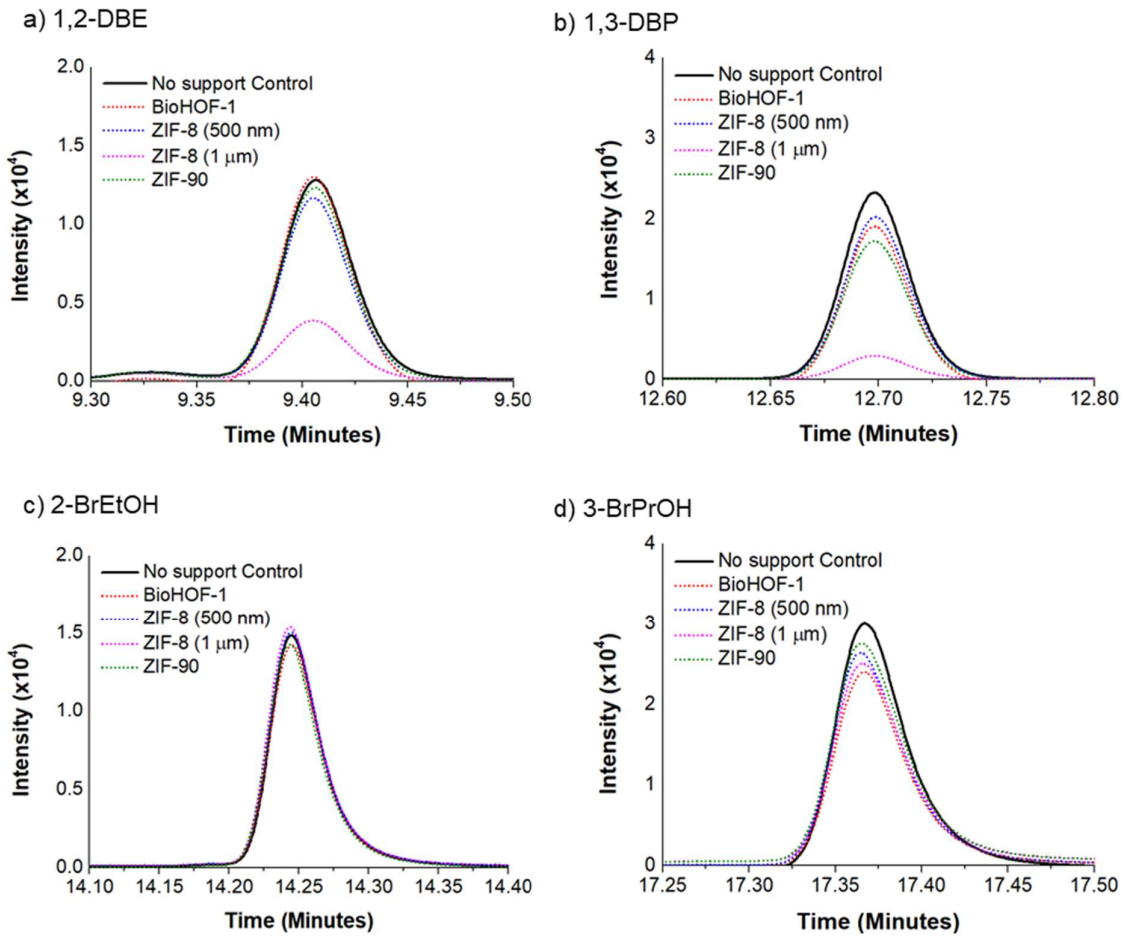

Figure S6.14: Substrate and product adsorption controls for 1,2-DBE (left) and 1,3-DBP (right) after 8 hours. The amount of BSA biocomposite was set to be equivalent to the LinB counterpart. As such, a larger mass of ZIF-8 (1 μm) compared to ZIF-8 (500 nm) would be present in solution and would contribute to the larger percentage of substrate loss. Only minor product adsorption was observed for each biocomposite.

Supporting Information 6.8 References

1. Nagata, Y.; Miyauchi, K.; Takagi, M., Complete analysis of genes and enzymes for γ-hexachlorocyclohexane degradation in *Sphingomonas paucimobilis* UT26. *J. Ind. Microbiol. Biotechnol.* **1999,** *23* (4), 380-390.

2. Rehm, F. B. H.; Chen, S.; Rehm, B. H. A., Enzyme engineering for in situ immobilization. *Molecules* **2016,** *21* (10), 1370.

3. Badieyan, S.; Wang, Q.; Zou, X.; Li, Y.; Herron, M.; Abbott, N. L.; Chen, Z.; Marsh, E. N. G., Engineered surface-immobilized enzyme that retains high levels of catalytic activity in air. *J. Am. Chem. Soc.* **2017,** *139* (8), 2872-2875.

4. Gasteiger E., Hoogland C., Gattiker A., Duvaud S., Wilkins M.R., Appel R.D., Bairoch A. *Protein Identification and Analysis Tools on the ExPASy Server*, The Proteomics Protocols Handbook, Walker, J. M., Ed. Humana Press: Totowa, NJ, (**2005**), pp. 571-607.

5. Kruger, N. J., *The Bradford Method For Protein Quantitation,* The Protein Protocols Handbook, Walker, J. M., Ed. Humana Press: Totowa, NJ, (**2009**), pp 17-24.

6. Liang, W.; Carraro, F.; Solomon, M. B.; Bell, S. G.; Amenitsch, H.; Sumby, C. J.; White, N. G.; Falcaro, P.; Doonan, C. J., Enzyme encapsulation in a porous hydrogen-bonded organic framework. *J. Am. Chem. Soc.* **2019,** *141* (36), 14298-14305.

7. Boer, S. A.; Morshedi, M.; Tarzia, A.; Doonan, C. J.; White, N. G., Molecular tectonics: a node-and-linker building block approach to a family of hydrogen-bonded frameworks. *Chem. Eur. J.* **2019,** *25* (42), 10006-10012.

Chapter 7.

Conclusions and Future Directions

Chapter 7. Conclusions and Future Directions

7.1. Outlook

This thesis describes the investigation of a selection of porous materials that have been developed as enzyme immobilisation supports. The work in this thesis has developed general protocols for protein immobilisation using porous supports, and in doing so has improved our understanding of how these processes can influence enzymatic activity. The chemistry of porous frameworks and enzymatic catalysis are both well established, independent fields. However, at the interface of the two, lies a burgeoning area of research, known as enzyme immobilisation using porous frameworks (MOFs/HOFs). This thesis investigated the immobilisation process, through systematic screening of conditions. Enzymatic activity assays were used to probe the compatibility of the framework for immobilisation. As a result, improved protocols were developed for the immobilisation of enzymes whilst maintaining their activity. In summary, this study has contributed to an increased understanding of the interplay between the framework and the enzyme chemistry.

In **Chapters 2 and 3**, we established consistent and predictable protocols for encapsulating proteins using ZIF-8 as the support material. In the initial screening, we observed that the biomimetic mineralisation methodology used for BSA@ZIF-8 could not be universally applied to all proteins. Through the screening of a diverse range of proteins, we now understand the impact that protein surface chemistry plays in seeding the biomimetic mineralisation of ZIF-8 in aqueous solutions. With this knowledge, we developed synthetic conditions to enhance the immobilisation process, through modulation of precursor concentrations and surface functionalisation of the protein.[1-2] An important outcome of this study was that the zeta-potential of the protein in a 2-mIM solution (both experimental and computational) can be used to determine the efficacy of ZIF-8 nucleation using proteins. Here, it was established that the isoelectric point (pI) of the protein could also be used as a predictive tool, i.e. proteins with a pI value of <6 afforded successful nucleation. This could be used to select suitable proteins for future studies or to determine how the protocol of immobilisation could be modified.[2] This work enabled us to encapsulate a range of structurally and chemically diverse proteins. However, the influence of protein surface chemistry on spatial distribution within ZIF-8, upon immobilisation, is still relatively unknown. Within our group, work has been previously undertaken to understand this process, however the focus of that study was limited to one encapsulation method.[1] Variation in the spatial distribution of the protein within the crystals (central, subsurface or surface bound) was seemingly dictated by the surface chemistry of the

fluorescently tagged proteins (fluorescein or rhodamine). However, the impact of both the protein surface chemistry, and the synthetic conditions on the growth phase and properties of protein@ZIF-8 biocomposites is still largely unknown, which necessitates further investigation. However, the work described in **Chapters 2 and 3**, enabled the development of consistent methods of forming different sized enzyme@ZIF-8 biocomposites to be examined for enzymatic activity.

In the literature, there have been many studies of enzyme@ZIF-8 biocomposites. However, there are inconsistencies in the reporting of the synthesis conditions, material handling and storage of materials which have resulted in conflicting activity data.[3-5] The work described in **Chapter 4** investigated the relationship between the synthetic conditions (for biocomposite formation) and enzymatic activity. Biocomposites of lipase (CALB) of different particle sizes and network topologies were obtained, through modulation of the precursor concentrations and washing protocols, and their enzymatic activity was measured using different reactions catalysed by lipase. The method of CALB@ZIF-8 formation was shown to impact the catalysis of both a transesterification and hydrolysis reaction. For the transesterification reaction, that was conducted in hexane, the CALB@ZIF-8 biocomposites synthesised using low ligand concentrations, outperformed the free enzyme, that was unable to catalyse the reaction in 100% hexane. Additionally, the smaller (low ratio) CALB@ZIF-8 biocomposites demonstrated the best activity for both reactions, with the larger (high ratio) samples being essentially inactive.

In order to account for the variation in synthetic protocols, careful reporting of the reaction conditions and sample treatment was necessary. Indeed, by investigating the use of reaction media, such as phosphate buffer, which cause framework degradation and enzyme leaching, we have begun to understand source of the variations that have been reported in the literature.[3, 6-7] The data presented in **Chapter 4** has expanded our knowledge of CALB@ZIF-8 catalysis, however, to fully comprehend the variations reported, additional studies with alternate enzymes are needed. With further investigation, we aim to understand how the protein surface chemistry, and the formation kinetics ZIF-8, dictate biocomposite activity and stability.

In order to understand why the larger (high ratio) CALB@ZIF-8 samples were inactive, **Chapter 5** investigated two structurally and chemically different frameworks as immobilisation supports for CALB; ZIF-90 and BioHOF-1.[3, 8] Similar to previous studies with catalase, CALB was shown to retain activity upon immobilisation with both ZIF-90 and

BioHOF-1 and thus highlights the potential advantages of these frameworks, over ZIF-8 as enzyme immobilisation supports. An important finding of this study was that CALB maintained its stereoselectivity for the transesterification of phenyl ethanol with vinyl acetate (*ee* 99%), suggesting that the immobilisation process was not significantly impacting the enzyme structure. However, studies which directly probe protein conformation are required to fully understand the relationship between the framework and the protein. There are inherent difficulties in analysing these interactions for the solid phase biocomposites, as the majority of methods which probe protein/peptide folding/unfolding are solution based and so new solid phase techniques must be developed to do so. The preliminary investigations with CALB@ZIF-90 and CALB@BioHOF-1, suggested that the enzyme was impacting the formation of both materials. However, there remains little understanding of the mechanism of framework formation was affected in each case. The systematic screening of different proteins may aid our understanding of this process to establish the rules and generality of biocomposite formation, in a similar manner outlined in **Chapters 2** and **3**.

Chapter 6 built upon our knowledge from the previous studies to extend our protocols to a new dehalogenase enzyme (LinB). Importantly this enzyme had yet to be immobilised in any of the frameworks tested here (ZIF-8, ZIF-90, or BioHOF-1). Additionally, there have been few examples of the immobilisation of recombinantly expressed enzymes using ZIF-8, ZIF-90 and none for BioHOF-1, as such this was described for the first time in **Chapter 6**. LinB could be immobilised in each material, however this study highlighted some of the challenges of using ZIFs for enzymatic catalysis. More specifically, for the two dehalogenation reactions tested, LinB@BioHOF-1 exhibited greater activity and stability, compared to both ZIF materials which were either inactive or degraded under the reaction conditions. The BioHOF-1 framework has only recently been applied as a support material for enzyme immobilisation, and as such has substantial scope for investigation.[8] Despite the infancy of using BioHOF-1, this method has already shown promise for the stabilisation of multiple enzymes to a range of non-biological conditions. In the investigation described in **Chapter 6**, LinB@BioHOF-1 was stable to thermal treatment at 60 °C, and could be reused for five cycles with minimal loss in activity. These findings have prompted further exploration of LinB@BioHOF-1, to examine the potential of the biocomposite, extending the substrate range and reaction conditions to more industrially relevant applications. This may include chiral resolution of small molecules. Additionally, the volatile substrates of LinB, make this enzyme an ideal candidate for gas phase catalysis testing.

This work could be extended to focus on understanding the variations highlighted above and broadening the application of these porous supports to new enzymes, and reaction conditions. We limited our investigation to specific enzyme/reaction systems, and thus have only begun to uncover the potential of porous frameworks (in particular BioHOF-1) for enzyme immobilisation. There is a diverse library natural, recombinant, and genetically engineered proteins that are available which can direct our focus towards the development of novel protein/enzyme biocomposites. However, due to the challenges associate with ZIF materials, and the complexity of the biocomposite formation, little attention has been given to multi-enzyme reactions, and systems requiring external cofactors. With the recent development of BioHOF-1, an exciting extension of this work is to examine the immobilisation of complex, multi-enzyme systems that have yet to be investigated. As such, targeting more complex, industrially relevant reactions is now possible.

7.2. References

1. Liang, W.; Ricco, R.; Maddigan, N. K.; Dickinson, R. P.; Xu, H.; Li, Q.; Sumby, C. J.; Bell, S. G.; Falcaro, P.; Doonan, C. J., Control of structure topology and spatial distribution of biomacromolecules in protein@ZIF-8 biocomposites. *Chem. Mater.* **2018,** *30* (3), 1069-1077.

2. Maddigan, N. K.; Tarzia, A.; Huang, D. M.; Sumby, C. J.; Bell, S. G.; Falcaro, P.; Doonan, C. J., Protein surface functionalisation as a general strategy for facilitating biomimetic mineralisation of ZIF-8. *Chem. Sci.* **2018,** *9* (18), 4217-4223.

3. Liang, W.; Xu, H.; Carraro, F.; Maddigan, N. K.; Li, Q.; Bell, S. G.; Huang, D. M.; Tarzia, A.; Solomon, M. B.; Amenitsch, H.; Vaccari, L.; Sumby, C. J.; Falcaro, P.; Doonan, C. J., Enhanced activity of enzymes encapsulated in hydrophilic metal–organic frameworks. *J. Am. Chem. Soc.* **2019,** *141* (6), 2348-2355.

4. Cui, J.; Feng, Y.; Jia, S., Silica encapsulated catalase@metal-organic framework composite: A highly stable and recyclable biocatalyst. *Chem. Eng. J.* **2018,** *351*, 506-514.

5. Du, Y.; Gao, J.; Liu, H.; Zhou, L.; Ma, L.; He, Y.; Huang, Z.; Jiang, Y., Enzyme@silica nanoflower@metal-organic framework hybrids: A novel type of integrated nanobiocatalysts with improved stability. *Nano. Res.* **2018,** *11* (8), 4380-4389.

6. Luzuriaga, M. A.; Benjamin, C. E.; Gaertner, M. W.; Lee, H.; Herbert, F. C.; Mallick, S.; Gassensmith, J. J., ZIF-8 degrades in cell media, serum, and some—but not all—common laboratory buffers. *Supramol. Chem.* **2019,** *31* (8), 485-490.

7. Velásquez-Hernández, M. d. J.; Ricco, R.; Carraro, F.; Limpoco, F. T.; Linares-Moreau, M.; Leitner, E.; Wiltsche, H.; Rattenberger, J.; Schröttner, H.; Frühwirt, P.; Stadler, E. M.; Gescheidt, G.; Amenitsch, H.; Doonan, C. J.; Falcaro, P., Degradation of ZIF-8 in phosphate buffered saline media. *CrystEngComm.* **2019,** *21* (31), 4538-4544.

8. Liang, W.; Carraro, F.; Solomon, M. B.; Bell, S. G.; Amenitsch, H.; Sumby, C. J.; White, N. G.; Falcaro, P.; Doonan, C. J., Enzyme encapsulation in a porous hydrogen-bonded organic framework. *J. Am. Chem. Soc.* **2019,** *141* (36), 14298-14305.